# STRUCTURE AND DEVONIAN STRATIGRAPHY OF THE TIMPAHUTE RANGE, NEVADA

Volume I

by
Alan K. Chamberlain

A thesis submitted to the Faculty and Board of Trustees of the Colorado School of Mines in partial fulfillment of the requirements for the degree of Doctor of Philosophy (Geology).

Golden, Colorado
Date____________

Signed:___________________________
Alan K. Chamberlain

Approved:___________________________
Dr. John E. Warme
Professor and Thesis Advisor

Golden, Colorado
Date____________

___________________________________
Dr. Roger Slatt,
Professor and Head,
Department of Geology and Geological Engineering

ABSTRACT


Sequences of Devonian rocks are advantageously exposed along a unique 40-mile-long east-west traverse in the greater Timpahute Range, southeastern Nevada. Study of these rocks casts light upon Devonian paleogeography, the Devonian Antler orogeny, an Upper Devonian cosmolite impact basin, this part of the Cretaceous Sevier fold-and-thrust belt, and the effects of Cenozoic extension. The greater Timpahute Range lies within the Timpahute Range 30' X 60' quadrangle and includes the region from Tempiute Mountain on the west to the Pahroc Range on the east.

Concealed major north-south trending normal faults caused by Cenozoic extension have been proposed to disrupt the Paleozoic rocks of the region. However, a structural interpretation using a new geologic map of the quadrangle requires no major north-south striking normal faults. Furthermore, the greater Timpahute Range is interpreted as a salient of stacked thrust sheets within the Sevier fold-and-thrust belt. The range is bounded on the north and south by thrust tear faults that may be related to basement fractures caused by the cosmolite impact.

Evidence for the Late Devonian cosmolite impact includes shocked quartz, iridium anomalies, ejecta spherules, and disturbed shallowing-upward sequences exhibiting intrasequence folding, brecciation, carbonate liquefaction, and graded bedding. Impact breccia thins radially from 510 feet at Tempiute Mountain to zero within 80 miles north and south of Tempiute Mountain, but within only 60 miles northeast and southeast of the impact site. Bed length measurements from a geometrically balanced cross section of the greater Timpahute Range show at least 64 miles of cumulative crustal shortening. When restored, the diameter of the concentric impact basin, centered near Tempiute Mountain, is 160 miles. A restored cross section suggests that the impact site is likely about 20 miles west of Tempiute Mountain.

Thrust sheets within the salient contain rocks of three contrasting facies above the cosmolite impact breccia marker: facies 1 is a peculiar, anoxic, deepwater, thin-bedded limestone characterized by soft-sediment slump folds and interbedded turbidites that may represent a crater fill that now is exposed in a proposed fenster on the west end of the range; facies 2 is a thick shallow-water quartz sandstone (as much as 1070 net feet thick) deposited on the west side of the impact basin that now is in an interpreted klippe in the middle of the range; facies 3 is a shallow-water platform carbonate deposited on the east side of the impact basin. It contains a large stromatoporoid reef.

Characterized by shallowing-upward cycles, a reference measured section for the carbonate platform facies 3 was correlated to surface and subsurface sections of the region using sequence characteristics and gamma-ray log patterns. Only 19 of 21 sequences are exposed in the reference section that lies in the footwall and east of the thrust sheet containing sandy facies 2. When viewed in order, isopach maps of the 21 sequences show a large (200 X 400 miles, unrestored) depression, the Sunnyside basin, the axis of which migrated from central Nevada to western Utah during the Devonian. A composite isopach map of the 21 sequences shows that the intrashelf Sunnyside basin is thickest and therefore centered over Sunnyside, 60 miles north of the Timpahute Range.

Quartz sandstone isolith maps show that Devonian quartz sandstones were deposited on the edges of the Sunnyside basin. It is proposed that sandstones on the west side were derived from the Devonian Antler orogenic forebulge. Sandstones on the east side were probably derived from the craton and more specifically from an east-west highland developed on the Uinta aulacogen in north-central Utah. Isopach patterns suggest that the highland or arch, herein called the Monitor-Uinta arch, extended into central Nevada.

Dolomite, a common constituent of much of the Great Basin Devonian, commonly occurs as penecontemporaneous dolomite caps on shallowing-upward cycles in facies 3. Sections of Upper Devonian strata near the edges of the Sunnyside basin are more dolomitic than those within the basin.  Dolomites, basinward of the sandy facies 2, are rich in the thin, stick-like stromatoporoid, *Amphipora*.  Basinward of the *Amphipora*-rich dolomites are limestones rich in corals and bulbous and tabular stromatoporoids.  A major unconformity, characterized by deep (100's feet) karst cavities, separates pervasively dolomitized Middle and Lower Devonian carbonates from Upper Devonian limestones.  Of the three Upper Devonian facies in the greater Timpahute Range, only the facies 3 reference section contains significant dolomite as caps on shallowing-upward carbonate cycles, suggesting supratidal depositional environments in the shallower parts of the Sunnyside basin.

TABLE OF CONTENTS

LIST OF FIGURES

LIST OF TABLES

LIST OF PLATES

## ACKNOWLEDGMENTS

I am grateful to those who reviewed and made recommendations for improvements to this manuscript: Dr. Dave Drowley (Amoco), Drs. Alton A. Brown and S. Judson May (Arco), Drs. Morris S. Peterson and Lehi F. Hinze (Brigham Young University), Dr. Gerald Friedman (Brooklyn College), Bruce Birge and Renae Wilkinson (Cedar Strat), Dr. Peter Verrall (Chevron, deceased), Dr. Steve Boyer (consultant, formerly University of Washington), Dr. William Jamison (consultant), Gerald G. Loucks (consultant), Bill Roberts (consultant), Dr. Dietrich H. Roeder (consultant, formerly University of Tennessee), Dr. John E. Welch (consultant), Joseph Kulik (Denver Earth Resources Library), Peter Hummel (Eagle Exploration), Dr. John Willott (Exxon), Karl E. Marlowe (Homestake), Dr. Eric Mountjoy (McGill University), James and Daniel Carpenter (Mobil), Dr. David Kopelman (Retired Prosecutor), Dr. Michael L. Morrison (Talisman), Drs. Kathryn M. Nichols and Norman J. Silberling (consultants, formerly USGS and Stanford University), and Rick Page (USGS).

Also thanks go to those who helped with field work and made helpful observations: Randy L. Chamberlain (Blue Eagle), Bruce Birge (Cedar Strat), Charles Gillespie (Tide Petroleum), Edgar Perez, Brian Ackman, Jane Estes, Anna J. Chamberlain and participants of several field trips to the greater Timpahute Range area. Chris Hansen and Greg Cameron (Cedar Strat) did much of the early field work. I picked the Devonian sequences and correlated them with surface and subsurface sections throughout the eastern Great Basin with the assistance of Bruce Birge. Also, many thanks go to participants of Cedar Strat's annual field conferences. Their comments were helpful.

I am thankful to the following for graciously providing data for this project: Martin A. Kopacz (Shell Western E&P Inc.) who gave me permission to use surface sections measured by Shell in the 1950's and 1960's. Ron Nowak (Maxus Energy

Corporation) provided cuttings, logs, and analyses for the Tikaboo Valley wells. Renee Davis (Helmrich & Payne) provided Total Organic Carbon data from the Mississippian Antler shales in a well in northern Railroad Valley. Anita Harris (USGS) graciously provided conodont dates for Guilmette equivalent rocks in the Reveille Range used in the isopach maps. Duane Harris (Harris-Hebrew Consulting, formerly with Shell Oil Company) provided helpful discussions, measured sections, and regional studies, and introduced me to much of the Great Basin stratigraphy. Dr. John Welch (Consultant, formerly with Shell Oil Company) also provided data and stimulating discussions on Great Basin stratigraphy. Dr. Gerald Waanders (Waanders Palynology) provided assistance and review of the Paleozoic biostratigraphy and Mississippian source rock quality, richness, and maturity and reviewed the dissertation. Dr. Alvin Smith, Professor of English at Saint Paul's College, Virginia, gave assistance on grammar and organization of the manuscript. Dr. Peter Jones (International Tectonic Consultants Ltd.) kindly provided the file to generate the balanced cross section using his *Thrustbelt* program.

I am grateful to the many companies that provided data or financial support. A partial list includes: Amoco, Anadarko, Anschutz, Arco (Vastar), BHP, Blair Petroleum, Chandler and Associates, Chevron, Connelley Exploration, Conoco, Diamond Shamrock, Exxon, Gary-Williams, Grace Petroleum, Hunt, Marathon, Maxus, Mobil, Moncrief, Moore McCormack, Occidental, Pawnee, Phillips, Pioneer, Shell, Sohio, Sinclair, Talisman, Texaco, Tide, Town Exploration, Union of Texas, and Unocal.

Nevada Bureau of Mines and Geology kindly gave me permission to photocopy all their well files up to 1990, and the Nevada Department of Minerals provided well completion reports from 1990 to 1998 and allowed me to photocopy all their well files and lithologic logs up to the present. Copyrighted data from regional measured sections and stratigraphic studies of wells incorporated into regional reservoir rock studies were provided by Cedar Strat Corporation. Also, Cedar Strat Corporation provided the detailed 7.5' geologic maps and aerial photographs used to compile the Timpahute Range 30' X 60' geologic map.

A small amount of the work in the Nevada Test Site area was supported by a grant from the United States Department of Energy administered by the State of Nevada Nuclear Waste Projects office to evaluate the oil and gas potential of the proposed high-level nuclear waste repository at Yucca Mountain. Political pressures caused suspension of much of that grant. Part of this work was supported by NSF Grant EAR-906324 awarded to Colorado School of Mines, John E. Warme, Principal Investigator.

I am grateful to Drs. Lehi Hintze, Morris Peterson, Ken Hamblin, Myron Best and other professors at Brigham Young University who led undergraduate field camps and many field trips to the eastern Great Basin. I am also grateful to have been employed by Exxon Minerals, USA, where I learned to use scintillation equipment to generate gamma-ray data that can be used to suggest depositional environments and correlate well logs. Gulf Oil Company gave me the opportunity to work in the Big Horn Basin, Wyoming, where I first conceived of using scintillation counters to generate gamma-ray logs of outcrops to correlate from surface to subsurface sections. Marathon Oil Company gave me the experience of exploring the eastern edge of the Great Basin in central and western Utah. Placid Oil Company allowed me to develop surface gamma-ray log methods and gave me the resources to learn the Great Basin Paleozoic stratigraphy from experts who had worked for Shell Oil Company and measured Great Basin stratigraphic sections in the 1950's and 1960's.

I give thanks to Drs. J. Lintz, R.A. Schweickert, P.A. Cashman, and J.H. Trexler (University of Nevada, Reno) who encouraged me to attend a school more equipped and oriented to applying sequence stratigraphy to mineral and oil and gas exploration. I give special thanks to those at the Colorado School of Mines who introduced me to the economic applications of sequence stratigraphy that has greatly enriched my eastern Great Basin stratigraphic data base.

Finally, I give thanks to my committee who have patiently given me the encouragement to finish this work and for carefully reviewing the manuscript. Many thanks go to Dr. John Warme who advised this work and spent many days in the field with me and who stimulated observations and interpretations. He worked hard and patiently to pull the geology from my head and get it on the written page. His generous investment of time for me will always be appreciated. Dr. Mark W. Longman (adjunct CSM professor and consultant) not only encouraged me to review current literature that guided my thinking and interpretations but also helped me with the carbonate petrology and carefully reviewed the dissertation. Dr. John B. Curtis (CSM professor and director Potential Gas Agency) encouraged me to relate this work to economic applications. Dr. Thomas L. Davis (CSM professor, Geophysics) encouraged me to relate the study area to the regional setting. Dr. Karl R. Nelson (CSM professor, Engineering) encouraged me to review the basic chemistry of dolomitization. The entire committee inspired me to reach for greater excellence in completing this dissertation.

Special thanks go to my wonderful wife, Yvonne, who willingly moved the Chamberlain family to the base of the greater Timpahute Range for seven years and encouraged me to finish this work. She and the family sacrificed greatly to see me complete this long-term dream.

## DEDICATION

This dissertation is dedicated to my younger brother, Rex J. Chamberlain, who spent hundreds of hours with me hiking and exploring the Oquirrh Mountains, near Cedar Fort, Utah, where we were raised. He later helped me measure hundreds of thousands of feet of Paleozoic strata in the eastern Great Basin. Although his premature death prevents him from reaching his dream of earning a degree in geology, his shadow will always be present in the rocks of the everlasting hills.

This dissertation is also dedicated to my father, Don D. Chamberlain, who took me on many field trips looking for fossils and minerals. He unselfishly shared his love of geology and mountains with me. It was on those excursions into the hills that I learned to love my grandfather, Jim, who had worked in the old Mercur, Utah, gold mines. Jim died shortly before I was born. Those family bonds, coupled with my mother's careful instructions on prayer, gave me faith in the Creator of this wonderful earth. That faith has carried me over many cliffs and obstacles in the mountains and in life to reach for the impossible dream.

# CHAPTER 1

## INTRODUCTION

The Timpahute Range in western Lincoln County, Nevada, provides a unique opportunity to study a 40-mile long, continuous east-west exposure of Paleozoic rocks in this region of the Great Basin where most outcrops are subparallel to the north-south structural grain. Devonian rocks should reveal subtle, gradual changes in facies over long distances across the broad, featureless western North American continental shelf because they were believed to be deposited during a period of relative tectonic quiescence (Osmond, 1962; Niebuhr, 1979). However, abrupt contrasts in facies above a late Devonian impact breccia occur between thrust faults that segment the greater Timpahute Range. These contrasting facies from three thrust sheets of the greater Timpahute Range include: facies 1, a peculiar, anoxic, deepwater, rhythmic, thin-bedded limestone characterized by soft-sediment slump folds and some interbedded turbidites that may represent a crater fill that now is exposed in a fenster on the west end of the range; facies 2, a unique shallow-water quartz sandstone (as much as 1070 net feet thick) deposited on the west side of the impact basin and now is in a klippe in the middle of the range; and facies 3, a shallow-water platform carbonate deposited on the east side of the impact basin and lies on the east side of the range. These features and contrasts were revealed by a new geologic map (**Plate 1a**) of the Timpahute Range 30' X 60' quadrangle or Timpahute Range quadrangle (study area) which provides insight into this part of the Sevier fold-and-fault belt (**Figure 1**).

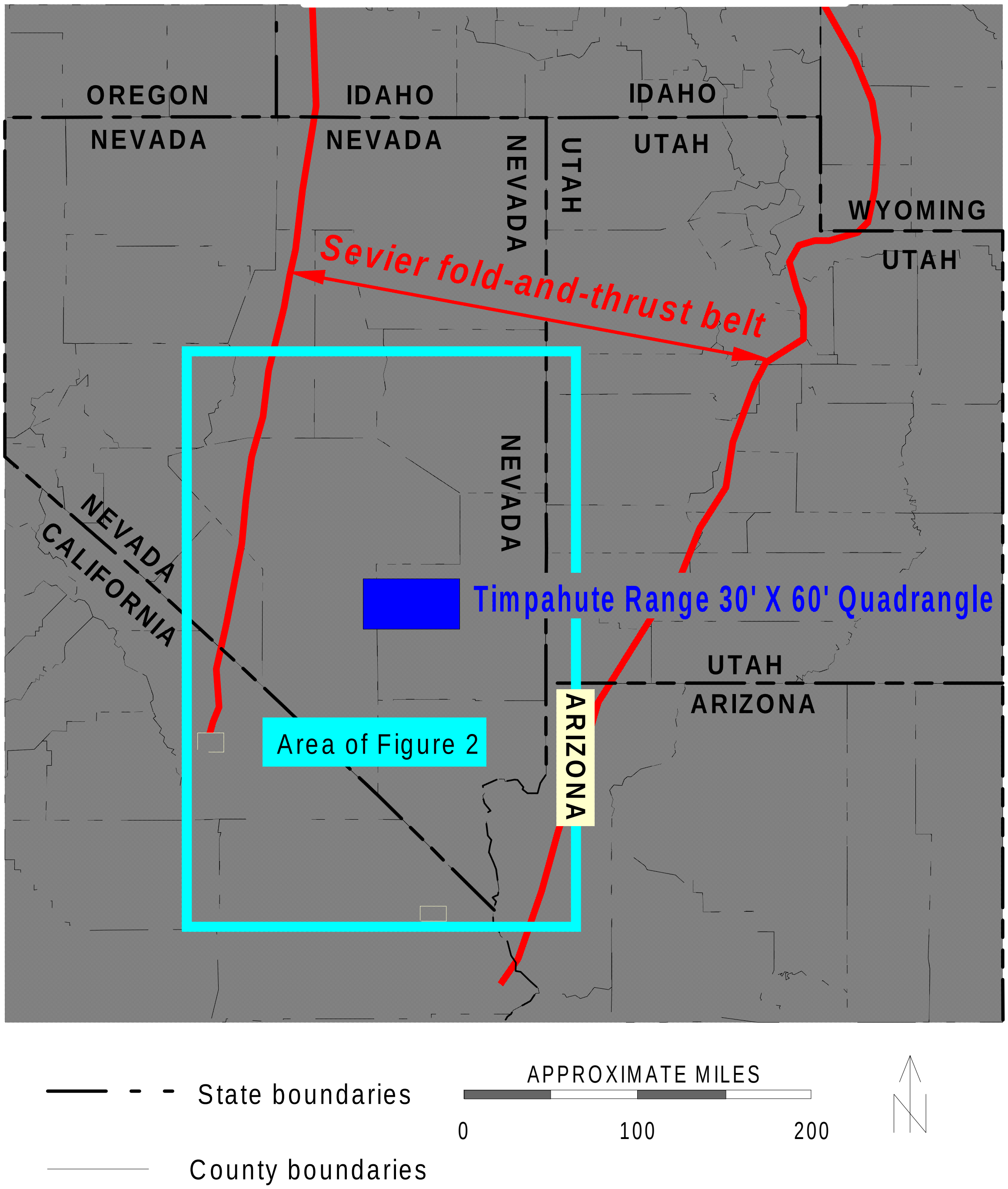


**Figure 1** Index map showing the location of the Timpahute Range 30' X 60' quadrangle within the Sevier fold-and-thrust belt. Some data are from references cited in **Figure 2**.

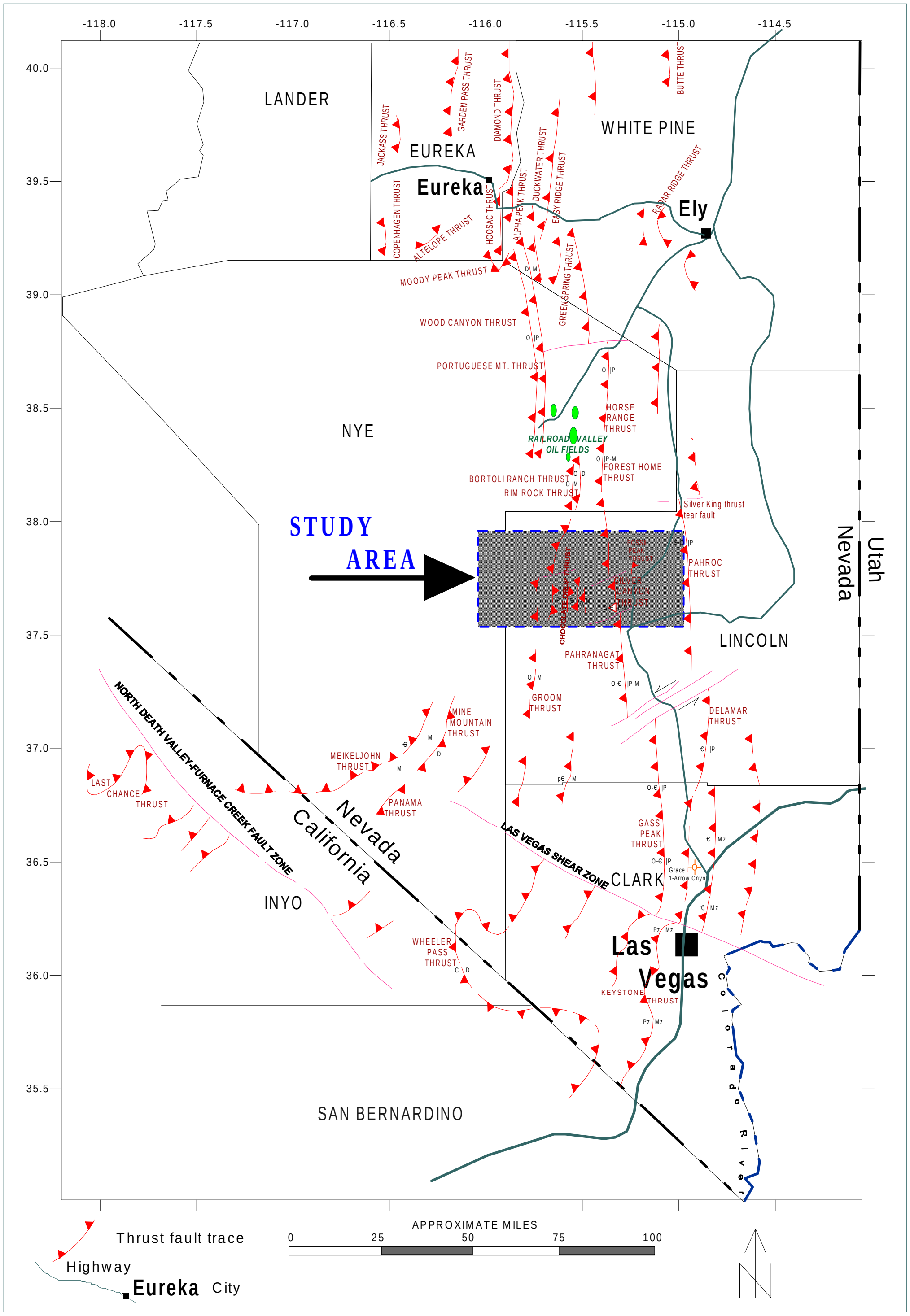


**Figure 2** Sevier age thrust fault traces in eastern Nevada (from Hazzard, 1954; Burchfiel,1961; Tschanz and Pampeyan, 1970; Kleinhampl and Ziony, 1984; Bartley et al., 1988; Cameron and Chamberlain, 1988; Carpenter et al., 1993; and proprietary mapping by the author). See **Figure 1** for index map.

## Author's Background Concerning Timpahute Range Research

I have worked in the Great Basin region for more than 20 years, and much of that time in the Timpahute Range quadrangle. Considerable field and laboratory work was carried out before my specific dissertation research, and discussions and interpretations herein have necessarily evolved over many years, involved many projects, and included interaction with many geoscientists. Every effort has been made to document my sources of data and interpretations. Some data are proprietary and some interpretations are based in part on work completed before the onset of my doctoral program at the Colorado School of Mines.

I was raised near the southern Oquirrh Mountains, 40 miles southwest of Salt Lake City, Utah, and attended Brigham Young University, Provo, Utah, to complete my Bachelor's and Master's degrees in geology. My Masters' thesis, *Biostratigraphy of the Great Blue Formation*, included discovery of fossil-plant-bearing terrestrial valley-fill sequences interbedded with open-marine carbonates in the Mississippian proto-Oquirrh basin, north-central Utah, indicating marine and nonmarine cycles that were previously overlooked. This work continued beyond my Master's research (Chamberlain, 1987; 1990b, 1999).

Employment by Exxon Minerals USA (Michigan, Pennsylvania, and New York, 1976-1978) and Gulf Oil Company (Wyoming, 1978) resulted in pioneering applications of surface gamma-ray logs for the interpretation of depositional environments (Chamberlain, 1983). I worked for Marathon and Placid Oil Companies in the Great Basin of Utah and Nevada from 1979 to 1984 measuring and describing stratigraphic sections, conducting source- and reservoir-rock studies, and exploring for hydrocarbons. During this time I met many consultants who had previously worked for Shell Oil Company in a large research program that involved measuring and describing many stratigraphic sections. They shared first-hand knowledge of Paleozoic stratigraphy, structure, oil source- and reservoir-rocks, and geomorphology of the Great Basin.

In 1984, I founded Cedar Strat Corporation, and managed teams of geologists that remeasured many Shell Oil Company sections and many new ones. We successfully employed the surface gamma-ray log techniques to aid in surface to subsurface correlations. I directed studies on Mississippian source- and reservoir-rocks, on Devonian reservoir rocks, on individual wells and fields, and organized and led annual Great Basin field conferences.

In recent years I undertook detailed mapping projects in several areas, most intensely within the Timpahute Range quadrangle. This mapping was streamlined by incorporating GPS and GIS techniques, reported in Chapter 3. The results are presented in the map of **Plate 1a**.

From 1991 to 1999 my home was in Hiko, Nevada, within the study area. This location eased the logistics for field research, but complicated my access to libraries and research laboratories. As a result, this report is mainly based on new field work, which I believe must be the basis for most new understanding of the complicated geologic history of the Great Basin.

## Purpose and Scope

This study provides the stratigraphic and structural data that constrain the restoration of the Devonian Sunnyside basin and allows a more accurate interpretation of its paleogeography (Chapter 7). The Sunnyside basin, named by Chamberlain and Birge (1997), is an intrashelf Devonian basin between the Antler forebulge (Carpenter et al., 1994) in central Nevada and the Utah hingeline in central Utah. Geologic mapping was limited to the Timpahute Range quadrangle and the study focuses mostly on Devonian sequences. A preliminary balanced cross section, restoration, and a surface geology profile of the east-west transect A-A’ from west of Tempiute Mountain (T4S R56E) to east of the Pahroc Range (T4S R62E) are provided (**Plates 4a** and **4b**). However, a rigorous structural analysis on the quadrangle is beyond the scope of this study.

This study illustrates the utility of applying the principles of “sequence stratigraphy” for geologic mapping of complex areas. Earlier workers using traditional lithologic formations were unsuccessful in accurately mapping the Timpahute Range quadrangle (**Plate 1b**). Twenty-one mappable Devonian sequences identified in Chapter 4 were used to map the structural elements presented in Appendix E, and to reconstruct the Devonian paleogeography in Chapter 7. Mapping the structural features in this complex region without knowledge of the order of sequences is untenable. Several obvious and accessible structural features had been described (e.g., Tschanz and Pampeyan, 1970; Armstrong and Bartley, 1993), but stratigraphic revisions on the new geologic map reveal significant structures--particularly folds, strike-slip faults, and thrust faults (Chamberlain and Chamberlain, 1990). Special attention has been paid in this study to the possible tectonic outcome of the Late Mesozoic Sevier orogeny on Paleozoic rocks in the Timpahute Range quadrangle, 100 miles west of the leading edge of the Sevier fold-and-thrust belt. Juxtaposition of different thrust sheets containing contrasting facies of Upper Devonian rocks in the Timpahute Range resulted from the Sevier compressional event. The overall goal of this research is to resolve these abrupt facies changes.

The specific goals of this research are threefold: 1) identify mappable sequences and interpret the Devonian strata using sequence stratigraphic concepts; 2) apply the mappable sequences to update the geology of the greater Timpahute Range on a map that shows the stratigraphy, folds, strike-slip faults, and thrust faults overlooked in previous mapping; and 3) reconstruct the Devonian paleogeography by evaluating the magnitude of deformation of this part of the Sevier fold-and-thrust belt using the new geologic map and correlations of Devonian sequences.

Realization of these goals is illustrated with plates 1 through 7. **Plate 1a** is a new geologic map discussed in Chapter 5 and Appendix E. A profile of surface geology along transect A-A' along the bottom of the map provides some constraints used to construct **Plate 4a**. In comparing it with **Plate 1b**, a geologic map of the Timpahute Range quadrangle modified after Tschanz and Pampeyan (1970) with a similar scale and color scheme, significant revisions of the old mapping are readily apparent. **Plate 2a** is a stratigraphic section illustrating the cycles and sequences of the Devonian rocks at Mail Summit discussed in Chapter 4. **Plates 2b** and **2c** provide detail about Devonian reef and reef flank facies at Mail Summit. **Plate 3** is an isopach map of the Devonian system which shows the shape of the Sunnyside basin described and named by Chamberlain and Birge (1997). **Plate 4a** is a balanced retrodeformable cross section along the line of section labeled A-A' in the greater Timpahute Range on **Plate 1a**. Although normal faults occur on the line of section, they were too small to illustrate in the cross section. **Plate 4b** is the restored or undeformed section. This new structural model of the greater Timpahute Range resolves the abrupt facies changes in Upper Devonian sequences between thrust sheets and provides a more comprehensive guide to the structural style of the region. The model gives insight into structures concealed by Tertiary volcanics and valley fill in other parts of the Sevier fold-and-thrust belt. Restoration of stratigraphic sections to their original positions using the structural model is essential for correct interpretations of the Devonian paleogeography (Chapter 7).

**Plate 5** is a diagrammatic facies belt chart after Wilson (1975) applied to the eastern edge of the Tempiute sub-basin. The Tempiute sub-basin is a basin at the south end of the Sunnyside basin created by a cosmolite impact (see Chapter 7). A cosmolite as used herein is an extraterrestrial body such as a meteorite or comet but of an uncertain composition. The facies belt chart lists microfacies characteristics and examples at Timpahute Mail Summit (TMS). **Plate 5** illustrates the correlation between microfacies in photomicrographs in Appendix C and the table of criteria to make facies assignments presented in Chapter 3. The microfacies helped refine facies assignments. Facies patterns and gamma-ray logs helped separate regional sequence boundaries from local cycle boundaries. Twenty-one regionally mappable sequences were identified (Chamberlain and Warme, 1996). These regional correlatable sequences were used to make isopach maps and to make the new geologic map of the Timpahute Range quadrangle. **Plate 6** is a geologic map showing the distribution of Devonian sequences at the measured section in the southwest corner of the Mail Summit 7.5' quadrangle (TMS herein). **Plate 7** is a distribution map of Pilot outcrops within the Timpahute Range 30' X 60' quadrangle. A detailed biostratigraphic analysis of the sequences is beyond the scope of this study. Gamma-ray log patterns of sequences usually provide greater resolution for regional correlations than do conodont zones. Therefore, conodont and other fossil zones tied to surface gamma-ray logs would greatly enhance regional correlations.

## Format

This report consists of nine chapters. Chapter 1 introduces the study area by presenting the format and purpose and scope of the study and describing the location and geologic setting of the study area. Chapter 2 provides a brief review of previous work in the study area. Chapter 3 introduces the methods used in the research. Chapter 4 consummated the first main research objective, which was to identify and interpret the mappable Devonian sequences in the study area. A well-exposed 5000-foot-thick composite stratigraphic section on the Mail Summit 7.5' quadrangle provided a useful reference section for Devonian depositional cycles and sequences across the eastern Great Basin and is called TMS (Timpahute Mail Summit measured section) in this report (**Figure 3**). Dolomite and dolomites, important components of the sequences, are discussed in Chapter 4. Recognition of the sequences was important in achieving research objective two, which was to make a geologic map of the Timpahute Range quadrangle. Defined sequences were used to make the geologic map and identify thrust sheets presented in Chapter 5 and structural elements described in Appendix E. The map and correlation of the sequences at TMS to sections exposed in different thrust sheets in the greater Timpahute Range support the stratigraphic significance of structural interpretations in Chapter 6.

The sequences defined at TMS were correlated with other surface and subsurface sections of the region. These correlations provided the basis for sandstone isolith maps and the total Devonian isopach map presented in Chapter 7. Sequences at TMS provide clues to Devonian tectonic events in the region. For example, the “Oxyoke Formation” at TMS may be a record of the first siliciclastic pulse of the Devonian-Mississippian Antler


**Figure 3** Index map showing the position of the Mail Summit 7.5' quadrangle (shaded gray) among the other 7.5-minute quadrangles (black lines) comprising the Timpahute Range 30' X 60' quadrangle. Surveyed townships and ranges are in blue and sections are in yellow. Several township and range values are indicated along two map edges. Digital land grid is from Premier Data Services, Denver (1997). Digital topographic index map was provided by Homestake Gold Company, Reno (1997). Degrees north latitude and west longitude are indicated on several map corners. See Chapter 3 for methods of constructing this and other maps from digital data bases.

orogeny. This and other tectonic events and features that affected the Devonian paleogeography are also presented in Chapter 7. The economic and academic applications of the stratigraphic sequences, the new geologic map and structural model, and the new paleogeographic interpretations of the Great Basin Devonian are discussed in Chapter 8. Conclusions and recommendations for further study comprise Chapter 9.

Appendices explaining abbreviations used in the text or sets of photographs and data too lengthy to be incorporated in the body of the text are provided for completeness. Appendix A provides an explanation for symbols and abbreviations used in maps, correlation charts and stratigraphic sections. Appendix B provides a detailed description of each cycle of TMS organized from the oldest sequence to the youngest. Appendix C provides descriptions of thin sections taken mostly from the lower Guilmette cycles. **Plates 8** through **14** contains selected photomicrographs of the thin sections. Appendix D is a CD-Rom originally presented as a poster session (Chamberlain et al., 1996; Chamberlain, 1998) and later published by SEPM (Hook et al., 1998). It is a digital presentation of a field trip in the Central Nevada Thrust Belt, and it contains annotated, animated, captioned, and plain digital images that compliment the text. Appendix E presents detailed descriptions of structural elements of the Timpahute Range 30' x 60' quadrangle geologic map. Appendix F is a table from a spreadsheet of control points of sections with the complete Devonian represented and used to label **Plate 3**.

## Location of the greater Timpahute Range

The Timpahute Range 30' X 60' topographic quadrangle is covered in the 1:100,000-scale metric topographic map series by the United States Geological Survey published in 1988. It lies within western Lincoln County in southeastern Nevada, centered approximately 100 miles north of Las Vegas, from 37° 30' to 38° N latitude and 115° to 116° W longitude. This quadrangle is within the Sevier fold-and-thrust belt

(**Figure 1**). The Timpahute Range is in the southwest part of the Sunnyside basin (Chamberlain and Birge, 1997; **Plate 3**). It lies south of prolific oil wells in Railroad Valley that produce mainly from Devonian carbonates. It is northeast of the Nellis Air Force Bombing Range where access to rock outcrops is restricted by the United States Department of Defense.

The greater Timpahute Range provides an unique 40-mile-wide east-west band of nearly continuous Paleozoic outcrops (see **Plate 1**) in a region where usually only crestal exposures in north-south trending ranges are exposed between broad areas of Tertiary cover. It includes Tempiute Mountain, Monte Mountain, Mount Irish, Mail Summit, Fossil Peak, Hiko Range, and the southern end of the North Pahroc Range (**Figure 5**). Other ranges within the Timpahute Range quadrangle with significant outcrops of Paleozoic rocks include the Worthington, Golden Gate, Seaman, and Pahranagat ranges. Extensive outcrops in the Timpahute Range quadrangle are especially favorable for study of Devonian strata in both north-south and east-west directions.

TMS (Timpahute Mail Summit measured section) is a composite measured section composed of three segments that mostly lie in the southern part of the Mail Summit 7.5' quadrangle (**Figure 4**, **Plate 6**). The lower parts of two of the segments lie in the northern part of the Mount Irish SE 7.5' quadrangle. However, because most of the section lies in the Mail Summit quadrangle, it is called TMS herein.

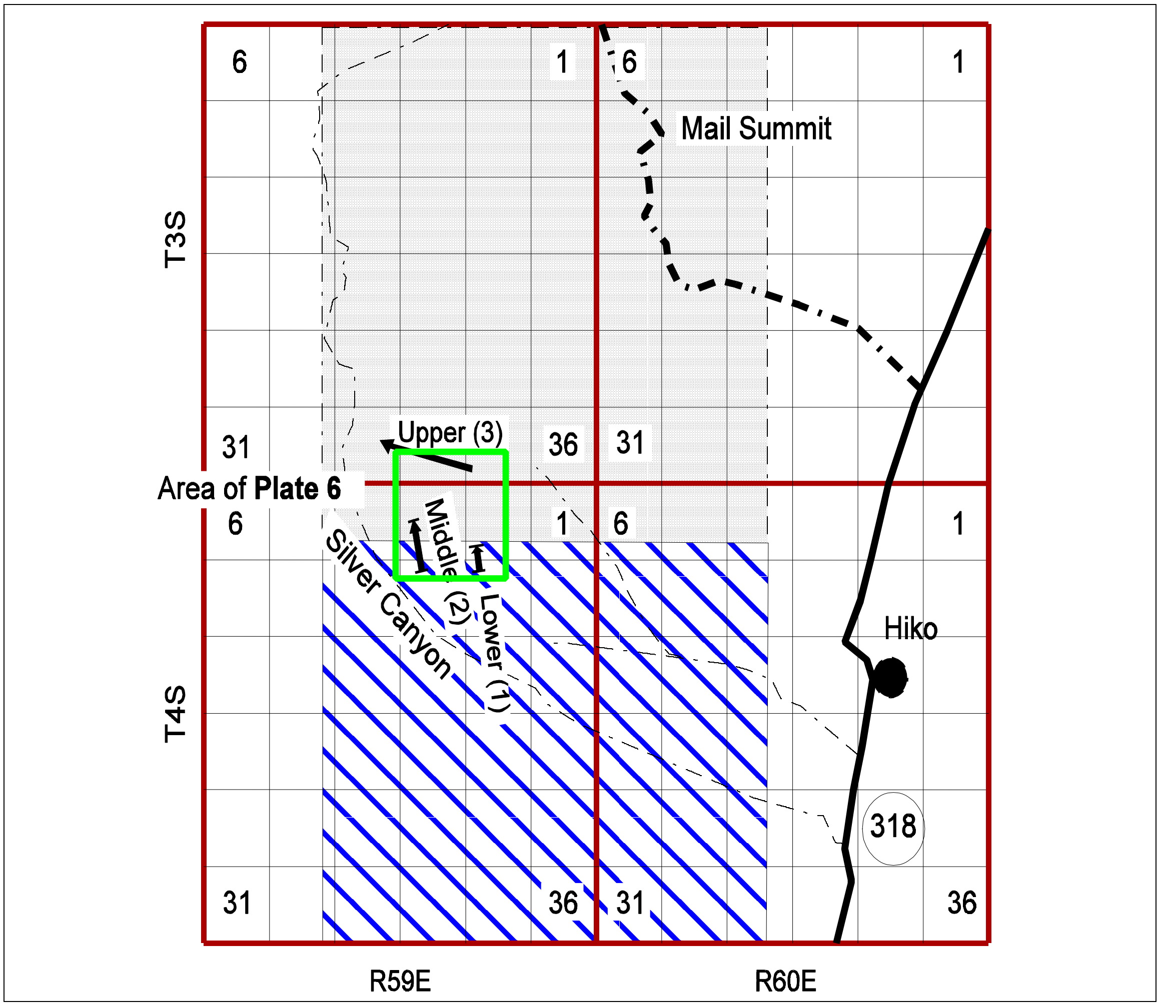


**Figure 4** Index map to the Mail Summit measured section (TMS) in the southwest part of the Mail Summit 7.5' quadrangle (stippled) and northern Mount Irish Se 7.5' quadrangle (hachured). The solid black line is Nevada State highway 318, the heavy broken line is the Mail Summit county road, and the light broken lines are jeep trails. The lower, middle and upper segments of TMS composite measured section are indicated by arrows that point up-section. The green box shows the area covered by **Plate 6,** a geologic map of the sequences mapped at TMS and an example of the detail used to compile the geologic map of the Timpahute 30' X 60' quadrangle.

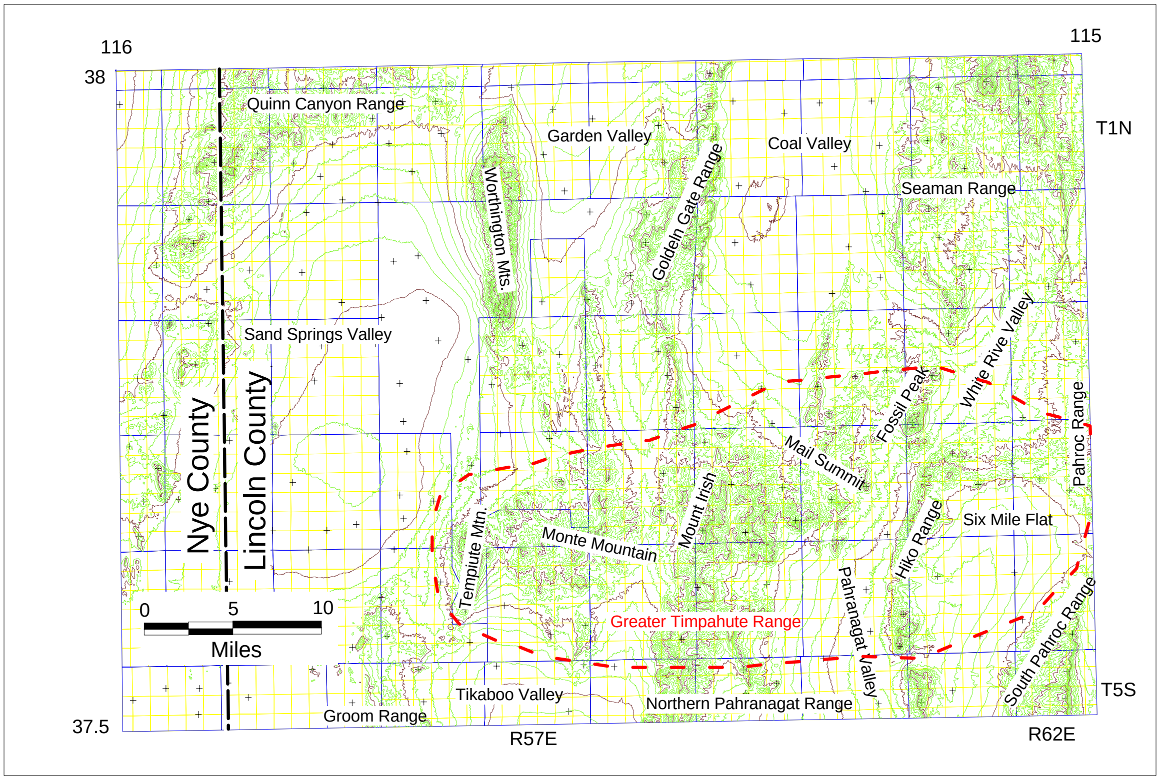


**Figure 5** Topographic elements of the greater Timpahute Range (outlined in red dashed line) including Tempiute Mountain, Monte Mountain, Mount Irish, Mail Summit, Fossil Peak, Hiko Range, and the North Pahroc Range in the Timpahute Range quadrangle. Digital topography was downloaded from the United States Geological Survey web site. The small black crosses are elevation bench marks.

## Geologic Setting of the greater Timpahute Range

The Timpahute Range lies in the Great Basin portion of the Basin and Range Physiographic Province. Deposition in the region was nearly continuous from Precambrian to Lower Triassic (Stewart, 1980). In this section, the tectonic setting that affected the Paleozoic rocks and their stratigraphic setting is discussed.

Tectonic Setting

North-south Precambrian rifting (Stewart and Poole, 1974) and east-west compression by the Mississippian Antler orogeny (Roberts, 1972) caused the north-south structural grain of the region that controlled or influenced all subsequent tectonic and depositional events. After the rifting and before the Antler orogeny, rocks in western North American were deposited on a passive margin. **Figure 6** is a diagrammatic cross section of the pre-Antler passive margin. A correlation chart and nomenclature of some units exposed in the study area will be presented later in this Chapter. Previous work that resulted in the evolution of **Figure 6** will be discussed in Chapter 2.

The greater Timpahute Range is perpendicular to the general north-south structural and physiographical grain of the Great Basin. It lies within the north trending Mesozoic Sevier fold-and-thrust belt that is responsible for much of the present-day regional structural grain and topography (**Figure 2**). Previous geologic mapping depicted the ranges in the study area as horsts and the valleys as grabens (Tschanz and Pampeyan, 1970). As a result, a fault-block model by Duey (1979) and Foster et al. (1979) has been used for oil exploration in the region. The fault-block model continues to be used in oil and gas exploration in Nevada (Bortz, 1998). However, the new geologic map shows that structures produced by east-west crustal shortening in the study area are also reflected by the topography (**Plates 1a, 4a**, Appendix E). Six thrust faults and their associated folds are exposed by Tertiary erosion in the greater Timpahute Range (**Plate 1a**). A seventh thrust fault, the Pahroc thrust fault, is exposed in the southern Delamar Range, 35 miles south-southeast of Hiko and beyond the area of **Plate 1**. It is interpreted to underlie much of the study area (**Plate 4a**). The ranges in the study area are generally anticlines and the valleys are synclines. Apparently they were not affected by an overprint of Cenozoic extension. Therefore, a lack of major normal faults with thousands of feet of displacement suggests that Cenozoic extension was minor in the Timpahute Range quadrangle. Major north-south normal faults are reported in other areas in the Basin and Range Province (Effimoff and Pinezich, 1986).

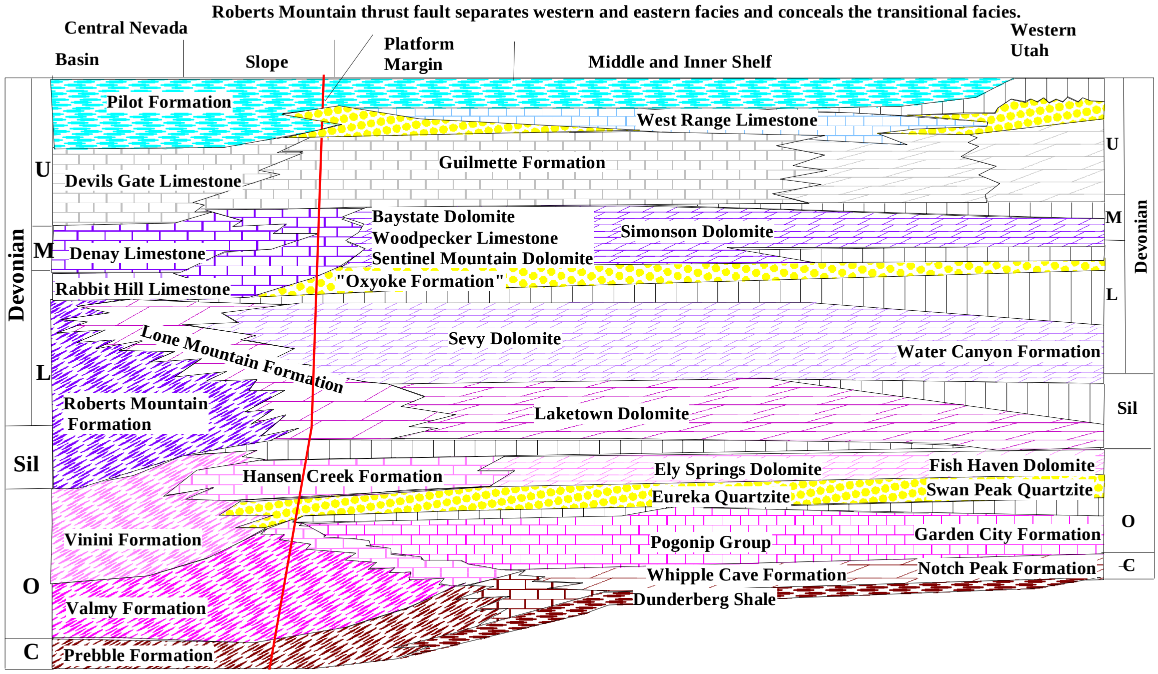


**Figure 6** Pre-Antler orogeny tectonic setting and depositional profile from western Utah to central Nevada showing formational terminology from the Upper Cambrian through the Devonian. Modified after Cook and Taylor (1985) and Langenheim and Larson (1973). No attempt was made to include the effects of the Antler forebulge. The slope/margin area is diagrammatic as it lies in the same area as the Roberts Mountain thrust fault (red line) where the transition facies are concealed. Siliciclastic intervals are in yellow.

Lake beds or synorogenic sediments associated with the Sevier Orogeny represent the only possible Mesozoic strata preserved in the Timpahute Range quadrangle. Many compressional structures are masked by Tertiary volcanic deposits that filled paleovalleys and canyons with ash falls and flows. Paleotopographic high areas (anticlines) received little volcanic cover. A few north-south trending normal faults that could have had hundreds of feet of displacement likely formed during Cenozoic extension (**Plate 1a**). Two large displacement faults, the north Worthington and Hiko Narrows faults, could be normal faults associated with extension but are likely deeper thrust faults.

An extensive cover of Tertiary volcanic rocks and thick Tertiary valley fill conceal most of the structures in the region. Headward erosion by tributaries to the Colorado River has exhumed some Sevier-age structural elements from the greater Timpahute Range southward. Most of the compressional features remain buried below Tertiary strata north of the greater Timpahute Range. **Figure 7** summarizes the tectonic events of the Great Basin from the Late Mesozoic Sevier orogeny to the present.

Generally, lower Paleozoic strata thicken from east to west (many studies, and Cedar Strat proprietary measured sections, 1984-1989). West of the study area, deposition on the passive margin was interrupted by the Devonian-Mississippian Antler orogeny (Roberts, 1972). Carpenter (1997) suggested that the orogeny was initiated during Yellow Slope Sequence time in the Frasnian Stage of the Late Devonian (**Plate 2a**, Chapter 4). Carpenter et al. (1994) interpreted an Antler forebulge uplift, a positive area in central Nevada within and west of the Shoshone and Toiyabe ranges, 80 miles northwest of the study area. A forebulge is an upwarp or flexure of the lithosphere caused by tectonic loading (e.g., Roberts Mountain allochthon) that occurs in front of a thrust front. The upwarping or forebulge develops because of isostatic response to crustal loading and flexural downwarping and is predicted by flexural modeling (Giles, 1996). A backbulge basin (e.g., Sunnyside basin) occurs between the forebulge and the stable craton. It is a broader and shallower downwarp or backbulge basin than the downwarping of the foreland basin (Giles, 1996). The bulge coincides with the western side of the Sunnyside basin described in Chapter 7. The forebulge is defined by the increasing age eastward of subcropping miogeoclinal Cambrian and younger rocks beneath the Roberts Mountain thrust. When the Roberts Mountain allochthon overrode it in the Late Devonian, the Lower and Middle Devonian forebulge was an eroded paleohigh (Carpenter et al., 1994). Fossils, such as conodonts, and quartz sand that are insoluble in weak acids from early Paleozoic rocks were shed eastward into the Sunnyside basin and are the source of Devonian sandstones on the western edge. Paleozoic rocks within the

Sunnyside basin were subsequently deformed during the Mesozoic Sevier orogeny (Chapters 2 and 6).

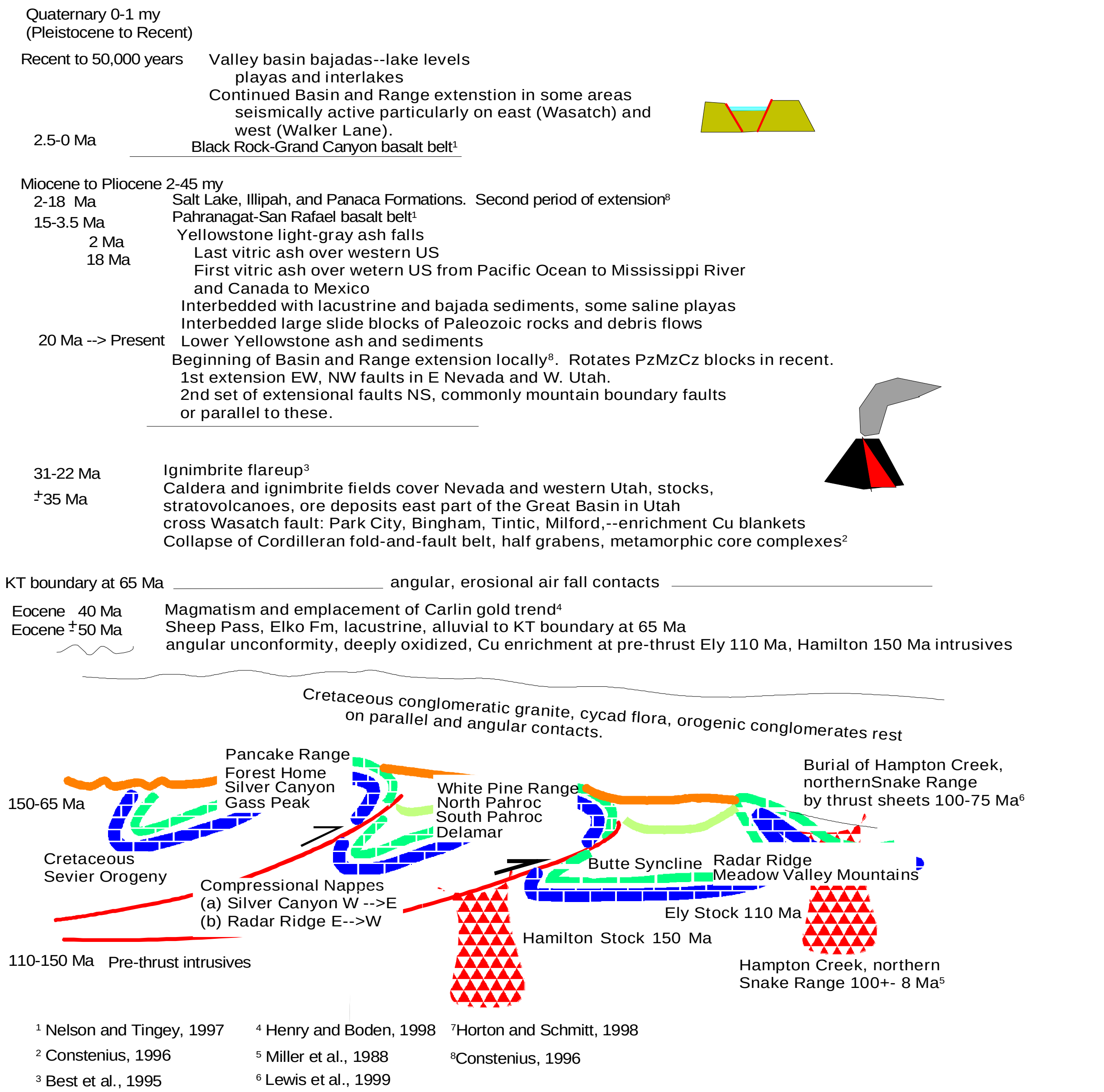


**Figure 7** Tectonic events at and since the Sevier orogeny in the eastern Great Basin. Data are from proprietary mapping, Cedar Strat data files, J. Welch (1998, personal communication), and other references that are indicated by the superscript numbers. Lists of locations are examples of fold and thrust features. Dark blue represents older Paleozoic rocks. Green represents younger Paleozoic rocks. Pale green represents the base of Tertiary valley fill. Orange represents present-day surface. Patterned red represents pre-thrust intrusives.

<u>Stratigraphic Setting</u>

Devonian rocks form a significant part of the 15,000 to 20,000 feet of Paleozoic rocks exposed in ranges of the area (**Table 1**). These are summarized in **Figure 8**, a correlation chart that compares Devonian rocks exposed at TMS with the Paleozoic units exposed in the Pahranagat Range 15 miles south of the study area (Stop #6, Appendix D) and those exposed in the Egan Range 65 miles north of the study area (Stop #13, Appendix D).

**Table 1** lists the formations illustrated in **Figure 8** and compares the nomenclature used herein with that of other workers in the region. Some of these units were grouped for the new geologic map. For example, Cambrian units, including Lower Cambrian Prospect Mountain Quartzite, Middle Cambrian Chisholm Shale, Middle and Upper Cambrian Highland Peak Formation, and Upper Cambrian undifferentiated limestone and dolomite, and Dunderberg Shale, are grouped together on the geologic map in the restricted area of the Groom Range (**Plates 1a** and **1b**). Only the Upper Cambrian rocks are exposed in the greater Timpahute Range. Access to extensive outcrops of Lower and Middle Cambrian rocks exposed in the Groom Range, eight miles southwest of Tempiute Mountain, is restricted by the United States Department of Defense.

On the geologic map, the Mississippian Chainman Shale facies and the interfingering Scotty Wash Sandstone facies are grouped together as Mississippian Antler clastics (Mac). This was done to avoid confusion where Scotty Wash facies are below or interbedded with the Chainman Shale facies as in the Egan Range (**Figure 8**). In its type locality in the northern Bristol Range, 20 miles east-northeast of the study area, the Scotty Wash Sandstone overlies the Chainman Shale.

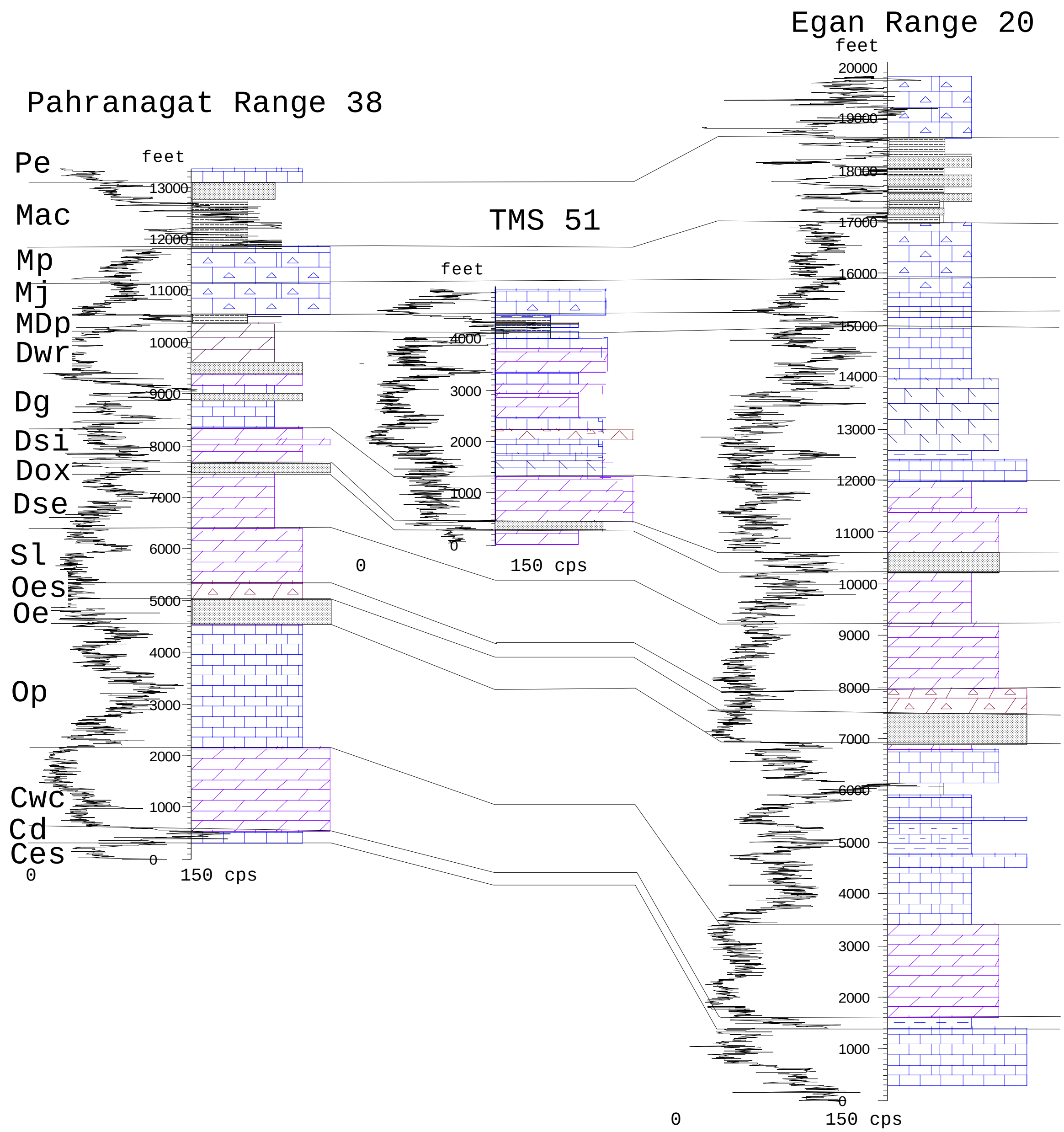


**Figure 8** Correlation diagram comparing the Devonian stratigraphy at TMS with the Paleozoic stratigraphy in the Egan and Pahranagat ranges. Numbers at the top of the stratigraphic columns are the section numbers listed in **Table 2** and **Figure 9**. See **Table 1** for abbreviations of the Paleozoic units. Gamma radiation varies from near 0 to over 150 counts per second. Placement of the gamma-ray scale varies between sections because the gamma-ray curve was placed to optimize amount of detail that is presented in the correlation diagram.

**Table 1** Paleozoic nomenclature in southeastern Nevada with abbreviations used in **Figure 8**. Numbers in the column headers correspond to section numbers on **Figure 9** and **Table 2**. Rocks above the Ely Limestone were omitted from the table and figure.

| Abbr. | Age | This paper TMS 51 | Kellogg (1963) Egan Range 20 | Reso (1963) Pahranagat Range 38 |
|---|---|---|---|---|
| Dwr | Devonian | West Range Limestone | Lower and Middle West Range Formation | West Range Limestone |
| Dg | | Guilmette Formation | Guilmette Formation | Guilmette Formation |
| Dsi | | Simonson Dolomite | Simonson Dolomite | Simonson Dolomite |
| Dox | | "Oxyoke Formation" (regionally mappable sandy, silty, and argillaceous dolomite) | sandstone lens (0-25 feet thick) near top of Sevy Dolomite | Basal Simonson Dolomite sandstone and upper Sevy Dolomite calcareous siltstone and chert |
| Dse | | Sevy Dolomite | Sevy Dolomite | Sevy Dolomite |
| Sl | Silurian | Laketown Dolomite | Laketown Dolomite | Laketown Dolomite |
| Oes | Ordovician | Ely Springs Dolomite | Fish Haven Dolomite | Ely Springs Dolomite |
| Oe | | Eureka Quartzite | Eureka Quartzite | Eureka Quartzite |
| Op | | Pogonip Group | Pogonip Group | Pogonip Group |
| Cwc | Cambrian | Whipple Cave Formation | Whipple Cave Formation | Desert Valley Formation |
| Cd | | Dunderberg Formation | Dunderberg Formation | Dunderberg Shale |
| Ces | | Emigrant Springs Formation | Emigrant Springs Formation | Highland Peak Formation |

**Table 1** (Continued) Paleozoic nomenclature in southeastern Nevada with abbreviations used in **Figure 8**. Numbers in the column headers correspond to section numbers on **Figure 9** and **Table 2**. Rocks above the Ely Limestone were omitted from the table and figure.

| Abbr. | Age | This Paper TMS 51 | | Kellogg (1963) Egan Range 20 | Reso (1963) Pahranagat Range 38 |
|---|---|---|---|---|---|
| Pe | Pennsylvanian | Ely Limestone | | Ely Limestone | Bird Spring Formation |
| Mac | Mississippian | Scotty Wash Sandstone facies | Antler clastics | Scotty Wash Sandstone | White Pine Group. Langenheim and Larson (1973) included Scotty Wash in upper part |
| | | Chainman Shale facies | | Chainman Shale | |
| Mp | | “Penoyer Limestone” | | Joana Limestone | Joana Limestone |
| Mj | | Joana Limestone | | | |
| MDp | Mississippian/ Devonian | Pilot Formation | | Upper West Range Formation | Pilot Formation |

Although it was not mapped separately on the final geologic map of the Timpahute Range quadrangle, the “Penoyer Limestone” was mapped separately on most of the field work maps (construction of field work maps is explained in Chapter 3). The slope-forming “Penoyer Limestone” is a mappable unit that lies above the cliff-forming Lower Mississippian Joana Limestone and is a useful field term. The “Penoyer Limestone” is composed of rhythmically bedded crinoid wackestones and mudstones that contain the trace fossil *Zoophycos*. It contrasts with the crinoidal grainstones and packstones of the underlying Joana Limestone and is more radioactive (**Figure 8**).

Surface gamma-ray logs, as shown in **Figure 8**, are valuable for regional correlations in frontier areas such as Nevada where few wells have penetrated the entire Paleozoic section. Note the similarity of the gamma-ray pattern for different units between the regional sections. Annotated unit thicknesses on the structural profile in the lower part of **Plate 1a**, constrain the structural cross section in **Plate 4a**.

Note in **Figure 8** how the Devonian rocks thicken northward toward the depocenter of the Sunnyside basin. Within the basin the sections are thicker and are mostly composed of coral and tabular stromatoporoid-bearing carbonates. They lack abundant *Amphipora*, a restricted platform and usually shallow-water fossil. In contrast, *Amphipora*-bearing carbonates and shallowing-upward cycles that imply shallow-water deposition in restricted marine conditions mostly occur in sections on the edges of the Sunnyside basin (**Plate 3**). Shoreward of the *Amphipora*-bearing carbonates are quartz sandstones. These changes in facies and a detailed discussion of the stratigraphic sequences and cycles in the Devonian rocks at TMS are presented in Chapter 4 and their paleogeographic significance is presented in Chapter 7.

The Devonian portion of the southwest Timpahute Range Mail Summit measured section, or TMS, is nearly 5000 feet thick. It lies in the footwall of the Silver Canyon thrust fault. The Silver Canyon thrust fault is near the middle of the greater Timpahute Range and in the northwest quadrant of the southeast quadrant of the Timpahute Range quadrangle (**Plate 1a**). TMS is a composite section consisting of three segments (**Figure 4**). Five formations comprise the Devonian at TMS. They are, in ascending order: the Lower Devonian Sevy Dolomite, Middle Devonian Simonson Dolomite, Late Devonian Guilmette Formation, very Late Devonian West Range Limestone, and Devonian-Mississippian Pilot Formation. Previous work on these formations and their previously mapped outcrop distributions are presented in Chapter 2 and **Plate 1b**. The newly mapped outcrop distribution of these formations and their sequences are presented in more detail in Chapter 4 and **Plate 1a**.

Devonian sequences of the TMS reference section were correlated to other sections in the region. **Figure 9** shows adjacent (inset) and regional surface and subsurface sections to which Devonian sequences in the TMS reference section were originally correlated (**Table 2**). Each measured section was measured at the same scale and detail as TMS but they are too voluminous to be included in this work. However, sequence thicknesses and other data from these sections were used to construct regional isopach maps herein.

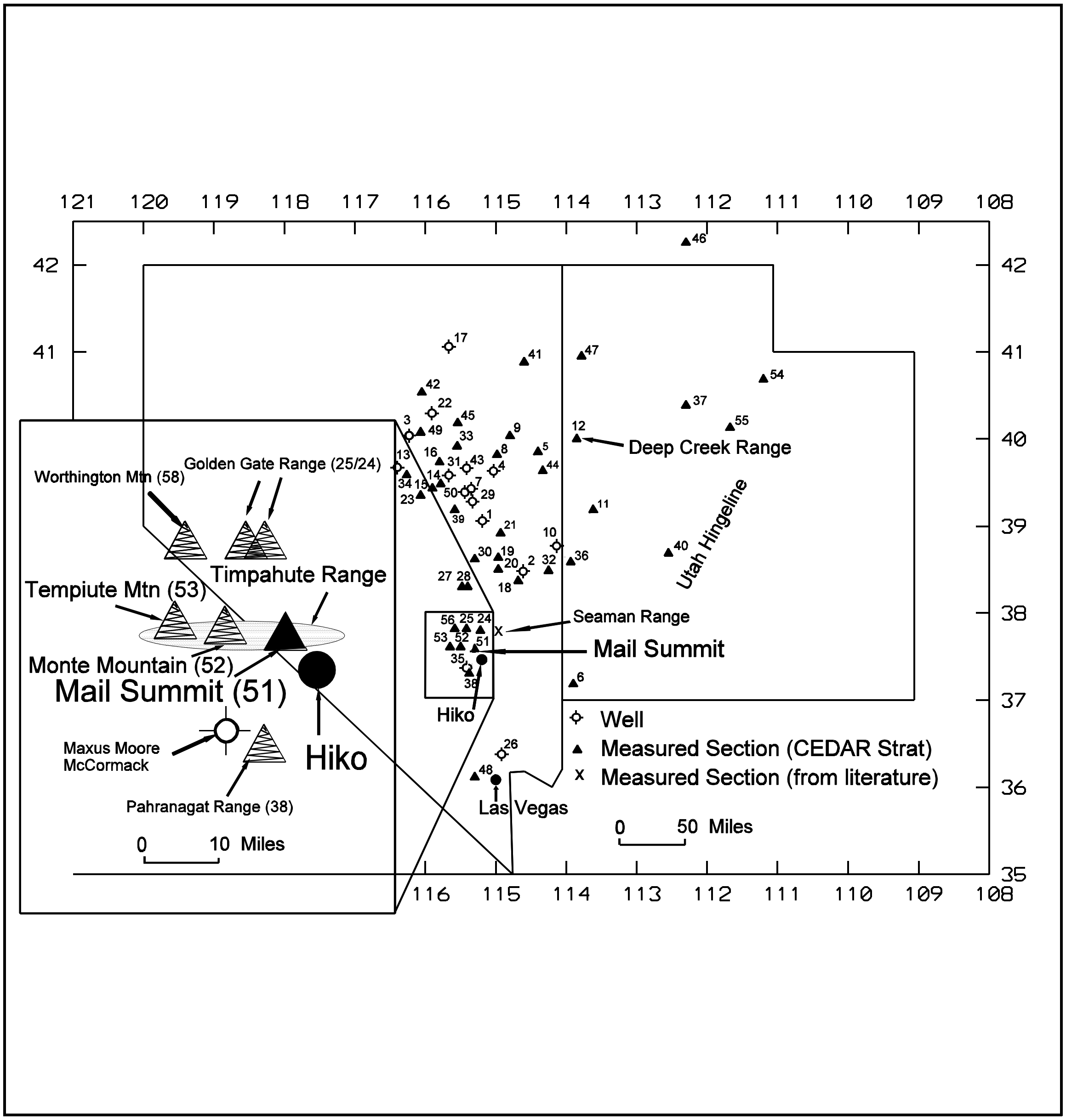


**Figure 9** Index map showing parts of Nevada and Utah with location of southwest Mail Summit composite stratigraphic section, in the greater Timpahute Range near Hiko, Nevada, and other sections to which the TMS was correlated and used to make **Plate 3.** Degrees latitude and longitude are indicated on the edges. The scale in miles is approximate. The number and name of the sections are listed in **Table 2**.

**Table 2** Wells and Measured Sections shown in **Figure 9**.

| # Well or Measured Section | # Well or Measured Section |
|---|---|
| 1. American Hunter Exploration, Blackjack Spring | 29. GW, Moorman Ranch |
| 2. Amoco, Dutch John | 30. Horse Range |
| 3. Amoco, East Henderson | 31. Keith Walker, Fed |
| 4. Anadarko, Combs Peak | 32. Limestone Hills |
| 5. Antelope Range | 33. Little Bald Mountain |
| 6. Beaver Dam Mountains, Horse Canyon | 34. Lone Mountain |
| 7. Blair, White Pine | 35. Maxus Expl., Moore McCormack 6-1 |
| 8. Cherry Creek Range, Egan Basin | 36. North Needles Range |
| 9. Cherry Creek Range, Goshute Canyon | 37. Oquirrh Mountains |
| 10. Commodore Resources, Outlaw Fed | 38. Pahranagat Range, Cutler Reservoir |
| 11. Confusion Range, Little Mile & ½ | 39. Pancake Range, Green Spring |
| 12. Deep Creek Range | 40. Pavant Range, Dog Valley Peak |
| 13. Depco, Willow Wash | 41. Pequop Range, Independence Valley |
| 14. Diamond Range, Newark Mountain | 42. Pinion Range, Pine Mountain Klippe |
| 15. Diamond Range, Oxyoke Canyon | 43. Ram, Long Jevity-1 |
| 16. Diamond Range, Rattlesnake Ridge | 44. Red Hills. |
| 17. Diamond Shamrock, Kimbark | 45. Ruby Range, Pearl Peak |
| 18. Dutch John Mountain | 46. Samaria Mountain, Idaho |
| 19. Egan Range, Ninemile | 47. Silver Island Mountain, Graham Peak |
| 20. Egan Range, Shingle Pass | 48. Spring Mountain, Lovell Canyon |
| 21. Egan Range, Water Canyon | 49. Sulphur Springs, Telegraph Canyon |
| 22. Exxon, Aspen Unit | 50. Tenneco Oil Co, Illipah-1 |
| 23. Fish Creek Range, Bellevue Peak | 51. Timpahute Range, Mail Summit |
| 24. Golden Gate Range, Lower Plate | 52. Timpahute Range, Monte Mountain |
| 25. Golden Gate Range, Upper Plate | 53. Timpahute Range, Tempiute Mountain |
| 26. Grace Pet., Arrow Canyon-1 | 54. Uinta Mountains, Hoyt Peak |
| 27. Grant Range, Forest Home Lower Plate | 55. Wasatch Range, Rock Canyon |
| 28. Grant Range, Forest Home Upper Plate | 56. Worthington Mountain |

Regional sequence correlations were used to refine the TMS sequences (Chamberlain and Warme, 1996). Once the sequences were refined, they were used with additional sections (Appendix F) to construct **Plate 3**, a total Devonian isopach map of the eastern Great Basin. Dry-hole symbols on **Figure 9** show wells that penetrated a significant part of the Devonian section. Triangles depict the location of measured sections containing Devonian rocks. The Devonian rocks generally thicken from approximately 500 feet east of the Utah hingeline to more than 6600 feet west of the hingeline. The Utah hingeline is a zone at the leading edge of the Sevier fold-and-thrust belt extending from southwestern Wyoming to southwest Utah where Paleozoic units are thick (1000's feet) to the west and thin (100's feet) to the east. Also shown in **Figure 9** is the location of the Seaman Range section (X) measured by Hurtubise (1989). Numbers on the map borders are degrees latitude and longitude. Nolan's (1935) type sections for the Devonian Sevy, Simonson Dolomite and Guilmette formations are in the Deep Creek Range, western Utah (**Table 2**, Number 12).

Most of the Devonian sections in the Sunnyside basin are similar to the TMS reference section. The Upper Devonian Guilmette Formation is composed of many shallowing upward cycles. However, the facies of the Upper Devonian sequences at TMS contrast sharply with the Upper Devonian sequence facies in other thrust sheets of the Timpahute Range. Examples include: 1) at Mail Summit (Number 51 on **Figure 9** and **Table 2**), reef-bearing carbonate rocks occur in the footwall of the Silver Canyon thrust; 2) at Monte Mountain (Number 52 on **Figure 9** and **Table 2**), thick quartz arenites dominate the hanging wall of the Silver Canyon thrust; 3) at Tempiute Mountain (Number 53 on **Figure 9** and **Table 2**), thin-bedded limestones comprise the hanging wall of the Tempiute Mountain thrust and footwall of the Chocolate Drop thrust (Chamberlain and Gillespie, 1993). Correlation charts showing these contrasts are presented in Chapters 4 and 8. The sharply contrasting facies are difficult to explain without taking into account evidences of post-Devonian crustal shortening in the greater Timpahute Range, probable east-west mixing of facies by the thrusting, and the presence of a Late Devonian impact crater and debris that were paleogeographically significant.

In this study, the lower Guilmette at TMS is described in more detail than other parts of the Devonian because it contains the impact breccia of Sequence Dgb2, and because it is unaltered, well exposed, and unstudied. Therefore, an understanding of the depositional setting immediately before and after the emplacement of the distinctive carbonate breccia is a primary focus of this study.

# CHAPTER 2

# RELATIONSHIP OF NEW RESEARCH TO PREVIOUS STUDIES

The geology of the Great Basin has been studied since the late 1800's (Hague and Emmons, 1877; King, 1870). This chapter, divided into three parts, contains reviews of mapping and the relationships between previous work on (1) stratigraphy and (2) structure in the region and the new research reported herein.

## Mapping

Stewart and Carlson (1978) compiled the regional county geologic maps into a 1:500,000 scale map of Nevada. The digital (Hess and Johnson, 1997) regional geologic map for Lincoln County, which contains the Timpahute Range quadrangle, was originally published at a 1:250,000 scale by the United States Geological Survey (USGS) in 1970. It was a cooperative program with the Nevada Bureau of Mines and Geology (Tschanz and Pampeyan, 1970). Twenty-two man-months were allotted by the USGS to map the 10,649 square miles of the entire County, and much of the geology was mapped on Army Map Service 1:60,000-scale aerial photographs. The region lacked 7.5-minute topographic base map coverage until about the mid 1980's. Moreover, up to the time of the cooperative program, only about 7 percent of the region, mostly in mining districts, had been previously mapped. Other geologic mapping of Paleozoic rocks in the area includes the Seaman Range (DuBray and Hurtubise, 1994), northern Worthington Range (Martin, 1987), Golden Gate Range (Armstrong, 1991), and sketch maps of parts of the Timpahute and southern Worthington ranges (Taylor et al., 1994). Tingley (1991) provided a sample location map of the Timpahute Range quadrangle but no geologic mapping. Tschanz and Pampeyan (1970) focused their attention on the mining districts.

## Stratigraphy

This section deals mostly with Devonian stratigraphy. However, earlier Paleozoic rocks are reviewed briefly. This section also briefly reviews younger Paleozoic rocks and Mesozoic and Cenozoic rocks of the study area. Earlier Paleozoic rocks were listed in Chapter 1 and **Table 1**. Also, cycle and sequence boundaries, mechanisms, regional comparisons, and their application to geologic mapping are discussed because they are important for understanding the stratigraphic framework.

### Pre-Devonian Stratigraphy

No Precambrian rocks are exposed in the greater Timpahute Range and access to those mapped in the Groom Range, eight miles southwest of Tempiute Mountain, is restricted by the United States Department of Defense. However, much work has been done on the Precambrian rocks beyond the study area. Poole et al. (1992) summarized the stratigraphy from the latest Precambrian to latest Devonian time. The sequence of rocks is dominated by carbonates that lie on Precambrian and Lower Cambrian siliciclastics. Most of the early Paleozoic carbonates are dolomites except Ordovician limestones and minor Upper Cambrian limestones (**Figure 6** and **Figure 8**). Exposed Upper Cambrian rocks in the greater Timpahute Range are limestones. They are overlain by limestone beds of the Ordovician Pogonip Group, which are overlain by the Middle Ordovician Eureka Quartzite (**Figure 8**, **Table 1**). Excluding the limey Upper Ordovician Ely Springs Dolomite in the Silver Canyon thrust sheet, the lower Paleozoic rocks between Devonian Simonson unconformity and Eureka Quartzite are dolomites (Chapter 4). The tectonic setting and evolution of these rocks are discussed more fully in this chapter.

<u>Devonian Lithostratigraphy</u>

Nolan (1935) first applied the names Sevy Dolomite, Simonson Dolomite, and Guilmette Formation to Devonian strata in the Deep Creek Range, western Utah, 125 miles north-northeast of the study area (**Figure 9**, No. 12). Later, Nolan et al. (1956) established the Nevada Formation in the Eureka area, 100 miles north of the study area (**Figure 9**, No. 15 and **Figure 10**). The establishment of the Nevada Formation and other correlative units between scattered outcrops illustrates the confusion caused by mapping lithostratigraphic units. Members of the Nevada Formation roughly correlate with the uppermost part of the Sevy Dolomite through the lowermost Guilmette Formation. Because the Nevada Formation is based on lithologic changes that span several sequences, it is not useful for mapping or correlation purposes in the Sunnyside basin. Units correlative with the "Oxyoke Formation" represent different facies of the same sequences and all the units are grouped together into sequences of the "Oxyoke Formation."

It appears to me that mapping and correlations in the Great Basin are difficult because narrow, north-south trending inselbergs of Paleozoic contain different facies. Scattered inselbergs only reveal fragments of the shelf to slope facies changes, and they are separated by broad, covered intervals. Furthermore, the thrust sheet fragments are tectonically shuffled. Puzzling facies changes between inselbergs commonly complicate lithostratigraphic correlations. As a result, dissimilar Devonian lithostratigraphic units were commonly given different names from inselberg to inselberg. Proliferation of Devonian nomenclature occurred mostly on the west side of the Sunnyside basin where structural deformation was the most intense (**Figure 10**).

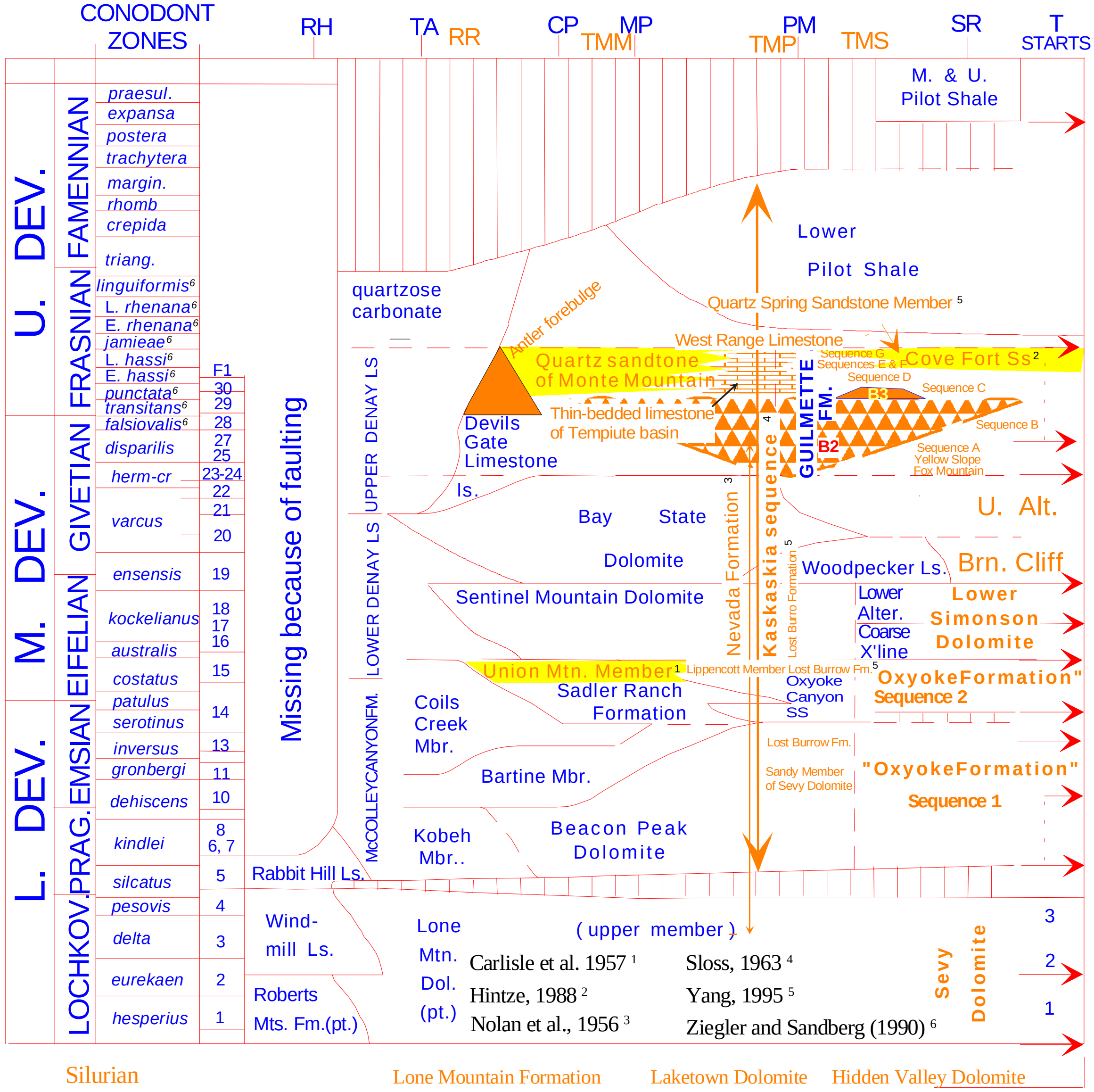


**Figure 10** Time-rock transect and correlation chart illustrating Devonian nomenclature of the Sunnyside basin (after Johnson et al., 1985). Red arrows indicate beginning of transgressions (T starts). RH=Rabbit Hill, TA= northern Antelope Range, CP= Combs Peak, MP= Modoc Peak, PM= Phillipsburg Mine area, Diamond Range, SR=southern Ruby Range. Orange and yellow depict modifications. RR= Reveille Range; TMM=Timpahute Monte Mountain; TMP=Timpahute Tempiute Mtn.; TMS=Timpahute Mail Summit. Credits for Conodont zone changes and other modifications are indicated in superscript and listed above. Note the proliferation of units on the left side of the chart representing the western edge of the Sunnyside basin. Disruptions of the stratigraphic record caused by the Devonian Antler (orange triangle) and subsequent orogenies resulted in structural complexities. Rare exposures of Paleozoic rocks in thrust sheet fragments make correlation and mapping difficult, and thus an inflated nomenclature.

For example, between the very light-gray, slope-forming Sevy Dolomite and the darker gray, ledge-forming Simonson Dolomite is a sandy, brown-gray slope- and ledge-forming interval. It includes the Oxyoke Canyon Sandstone Member of the Nevada Formation (Nolan et al., 1956) which corresponds to the uppermost sequence of the “Oxyoke Formation” presented in Chapter 4. The “Oxyoke Formation” as defined in Chapter 4 is correlative with the McColley Canyon Formation (**Figure 10**). Limestones of the Bartine Member of the McColley Canyon overlie correlative beds of the Sevy Dolomite (LaMaskin and Elrick, 1997). They are lithologically dissimilar to the “Oxyoke Formation” in other locations. In **Figure 10**, Johnson et al. (1985) correlated the Coils Creek Member of the McColley Canyon Formation and the Sadler Ranch Formation with the Oxyoke Canyon Sandstone member of the Nevada Formation. In the Inyo Mountains, 120 miles southwest of the study area, rocks correlative with the “Oxyoke Formation” correspond to the lower Lost Burro Formation (Beck, 1981). In the Sulphur Springs Range, 145 miles north-northwest of the study area (**Figure 9**, No. 49 and **Table 2**), it is called the Union Mountain Member of the Nevada Formation (Carlisle et al., 1957).

This study simplified the Devonian nomenclature of the Sunnyside basin. The Sunnyside basin was introduced in Chapter 1 and will be discussed in more detail in Chapter 7. Instead of creating new stratigraphic units at each facies change, sequences of six Devonian formations were employed for regional correlations and mapping. Sequences from the work maps were combined into mappable formations to make **Plate 1a**. Construction of work maps is described in Chapter 3. **Plate 6** is an example of a geologic work map using sequences at TMS. This sequence stratigraphic approach resulted in a more accurate map of the Timpahute Range quadrangle and more accurate regional isopach maps. A comparison of the number and area of formation outcrops between old and new geologic maps illustrate the differences between mapping lithologic units (i.e., formations) vs. mapping sequences. Following is a discussion of previous work on each of the six formations: Sevy, “Oxyoke,” Simonson, Guilmette, West Range, and Pilot.

Sevy Dolomite  Sevy Dolomite was the name given by Nolan (1935) to the dolomite exposures in Sevy Canyon, Deep Creek Range, Utah (**Figure 9**, No. 12). Later, Nolan et al. (1956) gave the name of Beacon Peak to the micritic, light-gray, slope-forming dolomite that overlies the Silurian Lone Mountain Dolomite (**Figure 10**). The lower Lone Mountain is probably partly equivalent to the Laketown Dolomite. The Beacon Peak is a member of the Nevada Formation in the Eureka area, Nevada, (**Figure 9**, No. 5). As Matti (1979) stated, the upper Sevy and Beacon Peak dolomites are correlative and lithologically identical. Sevy Dolomite has priority and Beacon Peak should be discarded. Johnson et al. (1985) placed the Sevy in the Lower Devonian (**Figure 10**). W.D. Roberts (1998, personal communication) collected Middle Devonian macrofossils from a limestone bed he placed in the upper part of the Sevy Dolomite in the Spotted range, 35 miles southwest of the study area. Access to the Spotted Range is now prohibited by the United States Department of Defense. His upper Sevy Dolomite is likely the “Oxyoke Formation” in this study. The digital geologic map (Hess and Johnson, 1997) of Tschanz and Pampeyan (1970) allowed me to compare their mapping with mine. The newly digitized geologic map of Tschanz and Pampeyan (1970) shows 48 outcrops of Sevy Dolomite that cover 24.46 square miles. In contrast, I show 68 outcrops covering 15.65 square miles using sequences on the new geologic map. Most of the difference is because Tschanz and Pampeyan (1970) combined the “Oxyoke Formation” with the Sevy Dolomite, and they mapped strata in the Hiko Range as Sevy Dolomite that is Guilmette Formation.

The Hidden Valley Dolomite, in the Inyo Mountains, California, 120 miles west-southwest of the study area, is approximately equivalent to the Sevy Dolomite or Laketown Dolomite. Tschanz and Pampeyan (1970) reported that fossils belonging to the *Spirifer kobehana* Zone occur in the upper 350 feet of the Hidden Valley Dolomite. Similar fossils were also found in the upper 65 feet of the Hidden Valley Dolomite at Quartz Spring by Beck (1981). These fossils are of Early Devonian Age and occur in rocks equivalent to the Sevy Dolomite.

"Oxyoke Formation" Previous investigators have been inconsistent in how they grouped and correlated the "Oxyoke Formation" and adjacent strata. As mentioned above, Nolan et al. (1956) established the "Oxyoke Formation" nomenclature naming the Oxyoke Canyon Sandstone Member of the Nevada Formation in the Eureka Mining District (**Figure 10**). Recognizing a faunal change between the argillaceous carbonate zone and the overlying quartzose carbonate zone, Johnson (1962) argued that the upper part of the Oxyoke Canyon Sandstone is correlative with the basal Simonson Dolomite east of the Diamond/Pancake ranges. The "Oxyoke Formation" in this study is possibly partly correlative with the basal part of the Coarse Crystalline Member of Johnson et al. (1989). However, the "Oxyoke Formation" was not mapped separately by Tschanz and Pampeyan (1970). They included rocks equivalent to the "Oxyoke Formation" in the Sevy Dolomite.

Southwest of the study area (120 miles) in the Inyo Mountains, California, Beck (1981) described the 164-foot thick sandy Lippincott Member of the Lost Burro Formation (**Figure 10**). It is probably partly correlative with the "Oxyoke Formation" at Mail Summit. Yang et al. (1995) divided the Lost Burro Formation into five units. The Lippincott lies above the Hidden Valley Dolomite and below their Unit 2 of the Lost Burro Formation.

Osmond (1962) described a persistent sandy interval between the Sevy and Simonson Dolomites and placed it at the top of the Sevy Dolomite. Hurtubise (1989), in his work in the Seaman Range, followed Osmond's convention and described it as the Sandy Member of the Sevy Dolomite (**Figure 10**). He measured 101 feet of sandstone in the northern Seaman Range in contrast to 46 feet reported by Osmond (1954).

However, Osmond (1962), Hurtubise (1989), and other early workers used different criteria to pick the contacts. They did not have the benefit of sequence stratigraphic perceptions at the time. To resolve the above stated problems and conflicts, I have chosen to establish an informal unit of formational rank which I name the "Oxyoke Formation." From **Figure 10**, it appears to range from upper Lower Devonian to lower

Middle Devonian.  I propose the TMS to be the type section because it is easily accessible and because it and its contacts are well exposed.  Though Tschanz and Pampeyan (1970) did not map “Oxyoke Formation” as a separate map unit (**Plate 1b**), I have found that it provides a key marker bed that reveals important structural details (**Plate 1a**).

The source for sandstone in the “Oxyoke Formation” is problematical.  Osmond (1954) argued for wind blown sands from an emergent area in the east or southeast. Johnson (1962) argued for a source from an arch on the north.  Paleocurrent directions from cross-bedding vary from a northwest transport direction at Fossil Peak (Hurtubise, 1989), southward in the Egan Range (Osmond, 1954; Reso, 1960)(**Figure 9**, No. 20 and **Table 2**), northeastward in the White Pine Range (Osmond, 1954)(**Figure 9**, No. 7 and **Table 2**), westward in the Grant Range (Osmond, 1954)(**Figure 9**, No. 27 and **Table 2**), south and southeastward in the Seaman Range and central Grant Range (Osmond, 1954), and southward in the Pahranagat Range (Reso, 1960).  Paleocurrent directions based on cross-bedding in the Hiko Range, however, vary from southwestward to northeastward. Herringbone cross lamination, bidirectional ripple marks, and cross-bedding all suggest that the sands--at least in this area--were deposited under the influence of tides.  A new “Oxyoke Formation” sand provenance is proposed in Chapter 4 and discussed in Chapter 7.

<u>Simonson Dolomite</u>  Nolan (1935) named the Simonson Dolomite after exposures in Simonson Canyon, Deep Creek Range, Utah (**Figure 9**, No. 12).  Osmond (1954) subdivided the Simonson Dolomite into four members.  His Coarsely crystalline, Lower Alternating, Brown Cliff Forming and Upper Alternating Members generally coincide with the sequences delimited in this study.  As defined herein, the Simonson Dolomite lies within the Middle Devonian (**Figure 10**).  The portion of the digital geologic map (Hess and Johnson, 1997) of Tschanz and Pampeyan (1970) of the Timpahute Range quadrangle shows 48 Simonson Dolomite outcrops covering 41.24 square miles.  In

contrast, I mapped 78 Simonson Dolomite outcrops covering only 17.67 square miles. Part of the discrepancy between old and new mapping is caused by the difference in defining the Simonson Dolomite and Guilmette formations. Tschanz and Pampeyan (1970) combined the Fox Mountain Sequence of the Guilmette Formation with the Simonson Dolomite. They also mapped large parts of the Hiko Range as Simonson Dolomite that should have been mapped as Guilmette and younger units (**Plate 2a**).

Elrick (1995) suggested that these Middle Devonian carbonates of the eastern Great Basin were deposited along a low energy, westward-thickening, distally steepened ramp. However, isopach maps of Middle Devonian sequences suggest that the carbonates were deposited in the Sunnyside basin, an intrashelf basin (see Chapter 7). Devonian rocks thicken westward (as suggested by Elrick, 1995) to the axis of the Sunnyside basin. However, they thin westward from the axis toward the Antler forebulge (**Plate 3**). Devonian rocks west of Eureka, Nevada, lie below the Mississippian Roberts Mountain thrust (i.e., Lone Mountain, **Figure 9**, No. 34 and **Table 2**). These thick, open-marine rocks were likely deposited west of the Antler forebulge and then thrust into their present location by Sevier thrust faults.

<u>Guilmette Formation</u> The Guilmette Formation was also named by Nolan (1935) after exposures in Guilmette Gulch, Deep Creek Range, Utah (**Figure 9**, No. 12). The basis for originally separating the Simonson Dolomite from the overlying Guilmette Formation at its Deep Creek Range type locality was the change from sucrosic dolomite to limestone (Nolan, 1935). The dolomite breccia that Nolan described at the base of the Guilmette Formation may be related to a karst surface at the top of the Simonson Dolomite. It also could be related to a transgressive lag over it, both of which are described in Chapter 4. As defined in this study, **Figure 10** shows that the Guilmette Formation began in the upper Middle Devonian and ended in the lower Upper Devonian.

Unfortunately, subsequent workers have chosen to redefine the base of the

Guilmette Formation rather than use Nolan's original definition. Reso and Croneis (1959) proposed that the base of a yellow slope-forming bed (the upper Yellow Slope Sequence in this paper) be the base of the Guilmette Formation in the Pahranagat Range. It is 40 to 90 feet above the highest bed in the Fox Mountain Sequence that bears the brachiopod *Stringocephalus* at TMS. The Fox Mountain Sequence herein is an interval between the major unconformity at the top of the Simonson Dolomite and at the base of the Yellow Slope Sequence. The sequence is present in some ranges. Following the convention of Reso and Croneis (1959), Tschanz and Pampeyan (1970) in their regional synthesis, Hurtubise (1989) in the Seaman Range, Ackman (1991) in the Worthington Range, and Estes (1992) in the Pahranagat Range all placed the top of the Simonson Dolomite at the base of the yellow slope-forming bed. They included the *Stringocephalus*-bearing Fox Mountain Member with the uppermost part of the Simonson Dolomite. Sandberg et al. (1997) formally proposed the Fox Mountain as a new formation lying between the Guilmette Formation and the Simonson Dolomite. However, the boundaries of their Fox Mountain Formation are under debate and are different from the Fox Mountain Sequence herein (Chapter 4).

Hurtubise (1989) defined the base of the yellow slope-forming bed as the base of a stromatolite bed. He did not identify which stromatolite bed. Most sections contain several stromatolite beds that occur above the sequence boundary that separates the Yellow Slope Sequence from the Fox Mountain Sequences as defined herein. Sandberg et al. (1997) did not mention criteria for a sequence boundary between the Yellow Slope Sequence and the Fox Mountain Sequence nor the karsted sequence boundary between the Fox Mountain Sequence and the underlying Simonson Dolomite. The karst surface they describe between their lower and upper members is likely the sequence boundary or the top of the Simonson unconformity herein. Crinoids, occurring only in their upper member and my Fox Mountain Sequence, suggest open-marine deposition. The base of the Fox Mountain Sequence defined herein most likely marks the Taghanic onlap or Event 1 of Sandberg et al. (1997). Therefore, application of sequence stratigraphy and recognition of the regional unconformity at the top of the type Simonson Dolomite returns us to Nolan's original definition of the lower contact of the Guilmette Formation as the change from underlying sucrosic dolomite to overlying limestone. A more detailed description of the Guilmette sequences, including the Fox Mountain, is presented in Chapter 4.

The number of Guilmette Formation outcrops and their distribution in the study area partly depends on how the Guilmette Formation is defined. The digital geologic map of Tschanz and Pampeyan (1970) shows 65 Guilmette outcrops covering 95.62 square miles in contrast my map that shows 142 Guilmette outcrops covering 89.07 square miles (Chapter 4). However, the large area Tschanz and Pampeyan (1970) mapped as undifferentiated Devonian and Mississippian in the Mail Summit 7.5' quadrangle (**Figure 3**), and the large area of Ordovician Pogonip Formation in the Monte Mountain 7.5' quadrangle they mapped as Guilmette, greatly increased the area they mismapped as Guilmette Formation. Nevertheless, they mismapped the Guilmette and younger beds in the Hiko Range as Simonson Dolomite (compare **Plates 1a** and **1b**).

Several workers have attempted to divide the Guilmette by lithology. In his work in the Pahranagat Range area, Reso (1960) divided the Guilmette into two members above and below the top of a prominent carbonate breccia (Dgb2 Sequence in this paper). Hurtubise (1989) divided the Guilmette into two members above and below the top of the yellow slope-forming interval. Sandberg et al. (1997) formally proposed to make the Guilmette Sequence Dgb2 breccia facies the Alamo Breccia Member of the Guilmette Formation. In contrast, in this report I have divided the Guilmette into nine stratigraphic sequences (Chamberlain and Warme, 1996) that can be mapped and correlated throughout much of the Sunnyside basin (**Plate 3**). These sequences are described in detail in Chapter 4.

Dunn (1979) studied a reef sequence at TMS. She reported *Thamnopora* corals, ostracodes, styliolinids, *Tentaculites*, and foraminifers (e.g., *Tikhinella*) from beds herein assigned to Sequence Dgb3, Cycle 1 just below the reef (**Plate 2c**). TMS sequences are described in Chapter 4 and cycles of the TMS sequences are described in Appendix B. Dunn (1979) reported that the high-energy assemblage of the reef (my Cycle 3, Sequence Dgb3) was characterized by tabular and massive stromatoporoids, tabulate corals *Thamnopora* and *Alveolites*, rhynchonellid and terebratulid brachiopods, crinoids, and gastropods. The reef was divided into three parts based on zonation of fauna within the reef. The first subdivision contains the rhynchonellid brachiopod *Hypothridina emmonsi*, terebratulid *Cranaena* sp., and the branching tabulate coral *Thamnopora* along with crinoids, horn corals and gastropods (Dunn, 1979). This subdivision probably included Sequence Dgb (reef core) Cycles 1 and 2 herein (**Plate 2c**).

Dunn's second subdivision probably extended near to sample MI-479 (Appendix C) at the 2,400-foot level in the TMS section (**Plate 2a**). **Plate 2a** shows the vertical position of samples from the TMS measured section. Dunn noted that this division contained many same fossils as in the lower subdivision with the addition of massive and tabular stromatoporoids and the colonial rugose coral *Pachyphyllum*. In addition, she listed the alga *Solenopora* sp. that would suggest the reef grew within the photic zone. Finally, *Renalcis* and *Sphaerocodium* algae and *Amphipora* stromatoporoids were noted in the middle or main subdivision. By comparing this reef with reefs in other parts of the world, she concluded that her tabular-massive stromatoporoid subdivision was constructed between storm and normal wave base. The uppermost subdivision contained more corals and fewer, thinner stromatoporoids and contained large colonies of the tabulate coral *Alveolites* that are rare in lower subdivisions, suggesting shallower water conditions.

Dunn (1979) pointed out that fossils from my Dgb3c at TMS (**Plate 2c**) were harder to identify than those of the reef flank equivalent beds due to the recrystallization of the reef core to coarsely-crystalline limestone. She listed the corals *Alveolites*, *Thamnopora*, and *Macgeea*, the mollusc (?) *Tentaculites*, the foraminiferans *Tikhinella*, *Nanicella*, *Elvania*, and *Multiseptada*, and the stromatoporoid *Trupetostroma*, as some fossils found in the reef flank equivalent beds. Dunn noted that the denser (thicker stemmed) stromatoporoid *Stachyoides* predominates near the reef and the delicate *Amphipora* is more common away from the reef. Tabular stromatoporoids decrease in abundance away from the reef.

The Dgb3 reef is the famous structure mentioned by Reso (1960), discussed by Chamberlain and Warme (1996), Warme and Sandberg (1996), Sandberg et al. (1997) and Chamberlain and Birge (1997). A color oblique aerial photograph of the reef is shown in Chamberlain and Warme (1996, Figure 11). Digital images of reefs occurring in the Hiko Range are shown at Stop 16, in Appendix D.

<u>West Range Limestone</u> Westgate and Knopf (1932) established the West Range Limestone in the Pioche Mining District 25 miles east of the study area. They named it after rocks exposed in the West Range which they described as "blue-gray fine-grained limestones, in some places nodular, commonly weathering to a characteristic yellow color." Kellogg (1963) in the Egan Range, Reso (1960, 1963) in the Pahranagat Range, Hurtubise (1989) in the Seaman Range and Sandberg and Ziegler (1973) at Bactrian Mountain all recognized the West Range Limestone above the quartz sandstone at the top of the Guilmette Formation (**Table 1**, **Plate 1a**). Bactrian Mountain in the northern Pahranagat Range is in T5S R59E on the south edge of the Timpahute Range quadrangle (**Plate 1**). Tschanz and Pampeyan (1970) did not map the West Range Limestone as a separate unit in their geologic map of Lincoln County. They probably grouped it with the Pilot Formation.

Johnson et al. (1991) suggested that the West Range Limestone intertongues with the Pilot Formation. It lies in the upper Frasnian (**Figure 10**). Sandberg et al. (1988) suggested that the Indian Ranch Tongue of the uppermost Guilmette Formation lies entirely within the Pilot Formation although it is "a time and lithogenetic equivalent of the West Range Limestone."

Pilot Formation Spencer (1917) established the Pilot Formation in the Ely Mining District 100 miles north of the study area (**Figure 2**). Reso (1963) in the Pahranagat Range, Hurtubise (1989) at Fox Mountain (50 miles north-northeast of Hiko), and Sandberg and Ziegler (1973) at Bactrian Mountain also recognized the Pilot Formation between the West Range Limestone and overlying Joana Limestone. Tschanz and Pampeyan (1970) mapped 49 outcrops of Pilot Formation covering 10.9 square miles in the Timpahute Range quadrangle. In contrast, the new map shows 91 Pilot Formation outcrops that cover 5.85 square miles.

Sandberg et al. (1988) concluded that the lower member of the Pilot Formation was deposited in the Pilot Basin at the start of the *Ancyrognathus triangularis* conodont zone that lies above the *Mesotaxis asymmetrica* (*liguiformis* in Sandberg et al., 1997) conodont zone of the upper Guilmette Formation. The *triangularis* zone began 364 Ma. (Sandberg and Ziegler, 1996). Johnson et al. (1985) placed the lower Pilot Shale at the end of the *Ancyrognathus triangularis* conodont zone (**Figure 10**). The *triangularis* zone ended 362.5 Ma. (Sandberg and Ziegler, 1996). Conodonts from the Dgb2 (Alamo Breccia) show the Alamo event occurred in the *punctata* zone (Warme and Sandberg, 1995) which ended three (Sandberg et al, 1997) or four (Sandberg and Zeigler, 1996) million years before the beginning of the *triangularis* zone. The Pilot Formation is divided into three members by major unconformities (Sandberg et al., 1997) but begins 356.5 Ma. In contrast, Carpenter (1997) suggested that the Yellow Slope Sequence could represent the earliest Pilot basin deposition. The Yellow Slope Sequence began about 371 Ma. (Sandberg et al., 1997).

According to Sandberg et al. (1988), the incipient Pilot basin is a small circular basin between the Utah/Nevada border and the Eureka area (**Figure 2**). It expanded slightly into westernmost Utah during the Lower *triangularis* Zone (Sandberg et al., 1988). In contrast, the Sunnyside basin began in Sevy Dolomite time and extended into Pilot Formation time and covered a much greater area than the Pilot basin (Chamberlain and Birge, 1997). The Pilot basin of Sandberg et al. (1988) lies within the Sunnyside basin.

Regional Comparison According to earlier research, Devonian rocks exposed at TMS are lithologically, depositionally, and biostratigraphically similar to those in the Specter Range (60 miles south-southwest of the study area), Nevada (Burchfiel, 1964), and the Panamint Range (80 miles south of the study area), California (Zenger and Pearson, 1969), and to those as far north as Alberta, Canada (Reso, 1960).

The Middle and Late Devonian Lost Burro Formation, exposed in the Panamint Range, is composed of mostly dolomite in the lower part and limestone in the middle and upper parts (McAllister 1952). This pattern is found elsewhere, over much of the Devonian shelf throughout the region. According to Beck (1981), the lowermost part of the formation is marked by the 50-meter thick sandy Lippincott Member. Johnson et al. (1989) correlated the Lippincott to the Coarse Crystalline Member of the Simonson Dolomite. However, as mentioned above, part of the Lippincott is probably partly correlative with the “Oxyoke Formation” herein (**Figure 10**). According to Stevens (1986), the Lost Burro Formation was deposited on the western North American passive margin under subtidal to supratidal conditions. He suggested that similar thick platform Devonian carbonates found in the central and western parts of the Inyo Mountains-Angus Range region probably accumulated on a moderately channeled slope in deep water. Similar Devonian carbonates in the Panamint Range and the easternmost and southern Inyo Mountains were deposited on the western edge of the carbonate shelf near the continental slope (Armstrong, 1980).

Yang et al. (1995) divided the 1969-foot thick Lost Burro Formation into five units. Most of Yang et al. (1995)’s Unit 2 (459 feet) and the uppermost part (66 feet) of Unit 1 of the Lost Burro Formation is probably correlative with the Simonson Dolomite. It is correlative because it lies above the *Spirifer kobehana* Zone and below rocks of

Givetian age. An *Amphipora*-bearing bed near the middle of their Unit 2 is most likely correlative with the Simonson Dolomite Brown Cliff Sequence at TMS. Yang et al. (1995) described the upper part of the Lost Burro Formation as shallowing-upward cycles of predominantly stromatoporoid-bearing limestones and minor sandstones. The uppermost part of their Unit 2 (82 feet) and the lower part of their Unit 3 (443 feet) most likely correlate to the upper part of the Simonson Dolomite Upper Alternating Sequence and the Guilmette Fox Mountain Sequence at TMS because of its Givetian age. Because of the interbedded sandstones and Frasnian age, the upper parts of their Unit 3 (262 feet thick) most likely correlates to Guilmette Sequences Dge and Dgf of TMS. A regional unconformity and major sequence boundary cuts out lower and middle Guilmette sequences in many Nevada and Utah sections to the north and probably removed lower middle Guilmette sequences in the Panamint Range. Unit 4 of Yang et al. (1995) is 426 feet thick and probably correlates to Sequence Dgg at TMS. Their Unit 5 (66 feet), the Quartz Spring Sandstone Member, correlates to the sandstone at the top of Sequence Dgg at TMS (**Figure 10**). It probably correlates to the Cove Fort Sandstone and its equivalents in Utah and eastern Nevada (Langenheim and Larson, 1973). An isolith map of net Guilmette sandstones in Chapter 7 shows the distribution of Late Devonian quartz sandstones in the Sunnyside basin.

## Younger Paleozoic Rocks of the Study Area

Although this study focuses on the Devonian rocks, the distribution of younger Paleozoic rocks is important to complete the geologic map. The Devonian Sunnyside intrashelf basin evolved into the Antler foreland basin in the Lower Mississippian. Synorogenic sediments shed off the Roberts Mountain allochthon filled the western side of the basin with siliciclastic sediments (Poole, 1974). Mississippian limestones with tongues of nonmarine valley-fill sediments filled the eastern side of the Mississippian basin (Chamberlain, 1981). The Timpahute area lies between thick (more than 4000 feet) Mississippian carbonates on the east and correlative thick (more than 6000 feet) siliciclastics on the west (Cedar Strat proprietary measured sections, 1984-1989). Reso (1963) reported more than 1000 feet of Lower Mississippian limestone and more than 1000 feet of shales and sandstones in the Pahranagat Range, five miles south of the study area. Tschanz and Pampeyan (1970) also estimated 1000 feet of Middle and Late Mississippian Antler siliciclastics in the Pahranagat Range. At Tempiute Mountain, the Mississippian Antler clastics are 2220 feet thick (Cedar Strat proprietary measured section). The thickness and presence of Mississippian Antler clastics, and especially the shales, are important in the study area because they form one of the most important thrust detachment layers. As defined in Chapter 1, the Mississippian Antler clastics include Chainman shale and Scotty Wash sandstone facies.

The digitized map of Tschanz and Pampeyan (1970) shows 53 outcrops of Joana Limestone covering 38.02 square miles in the Timpahute Range quadrangle. In contrast, I show 101 Joana outcrops that cover 40.26 square miles, in Chapter 4. The biggest difference occurs in the Monte Mountain 7.5' quadrangle where they mistakenly took Joana Limestone for Pennsylvanian rocks. Tschanz and Pampeyan (1970) mapped 44 outcrops of Antler clastics (Chainman Shale and Scotty Sandstone) covering 11.66 square miles in the Timpahute Range quadrangle (**Figure 11**). In contrast, I show 46 Antler clastics outcrops that cover 9.9 square miles.

Reso (1963) reported 764 feet of Pennsylvanian (undifferentiated but probably Ely Formation) rocks in the Pahranagat Range. Tschanz and Pampeyan (1970) noted that no complete section of Permian limestone exists in Lincoln County, but that in other sections in the region the Permian limestone is 2000 to 4500 feet thick. Rocks representing the uppermost Permian and Lower and Middle Mesozoic were not found in the study area.

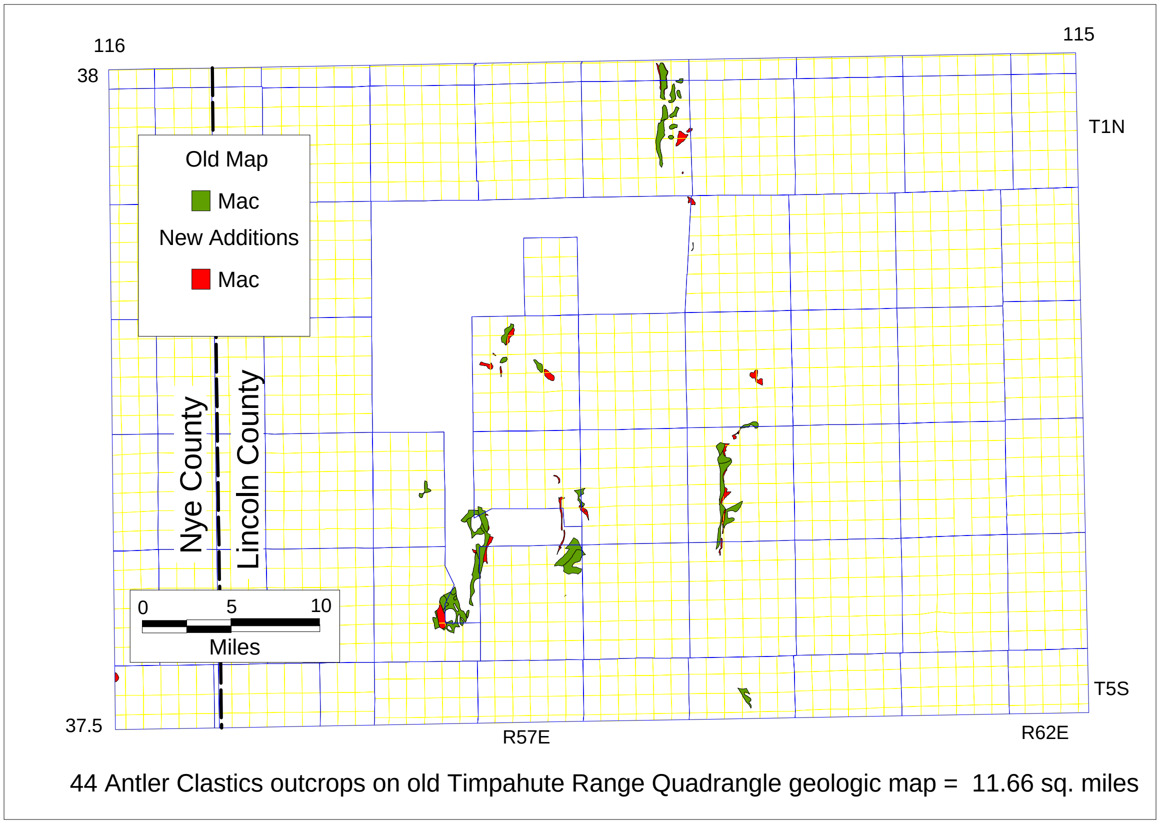


**Figure 11** Distribution of outcrops of Mississippian Antler clastics in the Timpahute Range quadrangle as reported by Tschanz and Pampeyan (1970). Added Antler clastics outcrops from the new map are marked in red. Degrees latitude and longitude are marked at the corners of the map.

<u>Sevier Synorogenic Sediments</u>

Sevier synorogenic sediments are present in the study area and in much of the Nevada part of the Sevier thrust belt. They provide constraints on the age of thrusting and thus resolve controversy concerning the age of the Sevier orogeny. Their distribution and stratigraphy provide insight into the evolution of the Sevier orogeny.

Age of Thrusting The age of thrust faults in the region is controversial. Some believe that most of the thrusting in Nevada is likely pre-Cretaceous (e.g., W.J. Perry, 1991, personal communication), and others contend that most thrusting occurred in the Late Cretaceous.

Synorogenic strata exposed near the leading edge of the Sevier fold-and-thrust belt in northern Utah and southwestern Wyoming confirm a Late Mesozoic age for thrusting. The Sevier wedge in northeast Utah and southwest Wyoming was shortened by 60 miles in three major and one minor events from Neocomian(?) to Eocene time (Decals, 1994). These events resulted in an overall eastward progression of thrusting that was punctuated by several episodes of out-of-sequence and hinterland vergent thrusting (Decals and Mitra, 1995). An out-of-sequence thrust fault is a thrust fault that does not fit the predictive pattern of thrust faults in a sequence becoming younger in their vergent direction but cuts across or through older thrust faults. Hinterland vergent thrusts are backthrusts with a vergent direction opposite to the thrust faults in a normal sequence.

An isopach map of the Aptian-Albian Cedar mountain Formation at the leading edge of the Sevier fold-and-thrust belt in central Utah clearly shows that the Sevier orogeny there is Late Cretaceous (Currie, 1997). The Sevier thrust wedge of central Utah was emplaced between early Albian and Campanian time and persisted by out-of-sequence thrusting until Lower Eocene (Lawton and Trexler, 1991). Late Cretaceous (Albian-Cenomanian) synorogenic rocks associated with thrusting are found in outcrops from northern to southern Nevada. Some researchers suggest that these rocks provide constraints on timing of the Sevier deformation in the region (Vandervoort, 1987; Carpenter et al., 1993a, 1993b; Carpenter and Carpenter, 1994a, 1994b). Tertiary/Cretaceous rocks preserved in many ranges of eastern Nevada, including the study area, were probably associated with the Sevier fold-and-thrust belt (**Figure 1**).

Additional evidence of Cretaceous age thrusting comes from a well 180 miles on strike to the north. The Gary-Williams Company Three Bar Federal No. 36-C, C SW Sec

6 T27N R51E drilled from Ordovician Vinini Formation through Cretaceous strata and into upper Paleozoic strata (Well files, Nevada Bureau of Mines and Geology).

Two methods help date the Sevier orogeny. One is crosscutting relationships of dated igneous intrusions, and the other is dating of fossils and volcanics in the synorogenic sediments associated with thrusting. The Sevier thrust belt is best dated by the associated Cretaceous deposits in eastern Utah (L. Hintze, 1998, personal communication). Geochronological data from igneous intrusions and cross cutting relationships can also be used to date the Sevier orogeny. These relationships in the Clark Mountain area, at the southern end of the Sevier belt (**Figure 2**), suggest that thrusting was initiated in the Late Jurassic and continued to the Middle Cretaceous (Walker et al., 1995). However, Stamatakos et al. (1998) suggested that paleomagnetic and Paleozoic zircon fission-track data suggest that the Meiklejohn Peak thrust fault (near the Nevada/California border, 100 miles southwest of the study area) predates Jurassic-Cretaceous (Sevier) deformation. They suggested that the deformation may have resulted from a Permian or earlier contractional event. In the study area, the emplacement of the Freiburg intrusions (25.1 Ma., Taylor et al., 1993) that intrude the footwall and hanging walls of the Freiburg thrust fault suggests that the fault is Oligocene or older (**Plate 1a**, T1N R57E). An age date of the Troy Peak stock is 86.5 ± 4.6 Ma U/Pb on Zircon. It intrudes the recumbent limb of the Timber Mountain and associated thrust faults in the Grant Range. Therefore it gives an upper limit on time of formation (**Figure 2**) as Late Cretaceous (Taylor et al., 1993).

<u>Distribution and Stratigraphy</u> A newly discovered unit southwest of Monte Mountain between Paleozoic rocks and Tertiary volcanic rocks may provide insight on the age of the compressional structures of the region (Sec 5 T4S R58E, **Plate 1a**). The unit is Late Cretaceous or Lower Tertiary and is called Tertiary/Cretaceous (Chamberlain et al., 1992b). It probably predates Tertiary volcanics as it lacks fragments of Tertiary

volcanics within it. The Tertiary/Cretaceous strata contain lacustrine limestone beds similar to the Sheep Pass Formation in east central Nevada, the Flagstaff Limestone in central Utah (Fouch et al., 1991), and the Claron Formation in southwestern Utah (Goldstrand, 1992). Conglomerate underlies both the Claron Formation (Goldstrand, 1994) and the Tertiary/Cretaceous strata of the Timpahute region. It may be correlative with the conglomerates of the North Horn Formation that underlie and are coeval with the Flagstaff Limestone in central Utah (Fouch et al., 1979). A similar unit of limestone above conglomerate beds occurs in the Grant Range, 30 miles north of the study area. These beds were mapped as Sheep Pass on the Nye County Geological Map (Kleinhampl and Ziony, 1985).

Hurtubise (1989) described an outcrop of whitish weathering lime mudstone on the west side of the Seaman Range, thirty-five miles to the northeast of Monte Mountain. Palynomorphs suggest an Eocene age for the limestone. He correlated the outcrop in the Seaman Range with Winfrey's Member "B" from the Sheep Pass type locality in the Egan Range, 35 miles north-northeast of Hurtubise’s location in the Seaman Range (Winfrey, 1960).

Limestones at Monte Mountain may yield an Eocene age (uppermost Refugian), similar to Hurtubise's (1989) assemblage. If they do, the underlying conglomerates could be correlated to Winfrey's Member A. If the beds are Sheep Pass age, then the Sheep Pass basin should be enlarged or another basin defined. It would reach at least thirty-five miles farther south than Hurtubise's newly discovered outcrops in the Seaman Range. I found similar limestones in the hanging-wall sheet of the Pahranagat thrust near the top of Tikaboo Peak, twenty miles south-southeast of Monte Mountain. As with the Monte Mountain Tertiary/Cretaceous strata, they lie between the Paleozoic rocks and the overlying Tertiary volcanics.

Tschanz and Pampeyan (1970) described similar beds in the Pahroc (30 miles east of Monte Mountain), Groom (25 miles south-southwest of Monte Mountain), Pintwater (40 miles south of Monte Mountain), and Spotted (45 miles south-southwest of Monte

Mountain) ranges. According to their map, these rocks cover a significant portion of western Lincoln County. They suggested that the conglomerates are Cretaceous to Oligocene and the overlying limestone is Miocene or younger. These Tertiary/Cretaceous conglomerates and lacustrine limestones occur near thrust faults, were probably shed off from thrust fronts, and could provide important insight into timing of the thrust faults if they are genetically related to them. Tschanz and Pampeyan (1970) estimated that the thickest conglomerates exposed in the Spotted and Pintwater ranges are 5000 to 6000 feet thick. Access to these rocks is now restricted by the United States Department of Defense. These Tertiary/Cretaceous rocks that are closely associated with thrust faults along the four-hundred-mile-long Sevier fold-and-thrust belt in Nevada could provide insight into timing and thrust form. Others (e.g., Fouch et al., 1991) believed that there are no ramping thrust faults in the immediate region of these localities.

The Sevier fold-and-thrust belt in central Utah may have localized deposition of the Flagstaff Limestone, North Horn Formation and Colton Formation (Stanley and Collison, 1979). However, Fouch et al. (1991) suggest that the Sevier orogeny was over and no foreland basin in central Utah existed by the time of Flagstaff deposition. Goldstrand (1992) suggested that the correlative Pine Hollow and Claron formations were deposited during the Laramide Orogeny and are related to partitioning of the foreland basin into individual, internally drained basins. These basins derived sediment from surrounding structural highs during Lower Paleocene and Middle Eocene time. A contrast of depositional environments occurred between the west and east side of Lake Flagstaff. Western-derived lithic quartz sandstones show evidence of thinning over Sevier-age folds. They also show evidence of steep topography and high-energy along the west side of the lake. These sediments contrast with the shallow, vegetated, and episodically flooded east shore sediments. The phase of subsidence and infilling of a foreland basin east of the Sevier fold-and-thrust belt probably controlled the facies contrast. The Late Cretaceous to Lower Tertiary tectonic pulse of Elison (1991) probably controlled deposition of the North Horn Formation and associated units. This pulse probably corresponds to the emplacement of Roeder's (1989) thick terrane such as the Silver Canyon thrust sheet. The thrust disrupted and reinvolved Roeder's (1989) thin terrane such as the Monte Mountain thrust sheet. The emplacement of Roeder's (1989) thin terrane could have been during one of two earlier Sevier tectonic pulses.

In contrast to the compressional synorogenic model supported by this research, some researchers (e.g., Newman, 1979) believed that the conglomerates in the Tertiary/Cretaceous beds were a result of erosion off normal fault horsts. Similarly, Constenius (1996) concluded that many valley fill deposits were deposited in Late Paleogene half grabens resulting from extensional collapse of the Cordilleran foreland fold-and-thrust belt. The new geologic map of the study area does not support these extensional collapse or horst and graben models (**Plate 1a**). However, the new geologic map shows more Late Cretaceous compressional features than do previously published geologic maps.

## Structure and Tectonics

Paleogeographic reconstructions of this structurally complex region not only require a detailed analysis of stratigraphy but also an understanding of the structural elements and tectonic evolution. This section presents a brief discussion of tectonic events that influenced deposition and deformation of the Paleozoic rocks of the area. An emphasis is given to the Cretaceous Sevier orogeny because of its importance in paleogeographic reconstructions and its poorly understood effects on the rocks of the region.

Pre-Antler Orogeny

Rifting in the late Precambrian (<850 Ma) resulted in the western North American continental margin along which a thick wedge of strata accumulated during the late Precambrian and lower Paleozoic (Stewart and Poole, 1974). Most of the latest Precambrian (<850 Ma) to Late Devonian (>345 Ma) strata deposited east of the Sr 0.706 line were deposited in shallow-water conditions on the continental shelf. They were deposited during a time of relative tectonic stability (Stewart and Poole, 1974).

The 0.706 Strontium isotope line probably represents the rift edge in the Precambrian crust. It is a north-south line in central Nevada that divides older continental and newer oceanic crustal domains. It occurs where $^{87}Sr/^{86}Sr = 0.706$ in granitic rocks and is taken as the western edge of Precambrian crust at depth (Suppe, 1985). Oceanic sediments west of the line have $^{87}Sr/^{86}Sr$ ratios less than 0.706. They are interpreted as representing younger oceanic crust than the older continental rocks east of the line that have $^{87}Sr/^{86}Sr$ ratios above 0.706. Oceanic rocks deposited west of the $^{Sr}0.706$ line were deposited in deepwater conditions. They are composed of chert, shale and volcanic rocks and were termed “western facies” by Merriam and Anderson (1942) and “siliceous facies” by Roberts (1972). These siliciclastic-rich oceanic rocks contrast sharply with the carbonate-rich eastern facies of the study area.

Stewart and Poole (1974) described the transition between western and eastern facies as abrupt. Crustal shortening during the Antler and Sevier orogenies probably account for the abrupt transition.

Monitor-Uinta Arch

**Plate 3**, an isopach map of the Great basin Devonian rocks, shows an east-west trend where the Devonian rocks are thinner with respect to correlative rocks north and south. This east-west trend was a tectonic ridge or arch. Unconformities truncate some Devonian sequences on the arch. It coincides with the Precambrian Uinta aulacogen and may be genetically related to it. Some 25,000 feet of Precambrian shales and sandstones accumulated in the east-west trending Uinta aulacogen, north-central Utah (Hintze, 1988). An aulacogen is a tectonic trough, bounded by radially oriented convergent faults, that is open outward (Bates and Jackson, 1987). In other words, the two successful arms of a triradial fault system become the rift edge. Two arms of each of several such triple-rift systems will eventually link to form a single accreting plate boundary, along which an ocean will open (Sengör, 1987). The third, or failed arm, forms a tectonic trough into the continent from the ocean, 120º from the other two arms. The Uinta aulacogen may represent a failed arm of early crustal rifting. Rifting likely started at 600 Ma (Poole et al., 1992). The successful arms of the rifting separate the thick Paleozoic accumulations to the west from thin accumulations to the east. This thick and thin transition zone from southwestern Wyoming through southwestern Utah is called the Utah hingeline.

The aulacogenic behavior of the Uinta failed arm ceased before Cambrian time. However, a positive east-northeast trending arch coincides with the aulacogen during much or the lower Paleozoic, including the Devonian. Carpenter et al. (1994) recognized the positive area near the western edge of the pre-Antler continent and named it the Monitor arch. Isopach patterns in **Plate 3** suggest that the Monitor arch is an extension of the Uinta arch. Therefore, it is named the Monitor-Uinta arch herein. If this arch represents the uplifted aulacogen or failed arm, then the rift edge or successful arms in the Precambrian crust are likely reflected by the 0.706 Strontium isotope line. Nd isotope data provide the first evidence that the Monitor-Uinta arch was present in the region in the latest Proterozoic (Farmer and Ball, 1997). Pb, Sr, and Nd isotope data were used to distinguish mantle isotope signatures of Pacific Ocean mid-oceanic ridge basalts (MORB) from Indian Ocean MORB basalts in southeastern Australia (Zhang et al., 1999). Nd isotope data were used in western North America to identify the source areas of siliciclastic detritus (Farmer and Ball, 1997). Mafic crust has higher Sm/Nd ratios and higher $\varepsilon_{Nd}$ values than intermediate to felsic composition crust within each province.

The Uinta/Monitor aulacogen became a topographic low in Carboniferous time into which more than 4000 feet of Mississippian limestones and valley fill siliciclastics were deposited (Chamberlain, 1981, 1988c). More than 26,000 feet of Pennsylvanian and Permian rocks were deposited in the Oquirrh basin that developed about the aulacogen (proprietary measured section by the author, Wallsburg Ridge, Wasatch Mountains, Utah). However, Geslin et al. (1999) disputed the unusually thick section by attributing it to repetition of beds due to thrust imbricates. Erskine (1999) attributed the unusually thick section to normal sedimentary processes. I agree with Erskine. Gamma-ray patterns and patterns of decreasing Conodont Alteration Indices should be repeated if the section were tectonic thickened by thrust imbricates. I found no repetition of gamma-ray patterns and a consistent decrease in Conodont Alteration Indices (CAI) from the base to the top of the 26,000 foot section. Therefore, the Uinta-Monitor aulacogen changed from a positive arch in Devonian to a trough or graben structure in the Carboniferous. Similarly, the Peace River Arch, a northeast-southwest Precambrian crustal flexure in western Alberta, changed from a topographic high during the Devonian to a graben structure in the Carboniferous (Ross, 1991; Mossop and Shetson, 1994).

Longwell et al. (1965) provided strong evidence for several pulses of Cretaceous thrusting in the Spring Mountains, 120 miles south of the study area (**Figure 2**). They mapped the Keystone thrust fault that overrode the older Contact thrust fault. Matthews (1988) added detail that also suggested several pulses. An older sequence of Tertiary/Cretaceous strata provides information on thrust relationships in the southern Spring Mountains. The Keystone thrust sheet deformed (folded and faulted) rocks in Lavinia Wash and underlying older rocks of the Contact thrust sheet. The synorogenic Lavinia Wash rocks have a radiometric age of 120 Ma (Carr, 1980). Similarly, the Silver Canyon thrust deformed the Monte Mountain thrust (**Plate 1a** and **Plate 4**). See Stop #1, Appendix D, for digital images of the Keystone thrust fault in the Spring Mountains.

An isopach map of the Devonian clearly shows that the Monitor-Uinta arch has the same orientation and location of the Uinta aulacogen (**Plate 3**). Poole et al. (1992) named the eastern end of the arch, the Uinta uplift-Tooele arch. They suggested that it was a prong of the Transcontinental basement arch that extended from Colorado through northern Utah to eastern Nevada. The Monitor-Uinta arch affected deposition of Devonian quartz sandstones on the west and east edges of the Sunnyside basin (Chapter 7).

Other depositional troughs may have developed along the Proterozoic rift and may have influenced deposition of Devonian rocks in the region. South of the study area, in the Grand Canyon-Las Vegas area, more than 13,000 feet of middle and late Proterozoic rocks were deposited in a depositional trough that later became an “arch,” similar to the Monitor-Uinta arch (Poole et al., 1992).

Diamictite and volcanic rocks overlain by a thick (20,000 locally) terrigenous detrital late Proterozoic and Lower Cambrian rocks lie above the Proterozoic rocks (Poole et al., 1992). Carbonate rocks predominate the stratigraphic section between the Lower Cambrian terrigenous detrital rocks and the Middle Ordovician Eureka Quartzite (Cedar Strat proprietary measured sections; Poole et al., 1992). Barring Devonian sandstones and shales discussed in Chapter 4, the stratigraphic section between the Eureka Quartzite and the Mississippian Antler clastics is composed of carbonate rocks (**Table 1**, **Figure 8**). Carbonate deposition was probably related to a sea-level rise related to lithospheric cooling (Bond and Kominz, 1984).

## Devonian-Mississippian Antler Orogeny

Recognizing the stratigraphic contrast between eastern carbonate facies and western siliceous facies, Kirk (1933) predicted the Roberts Mountains thrust. Merriam and Anderson (1942) first mapped the thrust fault in Nevada and employed the western and eastern facies terminology. Kay (1952) was the first to suggest a mid-Paleozoic Age for the thrust. The Mississippian overlap deposits were documented by Dott (1955). Roberts et al. (1958), and Roberts (1972) first recognized siliceous marine rocks thrusted eastward over Devonian and older shelf carbonate rocks along the leading edge of the Roberts Mountains thrust-and-fold belt in mountain ranges northwest of Eureka. Subsequent work provided evidence that the Roberts Mountain thrust movement occurred in Late Devonian to Lower Mississippian (Ketner, 1970, 1977; Smith and Ketner, 1968, 1975). Devonian and older rocks were moved 125 miles eastward in Nevada (Poole et al., 1992). In central Nevada, the Roberts Mountain allochthon consists of locally metamorphosed Middle Cambrian to Upper Devonian quartzo-feldspathic and orthoquartzite turbidites, chert and argillite, limestone, mafic volcanic rocks, and locally lowermost Mississippian strata (Johnson and Pendergast, 1981). Shelf strata are exposed in allochthon windows (Poole et al., 1992; Carpenter et al., 1994). Smith et al. (1993) concluded that the contractional orogeny resulting in the emplacement of deep basinal, submarine-fan, and mafic volcanic strata over autochthonous continental margin strata extended along the entire Cordillera from Nevada to the Yukon. Stewart and Poole (1974) described a persistent positive belt that coincides with the western side of the Sunnyside basin (Chapter 7). They suggested that this positive belt may account for local erosional truncation of lower Paleozoic strata. Carpenter et al. (1994) provided additional evidence of erosional truncation of lower Paleozoic rocks below the Roberts Mountains allochthon and suggested that the positive trend was a forebulge related to the Antler orogeny. They provided evidence that the Antler orogeny in Nevada was initiated as a forebulge in the Frasnian and that the orogeny continued into the Meramecian. It is likely the same as the Lower Silurian through middle Lower Devonian Toiyabe ridge of Matti and McKee (1977). This study provides evidence that the Antler forebulge was likely initiated in late Lower Devonian. It was probably the source area for Devonian sandstones on the western edge of the Sunnyside basin (Chapter 7).

Mesozoic Sevier Orogeny

King (1870) first noted compressive folds in the mountain ranges of the region, and Spurr (1903) first recognized thrusting in the Great Basin. Misch (1960) added detail to descriptions of thrust faults and folds in central northeast Nevada. Armstrong (1968) was the first to distinguish between Laramide and Sevier structures in western North America, and to synthesize faults and folds in the eastern Great Basin.

Sevier Fold-and-Thrust Belt Multiple working hypotheses (Chamberlin, 1897) exist regarding the structural interpretation of the Great Basin. One widely accepted hypothesis is that the geomorphology of the Great Basin is a result of normal faulted horsts and grabens created during Cenozoic extension. It is believed by some (e.g., Hamblin, 1985), that the crust was arched upward and pulled apart in the region forming a complex rift system from northern Mexico to southern Idaho and Oregon. If range-bounding faults extend to lower levels of the brittle crust, then the grabens are true rift valleys (Quennell, 1987). However, Quennell (1987) suggested that if the faults flatten at depth, the resulting graben may not be a true rift valley. Carpenter and Carpenter (1994b), from their work in southern Nevada, suggested that listric normal faults reactivating earlier thrust faults may be responsible for the modern basin-range physiography and extension of the crust. They concluded that rooted low-angle normal faults or detachments do not exist in their study area in the Muddy and Mormon Mountain area, 50 miles southeast of the Timpahute Range 30' X 60' quadrangle. They used seismic and well data to support their interpretations. In contrast, Wernicke (1981) and Axen et al. (1990) suggested that low-angle normal fault systems composed of mantle penetrating detachments controlled crustal extension in the area. They ignored well and seismic data. Broad playas separating inselbergs containing Paleozoic rocks in the area invite unsupported speculations in their study area in contrast to the nearly continuous exposures of Paleozoic rocks in the Timpahute Range 30' x 60' quadrangle that constrain interpretations.

The ranges in the region have also been called fault-block mountains. Some suggest that the Basin and Range Province is one of the most extensive fault-block mountain systems in the world (e.g., Skinner and Porter, 1989; Carpenter and Carpenter, 1994b). However, large parts of the Basin and Range Province have not been mapped in detail. The valleys and ranges may have been formed by another process.

Another hypothesis is that the geomorphology of part of the Great Basin may be partly caused by compression during the Mesozoic Sevier orogeny (Chamberlain and Chamberlain, 1990). The orogeny resulted in a north-south belt of east-vergent thrust faults and folds that embodies much of the western Utah and eastern Nevada Great Basin (**Figure 1**). The new geologic map of the Timpahute Range quadrangle reveals few major normal faults that may be related to Cenozoic extension. However, it reveals many newly mapped folds and thrusts related to the earlier Sevier compressional event (**Plate 1a**, Chapter 5, Appendix E).

Other researchers have linked the Sevier fold-and-thrust belt to this region. Hintze (1988), for example, saw it as a segment of the 3,000-mile-long mountain chain that extends from southern California to Alaska. The Sevier fold-and-thrust belt is also part of the Cordilleran fold belt of King (1969). Tschanz and Pampeyan (1970) assumed that the major thrust faults in Lincoln County were Laramide age. In contrast, Chamberlain and Chamberlain (1990) identified the faults and folds exposed in the greater Timpahute Range as part of the Sevier fold-and-thrust belt (**Figure 2**). Cenozoic units, including Tertiary volcanic ash deposits, thin and pinch out over the ranges (anticlines) and thicken in the valleys (synclines). Typically, the underlying Paleozoic rocks dip toward the valleys and away from the ranges.

In addition, Sevier compressional features have been recognized in a narrow band from southern Nevada, through southwest and central Utah, to northeast Utah and southwest Wyoming (Armstrong, 1968). Late Cretaceous to Early Tertiary Sevier thrusting shortened basement and cover rocks by more than 60 miles in northeast Utah and southwest Wyoming (Decals and Mitra, 1995). Assuming the same degree of shortening for the rest of the Sevier belt between southwest Wyoming and central Nevada, at least 200 miles of shortening would have occurred (See Chapter 5). Elison (1991) concluded that the western North American Cordillera from southeastern British Columbia to northern Nevada experienced 180 miles of east-west crustal shortening. The distance between central Utah and central Nevada (200 miles) is several times greater than the part of the thrust belt exposed in southwest Wyoming (40 miles) and contains many significant thrust faults in that distance (**Figure 2**).

In contrast, Dilles and Gans (1995) concluded that the western margin of the Basin and Range has moved progressively 60 miles westward during the Late Cenozoic and created the Walker Lane belt on the west side of the Great Basin. However, my research shows very little evidence of Cenozoic extension in the greater Timpahute Range area of the Great Basin.

Some workers have tried to divide the Sevier fold-and-thrust belt into smaller thrust belts and mix Sevier structures with other orogenies (e.g., Taylor et al., 1993). As used by Cameron and Chamberlain (1987, 1988) and Hook et al. (1998), the Central Nevada thrust belt is part of the Sevier fold-and-thrust belt only (**Figure 2**).

<u>Sevier Fold-and-Thrust Belt in Nevada</u> The band of compressional features accepted by the USGS as part of the Sevier fold-and-thrust belt has widened to include part of Lincoln County, Nevada (Page, 1993; Swadley et al., 1994). I believe that some workers such as Stewart and Poole (1974) erroneously correlated the north-south trending Gass Peak thrust fault, 24 to 98 miles south of the study area, to the Wah Wah thrust fault, nearly 100 miles to the east in western Utah (e.g., their figure 2). Structural features in the Sheep and Pahranagat ranges strongly suggest that the Gass Peak continues northward

into the Timpahute 30' X 60' quadrangle. Others (e.g., Elison, 1991) placed westernmost Utah and northeastern and east-central Nevada, including the study area, west of the hinterland-foreland basin boundary. In his figure 1, Elison (1991) shows the hinterland-foreland basin boundary as a north-northeastward trending line in western Utah west of which are areas of Mesozoic metamorphism and where he shows a lack of east vergent thrust fault traces. However, abundant Sevier orogenic compressional features including thrust fault traces and associated syntectonic sediments occur as far west as the Pancake Range in Nye County and the Roberts Mountains and the Sulphur Spring Range in Eureka and Elko Counties, Nevada (Cameron and Chamberlain, 1987, 1988; Scott and Chamberlain, 1988a, b; Chamberlain, 1990c, 1991; Chamberlain and Chamberlain, 1990; Chamberlain et al., 1992a, 1992b; Carpenter and Carpenter 1994a, 1994b). This recent recognition of Sevier age compressional structures in central Nevada has important implications for petroleum and precious metal exploration (Chapter 8).

<u>Sevier Fold-and-Thrust Belt Analogue</u> The Canadian Rockies provide a thrust belt model that can help interpret the complex structure of the study area. Roeder (1989) suggested evidence to assume that the Nevada part of the Sevier fold-and-thrust belt has “a Dahlstrom geometry” similar to the Canadian Rockies. Similarities between the Nevada and Canadian Rockies portion of the thrust belt include: 1) Imbricate thrust sheets: a series of thrust sheets detached at a common deep horizon and that imbricately overlie one another in both thrust belts; 2) Total Displacement: total displacement in the Canadian Rockies is measured in tens of miles and stratigraphic displacement in thousands of feet (Gretener, 1972). In Nevada, total displacement is measured in tens of miles and stratigraphic displacement in thousands of feet; 3) Sedimentary wedge: Gretener (1972) pointed out the rapid thickening of the sedimentary section from Calgary to the Rocky Mountain Trench. Likewise, Paleozoic rocks thicken from hundreds of feet in central Utah to tens of thousands of feet in central Nevada (Cedar Strat proprietary

measured sections); 4) Progression of thrusting: Gretener (1972) noted that thrusting progressing outward or from west to east is well documented in the southern Canadian Rockies. Younger thrust faults are both younger and deeper. Folded thrust faults in the study area also suggest west to east progression of thrust faults; 5) Undeformed rocks at the leading edge of a thrust belt: Rocks east of the Canadian Rockies foothills are essentially undeformed (Dahlstrom, 1969). Similarly, Paleozoic rocks east of the leading edge of the Sevier fold-and-thrust belt, or Utah hingeline, are essentially undeformed. Differences between the Canadian Rockies and Nevada thrust belts include: 1) Precambrian basement. The Precambrian basement extends unbroken beneath the Canadian Rockies foothills structures (Dahlstrom, 1969). The nature of the Precambrian basement in the study area is unknown. It could be broken by Cenozoic normal faults. Metamorphic core complexes may provide windows into the Precambrian basement; 2) Cenozoic extension: Extensive Cenozoic extension is not known in the Canadian Rockies. Although little evidence for Cenozoic extension is found in the study area, much of the Great Basin is believed to have experienced considerable Cenozoic extension (Wernicke et al., 1988). Cenozoic extension is discussed further below in this chapter.

<u>Thrust Detachment</u> The exact decollements in the Sevier fold-and-thrust belt are not yet known. However, a series of finite element models of contractional deformation show that orogen evolution is strongly influenced by crustal architecture during the first 240 to 320 miles of shortening. Harry et al. (1995) provided evidence that major decollements develop at midcrustal and lower crustal levels, partition strain into upper crustal, lower crustal, and mantle strain domains, and extend throughout the width of the orogen. The most intense shortening occurs in the shallow crust as deformation propagates continentward (Harry et al., 1995). A crystalline basement is caught up in thrust sheets south of the Clark Mountains but may not be involved in Sevier thrusts north of the Clark Mountains (Walker et al., 1995). None of the thrust traces observed by me in the study

area involve crystalline basement rocks (**Figure 2**).

What previous research has not discovered, however, is the depth to the crystalline basement along the axis of the eastern Great Basin. No outcrops of crystalline basement occur in the study area. The depth to a crystalline basement can only be inferred from potential field data (i.e., gravity and magnetics, Appendix E). It can also be interpolated from surface outcrops of younger stratified rocks. Moreover, the western thickening of Paleozoic strata further frustrates attempts to find the depth to the crystalline basement. The problem is not unique to Nevada. Gwinn (1964) reported that the depth to basement along the structural axis of the Appalachian Basin was also imprecisely known.

The results of the Hunt Oil Company USA # 1-30 well (NE SE Sec 30 T1N R66E), near Pioche, Nevada (25 miles northeast of the study area), could provide insight into depth to basement. R. Fink (1997, personal communication) reported that the well penetrated nearly 9000 feet of Precambrian Prospect Mountain Quartzite before cutting into Mississippian Antler clastics. The nearest Mississippian Antler clastic outcrops are 15 miles on strike to the north, north of Bristol Pass. The fault in the well is most likely a low angle thrust fault. Tschanz and Pampeyan (1970) mapped thrust faults near Bristol Pass, 12 miles on strike north of the test. However, without the benefit of data from the Hunt well, Page and Ekren (1995) attributed the structures to a pre-Oligocene extensional decollement of younger on older rocks.

<u>Tectonic Model of Thin-Skinned Deformation</u> Rodgers (1949) pointed out two schools of thought concerning the Appalachian fold-and-thrust belt. One school follows the so-called thick-skinned thrusting theory and maintains that all major faults extend down to, and are supported by, a crystalline basement. The other school, following the so-called thin-skinned thrusting theory, supports the view that major bedding-plane thrust faults decouple the sedimentary cover and move it across the crystalline basement.

A similar controversy occurs in the Sevier fold-and-thrust belt because of a lack of regional seismic lines. Lack of control also originally retarded interpretation of the Appalachian fold-and-thrust belt. No regional seismic lines are available that clearly establish thin-skinned style of deformation for the Sevier fold-and-thrust belt. Nevertheless, inferences from a few scattered outcrops and several bore holes provide evidence that a north-south thin-skinned thrust belt runs through central Nevada (**Figure 2**, Cameron and Chamberlain, 1987). Moreover, balanced regional structural cross sections based on this evidence provide some additional information (**Plate 4)**.

Conclusive evidence of the economic potential of the thrust belt may have to wait for regional seismic lines and additional bore holes deep enough to penetrate buried thrusts. Picha (1996) showed many examples of thin-skinned thrust belts, one of which is the eastern edge of the Sevier fold-and-thrust belt in southwest Wyoming, which involves the Cretaceous Fossil Basin source rocks. Although he discussed their economic potential, he did not mention the part of the thrust belt that involves the Mississippian Antler basin source rocks in Nevada. Thin-skinned thrusting in the Timpahute Range quadrangle is similar to productive thrust belts in other parts of the world. Chapter 8 includes discussions of the economic application of this research.

## Cenozoic Volcanism and Extension

Before Cenozoic extension, the topographic evolution of the boundary between the eastern Basin and Range and the Colorado Plateau implies a topographic high in the Basin and Range that permitted drainage onto the plateau (Mayer, 1986). The boundary or transition zone between the Basin and Range and Colorado Plateau coincides with the leading edge of the Sevier fold-and-thrust belt.

Constenius (1996) concluded that the Cordilleran fold-and-thrust belt collapsed and spread west during a Middle Eocene to Early Miocene (ca. 49-20 Ma) episode of crustal extension. He suggested two periods of extension. The first resulted in half grabens and was concurrent with the formation of metamorphic core complexes and regional magmatism. For example, Horse Camp basin, 75 miles north-northwest of Hiko, developed during Miocene time above a west-dipping detachment fault (Horton and Schmitt, 1998). Best et al. (1993) suggested that this localized extensional faulting in the Great Basin probably occurred before the ignimbrite flare-up (31 to 22 Ma) and that regional extension was minimal during most of the flare-up (**Figure 7**). Cenozoic listric normal faults causing the half grabens probably exploited Mesozoic thrust faults in some basins in Nevada (Effimoff and Pinezich, 1986).

A second period of extension (ca. 17-0 Ma) resulted in the Basin and Range overprint of earlier events (Constenius, 1996). A result of the second period of extension, among others, (Late Miocene to Holocene) is the development of Railroad Valley basin and exhumation the adjacent Horse Camp basin (Horton and Schmitt, 1998). Timing of the event is not precise. Bohannan (1983) concluded that the precise time of initiation of Basin and Range deformation in the Muddy Mountain area, 100 miles south-southeast of the study area, is difficult to pinpoint. Based on Cenozoic units found in some valleys, he suggested that the basin and range deformation might have begun as early as about 13 Ma locally. Guth et al. (1988) suggested that extension structures in the Sheep Range, 50 miles south of the study area, were formed about 13 Ma.

Associated with the second extensional event is basaltic volcanism in the transition zone between the Basin and Range and Colorado Plateau. Nelson and Tingey (1997) concluded that basaltic volcanism in the transition zone resulted from east-west extension and that the maximum thinning or extension of the lithosphere occurs near the transition zone (**Figure 7**). Earthquake studies in the transition zone led Arabasz and Julander (1986) to conclude that background seismicity is controlled by variable mechanical behavior and internal structure of individual horizontal plates within seismogenic upper crust.

Although the topographic high or crustal thickening is likely caused by stacked imbricate thrust sheets, Mayer (1986) favored asthenospheric diapirism as the basic mechanism for continental rifting or Basin and Range extension. Similarly, Liu and Shen (1998) proposed a model that links the late Cenozoic uplift of the Sierra Nevada to ductile flow within the lithosphere induced by asthenospheric upwelling under the Basin and Range province. However, Okaya and Thompson (1986) pointed out that inflow of dense mantle material beneath a crust thinned by extension required by isostatically rising crust would result in elevations below sea level. Therefore they argued for igneous additions to the deeper crust of material of crustal density or of anomalously low mantle density. Rey and Costa (1999) argued for buoyancy-driven extension under low elevation conditions. In contrast, Jones et al. (1999) considered the hypothesis of low elevations at the time of Cenozoic extension suspect.

Furlong and Londe (1986) suggested that the specific mechanism for continental extension or rifting appears to differ from that of oceanic spreading centers. They pointed out that both pure and simple shear models proposed for the Basin and Range extension fall short in matching the observed elevation profile. They also pointed out that a uniform stretching mechanism obscures the evidences of simple shear. Pure shear involves uniform stretching and simple shear occurs along discrete low-angle shear zones. These zones of extreme extension involve metamorphic core complexes and are usually exposed in younger uplifted blocks but are older than faults responsible for the present Basin and Range topography (Okaya and Thompson, 1986). MacCready et al. (1997) suggested that the Ruby Mountain metamorphic core complex, 180 miles north of the study area, formed when Eocene-Lower Oligocene granitic magmas invaded middle crust rocks and resulted in highly extended upper crust rocks. Most metamorphic core complexes emerged during Oligocene to Miocene time (~36-16 Ma) (Rehig, 1986).

Liu and Shen (1998) concluded that the Basin and Range tectonic province (Great Basin) is one of the most extended continental regimes in the world. Metamorphic core complexes suggest 100% extension in the Great Basin (Rehig, 1986). Wernicke et al. (1988) concluded that their correlation of Early Mesozoic thrust faults suggests 155 to

186 miles of Neogene crustal extension in southern Nevada.

Cenozoic rocks deposited during the extensional and volcanic events conceal most of the Paleozoic rocks of the study area and provide a record of post-Paleozoic deformation (**Figure 7**). Tertiary/Cretaceous rocks associated with the Sevier fold-and-thrust belt that lie between the Cenozoic volcanic rocks and Paleozoic rocks are discussed elsewhere. At least sixty Tertiary calderas are responsible for thousands of cubic kilometers of ash-flow deposits that draped the pre-Oligocene Great Basin landscape (Best et al., 1993). In the study area, ash flows filled paleotopographic depressions and valleys such as footwall synclines or in prevolcanic strike valleys associated with folding and thrusting. In the Timpahute Range quadrangle and in the surrounding area, Oligocene volcanic rocks overlie folded Paleozoic rocks of various ages. Bartley et al. (1988) showed also an angular unconformity between Tertiary volcanics and Paleozoic rocks in the north Pahroc Range, 20 miles northeast of the study area. The angular discordance between the Oligocene volcanic rocks and the Paleozoic rocks implies that the Paleozoic rocks were folded and eroded before emplacement of the Oligocene volcanic blanket.

Though the study area is cut by abundant minor (10 to 100's feet of displacement) normal faults, no evidence of major (1000's feet of displacement) normal faults or reactivated thrust faults associated with Cenozoic extension were found in the study area (Appendix E). Edwards and Russell (1999) suggested that northern Cordilleran volcanic province of British Columbia is geologically similar to other extensional, continental volcanic provinces such as the Basin and Range and the East African rift system. They noted that all three regions have high surface heat flow values, are dominated by mafic rock, and are chemically bimodal. However, as with the study area, the northern Cordilleran volcanic province lacks pervasive extensional faulting. The Tertiary volcanics in the study area were buried by valley fill deposits eroded from the surrounding mountains (**Figure 7**). The present-day landscape of the study area is essentially a series of north-south trending inselbergs surrounded by an extensive lowland erosion surface. Continuous, extensive east-west exposures of Paleozoic rocks are rare.

## Summary

Previous investigators laid the stratigraphic and structural groundwork of an understanding of Great Basin Paleozoic rocks. Devonian formations defined beyond the Timpahute region were correlated to rocks in the study area. The reconnaissance map of Tschanz and Pampeyan (1970) generally differentiated Paleozoic rocks from Cenozoic rocks and grossly differentiated some Paleozoic rocks. Their map also provided a general view of some structural elements of the region.

The greater Timpahute Range (**Figure 3**), composed of forty miles of nearly continuous east west Paleozoic exposures, provides constraints on structural interpretations of the region. TMS is located near the center of the greater Timpahute Range. Devonian rocks in the range were deposited in the Sunnyside basin, an intrashelf basin on the western North American passive margin (**Figure 6**). Correlating Devonian sequences defined in the TMS reference section with other sections throughout the Sunnyside basin greatly simplified the formational terminology (**Figure 6**). The new map of the Timpahute Range 30' X 60' quadrangle sheds light on deformation of the Devonian rocks caused by the Sevier orogeny and subsequent tectonic events (**Figure 7**).

Earlier attempts to reconstruct the Devonian paleogeography of the study area were misleading because Sevier shortening was not documented, and thus was not taken into account. Conversely, attempts to map the structural features of the study area were incomplete because the identification and order of stratigraphic sequences were not recognized and used to solve structural problems. Therefore, structural and paleogeographic interpretations of the area needed reevaluation. This study illustrates the utility of mapping sequences for solving structural problems. It also illustrates the importance of understanding the structural complexities of the region to reconstruct the paleogeography. Methods to provide accurate data that constrain a new structural model and paleogeographic interpretations of the study area are the subject of Chapter 3.

# CHAPTER 3

# METHODS USED

Having stated the goals of this research and reviewed previous work, the methods to achieve the goals are discussed. Methods of data identification, data collection, and data analysis are discussed in this chapter.

## Data Identification

Mapped patterns of Paleozoic rocks in the eastern Great basin show a north-south structural grain (Stewart and Carlson, 1978). Either Mesozoic east-vergent crustal shortening or Cenozoic east-west extension, or both, were responsible for the north-south structural grain. Because of its anomalous east-west outcrop pattern of Paleozoic rocks, the greater Timpahute Range allows testing various structural models that may be responsible for the physiography of the region. These structural models can be tested by comparing and contrasting the stratigraphy of correlative units on the east and west sides of north-south trending faults. Therefore, an accurate geologic map and detailed stratigraphic sections are required to make the test.

Reconnaissance mapping revealed extensive Devonian outcrops and uncharted structural elements in the study area (Chamberlain and Chamberlain, 1990; Appendix E).

The Devonian section was chosen because measured sections throughout the region suggested little change in facies over much of the eastern Great Basin. A well-exposed section of Devonian rocks mostly on the southern edge of the Mail Summit 7.5' quadrangle was measured to provide a reference section to which the other sections could be correlated and to identify mappable sequences in the region. Construction of this stratigraphic framework resulted in identification of 21 regional correlatable and mappable sequences reported by Chamberlain and Warme (1996). These sequences were used to map more than 150 7.5' quadrangles in the region, 32 of which make up the Timpahute Range quadrangle (**Figure 3**, **Plate 1a**). Quadrangles mapped beyond the study area provided the locations of many thrust faults shown in **Figure 2** and allowed for testing structural models beyond the study area.

## Mappable Sequences

Using bounding surfaces and associated facies such as Lowstand Surfaces of Erosion (LSEs) and Transgressive Surfaces of Erosion (TSEs), lithofacies, biofacies, inferred depositional processes, and gamma-ray response, I divided the Devonian section into 21 mappable rock sequences (**Figure 13**). Sequence criteria presented in Chapter 4 are useful in mapping complex structures in the region. After I mapped the sequences at larger scales (i.e., 1:12,000), I combined them into formations to produce the smaller scale map **Plate 1a**. **Plate 6** is an example of mapped sequences at TMS.

Sequence criteria presented in Chapter 4 were also useful in correlating sequences to other Great Basin surface and subsurface sections throughout the intrashelf basin and inner shelf. These correlations were used to make isopach maps of each sequence. Most of the sequences are composed of bundles of thinner (10's feet) cycles. Goldhammer et al. (1993) and Elrick (1995) used cycle stacking patterns to help define sequences. The use of cycle stacking patterns still holds promise as a tool for stratigraphic application.

However, gamma-ray responses of surface sequences may provide a more effective and practical means of correlation and chronostratigraphic analysis, especially when using subsurface information in the data set. Subsurface logging techniques have proven their worth because they have wide application in reconstructing major marine environments (Asquith, 1970).

## Measured Sections

Helicopters were used to reconnoiter the region and choose possible stratigraphic sections to measure. Once a section was chosen, a traverse of the least structurally disrupted and best exposed section was chosen. This was done by creating a 1:24,000 scale reconnaissance geologic map of each 7.5-minute quadrangle, including the southwest Mail Summit 7.5' quadrangle (**Figure 4** and **Plate 1a**). Dirtbikes, motorcycles designed for cross-country, off-road use, greatly eased desert mapping by allowing quick, easy access to remote outcrops and terrain not accessible to four-wheel drive vehicles without disturbing environmentally sensitive terrains. Mounted with a clinometer adjusted for structural dip, a five-foot Jacob's Staff was used to measure section thicknesses. The outcrop profile, description, and gamma-ray measurements at 2.5-foot intervals were recorded on audio tape.

The outcrop profile is divided into four categories. These are: 1) covered slope (CS) where only scree shows the composition of the buried rocks; 2) partly covered slope (PCS) where some bedrock protrudes between covered areas; 3) ledges (LDG) where rocks are well exposed but can be easily negotiated; and 4) cliffs (CLF) where prominent outcrops can be climbed over with some difficulty and where near vertical rocks faces are prominent. The profile is portrayed graphically as a histogram (profile of the lithologic column) on **Plates 2a, 2b,** and **2c**.

Outcrop descriptions included cycle boundaries, internal lithologies, colors, textures, fossils, sedimentary structures, bedding, lateral and vertical changes and other significant information. A numerical value representing facies environment was assigned to each facies change while in the field. These data were used to construct a relative water-depth (relative sea-level) curve. Criteria used to make facies assignments are summarized in **Table 3** and illustrated in **Plate 5**. Approximately 500 thin sections of samples from the lower Guilmette sequences at TMS were used to confirm and adjust facies assignments made in the field. Selected photomicrographs of the thin sections are presented in Appendix C. Appendix B presents a detailed description of the cycles and sequences. **Plate 2a** presents these cycles and sequences graphically in a stratigraphic column.

**Table 3** Criteria used to make facies assignments in the measured sections of the study area and beyond. The most characteristic properties are in bold type.

| Facies # (**Plate 2a**) | Interpreted Facies | Diagnostic Features/Depth Indicators |
|---|---|---|
| 1 | Supratidal | Usually **dolomicrite**, forms recessive slopes, **very light-gray to yellow-gray**, microcrystalline to very finely crystalline, stromatolitic, ripple, wavy or parallel **laminations**, mud-chip breccia, rip-up clasts, windblown (well sorted, frosted grains) **silt and sand grains**, paleokarst, **solution breccias**, vugs, paleosols, terra rosa, **desiccation cracks**, bird's-eyes, **tepee structures**; laminated dolomicrites commonly cap shallowing-upward cycles and exhibits a **higher gamma-ray log signature** than adjacent more seaward strata. The most diagnostic features are the light color, laminations, dolomicrite, desiccation or karst features, scattered quartz silt and sand grains and a high gamma-ray log signature. |

**Table 3** Criteria used to make facies assignments in the measured sections of the study area and beyond. The most characteristic properties are in bold type.

| Facies # (**Plate 2a**) | Interpreted Facies | Diagnostic Features/Depth Indicators |
|---|---|---|
| 1.5 | Low supratidal | Usually **dolomicrite**, forms resistive slopes, darker (**medium- to light-gray**) than 1 but lighter than 2, thin bedded to **weakly-laminated**, ostracode grainstone, transitional between supratidal and intertidal strata. Forms the cap on shallowing-upward cycles where erosion has cut out high supratidal strata. Exhibits a higher gamma-ray log signature than intertidal rocks below but lower than supratidal rocks above. The most diagnostic features are weak laminations, light-gray color, and dolomicrite. |
| 2 | Intertidal | Commonly dolomicrite or dolomitic lime mudstone, characteristically partly covered intervals, **mottled** light- to very light-gray to medium dark-gray, microcrystalline or very finely crystalline to sucrosic, parallel-ripple or low-angle cross-laminations, low angle cross-bedding, channel and tidal flat quartz sandstone, shelly **intraclast lags, rip-up clasts**, vugs, sparse chert. Commonly lies between restricted-shelf and supratidal strata in a shallowing-upward cycle. May form base of a shallowing-upward cycle. Gamma-ray log signature is higher than low intertidal strata below but lower than supratidal strata above. Intraclast lags and mottles are the determining features. |

**Table 3** Criteria used to make facies assignments in the measured sections of the study area and beyond. The most characteristic properties are in bold type.

| Facies # (**Plate 2a**) | Interpreted Facies | Diagnostic Features/Depth Indicators |
|---|---|---|
| 2.5 | Low intertidal | Commonly dolomicrite or dolomitic lime mudstone, forms low ledges, dark gray to medium-light gray, brown-gray to medium gray, intraclast mudstone-wackestone, medium bedded, commonly **mottled/burrowed**. May form the base of shallowing-upward cycles but commonly occurs between restricted-shelf and subtidal strata. Gamma-ray log signature is lower than intertidal strata above but higher than restricted-shelf strata below. Relative cycle position and mottles/burrows are the determining factors. |
| 3 | Restricted subtidal-shelf | Limestone or dolomite, forms ledges, medium dark- to medium-light gray, ***Amphipora*** wackestone-packstone, **low faunal diversity,** some thin-shelled brachiopods, uncommonly gastropod-rich and rare stromatoporoids. Usually occurs between transgressive basal open-shelf and shallow intertidal strata. Gamma-ray signature may be lowest value in the cycle, but commonly underlying open-shelf strata exhibit slightly lower radiation. The presence of *Amphipora* and low faunal diversity provide the most diagnostic criteria. |

**Table 3** Criteria used to make facies assignments in the measured sections of the study area and beyond. The most characteristic properties are in bold type.

| Facies # (**Plate 2a**) | Interpreted Facies | Diagnostic Features/Depth Indicators |
|---|---|---|
| 3.5 | Partially restricted subtidal-shelf | Limestone or dolomitic limestone, forms prominent ledges, medium light- to dark-gray or light brown-gray, **small rounded stromatoporoids** and *Amphipora* packstone-wackestone, burrowed/mottled mudstone, massive to medium bedded, dolomite/limestone, crinoids, rugose corals, grainstones, storm lags. Commonly forms the basal part of shallowing-upward cycles and emits less gamma radiation than adjacent strata. Small rounded stromatoporoids are the most significant criteria. |
| 4 | Open-shelf | Limestone (rarely dolomite), forms prominent ledges or cliffs, dark-medium gray, **crinoid**, coral (rugose or colonial) brachiopod, bryozoan, gastropod mudstone-wackestone-packstone, with **bulbous-tabular stromatoporoids**, rich **faunal diversity**, abundant fossil fragments. Commonly forms transgressive strata over the base of shallowing-upward cycles and usually exhibits a sharp decrease in gamma radiation. Crinoids, massive to tabular stromatoporoids and rich faunal diversity in limestone form the most important criteria. |

**Table 3** Criteria used to make facies assignments in the measured sections of the study area and beyond. The most characteristic properties are in bold type.

| Facies # (**Plate 2a**) | Interpreted Facies | Diagnostic Features/Depth Indicators |
|---|---|---|
| 4.5 | Deep open-shelf | Limestone, with rare early-formed dolomite, forms thin ledges, **medium dark gray**, nodular lime mudstone, with uncommon **crinoid** or **brachiopod fragments**, burrowed, with **chert stringers**, massive to thick bedded. Rarely forms the lower part of shallowing-upward cycles. Hummocky crossbedding at the base of some cycles. Gamma-ray log pattern is similar to open-shelf carbonates. Crinoids and brachiopods, darker gray limestone than open-shelf strata, and chert stringers provide diagnostic criteria. |
| 5 | Shelf edge | Limestone, forms thin ledges or partly covered slopes, medium gray-**black**, lime mudstone, very thin- to thin-bedded, laminated, **chert nodules and lenses**, rare fossils, abundant load casts/soft sediment deformation. Rarely forms the base of shallowing-upward cycles. Gamma-ray radiation is higher than with open-shelf strata. This and the next three facies occur almost exclusively in the Guilmette Formation above Sequence Dgb at Tempiute Mountain. The black color and chert are diagnostic features. |

**Table 3** Criteria used to make facies assignments in the measured sections of the study area and beyond. The most characteristic properties are in bold type.

| Facies # (**Plate 2a**) | Interpreted Facies | Diagnostic Features/Depth Indicators |
|---|---|---|
| 5.5 | Upper slope | Limestone, forms partly covered slopes, **dark gray**, **no fossils**, contains **bedded chert**. Gamma-ray log signature is relatively high but lower than the more shallow strata above. Rarely preserved between more basinward shelf slope strata and shoreward shelf-edge strata of 5. These and the two positions following are unique to the Tempiute Mountain section. Dark-gray limestone with bedded chert and lack of fossils are diagnostic features. |
| 6 | Slope | Limestone, forms covered slope with sparse prominent ledges, lime mudstone, rhythmic **thin-bedded limestone** with pale-red **siltstone partings**, isoclinally convoluted **soft sediment deformation**, sparse deepwater trace fossils. Gamma radiation is relatively low and is similar to the gamma-ray signature over open-shelf strata at the base of shallowing-upward cycles. Diagnostic features include, rhythmically, thin-bedded limestone and convolute, soft-sediment deformation. |
| 7 | Base of slope | Sandstone, forms thin ledges and partly covered slopes, light- to dark-gray, fine- to coarse-grained, **lithic graywacke**, deepwater sandstone (**turbidites**) and siltstone, interbedded thin-bedded unfossiliferous silty limestone, deepwater trace fossils. Occurs **rarely** in the Tempiute Mountain section above Sequence Dgb2 Guilmette Formation. A gamma-ray log signature is usually lower than overlying shelf-slope strata. Lithic graywacke is the most characteristic feature. |

Lithologies were determined visually in the field using hydrochloric acid to detect the presence of calcium carbonate and a hand lens to detect the presence of quartz grains and other inclusions. Color was determined by comparing rock chips with the GSA rock-color chart (Goddard et al., 1984). Texture was assigned in the field using Dunham's (1962) classification and in thin section using Folk's (1962) classification. Where possible, the standard grain size scale for inclusions was used. I used the same criteria for crystal size where primary texture was obliterated by recrystallization.

## Stratigraphic Terminology

In this report, I apply the most widely accepted sequence stratigraphic terms to describe and interpret the Devonian strata in Nevada (see Baum and Vail, 1988; Weimer, 1992). A sea-level Lowstand Surface of Erosion (LSE) is an unconformity or a significant hiatus formed during a relative lowstand of sea level that forms a sequence boundary of any scale. In carbonate rocks, LSEs are signaled by zones of karst, paleosols, or erosion. A Transgressive Surface of Erosion (TSE) is a hiatus within or at the base of every sequence. It is formed by intertidal to submarine erosion of the seabed during episodes of a sea-level rise and landward shifts of the shoreline. It commonly represents minor erosion, transgresses time surfaces, and may be a sharp surface or rendered vague by bioturbation. A Maximum Flooding Surface (MFS) is formed during sea-level transgression and highstand. It represents a surface or interval of deepest marine conditions with sediment starvation over much of the shelf. A Condensed Section (CS) represents beds accumulated during a sea-level highstand above the MFS where the rate of deposition is low over a wide area. It commonly consists of pelagic shale or lime mudstone. It may be lacking benthic fossils, have a depauperate benthic fauna, or contain "deep water" ichnofacies assemblages, hardgrounds, lags that shifted about during periods of zero net deposition.  It should have an enhanced nautiloid, conodont, and acritarch fauna (E. Brown, 1998, personal communication).

The base of a unique sequence (Guilmette Sequence Dgb2, Chapter 4) related to a Devonian cosmolite impact does not fit LSE or TSE criteria for erosional sequence boundaries.  High-pressure phenomena associated with the impact created a carbonate breccia fluidized zone between strata.  Because the fluidized zone was created by processes more closely related to impact tectonic processes than erosional processes associated with changes in relative sea level, a new sequence boundary term is applied herein.  A Disrupted Surface of Erosion or DSE connotes impact tectonic disruption of already deposited beds in contrast to TSE and LSE that connote erosion and deposition associated with sea-level changes.  A DSE occurs as a thin (one inch to several feet thick) zone of Dgb2 at the base of Dga2 at TMS.  Possible tectonic processes forming a DSE could include shearing between beds, shock pressure that liquefies the carbonate, or carbonate breccia liquefaction between beds under extreme high pressure and short duration conditions (see Appendix C for examples of liquified carbonate rocks in thin sections from the base of Guilmette Sequence Dgb2).

## Data Collection

Data were collected using a variety of modern techniques, equipment, and software all designed to increase accuracy and efficiency.  This section briefly reviews the technology used to measure the Devonian sequences and map the geology of the study area.

Global Positioning Systems (GPS)

A Pathfinder Pro global positioning system was used to assure accuracy in locating field stations to make geologic maps. Pathfinder Pro is a trademark of Trimble Navigation, Limited. The global positioning system affords precise locations (within a meter). It allows field attributes such as attitudes (dip and strike) of the strata, lithology, stratigraphic sequence, inclusions, and other descriptions to be recorded onto a hand-held computer in the field at each station. These field attributes are recorded along with location coordinates found by recording at least 25 satellite signals with a roving Pathfinder Pro receiver. These data are stored in a tabular form that could easily be used for additional analysis. Satellite positions were simultaneously recorded using a Trimble Navigation 4600LS Surveyor receiver at a precisely located base station in Hiko. Post-field processing and differentiation using the satellite signals from the base station and roving unit provided accurate sub-meter positions of field stations. The digital data were downloaded directly onto digitized 7.5-minute quadrangles formatted with *MapInfo*, a type of Geographic Information System (GIS) software. *MapInfo* is a trademark of MapInfo Corporation.

Accurate positioning provides a great advantage for field methodology because it reduces controversy over fault angles, location of formation contacts, and sample locations. It also provides for repeatability of results: Future investigators can use Global Positioning Systems to navigate to precisely the same location where geologic observations were made or where samples were taken. Furthermore, a Global Positioning System eliminates errors in transposing data from field notes to the final geologic map. As a result, interpretation controversies concerning some fault attributes can be eliminated and field data can rapidly and accurately be added to the geologic map. Approximately three times more area can be precisely mapped in the same amount of time than using less precise, cumbersome, and outmoded methods of the past such as mapping on aerial photographs without GPS support.

Aerial Photographs and Field Work Maps

Besides using GPS methods, geology of the Timpahute 30' X 60' quadrangle was mapped on 1:24,000-scale, color aerial photographs taken by Intrasearch Incorporated and on field work maps. Photograph stereo pairs were used to plan traverses, pick outcrops for study, and identify critical relationships to investigate. Mapping in the field was done directly on 1:24,000, or where needed, 1:12,000 or 1:6,000 work maps generated from digitized United States Geological Survey topographic quadrangles overprinted with digitized published geologic maps (e.g., Hess and Johnson, 1997). Colored field work maps were plotted using a Hewlett-Packard DesignJet 7500C plotter. Much of the detailed, 1:24,000 topographic data have become available only in the mid 1980's. Though much of the Timpahute Range quadrangle was mapped on large scale (1:12,000 or 1:6000) work maps using the 1:24,000 topographic base maps, only the smaller scale (1:75,000) compilation using the 1:100,000 topographic base map is necessary for the scope of this study.

Field notes made on the field work maps were compared with the images on color aerial photographs and then compiled onto a master map using *MapInfo*. Contacts, faults and other features were drawn directly onto the photographs with erasable ink. Predictions of trends were made on the photographs before going back to the field. The trends were confirmed or corrected after being field checked. The color aerial photographs allowed me to distinguish subtle differences between formations and identify areas of hydrothermal alteration. Hydrothermally altered areas commonly are associated with major fault systems. I discovered several, mostly concealed, outcrops in the pediments by using the color photographs. Also, color imagery allows for easy identification of jeep trails, subtle changes in vegetation related to underlying bedrock, and other subtle features that are not clearly visible on black and white imagery.

<u>Geographic Information System (GIS)</u>

Field data were readily downloaded into *MapInfo* from the Geographic Positioning System for quick generation of accurate, colored geologic maps. Digitized topographic base maps were prepared by using a line trace program that converted scanned raster images of U.S. Geological Survey topographic quadrangles into vector maps. The vector maps were imported into *MapInfo* using the Universal Transverse Mercator NAD 27, Zone 11 for the United States coordinate system. The digitized geologic map of Lincoln County was prepared by the Nevada Bureau of Mines and Geology. The scale of the vector 1:250,000 geologic map was changed to fit over the vector 7.5' topographic maps. Geologic features including fault and formation contacts were manipulated with *MapInfo*. Precisely pinpointed and oriented dip symbols and labels were created at each station using a complementary program, *Vertical Mapper*. Each attribute such as faults, attitudes, geologic attributes, geographic attributes, hydrology, cultural attributes, elevation contours, and labels were placed in separate layers within the mapping program. By putting attributes in each layer, maps that emphasized different features or various combinations of them could be easily generated. Because any part of the maps could be enlarged to any scale, much of the mapping was done with greater precision than the normal 1:24,000, namely at 1:12,000 or 1:6,000. Generating ancillary larger-scale maps, such as 1:24,000 or larger, using geology from published maps or new data was advantageous.

The geologic map made for this study was made by using the vector U.S. Geological Survey Timpahute Range 30' X 60' 1:100,000-scale topographic map. The digital format allowed for quick changes and productions of maps at any scale. **Plates 1a** and **1b** are the same scale (1:75,000) and have the same color scheme to compare new and old geologic maps.

## Gravity Data

Digital gravity data (Ponce, 1997) was contoured using *Surfer*, a contouring program. *Surfer* is a trademark of Golden Software, Inc. The digital contour map was reformatted for *MapInfo* and was used to create figures in Appendix E. Talisman Oil Company provided a much more refined digital contour map used to overlay the Timpahute 30' X 60' geologic quadrangle map during the interpretation phase of this study. However, because it cluttered the map, the gravity and magnetic map layers were turned off to produce **Plate 1a**.

## Computer-aided Structural Cross Sections

Dahlstrom (1969) suggested that the first step to construct a balanced cross section is to establish a pair of reference lines at either end of the section in areas of no interbed slip. His example in the Alberta foothills extends eastward into the undeformed Alberta plains. However, the portion of the Sevier fold-and-thrust belt in the study area lies more than 100 miles west of the correlative undeformed rocks in central Utah. Much of the intervening area is covered. Therefore, a balanced cross section of the study area is not possible using the method and ground rules outlined by Dahlstrom (1969). Roeder (1989) noted that his cross sections of the Timpahute Range and northward are open thrust systems and cannot be balanced. Furthermore, Mukul and Mitra (1998) noted that the assumptions that deformation within an individual thrust sheet are limited to flexural slip for line balancing and plane strain for area balancing breaks down into internal sheets where beds are penetratively deformed as in the Sheeprock thrust sheet, central Utah. Therefore, they stated that balanced cross sections constructed across the entire fold-and-thrust belt and their restoration will not be completely accurate.

Dahlstrom (1969) suggested that other ground rules will apply to other structural provinces beyond the Canadian Rockies foothills. Fortunately, the distinctive Guilmette Dgb2 breccia provides such a marker that allows for more accurate construction of balanced cross sections and restorations of the greater Timpahute Range (see Chapter 7). **Plate 4a**, constrained by the geologic map and distribution of the Guilmette Dgb2 breccia, exhibits a balanced cross section of the Timpahute Range that is probably more accurate than would otherwise be possible.

The new geologic map provides a spatial model of the structure and geology of the region. Verification of geometric balance of vertical models such as **Plate 4a** can be facilitated using computer programs such as *GeoSec*. *GeoSec* is a trademark of GeoScience Corporation. These programs take advantage of the vector topographic and geologic data and allow rapid construction of vertical profiles annotated with formation contacts, faults, and apparent dip directions of any desirable transect. These profiles are used to construct balanced structural cross sections and restorations. The software insures geometric precision and allows structural restoration in dimensions. Fermor (1999) suggested that in many areas of the Alberta Foothills structural restoration in only two dimensions is apparently invalid. However, the geologic models depend on both the operator's experience and the accuracy of the available data.

**Plate 4a**, a geometrically balanced structural cross section of the greater Timpahute Range, was constructed using the software program *Thrustbelt*. *Thrustbelt* is a trademark of International Tectonic Consultants, Limited. **Plate 4b** is the restored cross section. The program used a process of forward modeling.

First, thicknesses of stratigraphic units from sections along the line of transect were acquired. The line of transect is generally along A-A' on **Plate 1a**. Bends in the transect, minor faults and intrusives were ignored as they contribute little to the structural model. Thicknesses of units were compiled from Cedar Strat and Shell proprietary measured sections, published sections, and new measured sections for this study. Some thicknesses are noted on the geologic profile on the lower part of **Plate 1a**. The thrust fault angle through different strata was assumed. For dense carbonates, the angle was assumed to be greater (25º-30º) and for less competent shaly intervals it was assumed to be much less (5º-10º).

Second, based on the facies and thicknesses of the stratigraphic units, an undeformed stratigraphic cross section was assumed. The original positions of the stratigraphic sections within the cross section were partly determined from a previous structural cross section model by Chamberlain and Chamberlain (1990) using a snip-reconstruction or rigid body cut and paste restoration. The cross section was modeled after other cross sections in the Great Basin by Roeder (1989).

Third, the cross section was created through successive iterations until it matched the geologic map (surface geology, topography, well tops, etc.). Although the geologic interpretation may be flawed, the section is geometrically balanced and is a possible solution. The computer program helps to quickly eliminate impossible or geometrically unbalanced cross sections.

A more rigorous modeling program, *GeoSec* mentioned above, could be used to restore stratigraphic sections to their undeformed position. *Thrustbelt* used in this study employs only the vertical slip kinematic algorithm. In contrast, *GeoSec* uses many algorithms such as the fault propagation model, fault bend model, etc. that takes into an account flexural slip. However, such a rigorous analysis is beyond the scope of this study.

## Surface Gamma-Ray Logs

Surface gamma-ray logs were employed in this study to aid the correlation of stratigraphic sequences between structural sheets and subsurface sections (**Figure 12**). They provide much more resolution in local regions than correlations based on conodont zones. However, conodont zones provide worldwide correlations and show time gaps between sequences where zones are missing.  Furthermore, conodonts can be used as independent depth (paleoenvironment) indicators and thermal alteration indicators (Conodont Alteration Indices).  Nevertheless, gamma-ray patterns of sequences can provide more correlation resolution in the Sunnyside basin.  For example, most of the Guilmette is represented by the *diparilis*, *falsiovlais*, *transitans*, *punctata*, *hassi*, and *jamieae*, conodont zones (**Figure 10**).  Surface gamma-ray patterns of ten major regional correlatable Guilmette sequences and more than twenty subsequences greatly refine correlations in the Sunnyside basin.  Most sequences were broken down into regionally correlatable subsequences.  Each sequence and subsequence is marked by a unique gamma-ray pattern that can be correlated to sections within the eastern Great Basin.  The major advantage of using sequences over conodont zones in correlations is that they can be identified on outcrops and in well logs.  Furthermore, well cuttings may be too fine or not plentiful enough to yield diagnostic conodont faunas.  Also, extracting conodonts from dolomitized intervals is difficult.  However, gamma-ray logs are easy to obtain from wells and outcrops.  Gamma-ray sequence correlation methods were perfected during the study.  A future study could focus on correlations of conodont zones with sequences (Chapter 9).

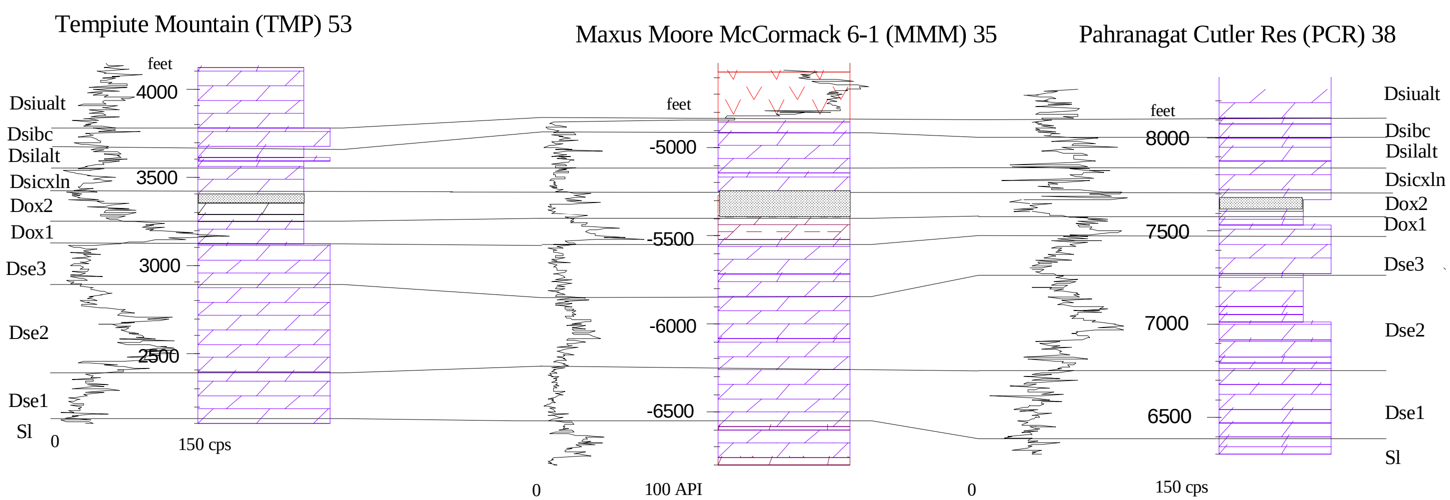


**Figure 12** A correlation chart of subsurface to subsurface Middle and Lower Devonian sequences from Tempiute Mountain southeastward (see **Figure 9** for section locations) illustrates the utility of using gamma-ray logs.

Surface gamma-ray logs provide a powerful correlation tool in frontier areas especially where surface and subsurface (wells) sections need to be correlated (Chamberlain, 1983). They provide physical measurements that tie exposures of stratigraphic sequences to seismic reflectors for use in seismic stratigraphy. **Figure 12** provides an example of surface and subsurface correlations in the Timpahute Range region (**Figure 9**). Sequences tied with gamma-ray logs can be tied to sonic and neutron density logs, which in turn are tied to seismic reflectors.

Correlations based on gamma-ray profiles can help where facies change between sections. For example, the gamma-ray spikes at the base and the top of the "Oxyoke Formation" allow correlation between sections, despite lateral changes in lithology. These gamma-ray spikes may be due to periods of greater amounts of radioactive dust falling from the atmosphere. These dusty periods likely occurred during periods of drought and high winds and could be possibly related to distant volcanic activity. Gamma-ray spikes most commonly occur at the top of cycles that contain evidence of subaerial exposure. Admittedly the correlatable gamma-ray spikes are subtle. Nevertheless, they can provide reliable markers for correlations. Examples of additional correlation charts using gamma-ray logs are presented in the summary of Chapter 4 and in Chapter 7.

Gamma-Ray Logs vs. Fischer Plots A Fischer plot is a graph in which cumulative cycle thickness of peritidal carbonates is corrected for linear subsidence and plotted versus time using an average cycle period (Read and Goldhammer, 1988). Whether Fischer Plots are useful guides to sea-level history and correlation between sections is controversial. Sadler et al. (1993) defended the usefulness of Fischer plots to track the cumulative departure from mean cycle thickness through a vertical sequence of continuous shallowing-upward units. However, Drummond and Wilkinson (1993) argued for the lack of a direct correlation between multiple-frequency eustatic sea-level variations and meter-scale cycle stacking hierarchies. The assumption that each individual cycle represents a single sea-level rise explicit in using Fischer Plots as guides to sea-level history may be flawed. Multiple autocyclic shallowing-upward cycles may originate during any single rise in sea level. Elrick (1995) concluded that Fischer plots are of limited use as a correlation tool for Devonian Great Basin carbonates. Thus, the gamma-ray curve provides an alternative, and practical, means for overcoming limitations of using Fischer plots and other stacking techniques for correlations. The value of gamma-ray profile correlations has been repeatedly proven by oil industry geologists.

Gamma-Ray Field Data Acquisition Consistent gamma-ray measurements were made by holding a scintillation counter waist high and recording the average counts per second from the digital display (Chamberlain, 1983). The count rate is set at one second intervals. I found that taking measurements at a consistent interval simplifies construction of gamma-ray logs. For most of my work in the eastern Great Basin, a five-foot Jacob’s Staff, mounted with a Brunton compass (clinometer), provided a convenient interval for measuring thicknesses of strata. The clinometer was set to correct for tectonic tilt of the strata and allowed measurement of the section in five-foot increments of true stratigraphic thickness.

Having two-man teams was helpful. One member of the team measured the interval, provided the tally of measured intervals and recorded the gamma-ray counts per second. The other described the strata in the five-foot interval. If the sections were reconnaissance sections, then the team could measure and record the data continuously as they moved up through the section. For detailed sections, as in this work, each five-foot interval is marked on the outcrop with biodegradable tree paint. The marked section allows for detailed description and study of the strata.

The Scintrex BGS-4, with its digital display, was the easiest to use, and it gave gamma-ray logs the best resolution. The Scintrex BGS-4 is a trademark of the Scintrex

Corporation. Fluctuating intensity of gamma radiation makes the Mount Sopris model with its analogue meter difficult to use. Mount Sopris is a trademark of Mount Sopris Corporation. The BGS-4 has a large enough iodide crystal to provide satisfactory resolution. For most work, only one measurement is needed. Others prefer to average three to five measurements (R.M. Slatt, 1997, personal communication). The reason for holding the scintillation counter waist high is to get an average measurement for the five-foot interval measured with a Jacob's Staff. The intensity of gamma radiation from the rocks is a mass effect. The closer the scintillation counter is held to the rocks, the higher the reading. This higher reading dampens the resolution of the gamma-ray log. Poor-quality logs result from inconsistencies in the distance the scintillation counter is held from the rocks. For shorter intervals, the scintillation counter is held closer to the outcrop. However, gamma-ray character can be sacrificed at the expense of an attempt to construct more accurate logs if the detector is held too close to the outcrop when measuring greater intervals of rock. Carefully collected, measurements can provide enough resolution to identify cycles in a gamma-ray log if the cycles are thicker than the interval measured.

I have found that calibrating the scintillation counters is not necessary if measurements are taken by the same instrument during a brief period. The reason for this is that only the relative changes in gamma-ray counts are necessary to create a correlatable gamma-ray profile. It would be necessary to calibrate the instruments if different segments of the measured interval were measured by different scintillation counters or if portions of the measured interval were measured between long periods.

A hand-held tape recorder simplified data collection in the field. By this method I could dictate a thorough description more quickly than by taking notes manually. If station number, a measured interval tally, gamma-ray measurement and lithologic descriptions are systematically dictated, the data can be transcribed onto spreadsheets for data manipulation and log construction.

## Data Analysis

Most of the data were analyzed using a computer. Measured sections were put on a spread sheet to aid in efficient data manipulation and presentation. Mapping was compiled from GPS data using a GIS to make presentation maps. The following section provides more detail on how the stratigraphic data were analyzed.

### Regional Correlations

Diagnostic features and water depth indicators listed in **Table 3** were used to help identify and group sets of shallowing-upward cycles into sequences in the regional correlations. I used significant features listed in **Table 4** (Chapter 4) to identify and differentiate sequences as I mapped. I found these sequences to be indispensable tools for mapping complex structures in the study area and beyond. The TMS reference section with its gamma-ray profile was also useful in correlating surface sections with other surface and subsurface sections at a higher level of detail and precision than otherwise possible (e.g., **Figure 12**). Also, by correlating sections in loops, miscorrelations could be detected and adjusted and significant sequence boundaries properly defined. Thus, the sequences of the Mail Summit reference section were refined. Examples of additional correlation charts are in the summary of Chapter 4 and in Chapter 7.

Predictable gamma-ray patterns were especially helpful in correlating the sections. At TMS and other sections in the Sunnyside basin, a genetic relationship between gamma-ray inflections and rocks associated with different depositional settings seems to occur. Wilson and Pilatzke (1987) suggested that gamma-ray inflections were caused by an increase of wind-blown, radioactive detrital grains that occur at the top of Devonian Duperow cycles in the Williston Basin. Altschuld and Kerr (1982) also noted increased radioactivity associated with supratidal dolomite and anhydrite at the top of shallowing-upward cycles that cause high radioactive reading on logs. Similarly, the Mission Canyon Formation in North Dakota displays argillaceous and sandy dolomite marker beds, as noted by Harris et al. (1966). Swart (1988) showed that uranium concentrations in a core taken from Miocene and Pliocene rocks, island of San Salvador, Bahamas, are higher at dissolution surfaces than in adjacent strata. Chan (1999) suggested that a surface gamma-ray log of a paleosol in the Mahogany member of the Triassic Ankareh Formation, north-central Utah could correlate to subsurface well logs. She showed the sharp gamma-ray decrease from the Mahogany member to the Gartra Grit. She also illustrated a gamma-ray spike at a paleosol at the top of the Mahogany member. Similar gamma-ray spikes occur at sequence boundaries in the Great Basin Devonian rocks.

In contrast to higher gamma radiation over dolomite caps at the top of shallowing upward cycles, gamma radiation is typically much lower over carbonates interpreted to have been deposited in open-marine conditions. Because these patterns are so predictable, it is likely that the radioactive particles were deposited during the Devonian. Uranium and the associated thorium mineralization in Devonian rocks of the Sunnyside basin have not yet been detected.

## Data Manipulation

Stratigraphic field data were transcribed onto a spreadsheet for further data manipulation and preparation for graphic output. Common spreadsheet programs such as *Excel* or *Lotus* 1-2-3 provided a simple way to format the data. *Excel* is a trademark of Microsoft Corporation and *Lotus 1-2-3* is a trademark of Lotus Corporation. Once the data are in a spreadsheet, statistical values for different lithologic characteristics such as gamma-ray intensity, color, texture, weathering profile, lithologies, etc. can be easily calculated and presented in detailed descriptions and graphics of cycles, sequences and formations. Statistics, such as average gamma radiation, standard deviations, etc.

presented in detailed descriptions of the lower Guilmette Formation in Chapter 4, were calculated in this manner. Because all the Cedar Strat proprietary sections were prepared in this manner, it greatly helped correlations of Devonian sequences throughout the Sunnyside basin.

Text editor programs such as *Word Perfect* were used to format the data for the graphics program, *Logger*. *Word Perfect* is a trademark of Corel Corporation and *Logger* is a trademark of Rockware Corporation. *Logger* was used to make combined gamma-ray logs and lithologic logs. A paper printout of the measured section at a large scale (e.g., one inch to 10 feet) allowed detailed correlation of the gamma-ray log with the outcrop description. A final printout at smaller scales (e.g., one inch to 200 feet) compressed the gamma-ray log and emphasized subtle, but significant, changes. These helped to discriminate sequence boundaries (**Plate 2a**). The gamma-ray log is compressed much more (e.g., one inch to 2000 feet) and the lithology greatly generalized in **Figure 8**.

# CHAPTER 4

# DEVONIAN SEQUENCES

The first objective of this research was to give a more detailed account of the Devonian sequences found in the study area and identify regionally correlatable sequences to be used to map the Timpahute Range quadrangle. Topics in this chapter include Devonian sequences, their relationship to the geologic map, sequence boundaries, and mechanisms for cycle and sequence development. It contains descriptions of each Devonian sequence at TMS and how they correlate to other sections in the region. Diagenesis and the occurrence of dolomite in the section are briefly discussed at the end of the chapter.

## Sequences

This section contains a brief discussion concerning the importance of recognizing Devonian sequences at TMS in constructing the geologic map and it provides examples of how sequences helped reveal overlooked geologic features. It also contains the framework for recognizing sequence boundaries at TMS and includes a review of some mechanisms for cycle and sequence development.

### Devonian Sequences

Recognition of stratigraphic sequences was essential for constructing an accurate geologic map to constrain a reasonable structural interpretation of the complexly deformed rocks in the Timpahute Range quadrangle. In this study, emphasis was placed on mapping Devonian sequences, which are widespread throughout the quadrangle. Obscured by the massive appearance of the thick (100's feet) formations in the Timpahute Range, many significant structural features were overlooked or misidentified. Division of the TMS Devonian formations into mappable sequences provided a way to enhance structural resolution. This higher resolution was necessary to map structural features overlooked in previous mapping using entire formations. Some formations were misidentified on previous maps.

<u>Stratigraphic Sequences and the Geologic Map</u> Using the stratigraphic order of Paleozoic sequences in mapping helped reveal important structural relationships. For example, few workers have recognized the overturned rocks in the Monte Mountain and Penoyer Springs footwall synclines (e.g., Taylor et al., 1993). Though Tschanz and Pampeyan (1970) showed the overturned fold on their map, Taylor et al. (1994) did not discuss the overturned Silver Canyon footwall syncline. It is understandable that the overturned rocks were overlooked because top and bottom indicators such as geopetal structures are rare. However, the order of shallowing-upward cycles in sequences reveals the up section sense of the beds and could be applied to geologic mapping.

Other subtle features were understandably overlooked. For instance, Taylor et al. (1993) published a geologic sketch map of the Penoyer Springs area that did not show the strike-slip displacement of the south Penoyer Springs and Tunnel Spring faults (see **Plate 1a**). In Appendix E, which contains discussions and illustrations of these faults, a map shows that the south Penoyer Springs fault offsets the Pilot Formation 1.3 miles and the Tunnel Springs fault offsets the Penoyer Springs thrust fault 1.4 miles. Armstrong and Bartley (1993) made conclusions about the lateral thrust termination in the southern Golden Gate Range without recognizing key units and faults at the thrust termination in Baseline Canyon discussed in Appendix E. They mismapped West Range Limestone and

Joana Limestone as Guilmette Formation at the Baseline Canyon fault that intersects their thrust fault termination. DuBray and Hurtubise (1994) reversed the thrust fault interpretation of the Fossil Peak thrust by Tschanz and Pampeyan (1970) without recognizing key beds involved in the faulting. It is shown in Appendix E that they mismapped Silurian Laketown Dolomite as Sevy Dolomite and that they did not map a thin exposure of Eureka Quartzite in fault contact with the Laketown Dolomite. Also, they overlooked the Fossil Peak footwall anticline highlighted by Devonian Sequences (Appendix E). Martin (1987) and Tschanz and Pampeyan (1970) did not recognize key stratigraphic and structural relationships and mistakenly changed the stratigraphic displacement at the north end of Freiburg Mountain from Ordovician on Devonian to Ordovician on Ordovician. Recognition of Devonian sequences in the footwall east of Worthington Peak improved the accuracy of the geologic map in this area. The revised map turns the fault eastward instead of westward and places Ordovician on Devonian rocks (Appendix E). Dunn (1979) interpreted the Guilmette Sequence Dgb2 breccia in the Mail Summit 7.5-minute quadrangle as local reef talus, but did not recognize the significance of its lateral continuity across many other ranges in the area (Warme et al., 1993; Warme and Kuehner, 1998). Therefore, detailed knowledge of the order, boundaries, and genesis of Paleozoic sequences is essential to making a geologic map that constrains structural and paleogeographic interpretations.

<u>Sequences and Sequence Boundaries</u> A sequence, as used in this paper, is a bundle of one or more conformable depositional cycles bounded by discrete bedding surfaces or boundaries that are widely traceable (Chamberlain and Warme, 1996). For practical purposes, the mappable sequences were grouped together into formations to produce **Plate 1a**. **Plate 6** is an example of a geologic map showing Devonian sequences at TMS. The sequences typically produce unique gamma-ray patterns that simplify regional correlations. Many preserved bedding surfaces or erosional surfaces represent significant

unconformities or their correlative conformities (Mitchum et al., 1977). Reid and Dorobek (1993), and many others, used this definition to study carbonate strata. They suggested that sequence-bounding unconformities show evidence of subaerial erosional truncation or subaerial exposure and represented significant depositional hiatuses. Many sequence bounding unconformities in TMS are karstified. Karstification can represent minor exposure with the removal of several inches of strata. It can also represent a significant drop in relative sea level resulting in karst cavities, extensive breccia, removal of tens to hundreds of feet of section, and freshwater phreatic diagenetic alteration 100 feet or more below the unconformity. Only the major karst intervals or dissolution surfaces (DIS) are illustrated in the TMS stratigraphic column (**Figure 13**).

Mechanisms for Cycle and Sequence Development The driving forces that create stratigraphic cycles and sequences, and particularly carbonate cycles and sequences, are not completely understood. Earlier work (e.g., Vail et al., 1977) attributed the mechanism for sequence generation to eustatic sea-level change. Others argued for tectonic or other forces (e.g., Wilkinsen et al., 1998). Many papers deal with the driving forces of cycles at all scales arguing all sides of the question. For example, Yoshida et al. (1996) found no independent evidence for eustasy controlling deposition of the siliciclastic Mesaverde Group of the Book Cliffs, Utah. However, the Mesaverde Group is one of one of the best-described and best-known instances of high-frequency successions in North America. New evidence from Yoshida et al. (1996) suggested that tectonism involving changes in intraplate stresses originating from thrust-belt compression may be the major mechanism for sequence generation in foreland basins. The researchers found no evidence of climatically induced changes in sediment supply for the Mesaverde Group. They saw no need to invoke eustasy as a mechanism to control sequences.

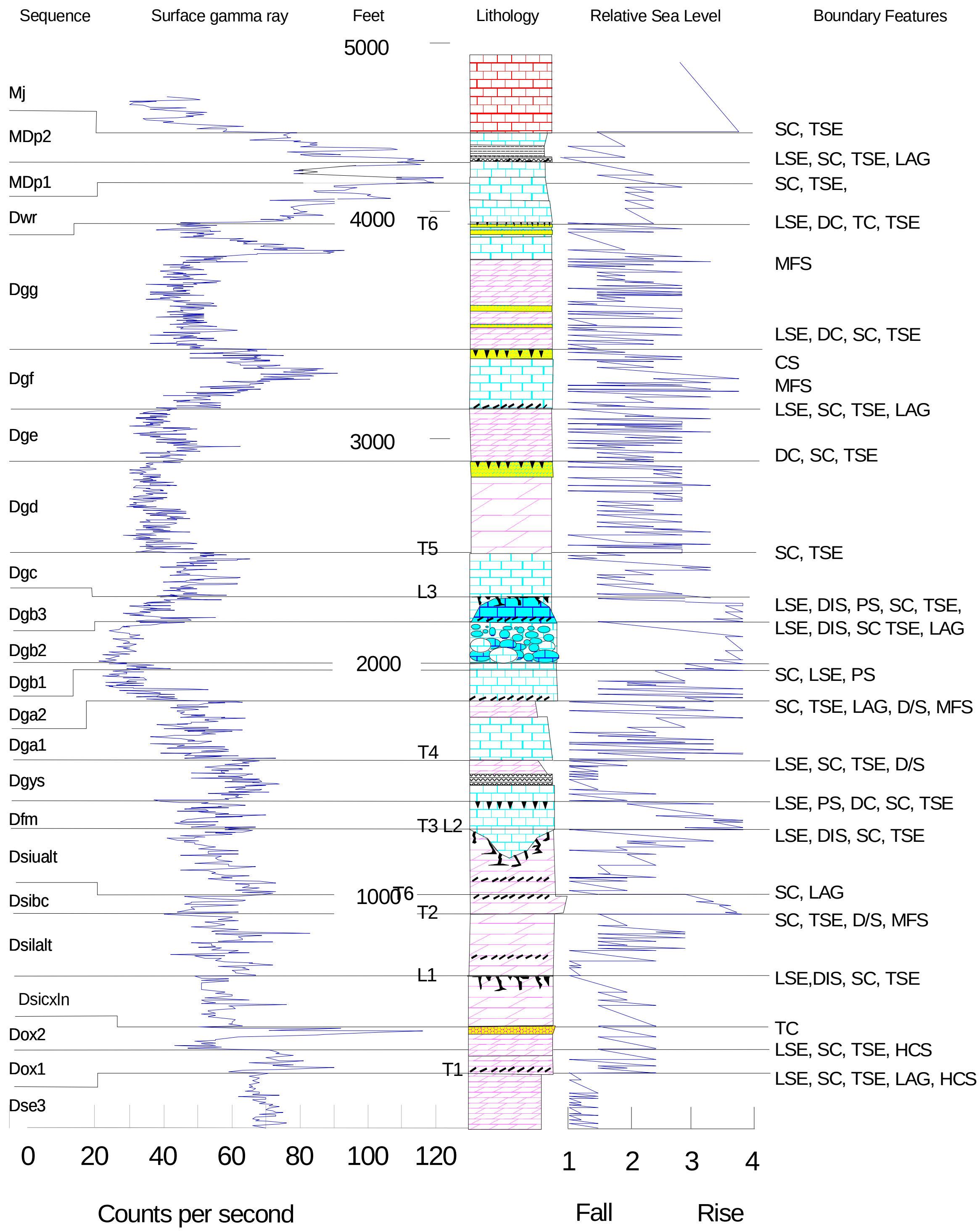


**Figure 13** Composite stratigraphic column of southwest Mail Summit section, TMS, showing sequences, surface gamma-ray log, sea-level lowstand and transgressive events (L1 to L3, T1 to T3), stratigraphic column, relative sea-level curve, and sequence-boundary features (Chamberlain and Warme, 1996). See **Figure 14** for the legend.

LEGEND

| Symbol | Sequence |
|---|---|
| Mp | "Penoyer Limestone" |
| Mj | Joana Limestone |
| MDp2 | Sequence 2, Pilot Formation |
| MDp1 | Sequence 1, Pilot Formation |
| Dwr | West Range Limestone |
| Dgg | Sequence G, Guilmette Formation |
| Dgf | Sequence F, Guilmette Formation |
| Dge | Seqeunce E, Guilmette Formation |
| Dgd | Seqeunce D, Guilmette Formation |
| Dgc | Sequence C, Guilmette Formation |
| Dgb3 | Sequence B3, Guilmette Formation (reef) |
| Dgb2 | Sequence B2, Guilmette Formation (breccia) |
| Dgb1 | Sequence B1, Guilmette Formation |
| Dga2 | Seqeunce A2, Guilmette Formation |
| Dga1 | Sequence A1, Guilmette Formation |
| Dgys | Yellow Slope Sequence, Guilmette Formation |
| Dgfm | Fox Mountain Sequence, Guilmette Formation |
| Dsiualt | Upper Alternating Sequence, Simonson Dolomite |
| Dsibc | Brown Cliff Forming Sequence, Simonson Dolomite |
| Dsilalt | Lower Alternating Sequence, Simonson Dolomite |
| Dsicxln | Coarsely Crystalline Sequence, Simonson Dolomite |
| Dox2 | "Oxyoke Formation" Sequence 2 |
| Dox1 | "Oxyoke Formation" Sequence 1 |
| Dse3 | Sequence 3, Sevy Dolomite |
| Dse2 | Sequence 2, Sevy Dolomite |
| Dse1 | Sequence 1, Sevy Dolomite |

BOUNDARY FEATURES

| | |
|---|---|
| CS | Condensed Interval |
| HCS | Hummocky Cross-stratification |
| MFS | Maximum Flooding Surface |
| LAG | Lag Deposit, Rip-up Clasts |
| D/S | Deep over Shallow |
| TSE | Transgressive Surface of Erosion |
| SC | Sharp Contact |
| TC | Transitional Contact |
| LSE | Low stand Surface of Erosion |
| DIS | Dissolution Surface (Karst) |
| PS | Paleosol |
| DC | Desiccation Cracks |

LITHOLOGY

| |
|---|
| Limestone |
| Cherty Limestone |
| Stromatolite Beds |
| Stromatoporoid Reef |
| Karsted Limestone |
| Dolostone |
| Karsted Dolostone |
| Calcareous Siltstone |
| Sandstone |
| Desiccation Cracks in Sandstone |
| Carbonate Breccia |

**Figure 14** Legend for **Figure 13** describing and defining Devonian sequences, features at sequence boundaries, and symbols. See **Figure 4**, **Figure 9**, and **Plate 6** for location of TMS.

In another system in another part of the world, Satterley (1996) suggested that Late Triassic eustatic sea-level fluctuations were ineffective in controlling sedimentation of the Dachstein Limestone, Austria. He suggested that vertical facies patterns are best explained by aperiodic fault-controlled downdropping.

On the other hand, Yang et al. (1995) suggested that Milankovitch climatic forcing was responsible for cycle periodicity of the Lost Burro Formation rocks in the Panamint Range over a large, low-latitude Devonian carbonate platform. However, in their work on the Virgilian and Wolfcampian Cisco Group in north-central Texas, Yang et al. (1998) pointed out the importance of distinguishing the roles of autogenic versus allogenic processes to establish a high-resolution (meter-scale) chronostratigraphy of any sedimentary record. An allocyclic Cisco record in the lower platform contains abundant autocyclic imprints because allogenic controls on cyclic sedimentation were accomplished through local autogenic processes. Elrick (1995) suggested that the cycles in the Great Basin Simonson Dolomite formed in response to glacio-eustatic sea-level oscillations. Similarly, McLean and Mountjoy (1994) attributed parasequence cycles in the Canadian Devonian Cairn Formation to high-frequency sea-level oscillations, but Wilkinson et al. (1996) concluded that meter-scale cyclicity was more apparent than real. They also suggested that perceptions of repeated and eustatically driven platform flooding were largely incorrect, and that much of the presumed stratigraphic order in peritidal carbonates reflected random migration of sedimentary subenvironments. From their work on the peritidal Upper Cambrian and Conococheague Formations, Virginia, Wilkinson et al. (1998) concluded that the frequence of stratigraphic recurrence of 265 shallowing-upward cycles is random. They believed that in most epicratonic peritidal sequences meter-scale variations in carbonate deposition are randomly controlled and are not related to recurrent intrabasinal or extrabasinal mechanisms that force rhythmic sediment accumulation. Furthermore, Wilkinson et al. (1999) showed that Phanerozoic peritidal sequences exhibit exponential thickness frequence distributions and that thickness distribution is independent of facies type. In other words, numbers, sizes, and compositions of carbonate units in the Phanerozoic imply a less deterministic relation between environment of accumulation that the lateral/vertical distribution of different stratal elements in cratonic peritidal sequences. The linkage between sea-level change and sequence shape and size relies on deterministic conjectures. In contrast, Gupta and Allen (1999) speculated that high-frequency episodic fluctuations in relative sea level of the French Early Tertiary Alpine foreland basin are a consequence of glacioeustatic sea-level oscillations of > 0.5 m.y. duration. These oscillations are superimposed upon a steady relative sea-level rise resulting from the background flexural subsidence. Their conclusion is based on data from which sediment supply can be eliminated as a variable. They analyzed the paleoshoreline features preserved along the Eocene Nummulitic Limestone Formation basal unconformity of the basin in southeastern France.

Sami and James (1994) inferred that small, meter-scale cycles in the Proterozoic upper Pethei Group, northwest Canada, were mainly autogenic, having formed in an aggradational tidal island model. They interpreted the formation-scale and decameter-scale cycles as controlled by changes in eustasy and subsidence rates. Along similar lines, Goldhammer et al. (1993) claimed those cycles in the Lower Ordovician Diablo Platform, west Texas, were probably driven by a combination of high-frequency, eustatic sea-level oscillations and autocyclic progradation.

Rankey and Walker (1994) suggested that carbonate platform cycles on the Cambrian Iapetan passive margin in the southern Appalachians are caused by autocyclic aggradation and progradation unrelated to sea-level fluctuations. In their model, the carbonate-producing mechanism shifts laterally to a more favorable location when the shallowing-upward cycle reaches its upper limits and the mechanism shuts off.

Another possible mechanism for cycle development involves tectonic activity. McLean and Mountjoy (1994), for example, attributed episodic longer-term regional development of Canadian Devonian sequences superimposed on a high-frequency cyclicity to episodes of tectonic loading related to the Antler orogeny. This hypothesis is important for the current research because Devonian rocks in the eastern Great Basin were deposited in the Sunnyside basin (**Plate 3**), next to and east of the region of the Antler orogeny.

In summary, agreement on the mechanisms for cycle and sequence development has not been reached. A combination of mechanisms could account for the cycles and sequences in the Sunnyside basin. Autocyclic mechanisms may have controlled development of cycles because cycles are not correlative throughout the basin. Some of these carbonate autogenic processes include variations in carbonate production and dispersal, intensity and frequency of tropical storms and monsoons, thermohaline circulation patterns, and ambient ocean chemistry and temperature as a control on cycles within the sequences. Tectonic or eustatic controls may have controlled regionally correlatable sequences. Tectonic pulses of the active Antler Orogeny likely affected relative sea-level changes in the adjacent Sunnyside basin. However, until more precise methods of dating the emplacement of the Antler thrust sheets can be made, the driving mechanisms for sequence development in the Sunnyside basin remain undetermined. Erosion at sequence boundaries precludes making useful conclusions of cycle stacking patterns between sequences in the Sunnyside basin because much of the record is missing.

In this report, the Sunnyside basin is identified and interpreted as the incipient Antler foreland basin that began to form in the Early Devonian. Episodic tectonic pulses of the incipient Antler orogeny may be responsible for some large-scale sequences in the Great Basin Devonian. Sequences defined in this study are correlatable throughout the Sunnyside basin. However, the composition, thickness, and number of shallowing-upward cycles within the sequences are highly variable across the Sunnyside basin. Similarly, Lehmann et al. (1998) found that composition, thickness and number of meter-scale cycles within their sequences of the Early Cretaceous carbonates and evaporites are highly variable across the Cupido and Coahuila platforms, northeastern Mexico. They attributed the cycle variability to interacting processes that created variable physiographic and oceanographic conditions across the platforms that complicated the sedimentary record generated by Milankovitch-driven sea-level changes.

## Devonian Sequences at TMS

**Table 4** provides a convenient reference for the thicknesses, numbers of cycles and significant features that locally distinguish each sequence. **Figure 13** is a composite stratigraphic column illustrating the surface gamma-ray log, generalized lithology, relative sea-level curve, and sequence boundary characteristics for sequence at TMS. It was constructed from three segments (**Figure 4** and **Plate 6**). Segment 1 starts in the Sevy sequence 3 and ends at the top of the Simonson Brown Cliff Sequence. Segment 2 starts at the top of the Brown Cliff Sequence and ends in Guilmette Sequence Dgd. Segment 3 starts near the top of Guilmette Sequence Dgb2 and ends in the Mississippian “Penoyer Limestone” (**Table 1**).

Overlap from the top of Sequence Dgb2 to the lower part of Sequence Dgd in segments 2 and 3 was intentional. In segment 2, Sequence Dgb3 is a stromatoporoid reef. This section is called reef core herein and a letter “c” is added to the sequence designation. For example, Dgbc is Sequence Dgb where Dgb3 is the stromatoporoid reef. On the other hand, Sequence Dgb3 in segment 3 is on the reef flank. A letter “f” is added to the sequence designation. For example, Dgbf is Sequence Dgb where Dgb3 is on the reef flank. **Figure 14** is a legend for symbols and abbreviations in **Figure 13**, **Table 4**, and **Figure 28**.

**Table 4** Thickness, numbers of cycles, and significant features of Devonian sequences in southwest Mail Summit measured section, Timpahute Range, Nevada.

| Seq. Abbrev. | Thickness in Feet | Cycles | Significant Features |
|---|---|---|---|
| Dga2 | 145 | 8 | Shallowing-upward cycles that successively deepen upward, predominantly limestone, open-marine fauna, ledges and slopes |
| Dga1 | 250 | 12 | Shallowing-upward cycles that successively deepen upward, predominantly dolomite, open-marine fauna, ledges and slopes |
| Dgys | 182 | 10 | Yellow, silty dolomite, stromatolites, and cycles capped by thin beds of very fine-grained quartz sandstone, ostracodes, forms slopes |
| Dgfm | 135 | 4 | Open shelf fauna, brachiopod *Stringocephalus*, resistant cliffs. |
| Dsiualt | 285 | 12 | Shallowing-upward cycles that successively deepen upward giving the dolomite an alternating dark and light band appearance, karst breccia, ledges |
| Dsibc | 85 | 4 | Open shelf fauna (corals, stromatoporoids), dark brown-gray dolomite cliff |
| Dsilalt | 265 | 12 | Alternating intertidal-supratidal or dark and light bands of dolomite ledges |
| Dsicxln | 225 | 4 | Coarsely crystalline dolomite capped by karsted interval, light-gray to light-gray brown cliffs |
| Dox2 | 95 | 2 | Quartz sandstone with hummocky cross-bedding at base overlain by sandy dolomite, ledge |
| Dox1 | 100 | 4 | Burrowed, silty dolomite with flat-pebble conglomerate at base, light-brown slope |
| Dse3 | 240+ | 12+ | Light-gray, fine-grained, laminated dolomite, slopes, base concealed |
| Total | 4370 | 189+ | |

| **Table 4** Continued | | | |
|---|---|---|---|
| Seq. Abbrev. | Thickness in Feet | Cycles | Significant Features |
| MDp2 | 115 | 2 | Silicified stromatolites and laminated black chert, slope |
| MDp1 | 130 | 2 | Silty limestone capped with fossil bone-bearing sandstone, slope |
| Dwr | 153 | 4 | Silty, burrowed limestone, partly covered slopes |
| Dgg | 567 | 29 | Carbonate cycles capped by thick (>10 feet) quartz sandstone beds |
| Dgf | 267 | 16 | Slightly deeper cycles and contains more limestone than in adjacent sequences |
| Dge | 235 | 17 | Carbonate cycles capped by thin (<10 feet) quartz sandstone beds |
| Dgd | 406 | 23 | *Amphipora* dolopackstone, dark-gray ledges and cliffs |
| Dgc | 188 | 6 | Silty limestone with abundant gastropods & burrows, slope |
| Dgb3 | 97 | 3 | Stromatotoporoid and coral reef facies, light-gray cliffs |
| Dgb2 | 179 | 1 | Graded bed of carbonate breccia, open-marine fauna, brown-gray cliffs |
| Dgb1 | 26 | 2 | Abundant corals, stromatoporoids, and *Amphipora*, limestone cliffs |

Although some sequence boundaries do not exactly coincide with formation contacts, the sequences are grouped into formations wherever possible. Characteristics of each formation, including lithology, weathering profile, gamma-ray character, distribution of the formation in the study area, cycle attributes and tectonic significance, are described in this chapter. Then each sequence is described. Detailed descriptions of each cycle within each sequence are presented in Appendix B. Photomicrographs and their descriptions from the lower Guilmette sequences are presented in Appendix C.

Recorded in the measured section are three major Devonian sea-level lowstand events (L1-L3, **Figure 13**) that produced regionally and economically significant karst intervals, and six major sea-level transgressions (T1-T6, **Figure 13** and **Plate 2a**). Bounding surfaces and internal features were interpreted for their relative sea-level changes and paleoenvironmental significance, and the results were used to create a relative sea-level curve. Criteria used to classify sequences are presented in **Table 3**, Chapter 3.

## Sevy Dolomite

Three mappable sequences comprise the Sevy Dolomite in the Sunnyside basin. Isopach maps of the sequences suggest that the center of the Sunnyside basin in Sevy Dolomite time was near Eureka, Nevada (see **Figure 2** for location of Eureka, Nevada). Only 240 feet of Sequence 3 are exposed at TMS. However the Sevy Dolomite is 980 feet thick in the Tempiute Mountain section where all three sequences are exposed (No. 53, **Figure 9**; **Figure 12**; see summary of this chapter for another correlation chart involving the Tempiute Mountain measured section). In the study area and areas east of the Diamond Range, the Sevy Dolomite lies unconformably on Silurian Laketown Dolomite. It lies unconformably on top of the Silurian Lone Mountain Dolomite in the Diamond Mountain vicinity (**Figure 9**, Nos. 14, 15, 16, 23, and 34).

### Characteristics of the Sevy Dolomite

The Sevy Dolomite is a 500 to 1,600-foot-thick, monotonously repetitive, micritic to finely-crystalline, laminated, light-to very light-gray, dense dolomite that occurs throughout the study area (**Plate 1a**). Typically, the sequence boundary at its base occurs at the change from cliff-forming, dark-gray, chert-bearing, fossil-rich Silurian Laketown Dolomite to the slope-forming, fossil-poor, laminated, light-gray Devonian Sevy Dolomite. Reso and Croneis (1959) reported Lower Devonian (Oriskany) fossils in the Sevy Dolomite in the Pahranagat Range, five miles south of the study area. Tschanz and Pampeyan (1970) suggested that the Lower Devonian fossils occur considerably below the Oxyoke Canyon Sandstone Member of the Nevada Formation west of Eureka. They occur above the *Halysites*-bearing dolomites of the underlying Silurian Laketown Dolomite. *Halysites* corals are marker fossils of the Laketown Dolomite.

On fresh surfaces, the color of the Sevy Dolomite varies much more than it does on weathered surfaces. Fresh color ranges from light gray to dark gray, to light olive gray to light brownish gray. The light olive gray to light brown gray is typical for most of the section throughout most of the region. The darker grays are generally limited to the uppermost part of the sequence. However, sections in Elko and northernmost White Pine counties in Nevada and Silver Island Mountains in northwestern Utah (**Figure 9**, Nos. 41, 42, 45, and 47) are different. In these sections, the darker grays are prevalent throughout the formation. Most of the rocks in the formation contain thin stromatolitic laminations. Osmond (1954) described the sequence as uniformly micritic. The outcrops that I observed show the average grain size to be closer to very finely crystalline.

The Sevy Dolomite maintains its lithologic character from southern Nevada to southern Idaho and central Utah. It is easily recognized in the field by its micritic to very finely-crystalline grain size, extensive laminated beds, distinctive very light gray-weathering color and its slope-forming weathering profile (**Table 4**). **Figure 15** illustrates the distribution of 68 outcrops of Sevy Dolomite covering 15.65 square miles in the Timpahute Range quadrangle.

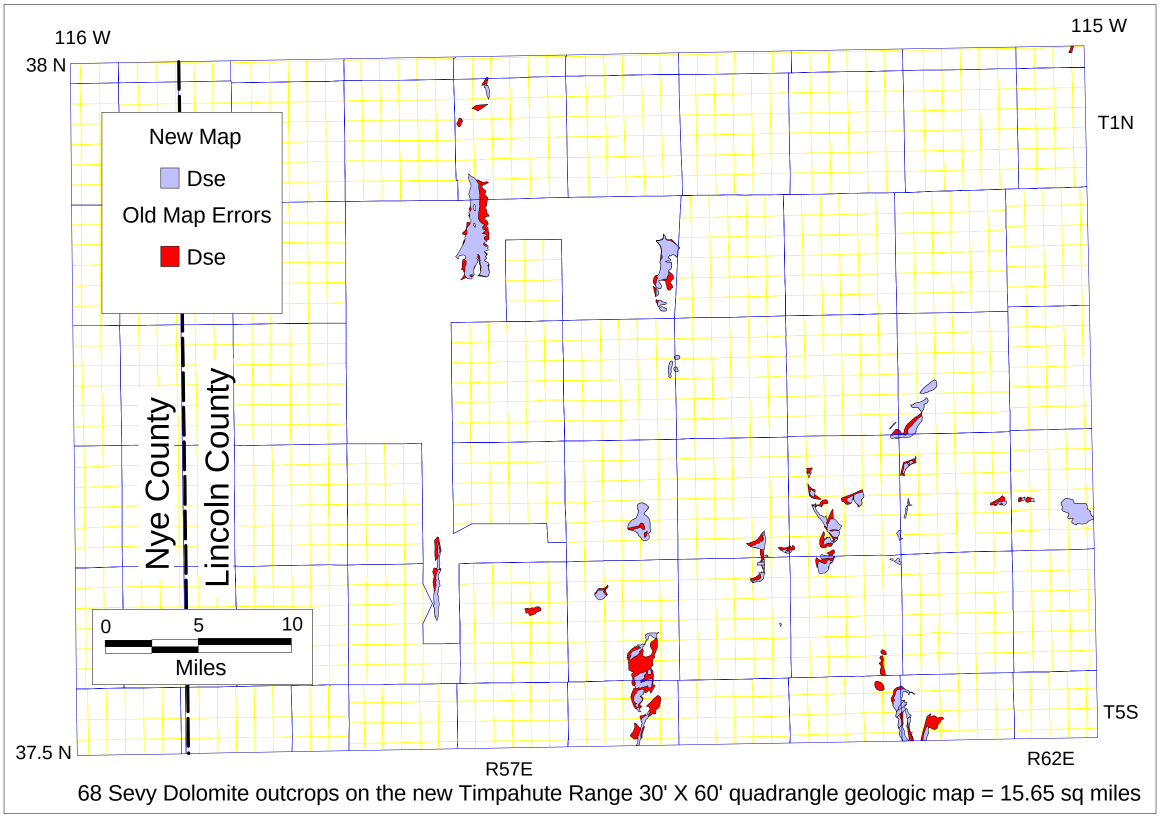


**Figure 15** Distribution of Sevy Dolomite outcrops on the new geologic map of the Timpahute Range quadrangle. Areas erroneously mapped as Sevy Dolomite on the old geologic map are marked in red. Degrees N latitude and W longitude are marked at the corners of the map. Surveyed township and range lines are blue and section lines are yellow.

<u>Lower Contact</u> As noted by Osmond (1962), the surface between the Silurian Laketown Dolomite and the Devonian Sevy Dolomite is a regional unconformity that can be readily recognized in some sections. In other sections, the unconformity is obliterated by recrystallization and dolomitization. This lower contact is picked in the measured sections at an abrupt decrease in fossils and bedded chert and where gamma radiation decreases. Locally a thin sandstone bed or sandy dolomite bed occurs at the base of the Sevy Dolomite, as Osmond (1962) reported. This boundary may also be subtle and occur on partly covered slopes.

Upper Contact Sharp in most measured sections, the upper contact of the Sevy Dolomite is picked at the unconformity between light-gray, supratidal, finely-crystalline stratal dolomite and light yellow-gray beds containing the first occurrence of "Oxyoke Formation" detrital sand grains. This erosion contact is overlain by breccia clast beds and sandy dolomite that is probably related to transgressive marine flooding and sedimentary reworking. Light gray clasts in the light yellow matrix are from the underlying Sevy Dolomite. A sharp increase in gamma radiation also marks the contact. Even without an obvious increase of siliciclastic grains in the carbonate beds, the increase in gamma radiation at the base of the overlying "Oxyoke Formation" is generally present.

In contrast to other workers who place the second order Kaskaskia sequence of Sloss (1963) at the base of the Sevy Dolomite, I place it at the top. I believe the unconformity at the top of the Sevy Sequence is the base of the Kaskaskia (**Figure 10**). The unconformity is marked by a more distinctive change in lithology and reflects a greater facies shift than the unconformity at the base of the Sevy Dolomite. Most of the Devonian strata at Mail Summit are incorporated in the Kaskaskia sequence of Sloss (1963) and as refined by Wheeler (1963). The paucity of fossils disallows placement of the lower Kaskaskia sequence boundary more precisely.

## Gamma Radiation

Gamma-ray logs help divide the Sevy Dolomite into three regionally correlatable sequences: lower, middle and upper. Gamma radiation is lower over Sevy Sequence 1 and Sequence 3 and higher over Sevy Sequence 2 (**Figure 12**). Sevy Sequence 1 is between 50 and 70 CPS (Counts Per Second) in the Tempiute Mountain measured section and is constantly about 20 API units in the Moore McCormack well. Sevy Sequence 2 is mostly between 70 and 110 CPS at Tempiute Mountain and 20 to 30 API units in the

Moore McCormack well. Sevy Sequence 3 is mostly 60 CPS at Tempiute Mountain, 20 API units in the Moore McCormack well, and 90 CPS in the TMS.

Environment of Deposition

Although the occurrence of fossils in the Silurian Laketown Dolomite suggests deposition in open-shelf conditions, I agree with Osmond (1962) who believed that the generally fossil-poor Sevy Dolomite originated mainly as a primary evaporitic dolomite in a supratidal setting. Most of the Sevy Dolomite is composed of the supratidal finely-crystalline stratal dolomite facies. This dolomite facies and other dolomite occurrences at TMS are described later in this chapter. Anhydrites have not been found in measured sections and wells listed in **Table 2** and in Appendix F. However, other characteristics common to sabkhas such as absence of fossils, thin pebble conglomerates, stromatolitic laminae, desiccation cracks, and other diagenetic modifications such as dolomite replacement to form finely-crystalline stratal dolomite, tepee structures, and disrupted bedding strongly indicate supratidal conditions and indirectly suggest hypersaline conditions.

The paleogeography of the eastern Great Basin during much of Sevy Dolomite time is interpreted as a vast sabkha, extending for hundreds of miles in width and perhaps a thousand miles or more along depositional strike. Just west of the Diamond Range, 100 miles north of the study area, was a narrow area of intertidal conditions next to an area of subtidal conditions (**Figure 9**, Nos. 14, 15). Correlative intertidal beds include the Beacon Peak, upper part of Lone Mountain, Wenban Limestone, Rabbit Hill, and the upper part of Roberts Mountain Formation, as Matti (1979) pointed out (**Figure 10**). Telescoping of the section by thrusting during the Sevier orogeny in the Diamond Range area is probably responsible for what now may be a very narrow, abrupt outer shelf (Chamberlain and Birge, 1997). Many workers have reported thrust faults in the area

(Nolan, 1962; Nolan et al., 1971; Nolan et al., 1974; Roeder, 1989; Carpenter et al., 1993; Camilleri, 1999). Outer shelf deposits now lie next to sections with supratidal and subtidal deposits. Thrust fault restorations suggest that they were probably deposited west of Sunnyside basin and have been subsequently thrust into their present position. Relative sea-level changed little during Sevy Dolomite time; most cycles begin in high intertidal conditions and end in high supratidal conditions.

In the Silver Island Mountain section (**Figure 9**, No. 47) in northwestern Utah, the typical Sevy Dolomite lithotype is missing. A local fossiliferous, medium dark-gray weathering dolomite, similar to the Lone Mountain Formation, occurs at the same stratigraphic interval. The interval contains a few beds of typical Sevy Dolomite lithology just beneath the Simonson Dolomite. This suggests the development of a marine embayment on the shelf. The presence of this lithotype at this location could also be due to tectonic transport from the west by the Sevier thrusting event. Also it could be the result of tectonic transport from the northwest by pre-Sevier thrusting (N. Silberling, 1998, personal communication). Farther north and east, at Samaria Mountain in southern Idaho (**Figure 9**, No. 46), the Lower Devonian Water Canyon Formation exhibits typical Sevy Dolomite-like stratigraphy. Other workers have previously correlated the Water Canyon Formation with the Sevy Dolomite (Hintze, 1988). However, more data are needed to better define the paleogeography of the Samaria Mountain area.

## "Oxyoke Formation"

The "Oxyoke Formation" at TMS is 195 feet thick and is composed of two sequences. It is a distinctive light-brown argillaceous and sandy interval between the light-gray Sevy and medium dark-gray Simonson Formations, and thus, an important regional marker bed. The lower contact at TMS is sharp and is marked by a regional LSE cut into the top of the Sevy Dolomite and merged with a TSE and associated rip-up clasts above the unconformity. It is distinct at TMS where light-gray dolomite is overlain by light-brown argillaceous dolomite of “Oxyoke Formation” Sequence 1. Forming a prominent brown cliff, sandstones of “Oxyoke Formation” Sequence 2 are the first prominent occurrences of regionally distributed quartz sandstones in the Paleozoic rocks above the Ordovician Eureka Quartzite. Sandstones become interbedded with coarsely-crystalline dolomite near the top of the sequence. The uppermost occurrence of quartz sandstone marks the upper contact with the base of the Simonson Dolomite Coarsely-Crystalline Sequence. Sharp inflections on the gamma-ray log mark the lower and upper contacts at TMS.

## Establishing the “Oxyoke Formation”

Inconsistencies in correlating the argillaceous and sandy interval between the Sevy and Simonson Formations were discussed in Chapter 2. Osmond (1962), Hurtubise (1989), and other early workers each used different criteria to pick the contacts. They did not use sequence stratigraphic concepts to do so. I have chosen to establish the “Oxyoke Formation” as a mappable unit bounded by unconformities between the Sevy and Simonson formations to avoid these inconsistencies. Establishing the “Oxyoke Formation” avoids confusion over arbitrary contacts based on facies variations.

The “Oxyoke Formation” is not to be confused with the Oxyoke Canyon Sandstone Member of the Nevada Formation of Nolan et al. (1956). The type section of the Oxyoke Canyon Sandstone Member of the Nevada Formation is in Oxyoke Canyon, Diamond Range (**Figure 9**, No. 15). It correlates with “Oxyoke Formation” Sequence 1 in **Figure 10**. However, the “Oxyoke Formation” as employed here is composed of two sequences: Sequence 1 that correlates to the Oxyoke Canyon Member of Nolan, and Sequence 2. A reference section of the “Oxyoke Formation” is TMS (**Figure 9**, No. 51, **Table 2**, and **Figure 13**).

Characteristics

The “Oxyoke Formation” is a distinctive grouping of facies assemblages and lithologies between the Sevy and Simonson Dolomites. It contains types of strata found in neither the underlying Sevy Dolomite nor the overlying Simonson Dolomite. The “Oxyoke Formation” includes sandstone beds, sandy dolomites, and other beds above the Sevy Dolomite unconformity and below the Simonson Dolomite Coarsely-Crystalline Sequence. It includes both the cherty argillaceous member and the sandy member described by Osmond (1954), Reso (1960) and Hurtubise (1989). At TMS and in much of the Sunnyside basin, the argillaceous member generally corresponds to Sequence 1 and the sandy member to Sequence 2. However, Sequence 1 may be mostly quartz sandstone with dolomite cement as at the type locality of the Oxyoke Canyon member of the Nevada Formation (**Figure 9**, No. 15) and at other western sections. In some eastern sections, Sequence 2 lacks quartz sandstones.

At TMS, the lower part of the lowermost shallowing-upward cycle of the 100-foot thick “Oxyoke Formation” Sequence 1 is a hummocky cross-stratified, light yellow-gray, sandy, finely-crystalline dolomudstone. Several inches of thin, light-gray Sevy Dolomite rip-up clasts that lie parallel to the bedding in sandy dolomudstone suggest a major transgressive surface and mark the basal contact of the “Oxyoke Formation” Sequence 1. Normally, the significance of an unconformity is determined by the number of missing faunal zones. However, the paucity of fossils in the supratidal beds of the Sevy Dolomite preclude identifying the unconformity based on missing fossils. Therefore, other physical evidence such as the transgressive lag, irregular contact, missing Sevy Dolomite cycles on regional correlations must be used to find the significance of the unconformity. The transgressive intraclast packstone lag is overlain by a burrowed light yellow-brown weathering dolomudstone with quartz sand and black chert nodules two to three inches in diameter (**Plate 2a**). Intensity of burrowing decreases upward. Near the top of Sequence 1, the dolomites become more laminated.

"Oxyoke Formation" Sequence 2 contains persistent quartz sand intervals that are about five to 60 feet thick in most sections in much of the Sunnyside basin. At TMS, a 54-foot thick quartz sandstone bed forms a prominent brown cliff in the 95-foot thick sequence. The sandstone weathers medium yellow-brown and is cross-bedded, fine- to medium-grained and is poorly cemented with dolomite. Throughout the Sunnyside basin, quartz grain size ranges from medium sand to silt size. Fine- to medium-grained sand is most common. Sandstones commonly are subordinate to quartz-sand dolomites and may be missing altogether. In sections that contain no distinct quartz sandstone, the "Oxyoke Formation" is characteristically a silty dolomite bearing quartz sand grains. At localities where the base and top of the sequence are difficult to find, the gamma-ray log signature is diagnostic.

In the type locality of the Oxyoke Canyon member of the Nevada Formation or "Oxyoke Formation" Sequence 1 (**Figure 9**, No. 15), the trough cross-bedded sandstone is light olive-gray on a fresh break. It is medium- to coarse-grained in contrast to "Oxyoke Formation" sandstones in sections farther east. Nolan et al. (1956) reported a transgressive bed containing many casts of large crinoid columnals near the base of the unit at Phillipsburg mine, 15 miles north of the type locality (**Figure 9**, No. 16). Fossils are lacking in the unit in sections farther east.

Throughout the Sunnyside basin, horizontally laminated and ripple laminated beds are common, and these may contain dolomite interlaminations. Many sandstone beds have sedimentary structures such as horizontal planar laminations and hummocky cross-stratification that suggest a lower shoreface environment. Typically, the sandstones grade up to fine-grained sandstones with desiccation cracks suggesting a tidal flat origin. Near the top of the unit, interbeds of dolomite are coarsely crystalline. Sparse quartz-sandy laminae and floating quartz grains occur in the upper part of many sections where carbonate beds dominate. The quartz grains are subrounded to rounded, well-sorted, and fine- to medium-grained. Laminae of quartz grains commonly appear as discrete lenses within cross-bedded dolomite.

Seventeen feet of upward thickening, finely-crystalline, quartz sand-bearing dolomite beds that weather medium yellow-brown lie on top of the sandstone interbed at TMS. The upper contact of the "Oxyoke Formation" is marked by an irregular surface of erosion and where sand content abruptly decreases zero. The less radioactive Coarsely-Crystalline Sequence of the Simonson Dolomite overlies the upper beds of the "Oxyoke Formation" at TMS. See Appendix B for a more detailed description of the "Oxyoke Formation" sequences and cycles at TMS.

Thickness

The "Oxyoke Formation" is 285 feet thick at Tempiute Mountain (53), 195 feet thick in the reference section at TMS (51), 430 feet thick at Monte Mountain (52), 285 feet thick in the Maxus Moore McCormack well (35), and 230 feet thick at Cutler Reservoir, Pahranagat Range (38)--see **Figure 9** and **Table 2** for surface and subsurface section locations. It thickens to a maximum of about 580 feet in Oxyoke Canyon, Diamond Range, Sec. 20 T18N R54E. The sandy member of Hurtubise (1989) at Fossil Peak, Sec. 30 T2S R61E, is 139 feet thick and at Timber Mountain, Sec.10 T2N R62E, it is 101 feet thick. Hurtubise (1989) measured 22 feet of net sand within the sandy member at Timber Mountain section but did not provide a figure for net sand at Fossil Peak, which probably ranges between 50 and 150 feet. Sandy beds are absent in the "Oxyoke Formation" of the Pequop Range (**Figure 9**, No. 41), Cherry Creek Range (**Figure 9**, Nos. 8 and 9), Ruby Range (**Figure 9**, No. 45), and the Silver Island Mountains (**Figure 9**, No. 47). Nevertheless, the distinctive gamma-ray signature persists in these sections that appear to have a higher silt and clay content than the underlying and overlying formations. An isopach map of the "Oxyoke Formation" and a discussion of quartz sandstones in the Sunnyside basin are presented in Chapter 7.

<u>Gamma Radiation</u>

In contrast to the smooth, nearly constant line of low radiation over the upper part of the Sevy Dolomite, the gamma-ray log exhibits sharp fluctuations over the more radioactive, argillaceous, and sandy “Oxyoke Formation.” The lower contact of the “Oxyoke Formation” is easy to pick and correlate on gamma-ray logs because of the sharp rightward inflection caused by an increase in gamma radiation and in cuttings. Higher radiation is typical of the argillaceous “Oxyoke Formation.” **Figure 12** provides an example of the correlation from surface to subsurface sections. In the Maxus Exploration Moore McCormack well (**Figure 9**, No. 35)--a well near the study area (Sec 6 T7S R58E) that penetrated Devonian rocks--the 285-foot-thick “Oxyoke Formation” exhibits the sharp rightward gamma-ray inflection at its base. As with the surface gamma-ray on nearby outcrops, the “Oxyoke Formation” produces more radiation than the underlying Sevy Dolomite and the overlying Simonson Dolomite. It is highest over argillaceous “Oxyoke Formation” Sequence 1 and lower over sandy Sequence 2 (**Figure 12**).

The anomalously low gamma radiation of “Oxyoke Formation” Sequence 2 at TMS is probably due to the abundance of medium to coarse quartz sand grains that dilute the finer-grained, more radioactive particles. Similarly, in the type locality of the Nevada Formation Oxyoke Canyon Member at Oxyoke Canyon near Eureka, Nevada, the gamma-ray signature of the light gray sandstone is less pronounced than in the adjacent dolomites of the Sevy Dolomite below and Simonson Dolomite above (Cedar Strat proprietary measured section, 1985).

A pronounced upward decrease in gamma radiation marks the top of the “Oxyoke Formation” in most sections (**Plate 2a**). In some sections the upward decrease in gamma radiation is gradational with the overlying Coarsely-Crystalline Sequence of the Simonson Dolomite.

Sand Provenance

As stated in Chapter 2, the source of the sandstone in the "Oxyoke Formation" is problematical. Osmond (1954, 1962) and Poole et al. (1992) suggested an easterly source for the sand. However, this study proposes an alternative source area. Introduced in Chapter 2, the Antler forebulge was likely the source area for "Oxyoke Formation" quartz sandstones in the western side of the Sunnyside basin. The quartz sandstones in the "Oxyoke Formation" coarsen and thicken westward toward the Antler forebulge where unconformities on the west flank of the Sunnyside basin have cut out older Paleozoic rocks including Eureka sandstones. For example, in the Toquima Range, a window through the Roberts Mountain allochthon of Ordovician rocks reveals that Mississippian rocks unconformably lie on Cambrian rocks (Cedar Strat proprietary measured section). Measured sections of the region suggest that the Ordovician Eureka Quartzite was at least 400 feet thick about the forebulge. Eureka sandstones eroded off the forebulge were recycled and were redeposited in the back-bulge Sunnyside basin during the Devonian. The implications of the distribution of quartz sandstones in the Sunnyside basin and the regional tectonic features affecting Devonian paleogeography are presented in Chapter 7.

Environment of Deposition

Burrows in silty dolomudstone above the hummocky cross-stratified sandy dolomudstone at the base of Sequence 1 suggest a shallowing-upward from above storm wave-base in open-shelf conditions to low-intertidal conditions (**Plate 2a**). J. Warme (1999, personal communication) reported *Zoophycus* at Six Mile Flat, nine miles northeast of Hiko, suggesting quiet water. The abundance of burrows decreases upward to laminated dolomudstone. This suggests a shallowing-upward cycle to supratidal conditions at the top of Sequence 1.

Overlying the laminated dolomudstones of Sequence 1 is a cliff-forming sandstone interbed containing hummocky cross-stratification in the lower part of "Oxyoke Formation" Sequence 2. The hummocky cross-stratification was probably deposited above storm wave-base in open-shelf conditions. These sandstones were overlain with a clean, well-sorted, bidirectional trough cross-bedded sandstones that were probably deposited as upper shoreface sandstones. Above the shoreface sandstones, tabular cross-bedded sandstones suggest beach or intertidal conditions. Above the sandstone interbed, quartz sand content decreases gradually upward for 35 feet to the top of the "Oxyoke Formation." The upper contact of the "Oxyoke Formation," marked by a leftward flexure in gamma radiation, is the uppermost occurrence of quartz sandstone at TMS. Although bedding is obliterated by dolomitization, the higher gamma radiation at the top of the "Oxyoke Formation" could be a result of supratidal dolomite typical of many shallowing-upward cycles of the Devonian at TMS.

### Oxyoke Formation at Tempiute Mountain and Monte Mountain

The "Oxyoke Formation" at Tempiute Mountain and Monte Mountain displays some variability of the unit. It is composed of four shallowing-upward cycles at Wildcat Wash, Tempiute Mountain (**Figure 9**, No. 53; see **Plate 1a** for measured section location), where its base is less conspicuous than at TMS because it lacks rip-up clasts at the contact. I place the basal contact where dark-gray weathering dolomite overlies light-gray weathering dolomite. It coincides with a significant increase in gamma radiation (**Figure 13**). A 52.5-foot quartz arenite occurs near the top of the "Oxyoke Formation." It is pale red gray on a fresh and weathered surface. Cemented with dolomite, its fine sand grains are trough crossbedded. It overlies a 60-foot bed of quartz sand-bearing dolomite. A sharp upper contact marks the change from sandstone to dark weathering, laminated dolomite of the Simonson Dolomite Coarsely-Crystalline Sequence. Gamma radiation is low over the sandstone and begins to increase over the dolomite above the sandstone (**Figure 13**). About a mile south of Wildcat Wash the "Oxyoke Formation" is shattered, liquified, and jammed upward into a set of dikes and sills associated with the cosmolite impact (Warme and Kuehner, 1998).

The "Oxyoke Formation" at Monte Mountain (No. 52, **Figure 9**) has one thick (35-foot) quartz arenite and three thin (5- to 10-foot) ones near the base. Approximately 100 feet of sandy dolomite beds occur near the top of the interval. Eleven shallowing-upward cycles produce a serrated gamma-ray pattern at Monte Mountain.

"Oxyoke Formation" Sequences

Two sequences, containing six shallowing-upward cycles, occur in the 195-foot thick "Oxyoke Formation" at Mail Summit. They are described briefly below and in detail in Appendix B.

"Oxyoke Formation" Sequence 1 "Oxyoke Formation" Sequence 1 at TMS is 100 feet thick and comprised of four of the six "Oxyoke Formation" cycles. The lower boundary of Sequence 1 is a merged LSE and TSE. It separates the underlying ledge-forming, laminated, quartz-free, light-gray Sevy Dolomite from the overlying slope-forming, light-yellow-brown, sandy, hummocky cross-stratified, intraclast (flattened rip-up clasts) packstone that grades upward to finely-crystalline, black chert nodule-bearing, burrowed "Oxyoke Formation" dolomudstone. In cuttings, the Sevy Dolomite and the "Oxyoke Formation" could be confused unless the silty and cherty nature of the "Oxyoke Formation" is observed. A minor rightward gamma-ray spike followed by a prominent leftward gamma-ray inflection marks the base of Sequence 1 (**Figure 13**). All four of the Sequence 1 cycles are shallowing-upward cycles and are interpreted as beginning in restricted-marine to intertidal conditions and culminating in low-intertidal to supratidal conditions.

“Oxyoke Formation” Sequence 2  “Oxyoke Formation” Sequence 2 is 95 feet thick and is composed of two cycles at TMS. The lower cycle is a light orange-brown quartz sandstone cliff that creates a regionally recognizable but intermittent stratigraphic marker. Hummocky cross-stratification at the base of the cycle suggests a second major deepening event within the “Oxyoke Formation.” Medium yellow-brown, fine- to medium-grained, crossbedded, poorly dolomite-cemented quartz sandstone comprises the rest of the cycle. Quartz sand content decreases upward, and the cycle appears to shallow upward. The second cycle is composed of finely-crystalline, medium dark-gray dolomite that contains upward-thickening sandy beds. Superficially, the transition upward from sandy “Oxyoke Formation” beds to the overlying Coarsely-Crystalline Sequence of the Simonson Dolomite seems gradual. However, a significantly sharp leftward gamma-ray inflection was used to define the boundary (**Figure 12** and **Figure 13**). In other sections, the contact between the sandy, light-brown “Oxyoke Formation” and the sand-free, medium-gray Simonson Dolomite is sharp on the outcrop and gamma-ray log.

## Simonson Dolomite

The Simonson Dolomite at TMS is 860 feet thick and is composed of four sequences (**Table 4**), which coincide with the four members of the Simonson Dolomite identified by Osmond (1954): Coarsely crystalline, Lower Alternating, Brown Cliff, and Upper Alternating. It is characteristically banded with light-gray and dark-brown bands that are one to tens of feet thick. The bands represent upward shallowing cycles. Elrick (1995) interpreted the banded dolomites of the Simonson Dolomite as peritidal cycles. However, the broad shelf and the Antler forebulge probably dampened the effects of tides. Two major karst surfaces, one at the top of the Coarsely-Crystalline Sequence and the other at the top of the Upper Alternating Sequence, make the Simonson Dolomite a potentially attractive hydrocarbon exploration target (**Figure 13** and Stop #7, Appendix D). The economic potential of this interval is discussed in Chapter 8. Pervasive dolomitization of the Simonson Dolomite is discussed in later in this chapter. **Figure 16** shows the distribution of the 78 Simonson Dolomite outcrops that cover 17.67 square miles in the Timpahute Range quadrangle.

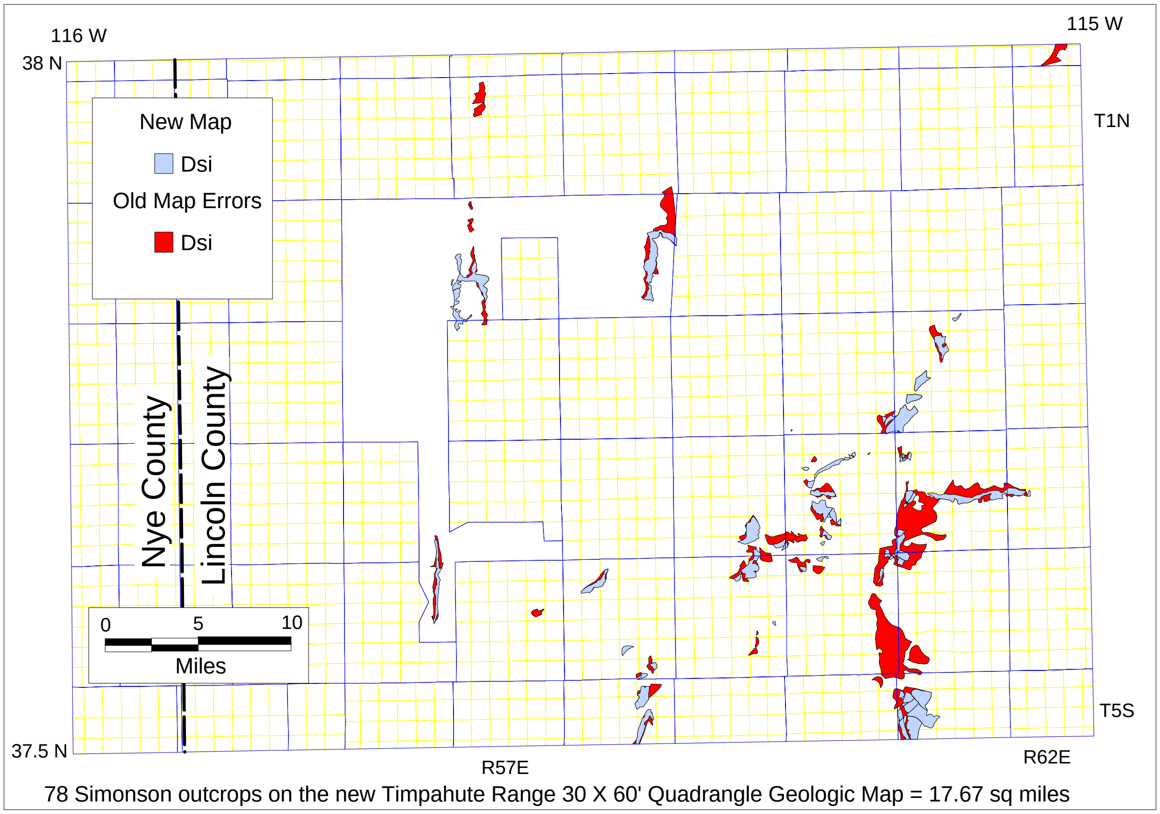


**Figure 16** Distribution of Simonson Dolomite outcrops on the new geologic map of the Timpahute Range quadrangle. Areas erroneously mapped on the old geologic map as Simonson Dolomite are marked in red. Degrees N latitude and W longitude are marked at the corners of the map. Surveyed township and range lines are blue and section lines are yellow.

Coarsely-Crystalline Sequence

Comprising four cycles, the Coarsely-Crystalline Sequence is 225 feet thick at TMS. Recrystallization of the dolomite to a very coarsely-crystalline texture has obliterated most primary depositional features in this basal member of the Simonson Dolomite (**Table 4**). Shallowing-upward cycles are subtle. Regionally, the base of the Coarsely-Crystalline Sequence appears to interfinger with the top of the “Oxyoke Formation.” At TMS, the base of the sequence is picked at a leftward flexure in the gamma-ray log coincident with a significant decrease in quartz grain content as described in the “Oxyoke Formation” section above. The top of the sequence is marked by a regional unconformity that separates coarsely-crystalline, karsted dolomite below from cyclic finely-crystalline dolomite above (**Figure 17**). Solution-collapse breccias and drusy cavity fillings occur tens of feet below the top of the unconformity. Intensity of karsting, width of fractures filled with white coarsely-crystalline dolomite, and crystal coarseness all increase to the upper sequence boundary, and must be related to the exposure surface there (**Figure 13**).

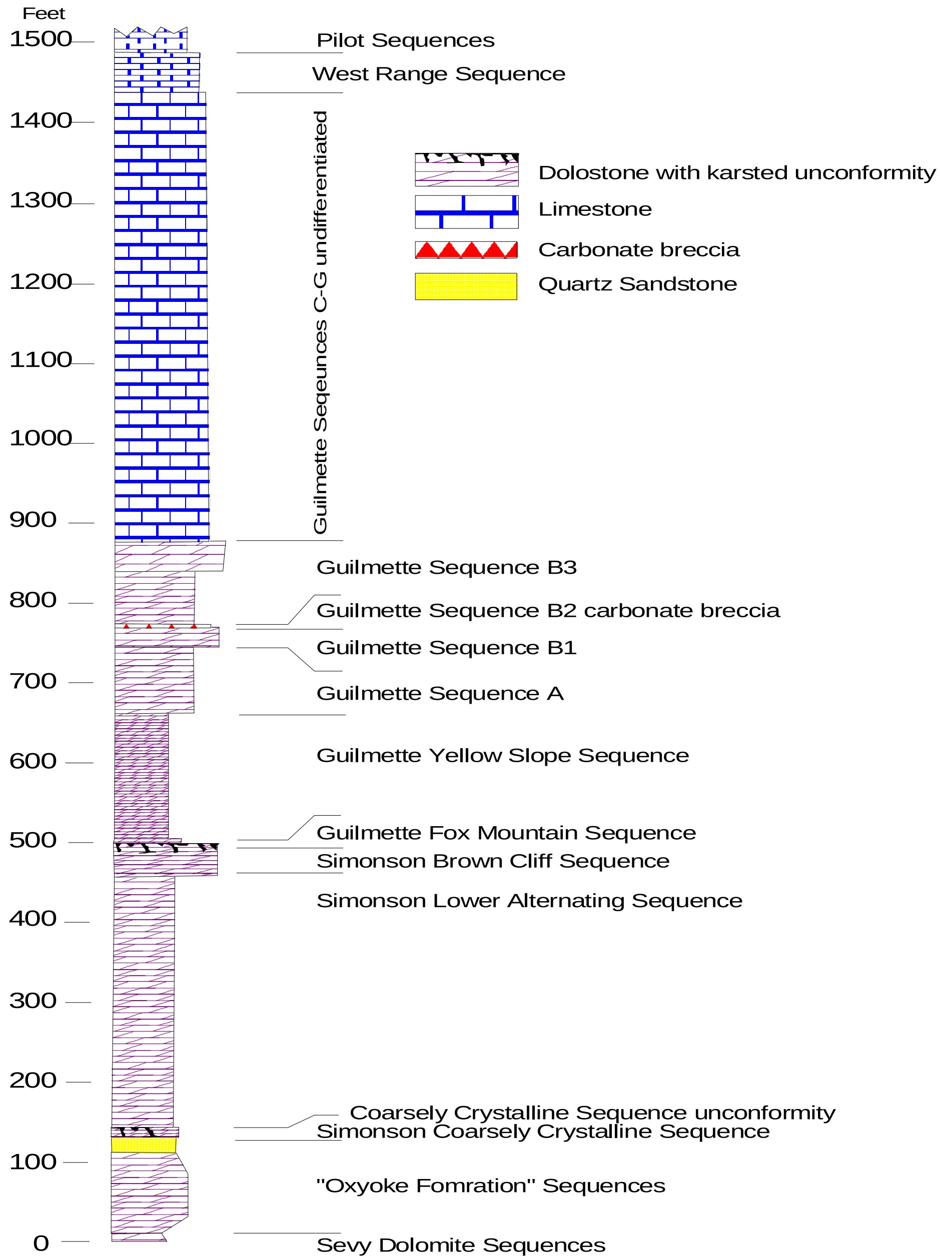


**Figure 17** Generalized stratigraphic column of Middle and Upper Devonian Rocks in the Meadow Valley Mountains, Longitude 114° 44' W, Latitude 37° N, Lincoln County, Nevada showing unusually thin Guilmette Sequence Dgb2 and thin Simonson Coarsely-Crystalline Sequence.

<u>Gamma Radiation</u>  A slight rightward gamma-ray inflection marks the top of the upper karsted surface of the sequence and correlates to other wells and sections (**Plate 2a**). The gamma radiation of the sequence is generally weak and forms a smooth pattern. Within the sequence, gamma radiation of each cycle gradually increases upward then abruptly decreases at the base of the succeeding cycle.

<u>Structural Implications</u>  If the Monte Mountain (TMM) section in the Silver Canyon thrust sheet is restored west of the Tempiute Mountain (TMP) section, the thickness of the Coarsely-Crystalline Sequence thickens progressively eastward to TMS. The depth of karsting also increases eastward from the study area and suggests that the Monte Mountain section was less emergent than the Tempiute Mountain section during the sea-level drop that produced the LSE at the top of the sequence.

In a section measured in the Meadow Valley Mountains about 50 miles southeast of Mail Summit, karst cavities associated with the LSE penetrate downwards into the "Oxyoke Formation" (**Figure 17**). Geopetal structures containing pale-red, laminated silty dolomite parallel to tectonic dip, the proximity of the karsting to the unconformity, and persistence of karsting in the same beds along structural strike, all distinguish Devonian karsting from recent karsting of this interval. In the Meadow Valley section, most of the Coarsely-Crystalline Sequence is missing and only 12.5 feet are remaining due to the unconformity. Overlying the unconformity is the Lower Alternating Sequence.

Therefore, the unconformity at the top of the Coarsely-Crystalline Sequence progressively cuts out more of the sequence eastward and the depth of karsting below the unconformity increases eastward. This regular eastward thinning of the Coarsely-Crystalline Sequence can be used to help restore thrust sheets.

Lower Alternating Sequence

The Lower Alternating Sequence is 265 feet thick and is composed of 12 cycles (**Plate 2a)**. A transgressive lag above the merged LSE and TSE marks the base of the Lower Alternating Sequence (**Figure 13**). Twelve prominent shallowing-upward cycles form the sequence. Each cycle is tens of feet thick and exhibits an alternating light and dark appearance at TMS. These cycles contain minor cycles (<10 feet thick). Subtidal, medium-gray to dark-gray, burrowed, medium-crystalline dolomite intervals that commonly contain *Amphipora* make up the lower part of the major cycles. They shallow upward to supratidal, light-gray, fossil-poor, finely-crystalline dolomite, some with tepee structures. Successive cycles become bathymetrically deeper, and become subsequently thinner to the middle of the sequence and then thicken to the top (**Figure 13**). Gamma radiation increases abruptly at the base of the sequence and gradually decreases upward (**Plate 2a**). Minor fluctuations superimposed on the upward decrease in gamma radiation roughly track the twelve shallowing-upward cycles, with each cycle marked by a subtle decrease at the base and a gradual increase upward.

Gamma Radiation A sharp increase in gamma radiation marks the base of the sequence and a sharp decrease in gamma radiation marks the top of the sequence (**Plate 2A**). Generally, the base of each of the ten cycles that comprise the sequence is marked by a sharp decrease in gamma radiation. Gamma radiation gradually increases upward within the cycles. A gamma-ray spike at the top of cycle 8 is higher (> 80 cps) than any other gamma-ray measurement in the Simonson Dolomite.

Brown Cliff Sequence

The Brown Cliff Sequence is 85 feet thick and comprised of four cycles. It lies above a regionally significant, undulating surface that cuts into the top of the Lower Alternating Sequence. The surface represents a merged LSE and TSE. This lower sequence boundary is directly overlain by an MFS. Recrystallization has largely masked a transgressive lag in the Brown Cliff Sequence above the erosional surface (**Plate 2a**). The Brown Cliff Sequence was probably deposited in more open marine conditions than any of the Simonson Dolomite sequences above or below. It is the first sequence above the Silurian to contain abundant marine fossils such as corals, large stromatoporoids and brachiopods. Though the Brown Cliff Sequence at TMS does not contain large reefs, Devonian reef building peaked during the Givetian worldwide (Webb, 1998). However, in other parts of the Sunnyside basin, Lower Givetian reefs were formed in the Brown Cliff Sequence. Givetian reefs are found in the Limestone Hills, 60 miles northeast of the study area and in the Meadow Valley Mountains, 40 miles south-southeast of the study area (Cedar Strat proprietary measured sections, 1985). Fossils are scarce in sequences between the Brown Cliff and the base of the Guilmette Formation at TMS.

Gamma Radiation The Brown Cliff-Forming Sequence contains more open-shelf fossils and exhibits weaker gamma radiation than any other sequence in the Simonson Dolomite. A sharp gamma-ray leftward inflection at the base of the sequence is regionally correlatable (**Figure 13**). Typically, gamma radiation decreases over fossiliferous, thickly bedded, darker-gray carbonates at cycle bases interpreted to be deposited in more open-shelf conditions. Gamma radiation increases toward cycle tops that consist of thinly-bedded, lighter-gray, fossil-poor carbonates interpreted to be deposited in more restricted to supratidal conditions. Slight increases in overall gamma radiation from base to top follows the same pattern of shallowing-upward cycles in other parts of the TMS. Thus, the gamma-ray pattern calibrated with fossil distributions suggests that the Brown Cliff-Forming Sequence is a shallowing-upward sequence.

Upper Alternating Sequence

The Upper Alternating Sequence is 285 feet thick and consists of 12 cycles at TMS (**Table 4**). A merged LSE and TSE marks its base (**Plate 2a**). Thin sections display ghosts of intraclasts near the base of the sequence, suggesting a TSE lag. Above the TSE, a pronounced lack of open-shelf fossils and increase in gamma radiation abruptly occurs. Depositional environments of this sequence are similar to the Lower Alternating Sequence. *Amphipora* in the lower, darker part of some cycles suggests intertidal conditions. Lighter-gray, fossil-poor, and the more finely crystalline upper parts of the cycles suggest supratidal conditions.

Gamma Radiation A sharp increase in gamma radiation marks the base of the Upper Alternating Sequence (**Plate 2a**). The general decrease in gamma radiation of each succeeding cycle upward supports the upward-deepening interpretation made from changes in lithology and biofacies (**Figure 13**). Gamma-ray spikes at the tops of internal shallowing-upward cycles may be due to concentrated, wind-blown radioactive detritus. A gamma-ray spike at the top of the sequence at TMS is probably caused by radioactive debris concentrated along the karsted interval.

Regional Simonson Dolomite Unconformity Extensive karsting at the top of the Simonson Dolomite marks the most persistent exposure surface of the Great Basin Devonian section (**Figure 13**). The regional unconformity, marked by karsting hundreds of feet deep, separates the calcareous Guilmette Formation from the underlying dolomitic Simonson Dolomite. However, the lower Guilmette that lies on the unconformity can be dolomitized as in the Meadow Valley Mountains where the unconformity cuts down into the Simonson Dolomite Brown Cliff Sequence (**Figure 17**). This LSE at the top of the Simonson Dolomite occurs in most outcrops and wells of Devonian rocks in eastern Nevada and western Utah (**Figure 9**).

The light and dark bands of the Upper Alternating Sequence become faded upward toward bleached dolomites below the unconformity. The bleached karsted Simonson Dolomite contrasts sharply with the darker gray limestones of the Fox Mountain and younger sequences on aerial photographs and outcrops. The karsted upper Simonson Dolomite is 55% dark-gray, 30% light-gray, and 15% medium-gray in contrast to 69% dark-gray carbonates in the overlying Guilmette Formation. Pervasively dolomitized, the Simonson Dolomite is easily distinguished from overlying limestone beds of the Guilmette Formation. Furthermore, the karsted, porous, and permeable Simonson Dolomite weathers into partly covered slopes and ledges whereas the Fox Mountain and younger sequences form ledges and cliffs (**Plate 2a**, **Table 5**).

Evidence for karsting includes karst breccia, drusy dolomite-lined cavities, dolomite crystal coarseness increasing upward, white dolomite spar-filled fractures that widen upward, bleaching, and geopetal structures filled with laminated yellow-gray, silty dolomite (Stop #7, Appendix D). At TMS, some karst cavities in the Simonson Dolomite are filled with Guilmette limestone that suggest that the transgression of the Guilmette sea must have been rapid. Some karst cavities, filled with dolomite breccia, occur as deep as 200 feet below the karst surface at TMS. The basis for separating the Simonson Dolomite from the overlying Guilmette Formation at its Deep Creek Range, Utah, type locality is presented in Chapter 2.

**Table 5** Gamma radiation and weathering profile for the lower Guilmette Formation at TMS. For gamma radiation, the average, maximum, minimum, and standard deviation in counts per second are presented. The average weathering for each sequence is presented from most resistant (cliff) to least resistant (covered slope). Note that the Yellow Slope Sequence emits the highest average radiation and that Sequence Dgb2 is more cliffy than the other sequences. The method for determining sequence values is explained in Chapter 2.

| SEQUENCE | GAMMA RADIATION Counts Per Second | | | | PROFILE PERCENT(%) | | | |
|---|---|---|---|---|---|---|---|---|
| | AVE | MAX | MIN | STD | CLF | LDG | PCS | CS |
| SEQUENCE Dgcc | 46 | 53 | 41 | 3.3 | 0 | 0 | 22 | 78 |
| SEQUENCE Dgcf | 46 | 64 | 36 | 8.8 | 0 | 31 | 43 | 26 |
| SEQUENCE Dgb3c | 24 | 41 | 18 | 5.4 | 44 | 49 | 7 | 0 |
| SEQUENCE Dgb3f | 38 | 57 | 28 | 7.2 | 3 | 92 | 5 | 0 |
| SEQUENCE Dgb2 | 27 | 34 | 21 | 3.3 | 100 | 0 | 0 | 0 |
| SEQUENCE Dgb1 | 30 | 37 | 24 | 3.9 | 60 | 20 | 10 | 10 |
| SEQUENCE Dgbc | 26 | 41 | 18 | 4.9 | 72 | 23 | 4 | 1 |
| SEQUENCE Dgbf | 33 | 57 | 32 | 7.3 | 65 | 32 | 2 | 1 |
| SEQUENCE Dga | 43 | 64 | 22 | 10.0 | 36 | 46 | 7 | 21 |
| SEQUENCE Dga2 | 32 | 53 | 22 | 6.5 | 50 | 40 | 8 | 2 |
| SEQUENCE Dga1 | 49 | 64 | 36 | 6.4 | 32 | 42 | 9 | 17 |
| YELLOW SLOPE | 62 | 74 | 48 | 5.5 | 0 | 26 | 49 | 25 |
| FOX MOUNTAIN | 53 | 70 | 37 | 7.6 | 13 | 58 | 27 | 2 |

Key: AVE: Average; MAX: Maximum; MIN: Minimum; STD: Standard Deviation; CLF: Cliff; LDG: Ledge; PCS: Partly Covered Slope; CS: Covered Slope

<u>Guilmette Formation</u>

Of the five TMS Devonian formations, the Guilmette Formation, which is 2,677 feet thick and consists of nine sequences and five subsequences, is the most lithologically variable (**Table 2**). It contains limestone, dolomite, siltstone, sandstone, reefs, and breccia. For convenience it was divided into two parts. The lower Guilmette Formation is composed of the Fox Mountain and Yellow Slope Sequences and Sequences Dga, Dgb, Dgc, and the upper Guilmette Formation is composed of Sequences Dgd, Dge, Dgf, and Dgg. All nine sequences are present at TMS (**Figure 13**), though the Fox Mountain Sequence is missing at Monte Mountain, and Sequence Dgb lies directly on the Simonson Dolomite at Tempiute Mountain.

Superficially, the Guilmette appears to be a massive carbonate with little internal character. However, a detailed analysis of the Guilmette sequences reveals a unit with enough internal character that it can be used to unravel complex structural relationships. Each sequence contributes an important part of the stratigraphic and structural picture. For example, the thickness of the Fox Mountain sequence suggests where within the Sunnyside basin each section was deposited before they were dislocated by Mesozoic thrusting. Sections with a thick Fox Mountain sequence such as at TMS and the Worthington and Golden Gate ranges were deposited near the center of the Sunnyside basin. In contrast, in the Silver Canyon thrust sheet, the Fox Mountain sequence is absent in the Monte Mountain (TMM) section and very thin at the Down Drop Mountain section deposited on the west edge of the Sunnyside basin. It is also thin in the Meadow Valley section (**Figure 17**) deposited on the east side of the basin.

Some Guilmette sequences are excellent marker beds and help delineate structural features. A good Guilmette marker bed in eastern Nevada is the nonresistant Yellow Slope Sequence (**Plate 2a**). It is easily recognized in the field and on areal photographs. Above the Yellow Slope Sequence are the well-developed, preserved and exposed cycles of Sequence Dga. Their upward shallowing nature helps restore deposition orientation in structurally complex areas.

Sequence Dgb, containing reefs and breccia, is easily identified in the field because it weathers into massive cliffs, whereas Sequence Dga and the rest of the Guilmette weathers into ledges and slopes. The unique concentric nature of the distribution of the Sequence Dgb2 impact breccia constrains restoration of thrust sheets containing the breccia. Above Sequence Dgb at TMS, the section is mostly shallow-water, cyclic carbonates that are predominantly dolomite with some limestone and minor sandstone beds higher in the section. These post-impact beds also constrain restoration of thrust sheets. Equivalent beds are predominantly quartz sandstone at Monte Mountain and deeper-water, thin-bedded limestone at Tempiute Mountain. The distribution of these post-impact sequences makes little sense without the thrust reconstruction presented in Chapter 5. Therefore, the Guilmette sequences in the Timpahute Range 30' X 60' quadrangle hold important keys to understanding this part of the Sevier fold-and-thrust belt. **Figure 18** illustrates the locations of 142 Guilmette outcrops that cover 89.07 square miles in the Timpahute Range quadrangle.

In this study, the lower Guilmette at TMS is described in more detail than other parts of the Devonian because it contains the impact breccia of Sequence Dgb2. Therefore, an understanding of the depositional setting immediately before and after the emplacement of the distinctive carbonate breccia is a primary focus of this study. Also, the shallowing-upward cycles in the lower Guilmette are unaltered (not pervasively dolomitized), well-exposed, and were overlooked in previous studies. They provide an unusual opportunity to study carbonates and carbonate environments. They provided the opportunity to test the usefulness of surface gamma-ray logs in cycle and sequence analysis. As a result, they were used to calibrate surface gamma-ray patterns in other sections throughout the Sunnyside basin. Microfacies analysis of thin sections from the lower Guilmette cycles and sequences provided additional detail and further calibrated the TMS cycles and sequences (**Plate 5**). Therefore, TMS is the reference section of Devonian sequences in the Sunnyside basin.

This section summarizes and compares the characteristics of the lower Guilmette sequences. These characteristics consist of general descriptions of weathering profile, color, gamma-ray patterns, lithology and texture, sequence and cycle thicknesses, fossil occurrences, and thickness patterns of cycles and are graphically presented in Tables 5-8 and Figures 20-22. Percentages were calculated from the number of measured increments of a particular characteristic divided by the total number of measured increments in the sequence (Chapter 2). Following this section summarizing the lower Guilmette sequences, a description of each Guilmette sequence is presented. Descriptions of each cycle within each sequence can be found in Appendix B.

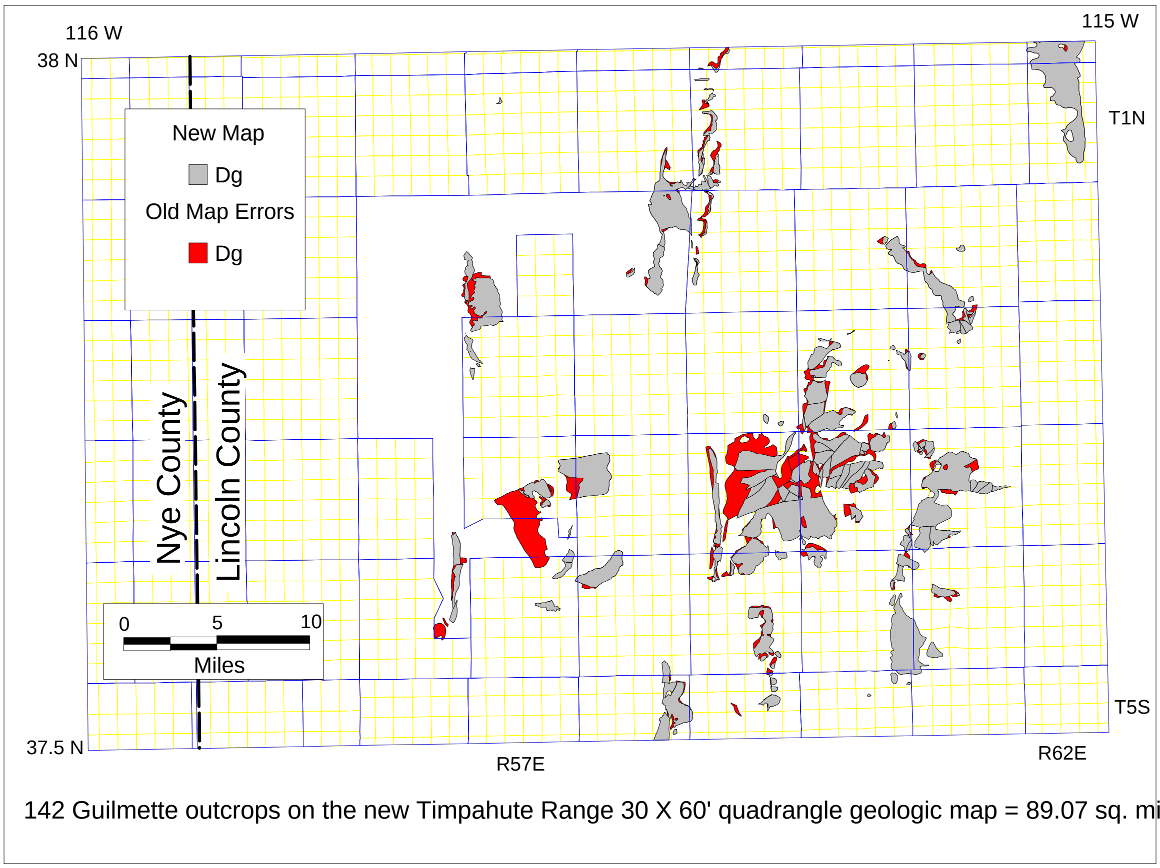


**Figure 18** Distribution of Guilmette Formation outcrops on the new Timpahute Range quadrangle geologic map. Areas erroneously mapped as Guilmette on the old geologic map are marked in red. Degrees N latitude and W longitude are marked at the corners of the map.

## Weathering Profile

Whereas the 135-foot-thick Fox Mountain Sequence is mostly cliffs (71%) and ledges, nearly 75% of the 182-foot-thick Yellow Slope Sequence weathers into covered and partly-covered slopes. Where present, the resistant Fox Mountain forms prominent ledges and cliffs (**Plate 2a**, **Table 5**). Ledges and cliffs make up 82% of the 395-foot-thick Sequence Dga, 95% of the 420-foot-thick Sequence Dgbc (reef core), and 97% of the 302-foot-thick Sequence Dgbf (reef flank). Sequence Dgc forms a 45-foot-thick slope above Dgbc and at Dgcf, forms a 188-foot-thick interval of ledges, partly covered slopes, and covered slopes above Dgbf (**Figure 4**). **Table 5** summarizes the weathering profiles of the lower Guilmette sequences.

## Lithology and Texture

**Table 6** summarizes thicknesses and lithologies of the lower Guilmette Formation sequences. Except the Yellow Slope Sequence and Sequence Dga1, limestone predominates in the lower Guilmette sequences. The percent of limestone in each sequence increases upward from the Yellow Slope Sequence to Sequence Dgc. The distribution of dolomite in the lower Guilmette sequences is significant because most of the dolomite occurs as finely-crystalline caps on the shallowing upward cycles. Sequences that contain a greater proportion of supratidal dolomite caps, such as the Yellow Slope Sequence, contain more dolomite than those composed mostly of open-marine carbonates such as Sequences Dgb1, Dgb3f, and Dgcc that contain almost no dolomite.

**Table 6** Thicknesses and gross lithologies of the lower Guilmette Formation sequences. The method for determining the gross lithology percent is explained in Chapter 2. Sequence Dgb3c is thicker than Sequence Dgb3f. The greater thickness could have been caused by accelerated growth and reef development at Dgb3c and lack of reef development at Dgb3f. Data in the table indicate that the percent of dolomite decreases upward from the Yellow Slope Sequence.

| SEQUENCE | THICKNESS in FEET | LITHOLOGY PERCENT (%) | | | | |
|---|---|---|---|---|---|---|
| | | LS | DOL | SS | BRC | SLTS |
| SEQUENCE Dgcc | 45 | 100 | 0 | 0 | 0 | 0 |
| SEQUENCE Dgcf | 188 | 72 | 20 | 3 | 0 | 5 |
| SEQUENCE Dgb3c | 228 | 90 | 10 | 0 | 0 | 0 |
| SEQUENCE Dgb3f | 97 | 100 | 0 | 0 | 0 | 0 |
| SEQUENCE Dgb2 | 179 | 0 | 0 | 0 | 100 | 0 |
| SEQUENCE Dgb1 | 26 | 100 | 0 | 0 | 0 | 0 |
| SEQUENCE Dgbc | 420 | 52 | 5 | 0 | 43 | 0 |
| SEQUENCE Dgbf | 302 | 41 | 0 | 0 | 59 | 0 |
| SEQUENCE Dga2 | 145 | 75 | 25 | 0 | 0 | 0 |
| SEQUENCE Dga1 | 250 | 50 | 50 | 0 | 0 | 0 |
| SEQUENCE Dga | 395 | 59 | 41 | 0 | 0 | 0 |
| YELLOW SLOPE | 182 | 39 | 58 | 3 | 0 | 0 |
| FOX MOUNTAIN | 135 | 93 | 7 | 0 | 0 | 0 |
| KEY: LS: LIMESTONE; DOL: Dolostone; SS: SANDSTONE; BRC: BRECCIA; SLTS: SILTSTONE | | | | | | |

A histogram of dolomite percentages in each cycle of the lower Guilmette Formation illustrates the distribution of dolomite in the section (**Figure 19**). Lithologies vary from 100% dolomite in Yellow Slope Sequence Cycle 7 and Sequence Dga1 Cycle 5, to 100% limestone in Fox Mountain Sequence Cycle 4 (**Table 6**). Dolomitization of 58% of the Yellow Slope Sequence is probably associated with early peritidal dolomitization. This finely-crystalline stratal dolomite contrasts with the medium- to coarsely-crystalline pervasive dolomite of the underlying Simonson Dolomite that is probably related to the regional unconformity at the top of that formation. The occurrences and significance of dolomite at TMS are discussed in more detail in later in this chapter.

Five sets of cycles in which the percentage of dolomite decreases upward occur in the lower Guilmette sequences (**Figure 19**). They are Fox Mountain Sequence Cycles 1 through 4, Yellow Slope Sequence Cycles 3 through 5, Yellow Slope Sequence 9 through Sequence Dga1 Cycle 3, Sequence Dga1 Cycles 5 through 11, and Sequence Dga2 Cycles 2 through 4. Two sets of cycles in which the percentage of dolomite increases upward include Yellow Slope Sequence Cycles 5 through 7 and Sequence Dga2 cycles 4 through 7. Repeated patterns of dolomite content in the histogram suggest that most of the dolomite in the reference section be related to selective early dolomite diagenesis at cycle tops. Most of the dolomite forms finely-crystalline stratal dolomite caps on shallowing upward cycles. These occurrences of dolomite contrast to later dolomitization associated with unconformities, faulting and porous zones.

Other than a small percent of sandstone in the Yellow Slope Sequence and in Sequence Dgcf, lower Guilmette sequences lack sandstone. Siltstone is a minor constituent in Sequence Dgcf, but is lacking in the other lower Guilmette sequences.

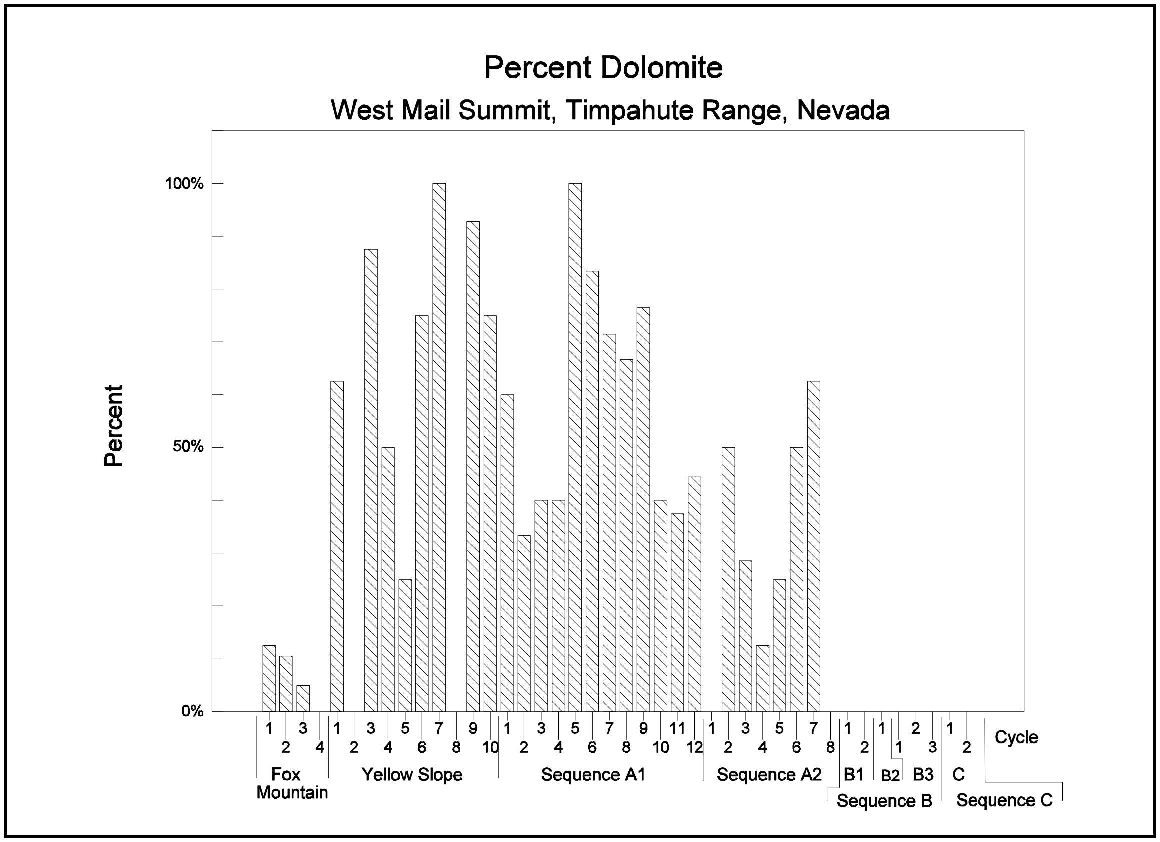


**Figure 19** Histogram of percent dolomite within each cycle of the lower Guilmette Sequences at TMS where Sequence Dgb3 is a stromatoporoid reef illustrates the abundance of dolomite in the Yellow Slope and Dga1 Sequences and the lack of dolomite in the Fox Mountain, Dgb, and Dgc Sequences.

**Table 7** summarizes the depositional textures of the lower Guilmette Formation Sequences. Texture coarsens upward from 72% mudstone in the Yellow Slope Sequence to 2% mudstone in the overlying Sequence Dgbc. Packstone predominates in five of the 13 lower Guilmette sequences listed in **Table 7**. Wackestone predominates in four of the sequences, mudstone in three of the sequences and boundstone in two of the sequences.

<u>Color</u>

**Table 7** summarizes the colors of the lower Guilmette sequences. The percent of dark-gray carbonates increases upward from 55% in the Simonson Dolomite to 69% in the Fox Mountain. In contrast, only 21% of the Yellow Slope is dark gray. However, the percent of dark-gray carbonates increases upward again from 36% in Sequence Dga to 45% and 62% in Sequence Dgbc and Dgbf respectively. Light-gray carbonates increase upward from 35% in Sequence Dga to 43% in Sequence Dgb reef core but decrease to 9% in Sequence Dgb reef flank. Medium-gray carbonates decrease from 29% in Sequence Dga to 12% Sequence Dgbc and 28% Dgbf.

<u>Percentage of Limestone</u>

A histogram of the percentage of limestone in each cycle illustrates the higher concentration of calcium carbonate in the Fox Mountain Sequence and in Sequences Dgb and Dgc with respect to the other sequences (**Figure 20**). Three sets of cycles in which the percent limestone increases upward occur. They are Fox Mountain Sequence Cycles 1 through 4, Yellow Slope Sequence Cycle 7 through Sequence Dga1 Cycle 4, and Sequence Dga1 Cycle 5 through Sequence Dga2 Cycle 5. One set of cycles shows an upward decrease in percentage of limestone from Sequence Dga2 Cycle 4 through Sequence Dga2 Cycle 7. Sequences Dgb and Dgc are all limestone except local non-stratal dolomite associated with fractures and porous zones. The cyclic pattern of the percentage of dolomite and the percentage of limestone suggests that dolomitization at the tops of shallowing-upward cycles occurred penecontemporaneously with deposition (**Figure 21**). Because dolomite-rich zones at the top of cycles occur at the same interval in other sections, it is likely that the zones were selectively dolomitized before Mesozoic thrusting and Cenozoic extension of the eastern Great Basin.

**Table 7** Color and texture of lower Guilmette Formation sequences expressed as percent of the sequence. The table indicates the unique abundance of pale yellow-brown rocks in the Yellow Slope Sequence and the muddy nature of the Yellow Slope Sequence and Sequence Dgc.

| SEQUENCE | COLOR PERCENT (%) | | | | TEXTURE PERCENT (%) | | | | |
|---|---|---|---|---|---|---|---|---|---|
| | LGY | MGY | DGY | PYB | MUD | WAC | PAC | GRN | BND |
| SEQUENCE Dgcc | 71 | 0 | 29 | 0 | 100 | 0 | 0 | 0 | 0 |
| SEQUENCE Dgcf | 42 | 40 | 18 | 0 | 74 | 36 | 0 | 0 | 0 |
| SEQUENCE Dgb3c | 86 | 7 | 7 | 0 | 0 | 2 | 3 | 5 | 90 |
| SEQUENCE Dgb2 | 14 | 18 | 68 | 0 | 2 | 0 | 98 | 0 | 0 |
| SEQUENCE Dgb1 | 0 | 50 | 50 | 0 | 0 | 21 | 79 | 0 | 0 |
| SEQUENCE Dgbc | 43 | 12 | 45 | 0 | 0 | 2 | 53 | 2 | 43 |
| SEQUENCE Dgb3f | 2 | 42 | 53 | 3 | 0 | 10 | 5 | 17 | 68 |
| SEQUENCE Dga2 | 12 | 38 | 50 | 0 | 24 | 39 | 33 | 4 | 0 |
| SEQUENCE Dga1 | 48 | 25 | 27 | 0 | 31 | 47 | 17 | 5 | 0 |
| SEQUENCE Dga | 35 | 29 | 36 | 0 | 28 | 44 | 23 | 5 | 0 |
| YELLOW SLOPE | 21 | 14 | 21 | 44 | 72 | 14 | 5 | 6 | 3 |
| FOX MOUNTAIN | 0 | 31 | 69 | 0 | 13 | 82 | 4 | 1 | 0 |

KEY: LGY: Light Gray; MGY: Medium Gray; DGY: Dark Gray; PYB: Pale Yellow Brown; MUD: Mudstone; WAC: Wackestone; PAC: Packstone; GRN: Grainstone; BND: Boundstone

Fossils

**Table 8** summarizes the occurrences of fossils in the lower Guilmette Formation. Fossil content changes from predominantly corals at the top of the Simonson Dolomite to brachiopods and gastropods in the Fox Mountain Sequence. Ostracodes, calcispheres and stromatolites commonly occur in the Yellow Slope Sequence. *Amphipora* and corals are more common in Sequence Dga. Tabular and bulbous stromatoporoids are more common in Sequence Dgb. Sequence Dgc is heavily burrowed, contains abundant gastropods, and contrasts sharply with the *Amphipora*-bearing beds of Sequence Dgd in the upper Guilmette Formation.

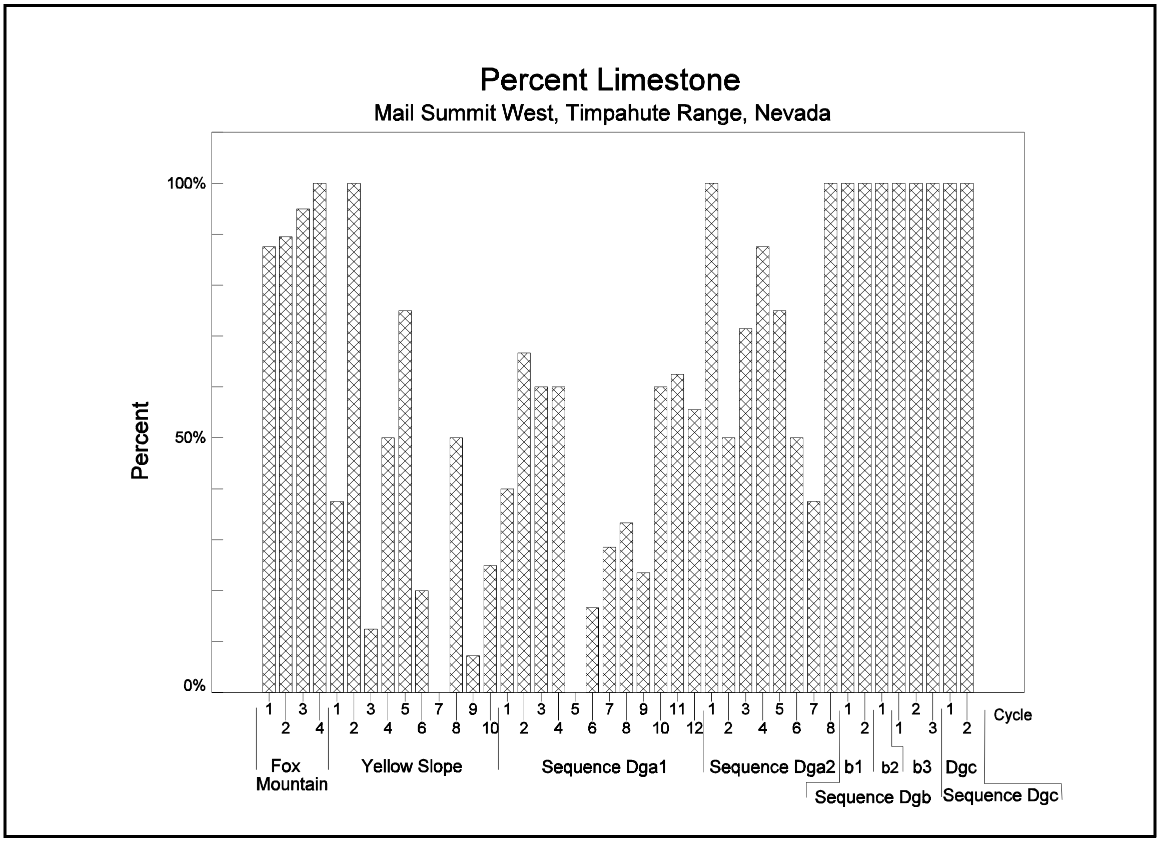


**Figure 20** Histogram of percent limestone within each cycle of lower Guilmette sequences at TMS where Sequence Dgb3 is a stromatoporoid reef. The highest percentages of limestone occurs in the Fox Mountain Sequence and in Sequence Dgb.

<u>Bedding</u>

Bedding in the five basal sequences of the Guilmette Formation varies from massive for the sedimentary breccia and reef in Sequence Dgb to stromatolitically laminated for the Yellow Slope Sequence. Sequence Dga is characterized by prominent shallowing-upward cycles whereas the Fox Mountain Sequence is characterized by subtle shallowing-upward cycles. Burrowed limestone beds help distinguish Sequence Dgc from the adjacent sequences.

**Table 8** Fossil occurrences in the lower Guilmette sequences at TMS ranked by abundance. Data in the table indicate that the abundance of fossil assemblages with an affinity for open-marine conditions increased from the Yellow Slope Sequence to Sequence Dgb3 at TMS.

| Formation Sequence | *Amphipora* | Bulbous Stromatoporoids | Tabular Stromatoporoids | Corals | Ostracodes | Brachiopods | Burrows | Stromatolites | Calcispheres | Echinoderms | Gastropods | Barren |
|---|---|---|---|---|---|---|---|---|---|---|---|---|
| Dgcc | N | N | N | R | R | R | C | N | N | N | C | C |
| Dgb3f | C | A | C | C | R | C | R | R | R | R | R | R |
| Dgb3c | C | A | A | A | R | C | R | R | R | C | R | R |
| Dgb2 | C | C | C | C | R | C | R | R | R | N | R | R |
| Dgb1 | C | C | R | C | R | C | R | R | R | N | R | R |
| Dgbf | C | A | A | A | R | C | R | R | R | R | R | R |
| Dgbc | C | A | A | A | A | R | C | R | R | R | R | R |
| Dga2 | C | C | R | C | R | C | C | R | R | N | C | R |
| Dga1 | C | C | R | C | R | C | C | R | R | R | C | R |
| YS | N | N | N | R | C | R | R | C | C | N | R | C |
| FM | R | R | N | C | R | C | C | R | R | C | C | R |

A =Abundant, C = Common, R = Rare, N = None
FM = Fox Mountain, YS = Yellow Slope,

Cycles

Four major shallowing-upward cycles and two minor cycles compose the Fox Mountain Sequence. Three of the cycles are limestone with a dolomite cap. It appears that open-marine limestones truncate intertidal carbonates. Perhaps serving as a dolomite cap of a large-scale cycle involving the Fox Mountain Sequence, the Yellow Slope Sequence is made of at least ten shallowing-upward cycles. Because open-marine fauna is lacking in the Yellow Slope Sequence, it is likely that the bases of the cycles are no deeper than intertidal. However, the tops of the cycles contain mudcracks filled with quartz sand grains characteristic of supratidal conditions. Two of the cycles are capped by very fine-grained quartz sandstones.

The lower parts of most of the 20 cycles of Sequence Dga contain open-marine fauna. Most of the cycles are capped by laminated, unfossiliferous dolomite. Only two minor shallowing-upward cycles occur below the sedimentary breccia in Sequence Dgb1. The sedimentary breccia or Dgb2 and overlying reef or Dgb3c form the rest of Sequence Dgb in the reef core measured section. All of Sequence Dgb appears to have been deposited in open-marine conditions. Karsting at the top of the Sequence Dgb3c marks an LSE between Sequences Dgb and Dgc. A pale red paleosol occurs at the unconformity and in some karst cavities 20 feet below the unconformity. Geopetals of laminated dolomitic siltstone within some karst cavities have the same attitude as strata above and below suggesting they were deposited before Mesozoic tilting. Burrowed, slope-forming limestone of Sequence Dgc lies above Sequence Dgb and marks another sequence of restricted-marine conditions.

Cycle Thicknesses

A histogram of thickness and content of cycles of the lower Guilmette Formation Sequences (**Figure 21**) provides insight into the nature of bundling of the cycles. It reveals a pattern in which groups of cycles thicken upward from the base of the Fox Mountain Sequence to Cycle 10 of Sequence Dga (UTK1, UTK2, UTK3, and UTK4). An exception to the upward thickening pattern is an upward-thinning pattern from Yellow Slope Sequence Cycle 3 to Yellow Slope Sequence Cycle 8 (UTN1). Above Sequence Dga Cycle 10, two groups of cycles thin upward to the top of Sequence Dgc. One group begins with Sequence Dga1 Cycle 10 (UTN2) and the other group begins with Sequence Dga2 Cycle 7 (UTN3). Admittedly, the trend lines marking bundles of upward thickening and thinning cycles are subjective and may be grouped and interpreted differently by other workers. If bundle thicknesses are related to sequence boundaries, perhaps they could be changed to reflect that relationship. However, the histogram show that there is no relationship.

An upward increase in cycle thickness or upward thickening probably represents an increase of accommodation space caused by an increase in the rate of relative sea-level rise. A comparison of the percentage of dolomite in **Figure 19** with the set of upward thickening Fox Mountain Sequence Cycles 1 through 4 illustrates that the percentage of dolomite decreases as cycle thickness increases upward. As the rate of relative sea-level rise increases, more accommodation space becomes available for open-marine carbonate deposition. Apparently this leaves less time for the formation of supratidal dolomite caps before the next transgression.

A major facies shift occurs at the base of the Yellow Slope Sequence with a greater percent (62%) of dolomite in Cycle 1 than any of the Fox Mountain cycles. The sequence is mostly composed of a set of upward-thinning cycles in which dolomite predominates. An upward decrease in cycle thickness or upward thinning suggests an upward decrease in accommodation space cause by a decrease in the rate of a sea-level rise. A slower rate of relative sea-level rise should provide a greater proportion of supratidal dolomites at the top of shallowing-upward cycles.

Two other facies shifts marking sequence boundaries are seen in the histogram of cycle thicknesses (**Figure 21**). Much of Sequence Dga1 is composed of a set of upward thickening cycles (UTK4) in which the percent of dolomite also increases. Another facies shift occurs at the base of Sequence Dga2, which is mostly a set of upward thinning cycles (UTN2). A greater facies shift occurs at the base of Sequence Dgb1. Sequence Dgb and Dgc cycles never shallow enough to preserve supratidal finely-crystalline stratal dolomite caps.

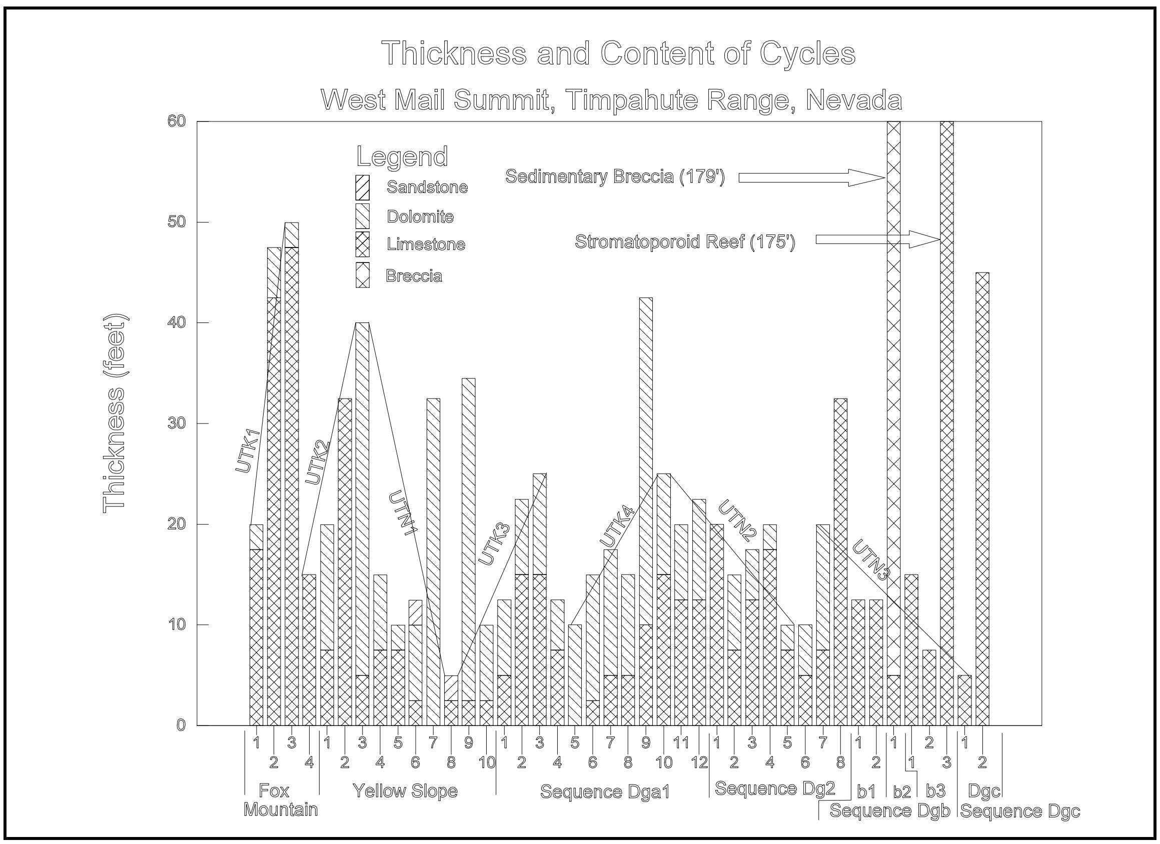


**Figure 21** Histogram of cycle thickness and content of lower Guilmette Formation suggest possible upward thickening (UTK) and upward thinning (UTN) trends at TMS where Dgb3c is a stromatoporoid reef. The sedimentary breccia (Dgb2) and reef (Dgb3c) were truncated at 60 feet to emphasize the other cycles in the lower Guilmette Sequences.
.

Gamma Radiation

**Table 5** summarizes the gamma radiation and weathering profile for lower Guilmette Formation sequences. Gamma radiation increases from about 38 CPS over the Simonson Dolomite Upper Alternating Sequence to an average of 53 CPS over the Fox Mountain Sequence. The radiation continues to increase to an average of 62 CPS over the Yellow Slope Sequence and then decreases to an average of 43 CPS over Sequence Dga and an average of 26 CPS over Sequence Dgbc or 33 CPS over Sequence Dgbf. Karsting at the top of the Sequence Dgb3 reef marks an LSE that merges with a TSE at the base of Sequence Dgc. Bioturbated and silty Sequence Dgc forms a regional rightward gamma-ray inflection that can be correlated with outcrops and wells throughout eastern Nevada and western Utah. Over Sequence Dgc, average gamma radiation increases to 46 CPS.

## Guilmette Sequences

The general characteristics and features of the lower Guilmette sequences were described above. All nine Guilmette sequences are described individually and in detail in this section. Again, emphasis is on the lower Guilmette sequences. Additional descriptions of each cycle and sequence are presented in Appendix B and **Plate 2a**.

Each sequence is composed of one or more cycles. Though cycle boundaries are marked by unconformities or hiatuses, almost no facies shift occurs at the cycle boundaries. On the other hand, major facies shifts mark sequence boundaries. Regionally correlatable gamma-ray log patterns accompany the sequence boundaries. However, gamma-ray patterns of cycles are not regionally correlatable.

Under each sequence described in this section a description may include color, texture, weathering profile, fossils, cycle thicknesses and patterns, and other features.

Next, the gamma-ray patterns of the sequence are described. Finally, for some sequences, a brief interpretation of depositional conditions is presented.

Fox Mountain Sequence

Overlying the regional unconformity at the top of the karsted, light brown-gray Simonson Dolomite is the transgressive 135-foot-thick cliff-forming Fox Mountain Sequence comprising four cycles that consist of medium dark-gray limestone and (**Figure 13** and **Plate 2a**). It represents the first occurrence of a significant amount of undolomitized limestone on the eastern Nevada Devonian shelf. Where the Fox Mountain Sequence is missing, by erosion or by nondeposition on adjacent topographic highs as at other measured sections, younger sequences overlie the Simonson Dolomite unconformity (see correlation charts that compare Timpahute Mountain with Mail Summit sections in the discussion in this chapter and in Chapter 7).

An abrupt deepening of the Fox Mountain Sequence above the Simonson Dolomite unconformity is illustrated by the relative sea-level curve in **Figure 13** and **Plate 2a**. The sequence is composed of four shallowing-upward cycles, mentioned above and described in Appendix B. The lower parts are composed of open-marine, medium dark-gray, burrowed, brachiopod, echinoderm, gastropod lime wackestones and upper parts of supratidal, medium-gray to light-gray, laminated dolomites. The lower two cycles have more open-shelf limestone than the upper two cycles. A regional LSE at the top of the Fox Mountain is marked with a pale-red siltstone paleosol, desiccation cracks, and a change from open-marine to restricted-marine fossils. As **Figure 13** shows, gamma radiation generally mirrors the relative sea-level curve. Open-shelf limestones of Fox Mountain cycle bases emit less gamma radiation than their supratidal dolomite tops.

<u>Summary of Descriptions</u> Tables in the previous section summarize some characteristics of the Fox Mountain Sequence. **Table 5** shows that the Fox Mountain sequence weathers into mostly ledges with some partly covered slopes. The table also shows that the gamma radiation over the Fox Mountain is lower than over the Yellow Slope Sequence but higher than the rest of the lower Guilmette sequences. Generally, the cycle bases are more resistant than the cycle tops. The weathering histogram in **Plate 2a** illustrates the weathering profile of the ledgy Fox Mountain Sequence. **Table 6** shows that the sequence is 135 feet thick and is predominantly limestone. **Table 7** shows the wackestone texture and the dark-gray appearance of the Fox Mountain Sequence. Texture descriptions were refined by thin-section analysis (Appendix C).

Brachiopods, crinoids, and gastropods typically occur at the base of the Fox Mountain cycles whereas the cycle tops generally lack fossils (see Appendices B and C). *Amphipora* is rare (**Table 8**).

<u>Fox Mountain, a Guilmette Formation Sequence</u> The controversy over whether to place the Fox Mountain Sequence in the Simonson Dolomite or Guilmette Formation was presented in Chapter 2. As explained in Chapter 2, the Fox Mountain Sequence is different from the Fox Mountain Formation proposed by Sandberg et al. (1997). They propose that their Fox Mountain Formation be composed of two members. Their lower member is composed of karsted dolomite that grades downward to the upper alternating member of the Simonson Dolomite. Their upper member is composed of open-marine limestone. I place the lower contact at the Simonson unconformity sequence boundary. The karsted interval below the unconformity may be the same as the lower dolomitized and karsted Fox Mountain member of Sandberg et al. (1997). Because this karsted interval is a diagenetic front, it has no definite boundary with the unaffected part of the Upper Alternating Sequence of the Simonson Dolomite. At TMS, the Fox Mountain Sequence is composed of four upward shallowing cycles. The lower parts of the cycles

contain crinoids, corals, and brachiopods deposited in open-marine conditions. The upper parts of the three lower cycles consist of finely-crystalline stratal dolomite deposited in supratidal conditions. My upper sequence boundary is marked by desiccation cracks and a thin exposure interval or paleosol on the uppermost Fox Mountain Sequence. Strata above this unconformity are rich in restricted-marine to supratidal fossils such as ostracodes and stromatolite bed. Sandberg et al. (1997) include part of the lower Yellow Slope Sequence into their Fox Mountain Formation. I regard the Fox Mountain Sequence as lower Guilmette Formation because: 1) the most pronounced regional sequence boundary in the Devonian occurs at the top of the Upper Alternating Sequence of the Simonson Dolomite; 2) the regional exposure surface separates fine-grained Fox Mountain limestones from underlying coarsely-crystalline, karsted, and pervasively dolomitized Simonson Dolomite carbonates; 3) the inconsistent occurrence of the Fox Mountain Sequence, which may be hundreds of feet thick in some sections near the middle of the Sunnyside basin and absent in others on the edges of the basin (**Figure 13**; see correlation charts in the discussion near the end of this chapter and in Chapter 7); and, 4) the pronounced geomorphic expression of the Fox Mountain cliffs (where present) above karsted Simonson Dolomite slopes and ledges are easily recognized in the field and on aerial photographs.

Fox Mountain Sequence Cycles The lower three Fox Mountain Sequence cycles are capped by laminated, light-gray dolomite that represents supratidal conditions (**Figure 22**). Cycle 1, a 20-foot-thick cycle, begins in open-shelf conditions and ends in restricted-shelf conditions. The lower 27 feet of Cycle 2 are composed of medium-dark limestone that contains an open-shelf fauna. A sharp decrease (leftward inflection) in gamma radiation marks the base of Cycle 2. Cycle 3, the thickest of the shallowing-upward cycles (50 feet), forms a complete (i.e., an open-marine base and supratidal cap) cycle as do Cycles 1 and 2. The lower parts of the cycles were probably deposited in partly restricted open-shelf conditions whereas their upper parts were deposited in peritidal conditions.

An erosional surface and missing facies (i.e., the supratidal cap is missing) suggest that the top of Cycle 4 was truncated by erosion before deposition of the Yellow Slope Sequence. Average thickness of the cycles is 34 feet (**Table 6**). Cycle thickness increases from 19 feet for Cycle 1 to 49 feet for cycle 2 and 52 feet for cycle 3. A histogram of cycle thicknesses illustrates the upward cycle thickening (**Figure 22**, **Plate 2a**). If the cycles are of similar duration and if no strata are missing, then the histogram suggests an upward increase of accommodation space or an increase in the rate of relative sea-level rise. This increase in the rate of relative sea-level rise is repeated at least four times, to the middle of Sequence Dga (UTK1-4, **Figure 21**). A relative sea-level lowering at the top of the Fox Mountain Sequence could have resulted in erosion of the top of Cycle 4 (base of UTK2, **Figure 21**). In other sections, karst cavities occur tens of feet below the Fox Mountain unconformity. In Chapter 9, it is suggested that an isopach map of the depth of karsting could provide a rough estimate of paleotopography at the end of Fox Mountain time.

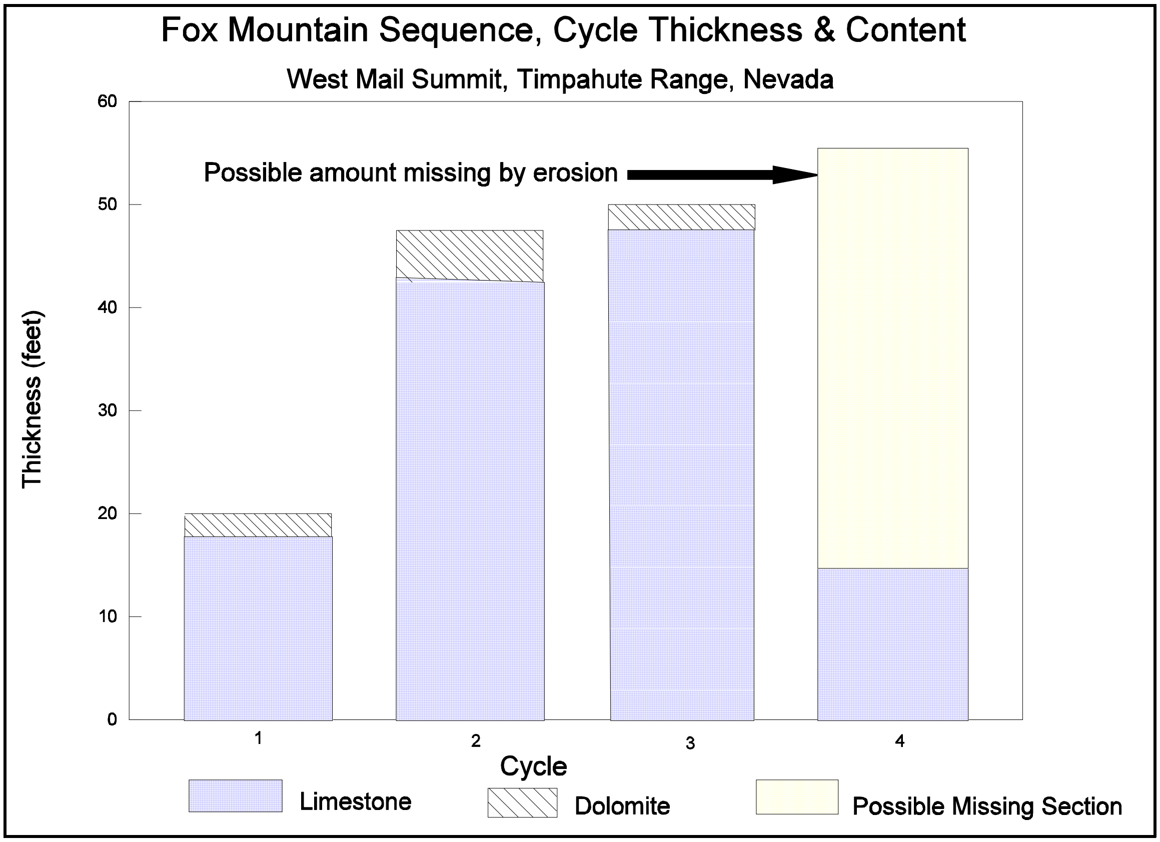


**Figure 22** Histogram of cycle thicknesses and content, Fox Mountain Sequence shows a pattern of upward thickening cycles and could be a clue to the amount of section missing at the unconformity a the top of the sequence.

<u>Distinguishing features of the Fox Mountain Sequence</u> The Fox Mountain can be distinguished from earlier Devonian rocks in the study area because it is the first mainly limestone formation above the Ordovician Eureka Quartzite, except the limey Ordovician Ely Springs Dolomite in the Silver Canyon thrust sheet. Also, the Fox Mountain limestones are finely crystalline whereas the underlying Simonson Dolomite is medium to coarsely crystalline. Fox Mountain Sequence Cycles can be distinguished from cycles of younger Guilmette sequences by their resistance to weathering and distinctive fauna (**Table 4**). Two cycles in the cliff-forming Fox Mountain Sequence typically contain crinoids. Crinoids are rare in the rest of the Guilmette Formation. Crinoids occur in the Fox Mountain Sequence of the study area as a thin bed in Cycle 3 and as Middle

Devonian two-holed crinoid columnals in Fox Mountain Cycle 2. However, crinoid columnals do occur locally above the Dgb2 breccia in the Hiko and Pahranagat ranges. Crinoids occur throughout the Guilmette equivalent rocks in the Reveille Range, Sec. 35, T2N R51½ E. Elrick (1986) reported crinoids in the Guilmette in the Goshute Range, T30N R68E. Besides crinoids, the highest known occurrence of the distinctive brachiopod *Stringocephalus* occurs in the Fox Mountain Sequence. It also occurs in the Simonson Dolomite Brown Cliff Sequence. Because of the affinity of *Stringocephalus*-bearing beds, Hurtubise (1989) and Tschanz and Pampeyan (1970) assigned the Fox Mountain limestone to the Simonson Dolomite.

Fox Mountain cycles are thicker than some Sequence Dga cycles (34 feet vs. 20 feet). Fox Mountain cycles thicken upward. They are more radioactive than the underlying Simonson Dolomite but are less radioactive than the overlying Yellow Slope Sequence. Changes in radioactivity occur at the two regional unconformities that bound the Fox Mountain sequence. Besides the sharp increase in radiation, a paleosol that partly fills mudcracks at the top of the Fox Mountain separates the sequence from the overlying Yellow Slope Sequence at TMS and in the Worthington Range. The Fox Mountain unconformity cuts out most of the Fox Mountain at Downdrop Mountain, 16 miles south-southeast of Monte Mountain, and all of the Fox Mountain Sequence at Monte Mountain and the Meadow Valley Mountains (45 miles southeast of Hiko).

<u>Gamma Radiation</u> Average gamma radiation over the sequence is 53 CPS with a maximum of 70, a minimum of 37, and a standard deviation of 7.6 (**Table 5**). In contrast, average gamma radiation over the upper Simonson Dolomite is 41 CPS with a maximum of 61, a minimum of 25, and a standard deviation of 8.7. Intervals of higher gamma radiation reflect concentrations of windblown siliciclastic detritus. Typically, sand grains that occur with siltstone at the top of some upward shallowing cycles are frosted and trough-cross bedded. Desiccation cracks provide evidence that the beds were periodically

subaerially exposed. Devonian supratidal flats in Nevada could have concentrated wind-blown siliciclastics. A potential source area could have been the Antler forebulge uplift, parts of which were subaerially exposed during lower Guilmette time (Chapters 2 and 8).

Other possibilities for increased windblown siliciclastic detritus include a change in prevailing wind direction or a more narrow shelf. However, no evidence of a change in the ocean-land shape resulting in a change of prevailing wind direction is found. Because the Guilmette is more widespread than the underlying Simonson Dolomite, it seems unlikely that the exposed shelf suddenly became reduced with time. Most likely the radioactive dust is from the Antler forebulge, the same area that eventually served as the source for mature quartz sandstones in the upper Guilmette Formation and was probably the source for the “Oxyoke Formation” sandstone below.

<u>Interpretation of the Fox Mountain Sequence</u> The Fox Mountain at Mail Summit was probably deposited in a topographic low near the center of the Sunnyside basin where marine limestone predominated. Other sections in the study area that lie near the center of the basin include the Golden Gate and Worthington ranges. In contrast, sections deposited on the edges of the Sunnyside basin either lack the Fox Mountain sequences such as at Monte Mountain or an unusually thin Fox Mountain Sequence as in the Meadow Valley Mountains (**Figure 17**).

Downdrop Mountain and Monte Mountain both lie within the Silver Canyon thrust sheet. The structural model presented in Chapter 5 and Devonian paleogeography presented in Chapter 7 suggests that the Silver Canyon thrust sheet was deposited on the west side of the Sunnyside basin and west of Tempiute Mountain. Thin Fox Mountain Sequence at Downdrop Mountain and no Fox Mountain Sequence at Monte Mountain suggest an eastward thickening of the Fox Mountain Sequence toward the center of the Sunnyside basin.

Similarly, thin Fox Mountain Sequence in the Hiko Range and in the Meadow Valley Mountains suggest an eastward thinning of the Fox Mountain Sequence (**Figure 17**). Probably more of the Fox Mountain Sequence was cut out by the Fox Mountain Sequence unconformity on the flanks of the Sunnyside basin than in the center of the basin. However, it is possible that more Fox Mountain Sequence was deposited in the center of the basin than on the basin flanks. Thin sections from the lower parts of TMS Fox Mountain cycles contain open-marine fauna including echinoderms, brachiopods, and corals (Appendix C). Therefore, the lower parts of Fox Mountain Sequence cycles in the center of the Sunnyside basin are interpreted to be deposited in open-shelf conditions (Appendix B). The upper parts of the cycles are fossil-poor, burrowed, and are composed of stratal finely-crystalline dolomite. They are interpreted to be deposited in low-intertidal conditions.

Yellow Slope Sequence

The Yellow Slope Sequence, 182 feet thick at TMS and comprising 10 cycles, is easily identified on aerial photographs and in the field (**Table 4**, **Figure 23**, **Plate 2a**). It erodes into a conspicuous, yellow slope between dark-gray cliff- and ledge-forming sequences above and below. It is predominantly (44%) pale-yellow brown (**Table 7**). The supratidal, silty dolomite cycles of the Yellow Slope Sequence mark an abrupt facies shift from predominantly open-shelf limestones of the Fox Mountain (**Plate 2a**). The TSE at the base of the Yellow Slope Sequence merges with a mud-cracked LSE at the top of the Fox Mountain Sequence. **Figure 13** illustrates the decrease in the rate of relative sea-level rise and the increase in gamma radiation at the sequence boundary (**Plate 2a**).

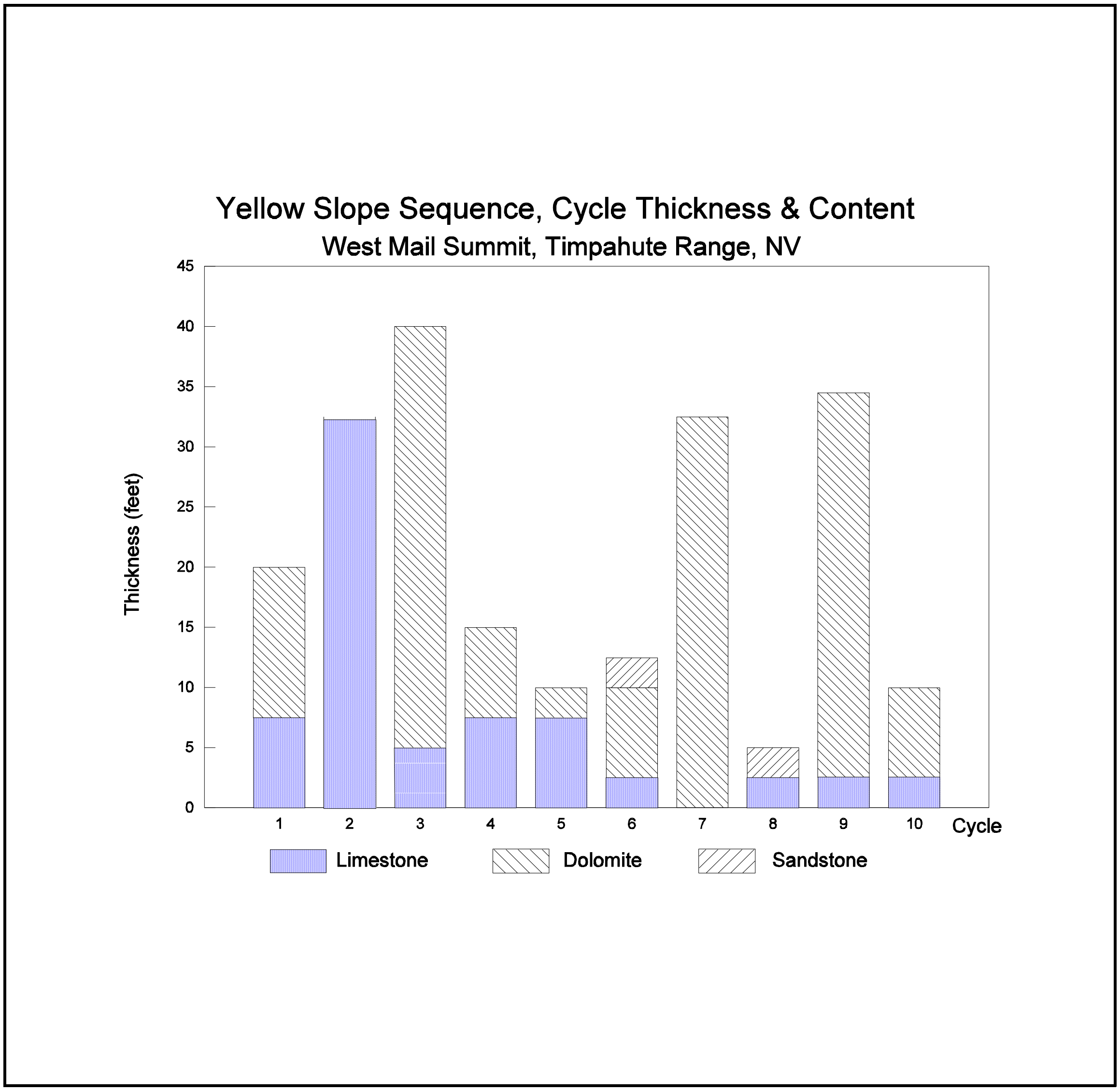


**Figure 23** Histogram of cycle thickness and content, Yellow Slope Sequence. Most of the sequence is set of upward thinning cycles. Limestone content also decreases upward.

Another significant facies shift occurs at the sequence boundary that marks the top of the Yellow Slope Sequence. The TSE at the base of Sequence Dga represents the first major transgression within the Guilmette. Here medium-dark-gray, burrowed, intraclast, brachiopod, pelletal lime bioclastic wackestone overlies medium-gray, laminated, lime mudstone. Barren, pale yellow-brown to light-gray, silty, laminated dolomudstone lies just below the mudstone whereas coral lime wackestone lies just above the wackestone. As seen on **Plate 2a** and as discussed in the section on gamma radiation, a sharp leftward inflection on the gamma-ray profile marks the Dga1 transgression.

<u>Marker Beds</u> The Yellow Slope Sequence is a prominent marker bed of the lower Guilmette Formation in southeastern Nevada (**Table 4, Plate 2a**). Early location of this marker bed helped in mapping and planning measured sections. At TMS, it is comprised of ten shallowing-upward cycles presented in more detail in the section on lithology and texture hereafter (**Figure 23**).

Although tops of other shallowing-upward cycles in other sequences are marked by yellow-gray, silty, laminated dolomudstone, beds of large, digitate stromatolites occur only in Yellow Slope Sequence Cycle 2 at TMS. Cycle 2 stromatolite beds serve as prominent regional marker beds within the Yellow Slope Sequence, as noted by Hurtubise (1989). He chose the base of a stromatolite bed as the base of Guilmette Formation as presented in Chapter 2. However, several stromatolite beds occur in many sections and at different levels above the base of the Yellow Slope Sequence. Therefore, although columnar stromatolites serve as excellent marker fossils for the Yellow Slope Sequence, the base of a stromatolite bed serves as a poor boundary between mappable units. Much of the sequence is laminated, but the stromatolites in Cycle 2 are uniquely diagnostic at TMS. Columnal stromatolites are thought to have formed by mucilaginous surfaces of cyanobacterial mats selectively trapping sediments (Ginsburg, 1991). At TMS, they form dark-gray, cyanobacterial boundstones with some columns reaching three to four feet high. Ostracodes and calcispheres are more abundant in the Yellow Slope Sequence than in any other Guilmette sequence (MI-316, Appendix C). The presence of the unique stromatolites alone is not adequate evidence for an intertidal zone or restricted circulation conditions because stromatolites can be found in normal marine settings (Ginsburg, 1991). However, no open-marine fossils such as crinoids, corals, or stromatoporoids have yet been detected in the Yellow Slope Sequence, which contains desiccation cracks at the tops of finely-crystalline stratal dolomite caps. Therefore, the sequence is interpreted to represent restricted subtidal to supratidal conditions. The lower parts of these cycles contrast with open-marine conditions of the lower parts of cycles in adjacent sequences, because they lack open-marine fossils.

Cycle Thicknesses Thickness patterns reveal that the average thickness of the ten Yellow Slope cycles is 18 feet in contrast with 34 feet for average cycle thickness in the underlying Fox Mountain and 21 feet for average cycle thickness in the overlying Sequence Dga1. Generally, cycles at the lower and upper parts of the sequence are thicker, and their bases were deposited in deeper water than cycles in the middle of the sequence. A histogram of cycle thickness versus cycle number shows that the first three Yellow Slope Sequence Cycles thicken upward (**Figure 23**). Thickening upward suggests an increase in accommodation space that in turn reflects an acceleration of relative sea-level rise (UTK2, **Figure 21**). The last three cycles, combined with the first three cycles of Sequence Dga, show another upward thickening trend (UTK3, **Figure 21**). Hematite/goethite/limonite(?) stains in fractures and stylolites have been detected in seven of the ten cycles (Appendix C).

Lithology, Texture, Erosional Profile, and Cycles The Yellow Slope Sequence can be readily differentiated from the underlying Fox Mountain and the overlying Dga1 Sequence based on lithology and texture. Yellow Slope Sequence Cycle 1 is a shallowing-upward cycle of limestone with a dolomite cap. It contains abundant ostracodes and rare large calcispheres in contrast to the brachiopod wackestone of the underlying Fox Mountain Sequence.

Most of the Yellow Slope Sequence eroded into covered slopes (25%) and partly-covered slopes (49%). Only 26% of the sequence forms resistant ledges (**Table 5**).

Seven of the Yellow Slope Sequence Cycles are capped by supratidal, fossil-poor, laminated, silty and sandy, pale yellow-brown to yellow-gray dolomudstone. Several exhibit desiccation cracks (**Plate 2a**). Nine of the ten cycles have a transgressive limestone base that is commonly marked by a leftward inflection in the gamma-ray log. These transgressive limestones are medium- to dark-gray, intertidal, calcisphere lime mudstone. Thin (less than 5 feet thick), yellow-gray, fine-grained, dolomitic, quartz sandstone interbeds cap the sixth and eight cycles in the section and contain intertidal ostracode lime mudstones (MI-316, Appendix C).

These thin beds of sandstone are the first occurrence of conspicuous quartz grains above the "Oxyoke Formation," as noted by Chamberlain and Warme (1996). Concentrations of quartz siltstone and sandstone in the Yellow Slope Sequence are probably due to wind-blown detrital grains trapped by moisture on peritidal flats. Except sparse, scattered quartz grains, the next occurrence of quartz sandstone in the section is at the tops of several shallowing-upward cycles in Sequence Dgd, nearly 1,000 feet above the Yellow Slope Sequence (**Plate 2a**).

<u>Gamma Radiation</u> The Yellow Slope Sequence emits higher gamma radiation than other Devonian sequence at TMS (**Plate 2a**). Its average gamma radiation is 62 CPS (**Table 5**). It ranges from a minimum of 48 to a maximum of 74 CPS. This is possibly due to wind-blown silt and sand.

The standard deviation of 5.5 CPS is lower than that of the adjacent sequences. The standard deviation radiation of the Sequence Dga of 10.0 CPS and that of the Fox Mountain is 7.6 CPS. At the base of the sequence, gamma radiation increases sharply above the LSE at the top of the Fox Mountain Sequence. An equally sharp decrease in gamma radiation occurs at the TSE marking the base of Sequence Dga above. **Plate 2a** illustrates these changes in gamma radiation.

Yellow Slope Sequence Interpretation  Desiccation cracks, stromatolites, and abundances of ostracodes suggest that the Yellow Slope Sequence was deposited in shallow water.  Most of the Yellow Slope Sequence is composed of stratal finely-crystalline dolomite caps interpreted to be deposited in supratidal conditions.  On a larger scale, the Yellow Slope Sequence is a shallow-water, dolomite cap on the shallowing-upward Fox Mountain Sequence with the Dga1 Sequence boundary marking the overlying transgression.

Though the thickness of the Fox Mountain varies greatly depending on its position in the Sunnyside basin, the thickness of the Yellow Slope Sequence remains nearly constant throughout the basin.  It is 182 feet thick at TMS, 140 in the Golden Gate and Worthington ranges, and 150 at Monte Mountain.  Apparently the Fox Mountain unconformity leveled the Devonian paleogeography making it possible for the supratidal Yellow Slope Sequence to be distributed uniformly over much of the Sunnyside basin. The uniform thickness of the Yellow Slope Sequence even persisted over the Monitor-Uinta arch, an east-west positive feature that affected deposition of all the Devonian sequences (Chapter 7).  Forming a vast sabkha that extended from western Utah to central Nevada (120 miles unrestored) and most of the length of Nevada (250 miles), the Yellow Slope Sequence was deposited in similar conditions as the Sevy Dolomite.  The main differences are that the Yellow Slope cycle bases are typically limestone, some cycles contain fossils including ostracodes, and two cycles are capped by thin sandstone units.

## Sequence Dga

Sequence Dga is 395 feet thick and contains 20 shallowing-upward cycles grouped into two subsequences in the TMS, but the subdivision was not always recognized in other sections (**Figure 9**).  Sequence Dga1 is predominantly dolomite and

Sequence Dga2 is predominantly limestone (**Table 6**, **Plate 2a**). The sequence boundary at the base of Sequence Dga is marked by a conspicuous facies shift from predominantly yellow-weathering ostracode-bearing dolomite to cycles of multifauna coral, *Amphipora*, stromatoporoid lime wackestones and light-gray dolomicrites. Another facies shift from multifauna coral, *Amphipora*, stromatoporoid wackestones to single-fauna stromatoporoid wackestones and a regional gamma-ray spike marks the top of the sequence.

Gamma Radiation and Weathering Profile A regionally correlatable leftward gamma-ray inflection marking a TSE over an LSE separates the sequence into two subsequences Dga1 and Dga2. A regionally correlatable slight decrease in gamma marks the top of the sequence. Average gamma radiation over Sequence Dga is 43 CPS (**Table 5**). It decreased from 49 CPS over Sequence Dga1 to 32 CPS over Sequence Dga2.

Sequence Dga becomes more resistant upward from the Yellow Slope Sequence that is 74% covered and partly covered slopes (**Table 5**) to Sequence Dgb that is 95% cliffs and ledges. Sequence Dga1 lies between the covered and partly covered slopes of the Yellow Slope Sequence below and the cliffs and ledges of Sequence Dgb above. It is 74% cliffs and ledges whereas Sequence Dga2 is 90% cliffs and ledges (see weathering histogram on **Plate 2a**).

Color, Texture, and Lithology **Table 7** summarizes the color and texture of the lower Guilmette sequences at TMS. The average dolomite content decreases from 58% in the underlying Yellow Slope Sequence to 41% in Sequence Dga and to 5% in Sequence Dgb above (**Table 6**). Limestone predominates in Sequence Dga (59%).

Subsequences Dga1 and Dga2 also reflect this upward decrease in dolomite content. Sequence Dga1 is 50% dolomite whereas Sequence Dga2 is only 25% dolomite (**Figure 19**).

Typical Sequence Dga Cycle The lower part of a typical shallowing-upward cycle in Sequence Dga is a coral-stromatoporoid open-shelf, medium dark-gray limestone above a TSE/LSE. It grades upward to a supratidal, laminated, light-gray dolomudstone facies bounded by an LSE at the top. *Amphipora* is an important constituent between the basal limestone and the dolomite cap.

Sequence Dga Cycles Depending on the amount of strata removed at the next TSE, some cycle tops are composed of light-gray, laminated dolomudstone. Eight of the 12 cycles in Sequence Dga1, but none of the cycles in Sequence Dga2, shallow up to light-gray, rarely mud-cracked, laminated dolomicrite facies. Either a TSE\LSE truncated supratidal strata or transgression occurred before the shallowing-upward sequence was completed in the partial cycles. Incomplete cycles in Sequence Dga2 are probably due to general deepening, and cycles only shallowed to intertidal environments before the next transgression. However, a histogram of cycle thickness for Sequence Dga1 and Dga2 illustrates that after Sequence Dga1 Cycle 9, cycles get thinner upward until Sequence Dga2 Cycle 6 (**Figure 21**). This thinning upward suggests an upward decrease in accommodation space caused by a decrease in the rate of relative sea-level rise. A similar decrease in accommodation space or a decrease in the rate of relative sea-level rise occurs from Sequence Dga2 Cycle 7 to Sequence Dgb3 Cycle 2 reef (see UTN2 and UTN3 in **Figure 21**).

Dolostone and Cycle Thicknesses  A histogram of the dolomite percentage for each cycle of Sequences Dga1, Dga2, and Dgb1 provides some interesting patterns (**Figure 19**). **Figure 24** illustrates two sets of thickening upward cycles in Sequence Dga1. Cycles 1, 2, and 3 thicken upward. **Figure 19** illustrates that the percent of dolomite in these cycles progressively decreases upward. Cycles 5 through 9 also thicken upward and the percent of dolomite decreases upward. The percent of dolomite continues to decrease upward to Sequence Dga2 Cycle 1 where no dolomite is preserved. The uppermost cycles in Sequence Dga1 and most of the Cycles in Dga2 form a set of upward thinning cycles (UTN2 on **Figure 21**). Dolomite percent decreases in Cycles 2 to 4 and increases from 4 to 7. This increase in percentage of dolomite is abruptly truncated at Sequence Dga2 Cycle 8, above which no supratidal dolomite occurs in cycles of Sequences Dga or Dgb. Sequences Dgc and Dgd lack shallowing-upward cycles with supratidal caps such as those in Sequence Dga1. An increase in dolomite thickness from the base of Sequence Dga to Cycle 9 is partly caused by an increase in accommodation space resulting from an increase in the rate of relative sea-level rise (UTK4 **Figure 21**).

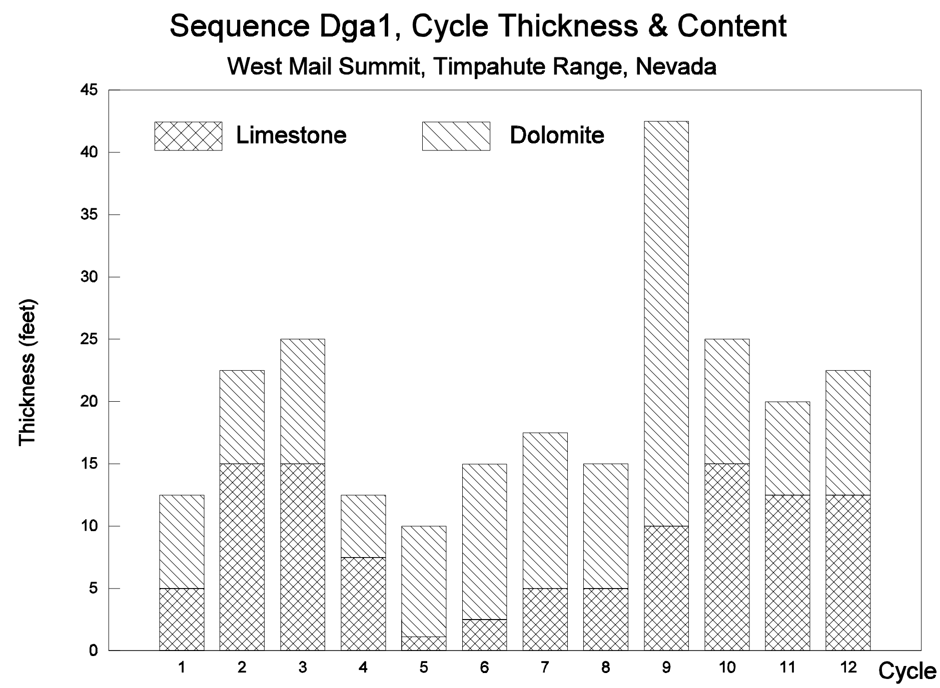


**Figure 24** Histogram of cycle thickness and content, Sequence Dga1. Two sets of upward thickening limestone cycles with dolomite caps characterize the sequence (cycles 1-3 and cycles 5-10). The first set is part of the upward thickening trend that begins with cycle 8 in the Yellow Slope Sequence (UTK3 in **Figure 21**) and the second is UTK3 in **Figure 21**. Cycles 11 and 12 are part of the upward thinning trend that continues to cycle 6 in Sequence Dga2 (UTN2 in **Figure 21**).

A decrease in the rate of sea-level rise resulted in less accommodation space and thinner cycles upward in Sequence Dga1 Cycle 10 through Sequence Dga2 Cycle 6 (UTN2 **Figure 21**). Less dolomite was preserved as dolomite caps in Sequence Dga because of the facies shift from predominantly supratidal environment to more open-marine environment at the top of the Yellow Slope Sequence. A cycle thickness increase from Sequence Dga1 Cycle 5 to Sequence Dga1 Cycle 10 reflects another increase in the rate of relative sea-level rise. However the percent of dolomite decreases upward suggesting that, although accommodation space was available, deepening occurred faster than carbonates could build up to supratidal conditions, or at least more deposition in open-marine conditions took place than in supratidal conditions. As a result, less supratidal dolomite is preserved at the top of the cycles. This pattern of decreasing amounts of dolomite preserved as dolomite caps continues upward to Sequence Dga2 Cycle 8 where no dolomite is preserved. This upward decrease in dolomite content may represent a local, deepening event superimposed on a general shallowing-upward pattern (UTN2 and UTN3 **Figure 21**).

Microfacies analyses and megascopic fossils show an overall deepening of cycles within Dga (compare photomicrograph descriptions for Wilson's (1975) microfacies in Appendix C with **Plate 5**). This deepening includes the sedimentary breccia Dgb2 and stromatoporoid reef Dgb3. Supratidal dolomite cycle caps of equivalent age (i.e., within the same sequence) are found shoreward in the Sunnyside basin. Correlative beds could have been the source for light yellow-gray, laminated dolomite clasts within the overlying Sequence Dgb2 sedimentary breccia. These dolomite caps are not preserved in beds next to the Dgb2 breccia at TMS. A thin lens of breccia associated with the overlying Dgb2 breccia sequence was emplaced or liquidized as a single bed and will be discussed later in this chapter.

<u>Subsequence Dga1</u> Subsequence Dga1 is 250 feet thick and is composed of 12 cycles (**Plate 2a, Figure 24**). A conspicuous facies shift separates the ostracode- and calcisphere-bearing Yellow Slope Sequence from the coral-, stromatoporoid-, and brachiopod-bearing Sequence Dga1 (**Figure 23**). Generally, the lower parts of the sequence cycles are composed of open-shelf, medium dark-gray to medium-gray, burrowed stromatoporoid, coral, brachiopod, *Amphipora* lime wackestone. Supratidal, light-gray, laminated dolomudstones with rip-up clasts cap most of the Sequence Dga1 cycles. **Plate 2a** illustrates the cycle thicknesses and contents. With few exceptions, Sequence Dga1 cycles exhibit a general upward-deepening trend from supratidal Yellow

Slope Sequence Cycles to open-shelf Sequence Dga2 cycles and a general upward decrease in gamma radiation from the underlying Yellow Slope Sequence (**Figure 13**).

A sharp leftward gamma-ray inflection marks the TSE/LSE at the base of the sequence. Within the sequence, each cycle begins with a sharp leftward gamma-ray inflection at the limestone base followed by a gradual increase in gamma radiation and dolomite content to the cycle top (**Plate 1a**, **Figure 13**).

<u>Subsequence Dga2</u> Subsequence Dga2 is 145 feet thick and comprised of eight cycles. A TSE/LSE at the base of Sequence Dga2 separates equal amounts of dolomite and limestone strata containing common open-shelf fossils of Sequence Dga1 from the overlying predominantly limestone strata characterized by abundant open-shelf fossils (**Table 6**, **Plate 2a**). **Figure 25** illustrates cycle thicknesses and composition of Sequence Dga2. A thin (1-2 foot) bed of distinctive Dgb2 carbonate breccia occurs 20 feet above the base of Sequence Dga2 and 392 feet from the top of Dgb2. It will be discussed later.

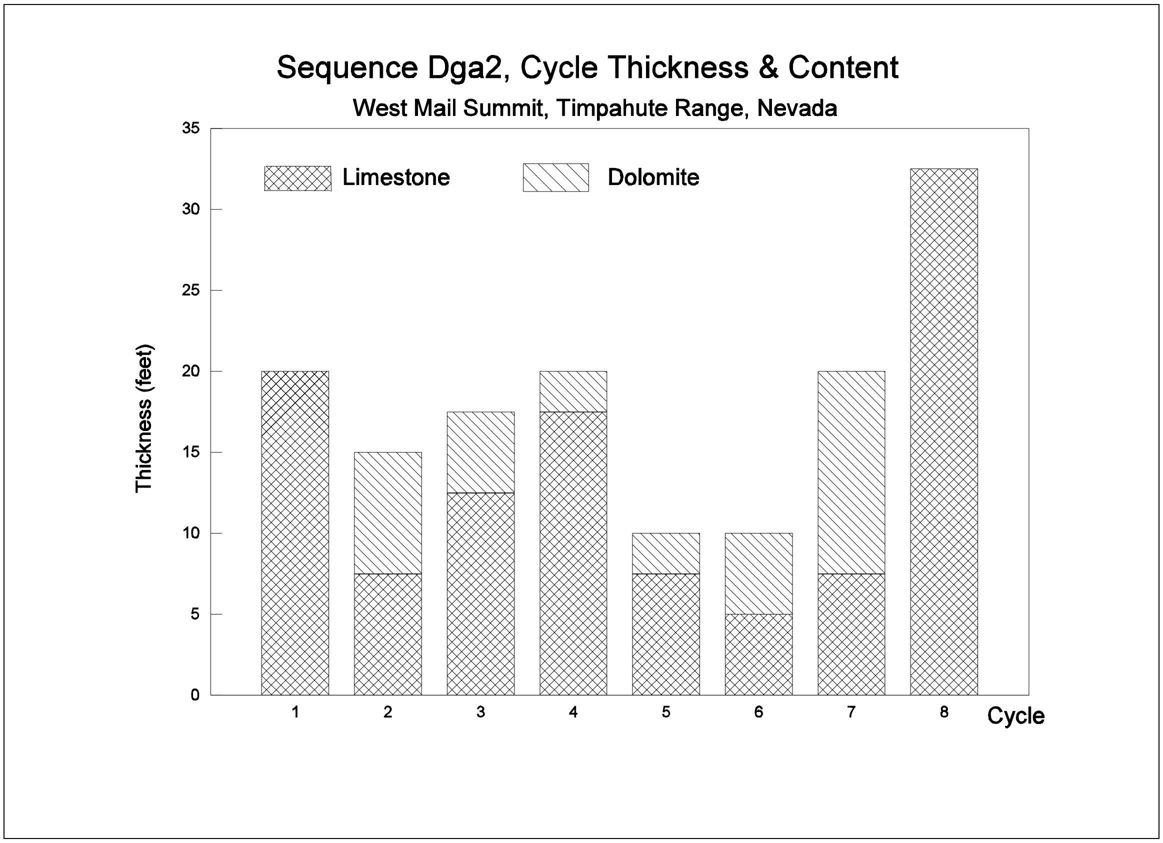


**Figure 25** Histogram of cycle thickness and content of Sequence Dga2 shows two sets of possible upward thickening cycles from cycle 2 to 4 and from cycle 5 to 8. However, cycle thicknesses and contents are probably random. Except for cycle 7, dolomite content tends to decrease as the cycles become thicker. Compare with **Table 9** which shows the percent of dolomite increasing from cycle 4 to cycle 7. The only dolomite from cycle 8 to Sequence Dgd is late diagenetic dolomite associated with fractures or porous parts of the Dgb2 breccia matrix.

Each shallowing-upward cycle in Sequence Dga2 shows a more pronounced change from the base to the top than in underlying Guilmette sequences. Generally, the base of each cycle is marked by an open-shelf, medium dark-gray to medium-gray, stromatoporoid, coral, brachiopod lime wackestone to packstone. Seven of the eight cycles are capped with subtidal, laminated, commonly burrowed, light yellow-gray, fossil-poor dolomite (**Plate 2a)**. Two cycles are capped by an extensively burrowed, medium-gray, lime fossil wackestone of a restricted-shelf environment.

A regionally correlative abrupt decrease in gamma radiation occurs at the base of Sequence Dga2 (**Figure 13**). The weak gamma radiation is interpreted to be caused by carbonate dilution of radioactive detritus in open-shelf conditions. Gamma radiation continues to decrease upward to a distinctive gastropod lime wackestone at the top of Sequence Dga2, above which gamma radiation abruptly increases.

Sequence Dgb

Though Sequence Dgb can be correlated to more remote outcrops such as the Egan Range (**Figure 9**), a sedimentary breccia, Subsequence Dgb2 restricted to the Timpahute region, divides the 301 foot-thick sequence into three subsequences, Dgb1, Dgb2 and Dgb3 at TMS (**Plate 2a**). **Figure 26** illustrates cycle thicknesses and composition of Sequence Dgb and overlying Sequence Dgc cycles where Sequence Dgb3 is a stromatoporoid reef. The distinctive sedimentary breccia (Dgb2) forms the middle part of Sequence Dgb. It provides an excellent marker bed in the Timpahute area. At TMS, Subsequence Dgb2 consists of an apparently single graded bed of sedimentary packstone megabreccia. It contains huge clasts up to hundreds of feet long at the base and mudstone at the top (Warme et al., 1993). Employing the grain-size classification of Blair and McPherson (1999), grain size decreases from “blocks” and “slabs” in the lower part to clay in the upper part. A thin layer of the megabreccia occurs tens of feet below the graded bed near the base of Sequence Dga2 at or just above the Dga2 gamma-ray marker bed at TMS and at other localities. It is described in a later section. Two shallowing-upward cycles below the sedimentary megabreccia comprise Sequence Dgb1. Two thinner cycles and the thick stromatoporoid reef cycle above the megabreccia comprise

Sequence Dgb3 (**Plate 2a**). Prominent rightward gamma-ray inflections at the base and top of Sequence Dgb are regionally correlative (**Figure 9**, **Figure 13**). Sequence Dgb emits less radiation, as low as 21 CPS, than any other sequence in the TMS. Except for the gamma-ray spike between Sequences Dgb2 and Dgb3, radiation increases steadily from the base to the top of Sequence Dgb (**Plate 2a**).

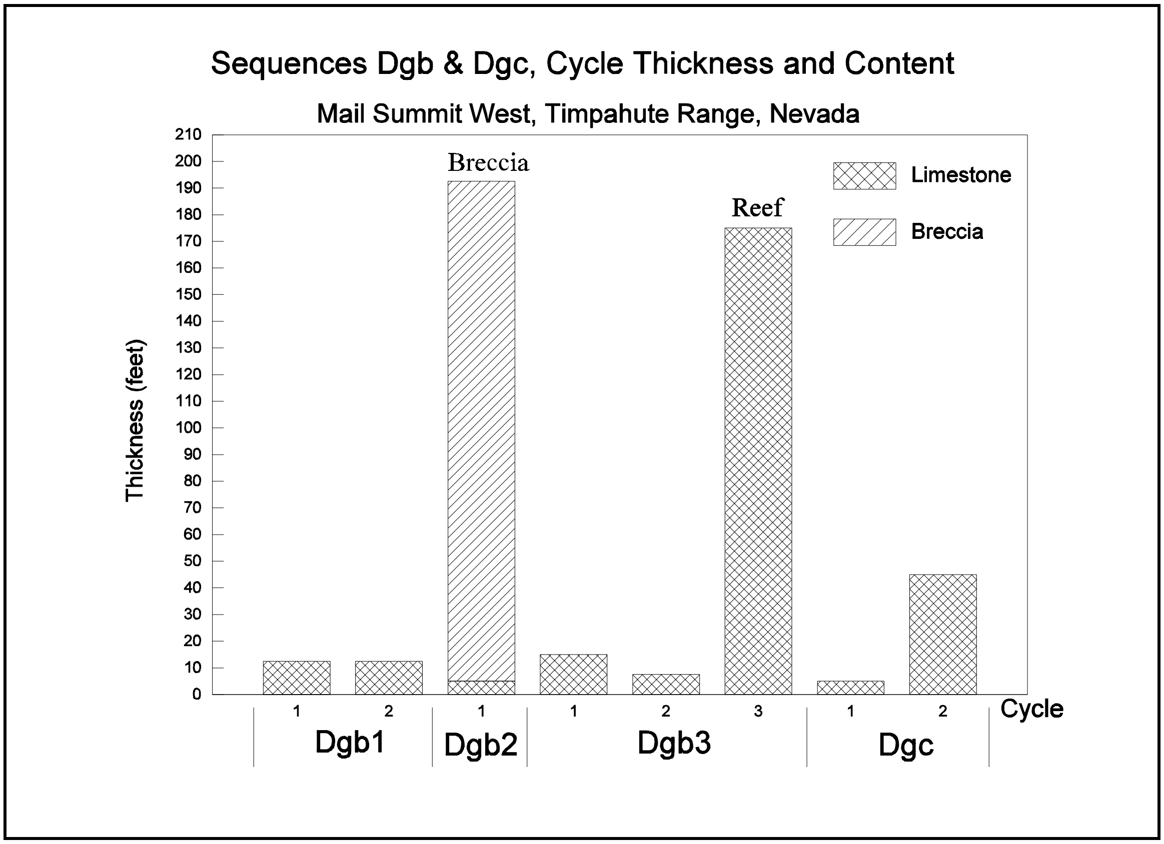


**Figure 26** Histogram of cycle thickness and content of Sequences Dgb and Dgc where Dgb3 is a stromatoporoid reef at TMS. The reef and Dgb2 breccia comprise most of Sequence Dgb and only two Sequence Dgc cycles overlap the reef. Cycles in the Sequence Dgb2 interval were obliterated by the Dgb2 breccia event and were replaced with breccia of the shattered cycles.

Weathering Profile **Table 5** and **Figure 28** summarize the weathering profile of

Dgbc and Dgbf. Most of the cliffy Dgbc profile is due to the 179-foot-thick Sequence Dgb2 breccia that forms 100% cliffs. It is also due to the 215-foot-thick Sequence Dgb3 measured on the reef core that forms 93% cliffs and ledges.

Lithology, Color and Texture **Figure 26** illustrates the thickness and composition of cycles in Sequence Dgbc and **Figure 27** illustrates the thickness and composition of cycles in Dgbf. **Table 6** and **Figure 28** summarize the lithologic components of the sequences.

Color of Sequence Dgb is summarized in **Table 7**. Sequence Dgb2 is another useful marker bed in the Timpahute region. Its dark gray cliff typically separates dark and light-gray cyclic beds of Sequence Dga and light-gray, cliff-forming reefy beds of Sequence Dgb3c. The lateral variability in color could be a pitfall to correct mapping and interpretation. For example, beds equivalent to the light gray reef are medium gray about a mile away and could be mistaken for a different sequence.

Significant lateral textural variations in Sequence Dgb occur between the two TMS sections. Textures for Sequence Dgb are summarized in **Table 7**. The lack of mudstone in Sequence Dgb suggests that it was deposited in a higher energy environment than sequences above or below.

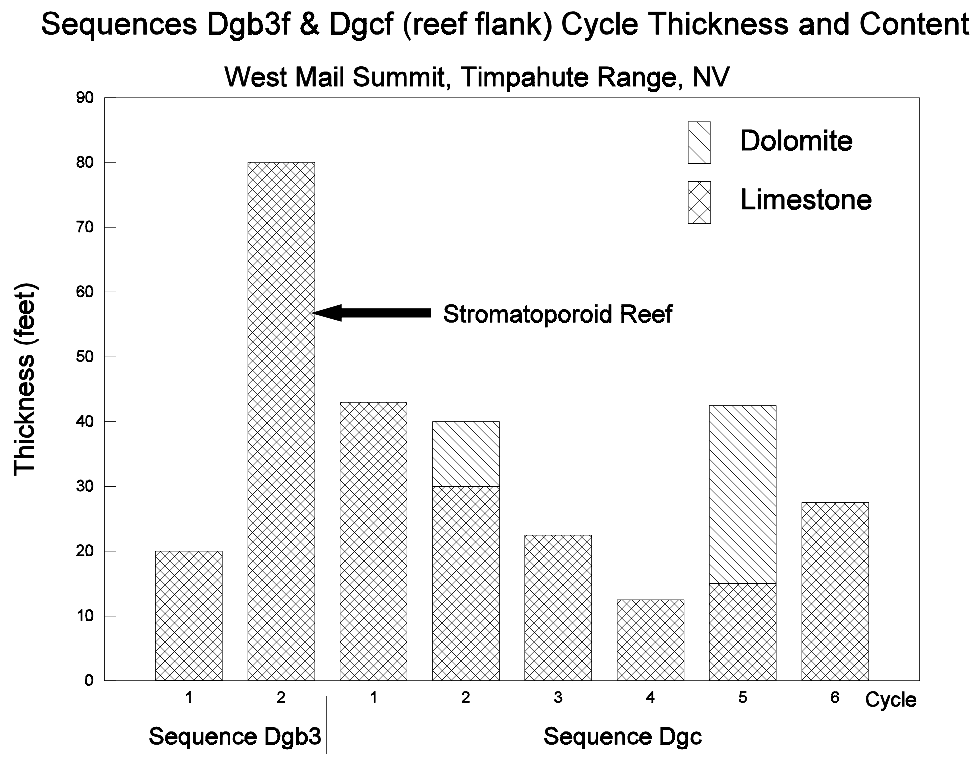


**Figure 27** Histogram of cycle thickness and content, Sequences Dgbf and Dgcf. Six cycles, four of w against the reef, comprise Sequence Dgc on the reef flank (see **Figure 28**).

Gamma Radiation Commonly, gamma radiation is higher over mudstones that contain more fine-grained detritus and less over higher energy boundstones and grainstones. This is the case with Sequence Dgb (**Plate 2a**). Gamma-ray response generally reflects the particle size of the matrix being measured. Because Sequence Dgb lacks mudstone with fine-grained detritus, it emits little gamma radiation. Average gamma radiation over Sequence Dgbc is thus only 26 CPS, less than that of any of the lower Guilmette sequences. In contrast, Dgbf has an average of 38 CPS. On the reef flank, increased percentages of fine-grained matrix results in higher gamma-ray intensity. Gamma radiation over Dgb1 is higher than over the rest of Sequence Dgbc and reflects higher content of mud-size matrix. Gamma radiation for Sequence Dgb is summarized in **Table 5**.

A low-intensity and featureless gamma-ray pattern over most of Sequence Dgb2 suggests that the entire sequence was deposited under uniform conditions. Average gamma radiation over Dgb2 is 27 CPS. Compositionally, Sequence Dgb2 is the most homogeneous of any of the Guilmette sequences. Therefore, the composition of its radioactive components remains uniform. B2 has the lowest standard deviation (3.3 CPS) of the three b subsequences. However, the texture of Sequence Dgb2 is highly heterogenous. A gamma radiation spike at the top of the sequence may reflect settling of impact dust after the event responsible for the megabreccia.

The Dgb2/Dgb3 contact is marked by a gamma-ray radiation decrease from the Dgb2 breccia to the overlying reefy Dgb3 strata in both the reef and reef flank segments of the measured section (**Figure 28**). The blocky, low-intensity, surface gamma-ray log response over the Dgb3 Cycle 3 in both sections is typical of an open-shelf depositional environment. However, the gamma-ray pattern for the reef is nearly a straight line whereas the reef flank facies produces a more undulating gamma-ray signature over shallowing upward cycles. Gamma radiation in both segments increases upward (**Figure 13**). A sharp, rightward gamma-ray inflection at the top of the Dgb3 Cycle 3 reef marks an LSE and a paleosol zone manifested on the outcrop as yellow-gray beds of silty dolomite. Above this unconformity, higher background radiation persists through Sequence Dgc up to the base of Sequence Dgd. This increase in background radiation is seen in surface and subsurface sections throughout the region (**Figure 9** and **Figure 13**).

Subsequence Dgb2  Dgb2 breccia is a unique rock body in the study area that deserves special treatment. In this section the evolution of understanding the breccia is presented along with a brief description of the breccia and its contacts. The distribution of the unique rock body has application to thrust reconstruction. Its unique origin provides a classic opportunity to study the effects of a cosmolite impact on a carbonate shelf.

Evolution of Understanding the Dgb2 Breccia  Previously described by Reso (1960), Estes (1991) and Yarmanto (1992) in the Pahranagat Range, Dunn (1979) at TMS, Cedar Strat geologists (1985) at Tempiute Mountain, and in the Golden Gate, Grant, and Worthington ranges, and Hurtubise (1989) and Ackman (1991) in the Worthington Range, Guilmette Subsequence Dgb2 breccia is a unique unit in the southern part of the Sunnyside basin. Its close association with reefs in the Pahranagat and Mount Irish ranges caused Reso (1960), Dunn (1979), and Estes (1992) to conclude that it is reef talus. Cedar Strat geologists first recognized the regional distribution of the breccia and concluded that it was caused by slumping of steep carbonate banks into an intrashelf basin (Devonian Reservoir Study 1996, a Cedar Strat proprietary study). Warme et al. (1993) concluded that it was caused by a cosmolite impact. Warme and Sandberg (1995) developed a classification scheme to describe the breccia. Their A unit was the obviously graded matrix near the top of the unit consisting of boulder, in some places to mud size grains. B is the main body of the breccia matrix consisting of cobble to boulder size clasts with a matrix of finer breccia. C consists of large clasts or slabs near the base of the breccia separated from the underlying strata by their Unit D, a megabreccia sill of fluidized carbonate rocks. Not all these elements are present in all sections. Chamberlain and Warme (1996) recognized the cyclic nature of the gamma-ray patterns and illustrated four subtle cycles in the breccia. Kuehner (1997) recognized subtle graded beds in the breccia. Some of his graded beds may be the same as the gamma-ray fluctuations and sea-level changes on **Figure 13** and **Plate 2a** that represent subtle cycles. Sandberg et al. (1997) formalized the breccia as the Alamo Breccia Member of the Guilmette Formation. Warme and Kuehner (1998) suggested that the breccia exhibits up to five subtle graded beds and proposed that each formed by a tsunami generated by the impact. Chamberlain (1999) used the distribution of the breccia to reconstruct the Sevier fold-and-thrust belt in the Timpahute Range 30' X 60' area.

<u>Description and Fossils of the Dgb2 Breccia</u> In the distance, the cliffy, dark gray nature of the breccia is easily recognized in many locations. Up close the breccia matrix is typically composed of medium gray clasts in a light gray matrix. At TMS, the dark-gray, massive cliffs of Sequence Dgb2 contrast sharply with the cyclic or banded sequences below and the light-gray stromatoporoid reef above (Figure 11 in Chamberlain and Warme, 1996). As reported by Warme et al. (1993), the breccia appeared to consist of a single graded bed of sedimentary packstone megabreccia. It contains huge clasts exceeding one thousand feet in length at the base and grades to mud at the top. Clasts are typically light-gray to medium light-gray limestone, in contrast to the commonly dolomitized fine-grained matrix that gives the outcrop a dark-gray appearance (Figure 10 in Chamberlain and Warme, 1996). The clasts are fragments of shallowing-upward sequences entrained into the breccia. If the strata between the thin breccia sill of Sequence Dga (Unit D of Warme and Sandberg, 1995) and the main breccia mass are included, then some clasts may be several miles long.

Fossils present in the Dgb2 breccia clasts at TMS include colonial corals, solitary corals, brachiopods, and clasts and matrix contain abundant stromatoporoids including *Amphipora*. MI-407 (two feet from the base of the cycle) is partially dolomitized (30%) coral, brachiopod, intraclast lime grainstone (See Appendix C for photomicrograph and descriptions of thin sections). MI-408 (seven feet from the base of the cycle) is dolomitized (80%) coral, intraclast, *Amphipora*, stromatoporoid, brachiopod packstone.

In the middle of the breccia, a chaotic interval of medium dark-gray, stromatoporoid, coral, and intraclast lime grainstone (open-marine) is medium brown-gray, with increasing stromatoporoids, corals, and intraclast matrix dolograinstone upward. Stromatoporoids are less abundant, and some clasts are flat. MI-421 (72 feet from the base of the breccia mass) is a brachiopod, calcisphere, coral, pelletal lime grainstone. MI-429 (112 feet from the base of the breccia mass) is an intraclast coral, gastropod, pelletal lime grainstone.

Lower Contact of Dgb2 Breccia  The base of Sequence Dgb2 varies from section to section due to its catastrophic nature of emplacement. It is generally defined as the first occurrence of a megabreccia matrix above shallowing-upward carbonate cycles of Sequence Dga. The base of the breccia is an erosional, undulating surface regionally and locally. At TMS the lower part of the breccia matrix (Sequence Dgb2) is a chaotic sequence of a medium dark-gray, dolomitized matrix, abundant coral, and *Amphipora* lime grainstone. However, a thin (1 to 10-foot) bed or a sedimentary “fluidized zone” of megabreccia, genetically related to Dgb2, commonly occurs tens of feet below Dgb2. It may represent a potential surface-of-detachment for the Sequence Dgb2 sedimentary megabreccia and is designated as Unit D by Warme and Sandberg (1995). It is a carbonate diamictite of fluidized bedrock. If it is fully detached, then all of Sequences Dga2 and Dgb1 above this level are a great clast of the megabreccia at TMS. It would be classed as a medium to coarse monolith (Blair and McPherson, 1999). At southwest Mail Summit (TMS), this unusual megabreccia bed occurs at or above the Dga2 gamma-ray marker bed, 20 feet above the base of Sequence Dga2, or 392 feet below the top of Dgb2. Apparently, the megabreccia “fluidized zone” was either fluidized or liquified at this horizon by the same catastrophic event responsible for the formation of Dgb2 megabreccia. Its sequence boundary is neither an LSE nor a TSE but is a DSE, a new term herein. As defined in Chapter 3, a DSE is a Disturbed Surface of Erosion caused by other processes other than changes in relative sea-level. Because the liquified zone does not look like the surrounding bedrock, it is likely that the clasts within the zone were "loosed" and "transported," and thus, satisfy the definition of erosion (Bates and Jackson, 1987). Zones of fluidized or liquified carbonates are described in thin sections from the top of Sequence Dga (MI-401, Appendix C), Sequence Dgb1 (MI-405 and MI-406, Appendix C), and from the base of Sequence Dgb2 (MI-407, Appendix C). An unusual abundance of circular structures in MI-400, MI-401, MI-402, MI-403, and MI-425 could be impact-related spherules described by Warme and Kuehner (1998). The liquified carbonates could have been caused by liquefaction processes briefly reviewed by Warme and Kuehner (1998).

At Monte Mountain, ten miles west of TMS, Dgb2 lies on a thin (145feet) Sequence Dga. The thin megabreccia fluidized zone or liquified carbonate also occurs at Monte Mountain. Farther west, at Tempiute Mountain, the Dgb2 breccia cuts down into the top of the Simonson Dolomite. The thin liquified layer is missing there.

Kuehner (1997) reported an anomalously thin (20 feet thick) Dgb2 breccia at Six Mile Flat. However, in a section less than two miles northwest of his section (Sec 10, T7N R61E), a thin layer of Dgb2 liquified carbonate lies about 200 feet below the top of the main breccia body. It is likely that the breccia fluidized zone was overlooked at Six Mile Flats.

<u>Upper Contact of the Dgb2 Breccia</u> A karstified surface of dissolution marks the upper contact of Sequence Dgb2 in some sections. It is characterized by silty terra rosa filling fractures and cavities found in the upper 20 feet of the sequence. The size and number of the fractures and cavities decrease downward. Attitudes of some strata within some cavity fillings are parallel to tectonic dip caused by Mesozoic folding. MI-440 (167 feet from the base of the sequence) is dolomitized (95%) intraclast packstone containing subvertical and subhorizontal fractures partially filled with coarsely-crystalline white

dolomite and calcite. This regional exposure surface at the top of the Dgb2 breccia suggests that the event responsible for the breccia was followed by a period of local exposure and carbonate dissolution. Open-marine carbonates above the karsted interval show that the exposed areas were drowned under the transgressive sea.

<u>Distribution and Thickness of the Dgb2 Breccia</u> This lithologically unique rock body is distributed over more than 10,000 square miles in western Lincoln County, east-central Nye County and northern Clark County, Nevada. After palinspastic thrust fault restoration, this breccia could have been distributed over more than 20,000 square miles. In sections beyond the breccia occurrence, Sequence Dgb is a more ordinary succession of carbonate shelf strata (**Figure 9**, **Table 2**, and **Plate 3**).

The Tempiute cosmolite created the 160-mile diameter Tempiute basin that is assumed to be concentric about Tempiute Mountain before Mesozoic thrusting (Chamberlain, 1999). Warme et al. (1993) noted that it is thickest at the west end of the greater Timpahute Range. It thins radially. It is 510 feet thick at Tempiute Mountain (Cedar Strat proprietary measured section, 1985). In the Forest Home hanging wall thrust sheet (**Figure 2**), eastern Grant Range, 50 miles north of Tempiute Mountain, it is 20 feet thick (Cedar Stat proprietary measured section, 1985; No. 28, **Figure 9**). Guilmette Sequence Dgb2 at TMS is 179 feet thick from the base of the matrix to the graded bed at the top. It is 392 feet thick from a liquified interval near the base of Guilmette Sequence Dga2 to the top.

<u>Origin of the Dgb2 Breccia</u> Warme and Sandberg (1995) recounted mounting evidence that the Dgb2 megabreccia is a massive debris slide triggered by a Late Devonian cosmolite impact. That model assumed that the Tempiute Mountain section is on the shelf edge. However, as shown in Chapter 7, after thrust restoration the Tempiute Mountain section is interpreted to be deposited in the southern end of the Sunnyside basin

and to contain depositional environments that become shallower westward toward the Antler forebulge. The depositional environment of the breccia is problematical, but the thickness of the unit and the size and grading of clasts suggest open-marine conditions. I believe the impact of the Tempiute cosmolite created the Tempiute basin and was responsible for the distribution of Dgb2 breccia. Warme and Kuhner (1998) summarized evidence for the Late Devonian cosmolite impact including shocked quartz, iridium anomalies, ejecta spherules, and disturbed shallowing-upward sequences including intrasequence folding, brecciation, carbonate liquefaction, and graded bedding

Clasts within the breccia are fragments of shallowing-upward cycles of Sequence Dgb. Evidence of earlier Devonian sequences being involved in the breccia only occur at Tempiute Mountain. No evidence suggests that earlier Paleozoic rocks were involved in the breccia other than Ordovician conodonts reported by Warme and Sandberg (1996). I believe it likely that the conodonts are part of the recycled insoluble residues eroded from early Paleozoic carbonates on the Antler forebulge and redeposited in the Sunnyside basin. T. Hutter (1998, personal communication) found recycled early Paleozoic microfossils in Devonian rocks throughout the Sunnyside basin. The Antler forebulge and Sunnyside basin are discussed in Chapter 7.

<u>Reef Core vs. Reef Flank</u> **Figure 28** compares the overlapping sections where Sequence Dgb3 is a stromatoporoid reef (reef core) and where it is composed of reef flank facies (reef flank). The middle segment on **Figure 4** and **Plate 6** was measured where Subsequence Dgb3 is mostly a stromatoporoid reef (**Figure 26**, **Plate 2a** ). Sequences Dgb and Dgc and Subsequence Dgb3 in the middle reef section are designated Dgbc, Dgcc and Dgb3c respectively in **Table 5**, **Table 6** and **Table 7**. The upper segment on **Figure 4** was measured where Subsequence Dgb3 is composed of off-reef facies (**Figure 27**, **Plate 2b**). Sequences Dgb and Dgc and Subsequence Dgb3 in the upper off-reef segment are designated Dgbf, Dgcf, and Dgb3f respectively in **Table 5**, **Table 6** and

**Table 7**. Correlative strata of the two sections exhibit different thicknesses, and erosional and weathering characteristics (**Figure 28**). Whereas the reef facies is a massive recrystallized body, the Dgb3f facies is more cyclic and less recrystallized. Also, the gamma-ray pattern for the reef is nearly a flat line whereas the reef flank facies produces a more undulating gamma-ray signature over shallowing upward cycles. Sequence Dgbc is 420 feet thick (**Plate 2a**). Sequence Dgbf is 302 feet thick (**Plate 2a**).

<u>Sequence Dgb3c</u> Sequence Dgb3c is 228 feet thick at TMS and is composed of three cycles (**Figure 28**). The base is marked by an LSE overlain by a transgressive lag that makes a sharp contact with the underlying Sequence Dgb2. Cycles 1 and 2 contain corals, crinoids and other open marine fossils (see Appendix B for more details). The uppermost cycle, Cycle 3, is a coral-stromatoporoid boundstone reef and is much thicker than the lower two cycles (**Figure 28**). The reef is a classic lens-shaped, open-shelf, stromatoporoid reef with associated flank beds (Figure 11 in Chamberlain and Warme, 1996). It is composed of recrystallized limestone with some dolomite patches and forms a prominent, light-gray cliff above the medium-gray Dgb2 megabreccia cliffs. The exposed thickness of the lenticular reef is 165 feet thick in the center. It can be traced laterally for about 500 feet.

At the base of the reef, stromatoporoids are tabular and are up to six feet in diameter whereas in the middle and upper part of the reef stromatoporoids are bulbous, decreasing in diameter upward (12 inches to two inches diameter). A photomicrograph shows MI-456 is light-gray, dolomitized (<1%), recrystallized, stromatoporoid lime boundstone with tiny authigenic quartz crystals. A subvertical stylolite provides no visual porosity but shows evidence of lateral compression. MI-479 is a light-gray, recrystallized, stromatoporoid, lime boundstone. Details of the reef architecture and biostratigraphy have previously been documented by Dunn (1979).

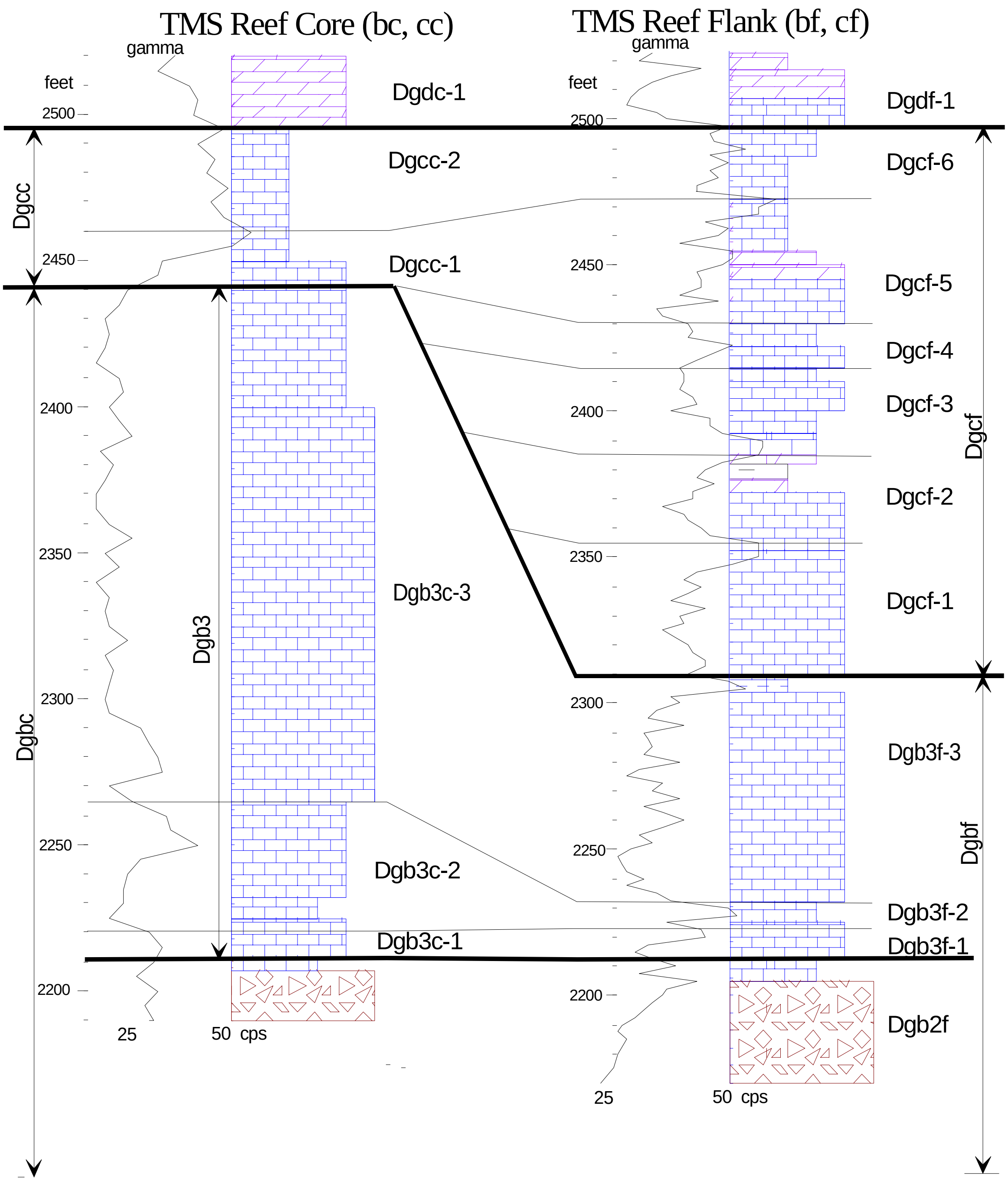


**Figure 28** Correlation chart comparing Guilmette cycles of Sequences Dgb3 and Dgc on a reef (Dgbc and Dgcc) with cycles on the reef flank (Dgbf and Dgcf) at TMS (i.e., middle and upper segments of TMS on **Figure 4**). Photographs suggest that the contact between the reef and reef flank beds is smooth (see Chamberlain and Warme, 1996, Figure 11).

Terra rosa and karst pockets characterize the LSE exposure surface at the top of the reef and at the top of Sequence Dgb3 on the reef flanks (**Figure 13**). Some karst cavities just below the exposure surface contain pale yellow-gray, laminated dolomudstone. The structural attitude of the dolomudstone is parallel to tectonic dip caused by Mesozoic folding.

Other stromatoporoid reefs of Sequence Dgb3, such as the one at Mail Summit, occur in the study area (Stop 16, Appendix D). They could serve as economically important hydrocarbon reservoirs in the region. Economic considerations are presented in Chapter 8.

Sequence Dgb3f Sequence Dgb3f is 97 feet thick and is composed of three cycles in the upper segment of TMS (**Figure 4** and **Figure 28**). Cycles 1 and 2 at the reef flank are similar to those in the middle segment of the measured section at the reef core. Cycle 3 is a 77-foot-thick shallowing-upward cycle of medium dark-gray, stromatoporoid coral lime packstone at the base (open-shelf) that becomes a burrowed, gastropod wackestone at the top (restricted shelf from 2,305 to 2,307 feet, **Plate 2a**). It is correlative with the 165 foot-thick stromatoporoid reef Guilmette Sequence Dgb3c, Cycle 3. The upper sequence boundary separates burrowed Sequence Dgcf rocks that lack marine fossils from underlying Sequence Dgb3f rocks that are rich in gastropods and other marine fossils.

Sequence Dgc

Two sections were measured TMS to compare and contrast Sequence Dgc strata deposited above the two different Dgb3 facies (**Figure 28**). Dgcf was measured in the upper segment at TMS where Dgb3 is reef flank facies (**Figure 4**, **Plate 6**). Dgcc was measured in the middle segment where Dgb3 is stromatoporoid reef facies. Sequence Dgcf is 188 feet thick and comprised of six cycles. Dgcc is 55 feet thick and comprised of two cycles.

Sequence Boundary The unconformity marked by a paleosol on a dissolution surface at the top of Sequence Dgb3 forms the major sequence boundary between Dgb3 and overlying Sequence Dgc (**Figure 13**). Above the unconformity, a TSE marks the base of Sequence Dgc, a silty, burrowed, gastropod lime wackestone (**Table 7**, **Plate 2a**).

Except for the uppermost part, the base of each shallowing-upward cycle in Sequence Dgc begins with sediments deposited in shallower water than the base of each previous cycle. The lower part of most of the cycles is composed of medium-gray, burrowed limestone. The upper part of each cycle consists generally of fossil-poor, medium to light-gray limestone, which was deposited in shallow-water conditions. Each successive cycle has more fossil-poor, light-gray limestone (**Figure 28**, see Appendix B for more details).

Gamma Radiation An abrupt gamma-ray increase at the base of Sequence Dgc is conspicuous and is correlatable on measured sections and well logs throughout the eastern Great Basin (**Figure 13**, **Figure 9**, and **Table 2**). The average gamma radiation of Sequence Dgc, 46 CPS, is almost twice that of the average gamma radiation of Sequence Dgb with an average of 26 CPS. The distinctive gamma-ray rightward inflection occurs because Sequence Dgc is more silty than adjacent sequences. Gamma radiation intensity increases upward from the open-shelf to slightly restricted-shelf bases to the more restricted-shelf tops of the shallowing-upward cycles. Gamma radiation of Sequence Dgc in the middle and upper segments of TMS is summarized in **Table 5**.

Depositional Indicators  The most characteristic features of Sequence Dgc rocks are the intensity of burrowing and the abundance of gastropods (**Table 4**). Sequence Dgc rocks lack open-marine fossils such as corals, stromatoporoids, and brachiopods and lack supratidal dolomites typical at the tops of shallowing-upward cycles of Sequence Dga below and Sequences e through g above. A dolomite cap on Cycle 5 of Sequence Dgcf is an exception and was probably deposited in supratidal conditions. The sandy limestone on dolomite and siltstone at the top of Sequence Dgc Cycle 2 was deposited in low-supratidal conditions.

Erosional Profile, Lithologies, Sequence Thicknesses, Textures, and Colors  Sequence Dgc tends to erode into a weathering profile of partly-covered to covered slopes (**Plate 2a** and **Table 5**). Typically, Sequence Dgc forms a saddle between the limestone cliffs of Sequence Dgb below and the dolomite ledges of Sequence Dgd above. **Table 5** summarizes the weathering profiles.

All of Sequence Dgcc is limestone and Dgcf is 72% limestone, 20% dolomite, 5% terrigenous siltstone, and 3% quartz sandstone (**Table 6**). Though the cumulative thickness of Sequence Dgb3 and Sequence Dgc in the two sections is similar, there is, nevertheless, a striking difference in the thickness of Sequence Dgc (**Plate 2a**, **Figure 26** and **Figure 27**). Cumulative thickness of Sequences Dgb3c and Dgcc is 260 feet and that of Dgb3f and Dgcf is 285 feet. Sequence Dgcc is only 45 feet thick. However, Dgcf is 188 feet thick.

Sequence Dgcc is 100% mudstone and Sequence Dgcf is 74% mudstone and 26% wackestone. Sequence Dgc mudstone contrasts with *Amphipora* wackestone of Sequence Dgd above and stromatoporoid packstones and boundstones of Sequence Dgb below. **Table 7** summarizes the sequence colors.

Cycle Thicknesses There are only two cycles in Sequence Dgcc. In contrast, six cycles with an average thickness of 31 feet make up Sequence Dgcf, approximately a mile away (**Figure 28**, **Figure 26**, and **Figure 27**). The thickest Sequence Dgcf cycle is 42.5 feet and the thinnest cycle is 13.5 feet. Similarly, Sequence Dgcc cycles average 28 feet thick, ranging from a maximum of 45 feet to a minimum of 10 feet. Cycle thickness can be used to distinguish Guilmette sequences. For example, the average Sequence Dgcf cycle is thicker (31 feet) than the average cycle of Sequence Dga (20 feet).

**Figure 27** illustrates that Sequence Dgcf cycles become thinner from Cycle 1 (43.5 Feet) through Cycle 4 (15 feet) and then thicken at Cycle 5 (42.5 feet). If the upward-thickening trend continued to Cycle 6, then erosion at the top of Cycle 6 could have removed 20 or 30 feet of supratidal dolomites. Because Sequence Dgcc is mostly (78%) a covered interval, it is unclear if it consists of more than two cycles (**Plate 2a**). All six cycles of Sequence Dgcf may merge into the two cycles of Sequence Dgcc. If they do, they thin over the reef core. Otherwise, Cycles 1 through 4 are missing over the reef core by onlap and Cycles 5 and 6 on the reef flank correlate to Cycles 1 and 2 on the reef core as shown in **Figure 28**. Cycles 1 through 4 on the reef flank represent a period of shallowing-upward or slowing of relative sea-level rise that would result in less accommodation space. Cycles 5 and 6 on the reef flank and Cycles 1 and 2 on the reef core represent a period of accelerated sea-level rise, creating more accommodation space upward. A deepening of sea level at the top of the shallowing upward Cycle 6 (reef flank) resulted in a merged LSE/TSE responsible for truncating the upper part of Cycle 6 on the reef flank and Cycle 2 on the reef core.

## Sequence Dgd

Sequence Dgd is 406 feet thick and comprised of 23 cycles. *Amphipora*-rich dolowackestone-packstone characterizes Sequence Dgd (**Table 7**). The medium dark-gray to medium brown-gray *Amphipora* wackestone-packstone facies suggests deposition in a restricted-shelf lagoon environment, an interpretation that concurs with Niebuhr (1979). A merged LSE/TSE marks the sharp basal contact of this sequence. Above the transgressive lag deposit associated with the TSE is an oncolite-bearing bed. Except for a few minor (10 feet thick or less) limestone intervals and several thin (less than 5 feet thick) quartz sandstone beds, 90% of Sequence Dgd is an *Amphipora*-rich dolopackstone that generally shallows upward (**Plate 2a**).

Quartz Sandstone Most of the cycles in Sequence Dgd are capped by thin, laminated, light-gray dolomite (**Plate 2a**). Four of the cycles are capped by thin sandstone beds less than five feet thick. The light-gray, medium-grained, well-sorted, dolomite-cemented, quartz sandstones are trough crossbedded. Commonly the crossbedding shows a prevailing southwest current direction. Some sandstones have desiccation cracks. Other than a few scattered medium-sized quartz grains and rare thin (1' thick) sandstone beds in the Yellow Slope Sequence, sandstone in cycle 16, near the middle of Sequence Dgd, contains the first occurrence of medium-grained quartz sand above the “Oxyoke Formation” sandstone.

Though quartz sandstone makes up a small part of the Guilmette at TMS, it predominates in the Monte Mountain Section above the Dgb2 breccia (**Figure 9**, No. 52). One massive sandstone unit, truncated at the base by the Monte Mountain thrust fault, is at least 700 feet thick (Stop 14, Appendix D). Net sandstone for the formation at Monte Mountain is 1,070 feet. The sandstone bodies are composed of well-sorted, well-rounded, frosted, fine to medium quartz grains (Chapter 7).

Gamma Radiation A prominent, regionally persistent, gamma-ray leftward inflection marks the base of Sequence Dgd, which lies on the unconformity at the top of

Sequence Dgc. **Figure 13** illustrates a slight increase in gamma radiation from the base to near the middle of the sequence. The gamma-ray pattern is generally smooth over the sequence except local inflections at cycle tops caused by concentrations of wind-blown radioactive dust. A regionally persistent gamma-ray leftward inflection occurs in the middle part of the sequence.

<u>Sequence Dge</u>

Sequence Dge is 235 feet thick and comprised of 17 cycles. Whereas Sequence Dgd is predominantly dolomite, Sequence Dge is a mixture of dolomite, limestone, quartz sandstone, and siltstone (**Plate 2a**). Denoting another merged LSE and TSE sequence boundary, the dolomite at the base of Sequence Dge directly overlies an unconformity at the top of Sequence Dgd. In some sections north of the study area, the unconformity cuts out much of Sequence Dgd.

<u>Gamma Radiation</u> A regionally correlatable gamma-ray rightward inflection marks the base of Sequence Dge (**Figure 13**). Cycles within the sequence are marked with a leftward gamma-ray inflection at the base and a gradual gamma radiation increase toward the top. Gamma-ray spikes are common where terrigenous grains are concentrated at the tops of some cycles.

<u>Sequence Dgf</u>

Sequence Dgf is 267 feet thick and comprised of 15 cycles. The sharp basal contact of Sequence f occurs where an LSE truncates the uppermost light-gray, laminated dolomite of Sequence Dge and is merged with a TSE. A six-inch lag deposit of light-gray, finely-crystalline dolomite clasts in medium dark-gray dolomite overlies the TSE. The sequence is predominantly limestone, except the uppermost 65 feet, which is composed of predominantly dolomite (**Table 6**). Medium-gray to medium dark-gray, medium to thin-bedded, locally *Amphipora*-bearing, lagoonal, burrowed limestones form the lower part of most cycles. Many cycles are capped by either supratidal, light-gray, laminated dolomudstone with tepee structures or one- to two-foot thick supratidal, light yellow-gray, fine-grained quartz sandstone beds. Many supratidal caps contain intervals of desiccation cracks.

The sequence is erosionally nonresistant, because 61% is partly-covered slopes, 15% are covered slopes and only 24% are ledges. Light colors dominate as 33% of the sequence is medium light-gray, 26% is light-gray, 4% is pale yellow-gray, 13% is medium-gray, and only 24% is medium dark-gray.

The rightward gamma-ray inflection at the base of Sequence Dgf is regionally correlative (**Figure 13**). As observed in other cycles, gamma radiation is generally higher over light-gray, unfossiliferous, laminated, finely-crystalline dolomite interpreted to have been deposited in supratidal conditions. Gamma radiation is lower over thick-bedded, open marine fossil-bearing limestone interpreted to have been deposited in open-shelf conditions. However, cycles 9, 10, and 11 not only provide the highest gamma-ray responses in the sequence, but also contain the uppermost occurrences of open-marine fauna in the TMS section including corals, bulbous stromatoporoids, and brachiopods. The higher gamma-ray response associated with open-marine carbonates is probably due to a higher influx of detrital material. Above cycle 9, the detrital material shut off the carbonate factory. Detrital influx from the incipient Antler orogeny and more restrictive circulation is probably responsible for the paucity of abundant open-marine macrofossils observed between Sequence Dgf cycle 11 and the Mississippian Joana Limestone at TMS.

Sequence Dgg

Sequence Dgg, with its 567-foot-thickness and its 29 cycles, is the most variable sequence of the Guilmette Formation in cycle lithologies and thicknesses. At TMS, the section is 59% dolomite, 24% quartz sandstone, and 17% limestone.

A regionally correlatable leftward gamma-ray inflection (lower gamma radiation) marks the base of Sequence Dgg (**Figure 13**). Otherwise, the contact between the light brown-gray dolomite of Sequence Dgf and that of Sequence Dgg is indistinguishable in the field. Indicators of a sequence boundary or unconformity are yet to be found in the covered interval. The covered interval probably formed on a nonresistant paleosol developed on the top of Sequence Dgf.

The top of the Guilmette Formation in many sections on the edge of the Sunnyside basin is marked by a prominent sandstone bed, representing the uppermost part of the uppermost cycle. This sandstone probably correlates to the Cove Fort Sandstone in other sections of western Utah. Hintze (1988) showed the Cove Fort Sandstone at the top of the Guilmette Formation in western Utah sections.

Weathering Profile and Color Most (57%) of Sequence Dgg is resistant and forms ledges. Nevertheless, 39% of the sequence erodes into partly-covered slopes and 4% is covered. In contrast to earlier sequences, Sequence Dgg lacks cliffs. The sequence weathers to shades of gray and brown-gray. It is 42% light-gray, 36% medium-gray, 11% brown-gray, and 11% light brown-gray.

Gamma Radiation The sequence has a variable gamma-ray log response. It has a standard deviation of 10.3 CPS, higher than the standard deviation of Sequence Dga (**Table 5**). Average gamma radiation of the sequence is 49 CPS. It ranges from a minimum of 32 CPS to a maximum of 92 CPS. The abrupt decrease in gamma radiation at the base of the sequence provides a leftward inflection that is regionally recognizable. Another regionally correlative gamma-ray spike occurs at the top of the sequence. Gamma radiation intensity in Sequence Dgg is low compared with subjacent Sequence Dgf (average of 49 in Dgg versus 61 CPS in Dgf) and superjacent West Range Limestone Sequence (average of 49 CPS in Dgg versus 82.6 CPS in West Range Limestone (**Figure 13**).

The Uppermost Occurrence of *Amphipora* The uppermost occurrence of *Amphipora* in TMS Devonian occurs in the lower part of Sequence Dgg Cycle 25 (see **Plate 2a**). The last occurrence of rugose corals at TMS occurs in Sequence Dgf Cycle 11 and the last occurrence of stromatoporoids occurs in Sequence Dgf Cycle 5 (Appendix B). The lack of reef-building stromatoporoids and corals and the last occurrence of *Amphipora* could represent the Frasnian-Famennian boundary. Sandberg et al. (1997) also placed the Fransian-Famennian above the cyclical carbonate rocks and within the sandy member in their time-rock chart of the north Pahranagat Range and Mount Irish Range. They place it much lower in their Tempiute Mountain section. However, if their top of the Dgb2 breccia is the same as TMS herein, then using their thicknesses, the boundary is in Sequence Dgd. Either the measured thicknesses are different or Sequences Dgc-Dgg are unusually thin at TMS and the section needs to be recorrelated. It would have been most helpful if Sandberg et al. (1997) would have added a surface gamma-ray log to their chart so that the sections could be correlated directly. It is recommended in Chapter 9 that conodont zones of the region be tied to surface gamma-ray logs to tighten and refine sequence correlations of the region. The extinction of most reef-building stromatoporoids and corals at the Frasnian-Famennian boundary correlates to the collapse of North American stromatoporoid-dominated reefs (Webb, 1998). *Amphipora* does not occur in the uppermost cycles of Sequence Dgg in other sections throughout the

Sunnyside basin where the uppermost part of the sequence is preserved. Therefore, the Frasnian-Famennian boundary probably occurs at the top of Sequence Dgg Cycle 25.

## West Range Limestone

The West Range Limestone is 153 feet thick at TMS and comprised of one sequence and four cycles (**Plate 2a**). The basal contact of the sequence is marked by a transgressive erosional surface over the unconformity at the top of Sequence Dgg. In some sections north of the study area, the unconformity cuts out much of Sequence Dgg. The West Range Limestone consists of intertidal lime mudstones. They overlie the uppermost intertidal to supratidal quartz sandstone bed of Sequence Dgg (**Figure 13**). The West Range Limestone is readily eroded into recessive, partly-covered slopes. It is typified by light-gray, burrowed lime mudstone that contains few macrofossils. It is commonly mottled or burrowed, silty, argillaceous, partly laminated, and thin-bedded.

If the Monte Mountain (TMM) section is restored to west of Tempiute Mountain (TMP) as proposed in Chapter 5, then the West Range Sequence regularly thins westward. It is 153 feet thick at TMS, 125 feet thick at TMP, and 58 feet thick at TMM.

The West Range Limestone has a higher gamma-ray intensity than the underlying Guilmette. The highest gamma-ray count in the West Range Limestone is 106 CPS and the lowest is 61 CPS. The average is 82.6 CPS. The standard deviation is 10.7 CPS. A sharp, distinct, rightward gamma-ray inflection marks the base of the sequence on surface and subsurface logs (**Figure 13**).

The top of the West Range Sequence herein is defined by a sequence boundary with a sharp rightward gamma-ray inflection. It is different from the lithologic formation boundary by Sandberg and Ziegler (1973) who did not employ principles of "sequence stratigraphy" to their measured section at Bactrian Mountain. They included the upper part of the West Range Sequence in their Pilot Formation.

## Pilot Formation

The Pilot Formation is 245 feet thick and comprised of two sequences at TMS. **Plate 7** illustrates the distribution of 91 Pilot Formation outcrops in the Timpahute Range 30' X 60' quadrangle that cover 5.85 square miles. The poorly exposed Mississippian-Devonian Pilot Formation occurs above the cyclic Devonian carbonates (**Plate 2a**, **Figure 13**). The Mississippian-Devonian boundary lies within the Pilot Formation. The sequence boundary could be the unconformity at the top of Sequence 1. Sandberg and Ziegler (1973) pointed out that erosion at the unconformity cuts out eight conodont zones in the Pilot Formation at Bactrian Mountain, on the north end of the Pahranagat Range, seven miles south of the TMS section. The Pilot Formation manifests a unique gamma-ray signature with the highest radioactivity of all the Devonian system. It has a high clay content and probably high concentrations of radioactive potassium. In measured sections and well cuttings of the Mississippian Antler clastic shales, those which exhibit higher radiation are also higher in Total Organic Carbon or TOC (Chamberlain, 1988c). Similarly, the high organic carbon in the siliceous stromatolites and black siltstone is probably the source of the high gamma radiation in the Pilot Formation.

At the beginning of this chapter, it was proposed that the sequence boundary at the top of the Sevy Dolomite is probably the base of the Kaskaskia sequence of Sloss (1963) and the Piankasha Holostrome of Wheeler (1963). The Kaskaskia or Piankasha is one of several major continental sequences bounded by continent-wide unconformities. It began in the Early Devonian and ended in the Late Devonian. The top of the Kaskaskia or Piankasha may correspond to the sequence boundary between Pilot Formation Sequences 1 and 2. Wheeler called the missing interval at the unconformity the Acadian Hiatus. Most of the sequences described in this chapter lie in the Kaskaskia sequence (**Figure 10**).

Sandberg and Ziegler (1973) reported 426 feet of Pilot Formation at Bactrian Mountain in the study area, 60 miles south of the southern edge of the Pilot basin of Sandberg et al. (1988). Pilot Sequences are thickest (815 feet) in the Confusion Range

(No. 11, **Figure 9**), are absent in the Forest Home footwall thrust sheet (No. 27, **Figure 9**), and 233 feet thick in the Forest Home hanging wall thrust sheet (No. 28, **Figure 9**). Pilot Sequences in the Pancake Range, near the Pilot basin of Sandberg et al. (1988), are 365 feet thick (Cedar Strat files). The sequences thin over the Monitor-Uinta arch and thicken to 230 feet at Pearl Peak (No. 45, **Figure 9**) and 275 feet in the Pequop Range (No. 41, **Figure 9**) north of the arch (Cedar Strat files). Sandberg et al. (1988) neither show the thinning of the Pilot Formation over the Monitor-Uinta arch, nor do they mention the shuffling of sections caused by Sevier thrusting. Therefore, their paleogeographic maps may be misleading.

Correlation charts in Chapter 6 illustrate the thicknesses of Pilot Sequences in different thrust sheets in the Timpahute Range. It is 300 feet thick at Tempiute Mountain, 117 feet thick at Monte Mountain, and 245 feet thick at TMS. If the Silver Canyon thrust sheet is restored to west of Tempiute Mountain, then a consistent thinning of the Pilot Sequences occurs from near the center of the Sunnyside basin at Tempiute Mountain to Monte Mountain on the west and TMS on the east.

### Pilot Formation Sequence 1

Pilot Formation Sequence 1 at TMS is 130 feet thick and is comprised of two cycles (**Plate 2a**). It consists of most of the West Range Limestone upper unit and all of the Pilot Shale lower unit of Sandberg and Ziegler (1973). It lies in the lower *marginifera* conodont zone (**Figure 10**). The base of Sequence 1 occurs where recessive limestones of the West Range Limestone abruptly give way to mostly covered intervals. These slopes, bearing fragments of light-gray, silty limestone, produce an increased gamma-ray measurement. The top of the sequence is marked by a thin, ferruginous, fossil fish plate-bearing quartz sandstone only five to ten feet thick that overlies ten feet of pale-yellow, calcareous siltstone. This may be correlative with the planar, crossbedded, coarse-grained, quartz sandstone, containing abundant abraded fish bones and teeth, conodonts, and phosphatic pellets between sequences three and four of Giles (1994) in the Confusion Range, western Utah. However, Giles (1994) placed a regional unconformity below the sandstone.

The Pilot Formation Sequence 1 is more radioactive than the underlying West Range Limestone. Furthermore, two of the highest gamma-ray spikes in the TMS occur in Pilot Formation Sequence 1 (**Figure 13**). The first occurs at the base of Cycle 1, and the second occurs near the top of Cycle 2 in the ferruginous sandstone. Although thick cover commonly masks the base of the sequence, the contact can be picked on the surface gamma-ray log where an abrupt gamma-ray intensity increase occurs. This provides an example of the usefulness of surface gamma-ray logs for interpreting changes in lithology otherwise hidden by scree or soil.

## Pilot Formation Sequence 2

Pilot Formation Sequence 2 at TMS is 115 feet thick and comprised of 2 cycles. As mentioned above, the major unconformity that cuts out eight conodont zones in the Pilot Formation at Bactrian Mountain (Sandberg and Ziegler, 1973) may be the sequence boundary between Sequences 1 and 2. The ferruginous quartz sandstone at the top of Sequence 1 is overlain by the pale-red, cherty siltstone of Sequence 2. Its base lies in the Middle *costatus* conodont zone of Sandberg and Ziegler (1973) at Bactrian Mountain (**Figure 10**). Black, laminated, silicified stromatolite beds of cycle 1 are capped by a 2.5-foot-thick bed of bioturbated sandstone (**Table 6**). The second cycle is a silty limestone that is commonly covered.

The ferruginous sandstone at the top of Sequence 1 produces a gamma-ray peak in contrast to the abrupt gamma-ray leftward inflection at the base of Sequence 2 (**Figure 13**). The gamma-ray spike mentioned in the first paragraph of this section on the Pilot

Formation is associated with silicified stromatolites that occur at the top of Cycle 1. Gamma radiation abruptly decreases at the base of Cycle 2, and continues to decrease gradually to the base of the overlying Joana Limestone where a distinct gamma-ray leftward inflection at a sharp erosional break occurs (**Plate 1a**).

## Joana Limestone

The Mississippian Joana Limestone (note that only the base of the formation is shown in **Plate 2a**) represents a major transgression over the uppermost Pilot Formation Sequence 2 Cycle 2. The Joana Limestone contains abundant bedded chert and open-marine fossils including crinoids and corals in contrast with the uppermost Pilot Formation that lacks bedded chert and open-marine fossils. Joana Limestone sequences from the base to the top include: (1) ledge-forming, silty lime wackestone; (2) prominent, cliff-forming crinoid grainstone; (3) prominent, cliff-forming crinoid grainstone banded with chert; and (4) cliff-forming crinoid grainstone. The formation is mostly a medium-gray weathered, massively bedded crinoid packstone. **Figure 29** illustrates the distribution of 101 Joana Formation outcrops in the Timpahute Range 30' X 60' quadrangle that cover 40.25 square miles.

Although the Joana Limestone-Pilot Formation contact is generally covered with scree from the from overlying Joana Limestone, it can be picked at a pronounced decrease in gamma radiation. This gamma-ray shift is an abrupt change to some lowest values measured in the TMS (**Figure 13**). The leftward gamma-ray inflection at the erosional break is interpreted to be a merged LSE and TSE that separates Pilot Formation slopes from overlying Joana cliffs. Gamma radiation generally increases upward to the top of the Joana Limestone.

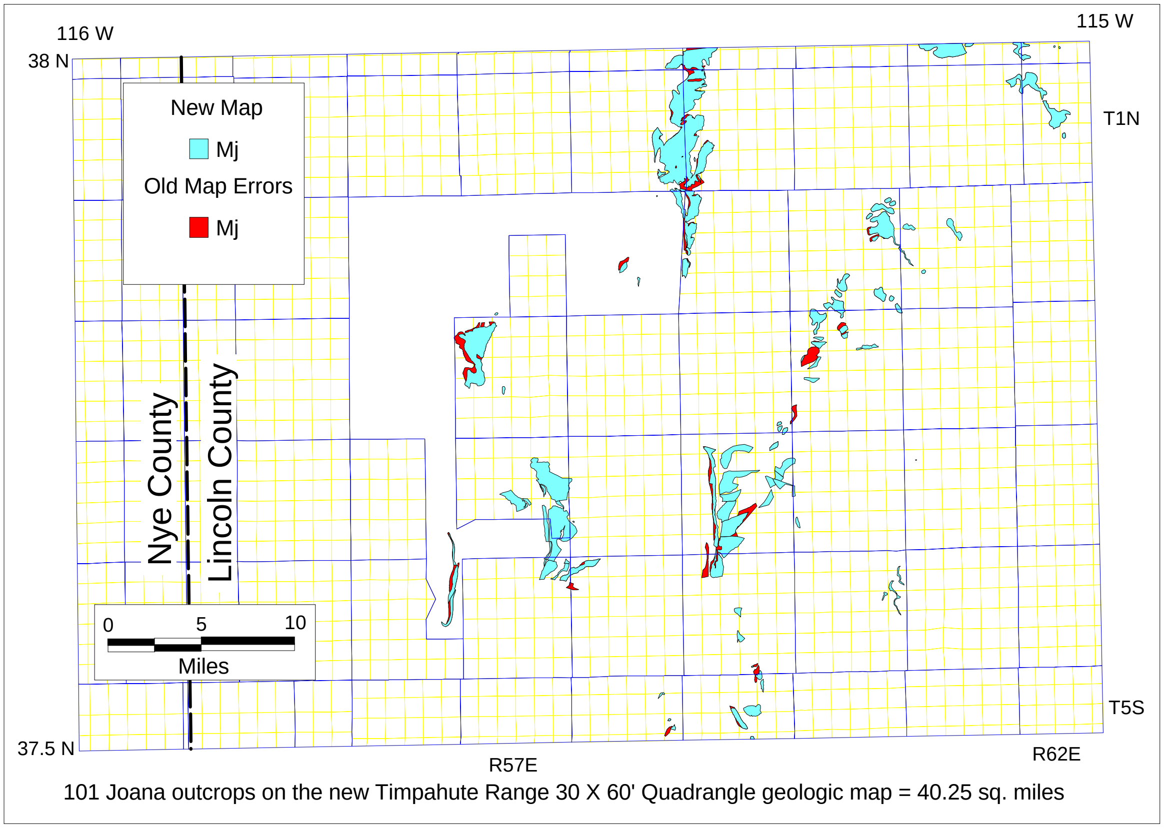


**Figure 29** Distribution of Joana Formation outcrops on the new geologic map of the Timpahute Range 30' X 60' quadrangle. Areas erroneously mapped on old map as Joana are marked in red. Degrees N latitude and W longitude are marked at the corners of the map. Blue lines are surveyed townships and ranges and the yellow lines are surveyed sections.

## Discussion

Devonian sequences at TMS serve as a reference section for the rest of the Sunnyside basin and fulfill the first objective of this research, namely to give an account of the 21 mappable Devonian sequences at TMS (**Figure 13**). These regionally correlatable sequences at TMS were correlated to more than 500 other Great Basin surface and subsurface sections measured and described in Nevada and western Utah (**Figure 9**, **Plate 3**). However, **Table 2** and Appendix F lists only those sections and wells where the complete Devonian interval is represented or where no Devonian rocks were deposited. All Cedar Strat sections listed in the tables were measured at the same scale and detail as TMS. They all contain surface gamma-ray logs for correlating. Cuttings from most of the wells listed in the tables were described by Cedar Strat. These descriptions, combined with gamma-ray logs, were used for correlations. Many other sections are described in the literature or in proprietary studies. Though they lacked the detail and surface gamma-ray logs, less exact correlations based on lithologic and fossil descriptions were made using these other sections. They did provide additional control points. Most of the surface and subsurface sections are composed of only parts of the Devonian interval because of faulting, cover, erosion, or not drilling deep enough. A spreadsheet of all the data points, sequence thicknesses, thicknesses of sandstones and other information provided a method of organizing the data set. Every section that contained one or more sequences was added to the spreadsheet. Data from the spreadsheet were used to construct isopach and isolith maps presented in Chapter 7. As each isopach map of each of the 21 sequences was made, errors in correlation were detected and corrected. The final product was an isopach map of the total Devonian (Chapter 7, **Figure 9**, **Plate 3**). Viewed in order, the 21 isopach maps reveal the evolution of the Sunnyside basin. This evolution aided in inferences and interpretations. For example, unconformities cut out some sequences over the Monitor-Uinta arch. These unconformities provided some basis for determining the sequence boundaries at TMS. However, a detailed analysis of the evolution of the Sunnyside basin is beyond the scope of this study.

Facies of sequences in most sections and wells throughout the Sunnyside basin are similar to TMS. However, abrupt contrast occurs in facies of post Guilmette Sequence Dgb2 in sequences from different thrust sheets in the greater Timpahute Range. For example, post Sequence Dgb2 facies at TMS are composed of limestone to dolomite shallowing upward cycles. Correlative rocks in the Silver Canyon thrust sheet are uniquely predominantly quartz sandstones and those in the Tempiute Mountain thrust sheet are uniquely predominantly thin-bedded limestones. The contrasting facies are illustrated by an east-west correlation chart (**Figure 30**). Gamma-ray log patterns of the sequences allow correlation of these sequences of different facies. Concentrations of greater amounts of wind-blown radioactive dust were not facies sensitive and left their chronostratigraphic imprints in the rock record. These imprints, much like bentonite beds in the Cretaceous Rocky Mountain seaway, mark the sequences with unique gamma-ray patterns that are regionally correlative. Because these patterns are not facies sensitive, sequences with sharply contrasting facies can be correlated between the thrust sheets.

Small, meter-scale, shallowing-upward cycles at TMS were probably controlled by local depositional systems involving autocyclic aggradation. These small-scale cycles can be traced laterally only locally. Cycle thicknesses and stacking patterns seem random and unpredictable. In contrast, the sequence and formation-scale cycles were probably controlled by changes in eustasy and subsidence rates. They are predictable and can be traced regionally. Some sequence boundaries are subtle on the outcrop but all the boundaries have recognizable gamma-ray signatures. Other sequence boundaries such as the change from light-gray dolomudstone to argillaceous dolomite at the Sevy Dolomite/“Oxyoke Formation” contact are more obvious on the outcrop. The unconformity at the top of the Simonson Dolomite is a regionally correlatable sequence boundary.

The upper parts of most of the cycles that make up the Guilmette sequences are dolomudstone and all the sequences below the Simonson Dolomite unconformity are pervasively dolomitized. However, thin-bedded limestones above the Dgb2 breccia in the Timpahute Mountain (west Pahroc) thrust sheet are not dolomitized. Less dolomite occurs in the sandy Silver Canyon thrust sheet than in the reefy east Pahroc thrust sheet. The dolomite occurrences and possible dolomitization mechanisms are the subject of the next section.

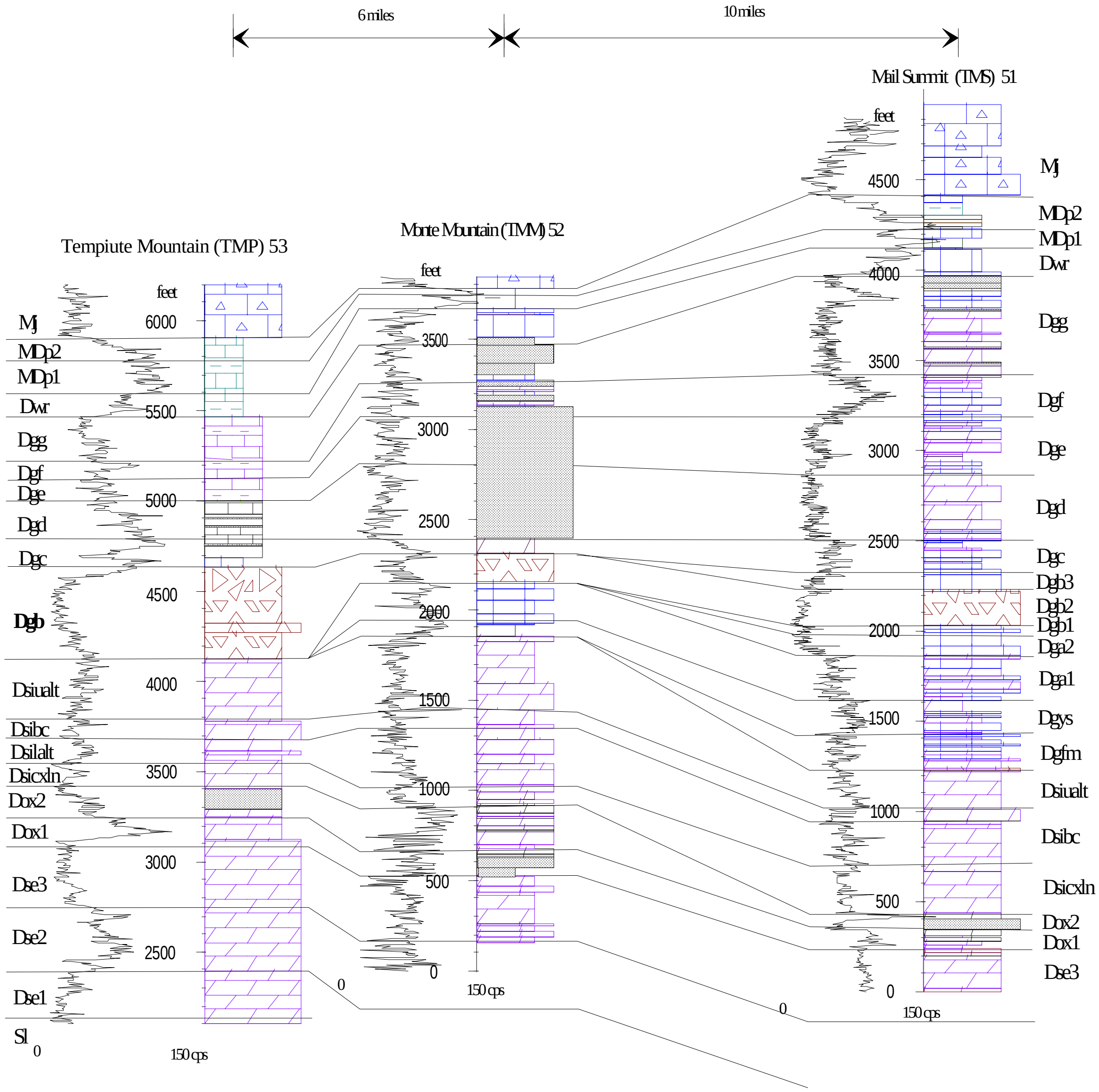


**Figure 30** Correlation of three measured sections in the greater Timpahute Range separated by Mesozoic thrust faults which shows the three contrasting facies above Guilmette Sequence Dgb2 breccia.

Dolomite at TMS

Much of the Devonian section in the study area has undergone diagenetic transformation to dolomite, particularly in the Sevy and the Simonson formations. However, classifying Devonian dolomite types in the study area is limited to dolomite fabrics, field relationships, and limited petrography. Using these data, a paragenetic sequence is suggested (**Figure 31**). Fabric refers to size and mutual relationships of crystals, whereas texture refers to shape of crystals (Friedman and Sanders, 1967). Other workers have developed crude paragenetic sequences based on limited data. Fischer (1988) classified dolomites of the Cambrian Metaline Formation, northwest Washington, based on crystal fabric.

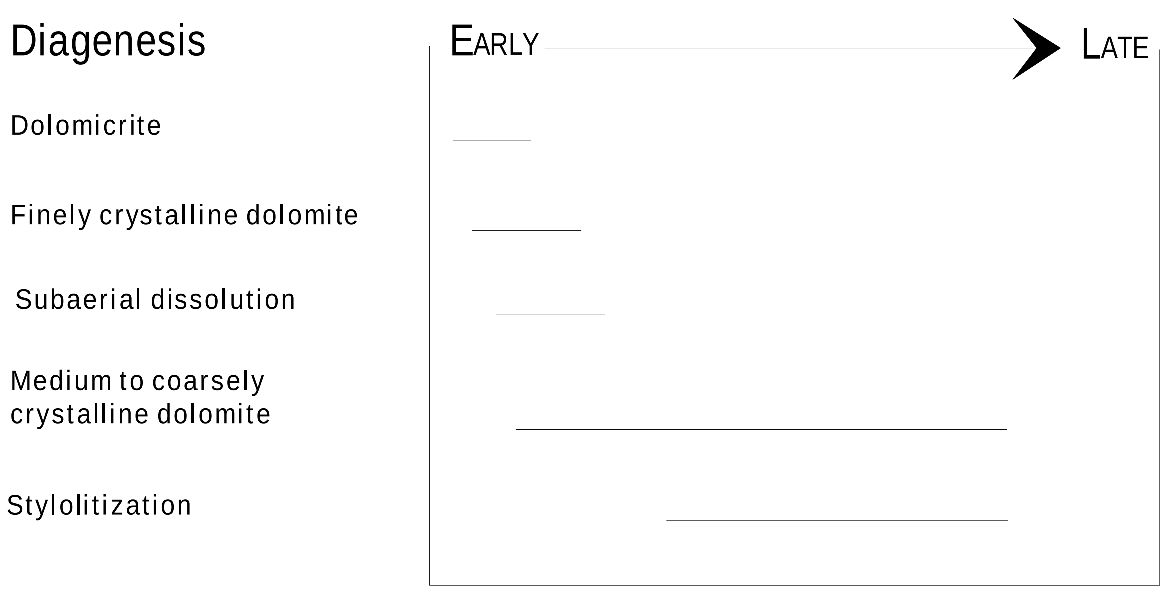


**Figure 31** Generalized diagenetic sequence for dolomites at TMS. Micrite caps on shallowing-upward cycles were probably diagenetically altered to stratal finely-crystalline dolomite penecontemporaneously. Porous zones created by subaerial dissolution during low sea-level stands channeled dolomitizing fluids resulting in medium to coarsely-crystalline dolomite. Regional burial and tectonism resulted in later-stage stylolitization.

At least four types of dolomite or dolomite facies occur in the study area. They are: 1) finely-crystalline stratal, 2) coarsely-crystalline stratal, 3) pervasive, and 4) non-stratal dolomite. All four types are considered to be replacement dolomites. Dolomitization of the cycle caps to finely-crystalline stratal dolomite probably occurred penecontemporaneously and the other types occurred later. Besides the dolomite bodies, Devonian sandstones discussed in Chapter 7 are cemented with dolomite. The four principal types of dolomite fabrics or dolomite facies at TMS are summarized in **Table 9**.

Pervasive dolomite is most important below the Simonson unconformity. TMS was intentionally picked to avoid secondary dolomitization and alteration associated with faults. Therefore, finely-crystalline stratal dolomite is most important in the Guilmette cycle caps above the Simonson unconformity.

Finely-Crystalline Stratal Dolostone (Type 1)

Most of the Sevy Dolomite and much of the Simonson Dolomite is composed of finely-crystalline, stratal dolomite. However, some of it has been modified to fine- to coarsely-crystalline fabrics. In the Guilmette Formation, finely-crystalline stratal dolomite is mostly restricted to the upper part of many shallowing-upward cycles. The finely-crystalline fabric provides some light on the diagenetic sequence. Shukla (1988) suggested that penecontemporaneous dolomites are more finely crystalline than diagenetic dolomites. Fischer (1988) also interpreted his finely-crystalline fabric type A dolomite as a penecontemporaneous dolomite formed by supratidal processes.

**Table 9** Dolostone types, characteristics, distribution, inferred timing, and examples at TMS and in other parts of the study area.

| TMS dolomite type | Characteristics | Distribution | Timing | Example |
|---|---|---|---|---|
| 1. Finely crystalline stratal dolomite | Finely crystalline, laminated, unfossiliferous, upper part of shallowing-upward cycles. | Restricted to upper parts of local carbonate cycles | Very early- syn-depositional. | Cycle tops in the Guilmette, Simonson Dolomite, and Sevy Dolomite |
| 2. Coarsely crystalline stratal dolomite | Coarsely crystalline, crystal coarseness and size of fractures filled with coarsely-crystalline dolomite increase upward toward sequence boundaries. Unaltered patches of limestone. Commonly contains zebra dolomite. | Local (not correlative with other sections in the basin) to regional (correlative with other sections in the basin) | Intermediate, restricted to sequence boundaries suggesting dolomitization before deposition of overlying unit. | Dolostone zones below some Guilmette Dgd, Dge, Dgf, and Dgg sequence boundaries |
| 3. Pervasive dolomite below the Simonson Dolomite unconformity at upper contact of the Simonson Dolomite | Finely to coarsely-crystalline dolomite, dolomitization complete Associated with karst breccia and coarse dolomite-filled fractures that increase in abundance and thickness upward to major sequence boundaries. | Regional, associated with major LSE and karsting | Intermediate, restricted to below the Simonson Dolomite unconformity suggesting dolomitization before Guilmette deposition | All carbonate rocks below the Simonson Dolomite unconformity and above the upper Pogonip Group limestones except in the Silver Canyon thrust sheet. |
| 4. Non-stratal dolomite | Frequency of zebra dolomite and fractures filled with sparry, saddle? dolomite crystals and coarseness of crystals increase toward faults. | Local, near faults or selective porous zones | Very late, cuts across all other dolomite types and sequence facies. | Dolostone associated with the Silver Canyon thrust fault and some normal faults and porous intervals that have no obvious association with faults |

<u>Sevy Dolomite Finely crystalline Stratal Dolostone</u> The Sevy Dolomite is composed of finely-crystalline dolomite that I interpret to have been deposited in mostly supratidal conditions at TMS (Chapter 4). Evidence of supratidal conditions includes lack of fossils, laminated dolomudstone, light-gray color (suggesting an oxidizing environment), tepee structures, desiccation cracks, and fenestral textures. The Sevy Dolomite is composed of many shallowing-upward cycles. Bases of the cycles were deposited in low tidal flat conditions and the tops of cycles were deposited in high supratidal conditions. The dolomite in the Sevy Dolomite cycles is similar to the finely-crystalline stratal dolomite in the Guilmette cycle caps.

<u>Simonson Dolomite Finely crystalline Stratal Dolostone</u> The succession of alternating light and dark layers (1-10's feet thick) that form the cycles within the Simonson Dolomite gives it a banded appearance. The banded layering is interpreted as a repetition of the alternating lower and upper parts of shallowing-upward cycles. Rarely *Amphipora* occurs in the darker, coarser-crystalline dolomite in the lower part of the shallowing-upward cycles. *Amphipora* suggests open-shelf to restricted marine near-shore conditions. The upper part of the shallowing-upward cycles consists of unfossiliferous, light-gray, fine- to medium-crystalline dolomite. Tepee structures and fenestral texture suggest that it was probably deposited in highly restricted to supratidal conditions. The dolomite was probably penecontemporaneously altered to finely-crystalline stratal dolomites in supratidal conditions. Capillary upward movement of sea water becomes concentrated by evapo-transpiration in supratidal environments (Friedman and Sanders, 1967).

Finely crystalline stratal dolomites probably occurred in the upper parts of shallowing-upward cycles of the Coarsely-Crystalline Sequence between the “Oxyoke Formation” and the Lower Alternating Sequence. Primary bedding and sedimentary structures in this interval have been obliterated by dolomitization and recrystallization.

The alteration may be associated with an unconformity at the top of the Coarsely-Crystalline Sequence. Upward-shallowing cycles in this sequence are similar to the Lower and Upper Alternating Sequences above the unconformity. The main difference is that they are recrystallized to coarsely-crystalline dolomite below the unconformity and they are not recrystallized to coarsely-crystalline dolomite above the unconformity. The unconformity apparently separates an earlier diagenetic event from a later one.

Guilmette Finely-Crystalline Stratal Dolostone Most of the upward-shallowing cycles in the Guilmette at TMS are capped by finely-crystalline stratal dolomite. An example of a shallowing-upward cycle with a dolomite cap is Cycle 9 in the Guilmette Yellow Slope Sequence (Appendix B). Three feet above the base of the cycle is an intraclast, ostracode, pellet lime packstone (see MI-317, Appendix C). At the top of the 20-foot cycle is a silty, laminated dolomudstone (see MI-320.95, Appendix C). This is an unfossiliferous, silty, light-gray dolomite that weathers gray-yellow. Based on evidence for desiccation and subaerial exposure, calcium carbonate was probably deposited in sabkha conditions and penecontemporaneously converted to dolomite in this and other shallowing-upward cycles. Evidences for supratidal conditions are listed in **Table 3**.

Some workers favor evaporative processes for diagenetic transformation to dolomite. Friedman and Sanders (1967), Sun (1994), and Friedman (1995) concluded that most dolomite in the rock record formed under hypersaline conditions. Though evidence of hypersalinity is sparse in the Devonian rocks in Nevada, Niebuhr (1979) found evidence of pseudomorphs after salt crystals in the finely-crystalline stratal dolomites of the Guilmette 75 miles north of the study area. However, indirect evidence such as exposure and deflation surfaces, solution-collapse breccias, zebra dolomite, tepee structures, desiccation cracks, and replacement chert nodules suggest that elevated salinity was likely at the time of deposition or shortly afterwards.

Zebra dolomite and tepee structures at TMS look like those illustrated by Beales and Hardy (1980) in the Mississippi Valley-type ore deposits. Zebra dolomite that is parallel to bedding and associated with the upper part of shallowing-upward cycles could be associated with dissolved evaporite deposits as discussed by Beales and Hardy (1980). However, the creation of zebra dolomite by evaporative processes was not proven by Beales and Hardy (E. Mountjoy, 1998, personal communication). Zebra dolomite that is closely associated with non-stratal dolomite near faults is most likely to have formed under hydrothermal burial processes.

Examples of dolomudstone forming the upper parts of shallowing-upward cycles at TMS include MI-329.8, MI-334, MI-342, MI-344, and MI-383.6 in Appendix C. These photomicrographs exhibit common wispy laminations, mud-size grains, 100% dolomite, absence of fossils, and sparse burrows.

Coarsely-Crystalline Stratal Dolostone (Type 2)

The same processes may be responsible for both coarsely-crystalline stratal dolomite (Type 2) and pervasive dolomite (Type 3). They differ in the intensity of dolomitization. No limestone remnants occur in the pervasively dolomitized rocks below the Simonson Dolomite unconformity. Limestone remnants commonly occur in coarsely-crystalline stratal dolomites in the Guilmette above the unconformity. Several intervals at TMS are composed of stratally confined coarsely-crystalline dolomite. They include: from oldest to youngest 1) Guilmette Sequence Dgd cycles 3, 7, 9, 10, 14, 17, 22, and 23; 2) Guilmette Sequence Dge cycles 3, 12, and 13; 3) Guilmette Sequence Dgf cycle 7; and 4) Guilmette Sequence Dgg cycles 9, 20, and 23. Zebra dolomite is common in these intervals of coarsely-crystalline stratal dolomite and is probably genetically related to it. Zebra dolomite consists of bands of white sparry dolomite separated by bands of dark-gray finely-crystalline dolomite. Cavities lined with drusy dolomite in the white sparry dolomite are common (see Beales and Hardy, 1980, Figures 2E and 3A-E, for examples of zebra dolomite). These intervals typically occur just below dissolution surfaces in the upper parts of sequences and cycles that contain karst breccia.

Typically, coarsely-crystalline drusy dolomite crystals line karst cavities, many of which are partly open. Terra rosa and hematite staining at cycle boundaries provide additional evidence of exposure and indirectly suggest periods of erosion. These periods of erosion could result in elevated salinity of ephemeral pools trapped on a low-relief exposure surface. If evaporite minerals formed in these pools, then the residual fluids could contribute to the dolomitization of the underlying karst zone.

Dunham and Olson (1980) provided evidence that dolomitization of the Ordovician Hansen Creek Formation carbonate platform was an early diagenetic process related to the Ordovician-Silurian paleogeography of the region. As with the Hansen Creek Formation, the shallowing-upward cycles in the Guilmette represent transgressions and regressions of the shoreline that controlled the western limit and seaward extent of the freshwater phreatic aquifer system. Similar to the Hansen Creek example, dissolution surfaces or karst zones developed at some Devonian sequence boundaries. Therefore, based solely on field evidence, I propose a similar model for the coarsely-crystalline, strata-bound dolomite at TMS. Dolomitization by brines resulted in intervals of coarsely-crystalline, strata-bound dolomite.

Coarsely-crystalline stratal dolomite intervals in the Guilmette commonly are associated with several feet of breccia and zebra dolomite. Breccias associated with cycle and sequence boundaries are likely karst breccias. They are regionally correlative. Other strata-bound breccia bodies may be a result of solution collapse. The solution collapse breccia occurs locally, is not associated with unconformities, and is not regionally correlative. Coarsely crystalline stratal dolomite intervals associated with cycle and sequence unconformities contain white, sparry dolomite that fills most of the fractures and voids in the karst zone. Open voids are lined with drusy dolomite. Subvertical fractures in the karst zone widen upward and are truncated by the unconformity. They do not continue into the base of the overlying cycle. The coarseness of the dolomite crystallinity increases upward to the unconformity. Primary structures become more obliterated upward to the unconformity. Without fluid inclusion work, the origin of the coarsely-crystalline stratal dolomite is unknown.

Pervasive Dolostone below the Simonson Dolomite Unconformity (Type 3)

Carbonate rocks between the top of the Ordovician Pogonip Group and the regional unconformity at the top of the Simonson Dolomite were pervasively dolomitized in the Fossil Peak and Tempiute Mountain thrust sheets (see **Table 1** for Paleozoic nomenclature). In the Silver Canyon thrust sheet, carbonate rocks are pervasively dolomitized from the top of the Ordovician Ely Springs Dolomite to the top of the Simonson Dolomite. The significance of the anomalous occurrence of undolomitized limestone in the Ely Springs Dolomite of the Silver Canyon thrust sheet is discussed under structural interpretations in Chapter 6. The Silver Canyon thrust juxtaposed an Ely Springs limestone facies with a dolomite facies that probably experienced different paleogeographic and diagenetic histories.

The Simonson Dolomite unconformity truncates the Upper Alternating Sequence, which consists of shallowing-upward cycles that resemble those found in the overlying Guilmette. Pervasively dolomitized rocks below the top of the Simonson Dolomite are more coarsely crystalline and occur more regionally than finely-crystalline stratal dolomite cycle caps of the Guilmette Formation. Vuggy, coarsely-crystalline dolomite occurs in the karsted interval below the unconformity at the top of the Simonson Dolomite (Stop 7, Appendix D; Chamberlain and Warme (1996) Figure 4). Dolomites occur in the Guilmette above the unconformity. However, the pervasively dolomitized rocks differ from coarsely-crystalline stratal dolomites of the Guilmette in that no limestone remnants are preserved below the Simonson Dolomite unconformity. This section on pervasive dolomite contains discussions including: 1) pervasive dolomite in Paleozoic rocks at TMS; 2) karsted Simonson Dolomite unconformity; 3) possible sources for dolomitizing fluids; and, 4) timing of dolomitization.

Pervasive Dolomite in Paleozoic Rocks at TMS The Simonson Dolomite unconformity divides the Paleozoic section at TMS and Tempiute Mountain and most sections in the Sunnyside basin from predominantly dolomite below (at least down to the top of the Pogonip) to predominantly limestone above the unconformity.

Ely Springs Dolomite (**Table 1**) is correlative with the Ordovician Hansen Creek and Vinini Formations in the Eureka area. Because of the lack of associated evaporite minerals or their traces, Dunham and Olson (1980) concluded that models involving hypersalinity were inadequate to account for the origin of regionally extensive replacement-dolomite formations. They provided evidence that dolomitization of the carbonate platform was an early diagenetic process related to the Ordovician-Silurian paleogeography of the region. Finney, et al. (1999) noted that the embayed platform margin Hansen Creek Formation in the Monitor Range (35 miles southwest of Eureka) is composed of lime mudstone rich in a diverse open-marine fauna. It lies in a facies between off-platform to basin Vinini Formation shales and limestones at Roberts Mountains (40 miles north-northwest of Eureka) and the shallow-marine pervasively dolomitized Hansen Creek Formation at Lone Mountain (25 miles west-northwest of Eureka). Similarly, dolomitization of the Ordovician-Devonian carbonate platform was also likely an early diagenetic process related to the paleogeography of the Timpahute region.

The Simonson Dolomite unconformity marks the last regionally extensive, pervasive, replacement- coarsely-crystalline Paleozoic dolomite (Type 3) in this part of the Great Basin. Its regional occurrence contrasts with the irregularly distributed late diagenetic products in the Western Canada Sedimentary Basin. These products include coarse-crystalline replacement dolomites, minor occurrences of late-diagenetic saddle dolomite, and thermochemical sulfate reduction products formed during intermediate to deep burial (Mountjoy et al., 1997).

Karsted Simonson Dolomite Unconformity  A regional major zone of karstification occurs immediately below the post-Simonson Dolomite unconformity (Chapter 4). This 20 to 100-foot thick zone is characterized by bleaching, karst breccia, upward thickening fractures filled with a dolomite spar and lined with coarsely-crystalline drusy dolomite crystals, and laminated cave deposits (Stop #7, Appendix D). Typically, the laminated cavity-filling cave deposits are pale-red, silty dolomite with angular carbonate fractures, and contain some small-scale cross bedding. Because the bedding of most of these cavity-filling sediments is parallel to the present-day tectonic dip, they must have been deposited before Mesozoic folding.

Simonson Dolomite unconformity karst differs from the zone of hydrothermal dissolution vugs, caverns, and breccia that host Mississippi Valley-type ore deposits in Devonian rocks at Pine Point, Northwest Territories, Canada. The Simonson Dolomite karst zone does not contain saddle dolomites, sulfide minerals, late-stage calcite, or pyrobitumen that Qing and Mountjoy (1994) attribute to hydrothermal fluids. At Pine Point, the hydrothermal dissolution zone follows a regional conduit and occurs both above and below the Watt Mountain unconformity. In contrast, the regional Simonson Dolomite unconformity karst zone is restricted to the strata immediately below the unconformity. Some karst cavities near the top of the Simonson Dolomite contain unaltered limestone from the overlying Fox Mountain Sequence. Furthermore, the Sulphur Point Formation below the Watt Mountain unconformity comprised of reef and shallow subtidal packstones, grainstones, floatstones and boundstones that could have had 5 to 10% porosity before dolomitization (Qing and Mountjoy, 1994). In contrast, the shallowing-upward cycles of the Upper Alternating Sequence below the Simonson

Dolomite unconformity are composed of wackestones and mudstones. They probably had very little porosity before karsting and dolomitization.

Some karst breccias in this interval extend several hundred feet below the unconformity. The upward thickening fractures filled with a dolomite spar and the coarsely-crystalline dolomite are truncated at the unconformity in most sections in the Sunnyside basin. Laminated cave deposits, described above, occur throughout the karsted zone. Bleached dolomites in the karst zone are distinct on the outcrop and on aerial photographs. The 100-200 foot bleached zone grades downward into the darker, underlying, non-karsted dolomites. Fluids moving through the well-developed pore system created in karsted carbonates is postulated to be related to the pervasive dolomitization below the unconformity. Large-scale and basin-wide process(es) involved in the dolomitization of the pre-Guilmette strata in the Great Basin could be similar to the processes involved in dolomitization of the Leduc in western Canada as discussed by Dix (1993).

<u>Sources of Dolomitizing Fluids</u> Almost no evaporite minerals occur in the Devonian carbonate section of the eastern Great Basin. Only two reports suggest anhydrite in Devonian rocks and both occur as cement in two wells: the Shell Oil Company Sunset Canyon #1 Unit well (Sec 21 T22S R4W, Millard County, Utah) and Tide Petroleum Baseline Canyon Unit #2 well (NE SW SW Sec 21 T1N R59E, Lincoln County, Nevada; Cedar Strat well files).

To the northeast of the Great Basin region, however, thick evaporite accumulations of the Prairie Formation were deposited in the Elk Point basin of western Canada and the Williston basin, Montana and North Dakota (Loucks, 1977). Also, a salt (halite) unit in the upper Duperow (Frasnian), the Flat Lake Evaporite, is locally preserved in northeast Montana and in southern Saskatchewan (Burke and Stefanovsky, 1984; Weinzapfel and Neese, 1986). It may have been deposited over a much wider area and then subsequently removed. Similarly, the cycle cap breccias at the top of Guilmette cycles may be evidence of evaporites removed. No direct evidence of evaporites has been found. However, indirect evidence of removed evaporite minerals includes zebra dolomite at the top of shallowing-upward cycles, desiccation cracks, tepee structures, and salt casts in finely-crystalline dolomite.

The Williston basin Middle Devonian evaporites were deposited about the time of deposition and dolomitization took place in the Simonson Dolomite. The Simonson Dolomite is Emsian to Givetian (Johnson et al., 1989) and the Prairie Evaporite is Eifelian to Givetian according to the northern Rockies/Williston basin Region COSUNA chart by the American Association of Petroleum Geologists. The southwestern depositional edges of the Prairie Evaporite basin are not preserved because of periodic episodes of subsurface salt dissolutions from Late Devonian to the present (Horita et al., 1996). Thus, the Simonson Dolomite could have also contained evaporites that were not preserved.

Timing of Dolomitization There is an abrupt lithologic change across the Simonson Dolomite/Guilmette unconformity regionally. This abrupt change from pervasive dolomite to predominately limestone above the unconformity suggests that pervasive dolomitization in the Simonson Dolomite occurred before deposition of the overlying Guilmette. Unaltered limestone infiltration from the overlying Fox Mountain limestone into the aquifer provides the key to timing of dolomitization. The Fox Mountain lies between the karsted aquifer of the upper Simonson Dolomite and the aquitard of the Guilmette Yellow Slope Sequence. If dolomitization of the Simonson Dolomite occurred after deposition of the Guilmette Fox Mountain Sequence, then dolomitizing fluids should have also altered the overlying Fox Mountain limestones, provided they were porous and permeable. Preferential Cenozoic karsting of the Fox Mountain suggests that the limestone is still porous and permeable. Leviathan Cave in the Worthington Range is a good example of selective Cenozoic karsting of the Fox

Mountain limestone. Simonson Dolomite unconformity dolomitizing fluids should have been confined to carbonates below the Yellow Slope Sequence aquitard. In most stratigraphic sections of the Sunnyside basin, the Fox Mountain is limestone and not dolomite. This suggests that the dolomitizing fluids responsible for pervasive regionally correlatable dolomitization must have been restricted to Simonson Dolomite carbonates and older carbonates. Most dolomites in Devonian rocks above the unconformity occur locally as finely-crystalline stratal dolomite caps on upward shallowing cycles or as non-stratal dolomite associated with faults. Some dolomites, above the unconformity, occur as coarsely-crystalline stratal dolomite associated with minor unconformities.

The extensive, pervasive dolomite below the Simonson Dolomite unconformity occurs regionally throughout the Sunnyside basin. Similarly, extensive replacement dolomitization affected much of the Western Canada Sedimentary Basin during shallow burial and resulted in early-diagenetic porous matrix dolomites (Mountjoy, et al, 1997). In contrast to the regionally distributed pervasive dolomite below the Simonson Dolomite unconformity, the other three types of dolomite are more irregularly distributed.

Non-stratal Dolostone (Type 4)

In the Guilmette Formation, non-stratal dolomite occurs locally in zones from several feet to tens of feet wide. It occurs near major faults and fractures. Typically it cuts across strata. Commonly, this Type 4 dolomite exhibits “zebra” structures or zebra dolomite near faults. Zebra dolomite is an altered rock that exhibits alternating light and dark bands. The light bands are composed of coarsely-crystalline dolomite crystals or dolomite spars and the dark bands are composed of finely-crystalline dolomite crystals. Zebra dolomites in non-stratal dolomites are the most intensely altered carbonates at TMS. Similarly, Fischer (1988) also noted that zebra dolomite is found in his intensely altered fabric D dolomite of the Metaline Formation, northeast Washington. In the

Metaline Formation, Zebra dolomites occur in association with lead-zinc mineralization. Fischer (1988) interpreted it as an advanced diagenetic alteration. Emsbo et al. (1999) also noted that the Roberts Mountains Formation is pervasively dolomitized adjacent to vertical faults and that the resulting dolomite exhibits zebra texture. They suggested that basinal brines moved upward along synsedimentary faults where they dolomitized the Silurian-Devonian Roberts Mountains Formation and deposited barite and base-metal sulfides in fractures and cavities. Similarly, the non-stratal dolomite at TMS is probably attributable to a late stage hydrothermal alteration event. Some early-formed, east-west faults in the Silver Canyon footwall sheet are mineralized with jasperoids and are associated non-stratal dolomite containing zebra dolomite. The intensity of alteration along these faults decreases to no observable alteration about a mile from the Silver Canyon thrust fault. Intensity of dolomitization and abundance of zebra dolomite decreases away from the faults. Non-stratal dolomites are interpreted to be caused by late dolomitization along Mesozoic and Cenozoic fractures and faults. Dissolution or alteration of calcite and replacement by dolomite was the result of hydrothermal fluids or deep-basin brines moving along the fractures.

A non-stratal style of local dolomitization is evident in the outcrops of the Guilmette at Timber Pass, Seaman Range (Hurtubise, 1989), and in the northern Pahroc Range. Hurtubise (1989) suggested that dolomitization was related to the east-west Tertiary Timber Pass fault. Hurtubise and Dubray (1988) suggested that secondary dolomitization along this fault is evidence for a deep-seated crustal structure they called the Silver King lineament. They showed that the intensity of dolomitization in the Guilmette decreases away from the fault. Similarly, local dolomitization of the Guilmette limestones in the northern Pahroc Range, seven miles east of the study area, is probably related to the Late Mesozoic Pahroc thrust fault (Chapter 5 and Appendix E). Non-stratal dolomite also occurs in the Joana Limestone near a thrust contact at Hancock Summit, two miles south of the study area (Stop 6, Appendix D). This type of dolomite also occurs near Hiko Narrows (**Plate 1a**) where much of the Guilmette Formation is dolomitized near faults. The intensity of dolomitization decreases away from the faults. Dolomitization may extend 100's of feet from larger faults such as at Hiko Narrows and only 5-10 feet from minor faults in the Hiko Range.

Much of the late dolomitization along fractures and faults in the Mail Summit section could be related to mineralization of the Pahranagat (Mount Irish) mining district. Mineralization probably occurred about the time of Late Mesozoic Sevier compression and before Early Tertiary volcanism. Mineralized veins and fractures in dolomitized carbonates along the Silver Canyon thrust do not penetrate the overlying Tertiary volcanic rocks. Devonian carbonates in the fault bounded overturned western limb of the Silver Canyon syncline are pervasively dolomitized but they are not pervasively dolomitized in the upright, eastern limb (Appendix E).

Most of the thin sections in this study were taken from lower Guilmette sequences at TMS (Appendix C). All of them were stained with potassium ferricyanide. None of them developed a bluish hue typical of iron-rich crystals. TMS was selected to avoid faults. Therefore, the section lacks non-stratal dolomite except the dolomitized matrix of the lower part of Sequence Dgb2 breccia that may have been fed from nearby faults. Furthermore, none of the thin sections exhibit saddle dolomite that might be found in dolomite-filled fractures associated with non-stratal coarsely-crystalline dolomite. Also, the lack of pyrite in the thin sections suggests that bacterial sulfate reduction did not play a major role in the origin of dolomites in the section, a criterion used by Holail et al. (1988) for dolomite in the Upper Cretaceous of Egypt.

## Summary

At least four types of dolomite occur in the Devonian section at TMS. Finely crystalline stratal dolomite (Type 1) at the top of shallowing-upward cycles is the most common type of dolomite in the Devonian rocks at TMS. The abundance of finely-crystalline stratal dolomite decreases upward from the Sevy Dolomite to the Guilmette Formation. Finely crystalline stratal dolomite forms most of the Sevy Dolomite, about half the Simonson Dolomite, and is restricted to the upper parts of shallowing-upward cycles in the Guilmette Formation.

Stratal dolomite (Type 2) occurs locally below cycle boundaries that are not regionally correlatable. The upper part of Cycle 3, Guilmette Sequence Dgd at TMS is an example.

Pervasive dolomites below the Simonson Dolomite unconformity (Type 3) are widespread and predictable. The unconformity marks a major sequence boundary and a major lithologic change from pervasive dolomite below to predominately limestone above. Unaltered (undolomitized) limestone infiltrating into aquifer cavities from the overlying Fox Mountain Sequence shows that regionally correlative pervasive dolomitization below the unconformity took place before deposition of the Fox Mountain limestones.

Non-stratal dolomites (Type 4) are associated with faults. Their occurrence is irregular and they are not regionally correlatable. Dolomitized Guilmette in the fault-bounded overturned west limb of the Silver Canyon syncline is an example of this type of dolomite.

These four dolomite types can be roughly separated into penecontemporaneous dolomite and diagenetic dolomite. Penecontemporaneous dolomites are enriched in Sr and are more finely crystalline than diagenetic dolomite (Nichols and Silberling, 1980; Shukla, 1988). Type 1 or finely-crystalline stratal dolomite is penecontemporaneous and is probably more enriched in Sr than the other three types that are diagenetic dolomites. However, Sr analysis is beyond the scope of this study. Of the different processes or models of dolomitization discussed below, penecontemporaneous dolomites were likely formed from either primary precipitation, evaporative processes, marine water pumping, or seepage reflux. Diagenetic dolomites could have resulted from either mixing processes, large-scale basin-wide processes, burial compaction, tectonics and sedimentary loading, or hydrothermal processes.

## Conclusions

Many processes of dolomitization could explain the four dolomite fabric types at TMS. Capillary compaction is most likely the dolomitization process forming the finely-crystalline stratal dolomite upward-shallowing cycle caps at TMS. Hydrothermal processes probably resulted in the non-stratal coarsely-crystalline dolomite associated with faults. However, until they are thoroughly analyzed, the processes, timing, and sequences of dolomitization of TMS carbonates are unknown. Even with the availability of trace element, fluid inclusion, and detailed petrographic analyses, distinguishing conclusively between alternate processes and combinations of processes may be difficult (Zenger and Dunham, 1988). However, the Great Basin with its widely distributed outcrops offers an opportunity to resolve some "dolomite problems."

# CHAPTER 5

## TIMPAHUTE RANGE STRUCTURAL ELEMENTS

Structural elements including thrust faults, folds, strike-slip faults, and normal faults of the greater Timpahute Range are summarized in this chapter and described in Appendix E. They set the stage for restoring thrust sheets containing measured sections (Chapter 6) and reconstructing the Devonian paleogeography (Chapter 7). The second goal of this study is to provide a new geologic map of the greater Timpahute Range. Upon completion, the new map illustrated the structural elements separating the sharply contrasting Upper Devonian facies of the study area. It is beyond the scope of this study to provide a detailed analysis of the structural elements, but this study provides constraints for a future comprehensive structural analysis recommended in Chapter 9.

As a step toward the new analysis I have generated a geometrically balanced structural cross section (**Plates 4a and 4b**). It shows that the greater Timpahute Range is composed of a stack of at least three main thrust sheets--Meadow Valley Mountain, Pahroc, and Silver Canyon--separated by two main thrust faults--Pahroc-Delamar and Silver Canyon-Chocolate Drop. The Penoyer Springs and Monte Mountain thrust faults are splay thrusts riding on the Silver Canyon thrust fault. The Fossil Peak, Tempiute Mountain, and an unnamed (5 on **Plate 4a**) thrust faults are splays on the Pahroc thrust fault. The Pahroc thrust fault may be a splay off another unnamed thrust fault (8 on **Plate 4a**). See thrust faults in Appendix E for detailed descriptions of these features.

Structural elements on the new Timpahute Range 30' X 60' geologic map include twelve thrust faults, 21 folds, thirteen strike-slip faults, but only five significant north-south striking normal faults in the Paleozoic rocks. These structural elements are named, classified, and described in Appendix E. They are indexed in a table of contents for Appendix E (page 345). In this chapter, the structural elements are grouped and discussed in four categories: 1) thrust faults, 2) folds, 3) strike-slip faults, and 4) normal faults. Names for all the structural elements on **Plate 1a** are new except the Freiberg thrust fault and the Seaman Wash fault both named by Tschanz and Pampeyan (1970) and the Golden Gate thrust fault and Garden Valley anticline named by Armstrong (1991). These names are used herein but names of other structures used by Tschanz and Pampeyan (1970) were discarded to avoid confusion with structural elements that were incorrectly mapped or which I interpreted differently. Two unnamed thrust faults shown on **Plate 4a**, but not exposed or mapped in the study area, were inferred on the cross section to explain the attitude of the overlying beds. Because of discontinuous outcrops, some of the twelve separately mapped thrust faults may represent structures that connect or that were connected before being offset by other faults.

Mappable stratigraphic sequences introduced in Chapter 4 were used to map the study area and helped refine structural elements presented in this chapter. As mentioned in Chapter 3, stratigraphic sequences along with other field attributes were recorded at each station. Stations are precise locations in the field where geologic attributes are measured and described. They are shown on my geologic maps as dip and strike symbols. Methods of plotting stations, tracing faults and formation contacts, and constructing map compilations are described in Chapter 3. Some stations are not shown on the maps because the symbols overlap. A table of approximately six thousand stations with all their field attributes would be impractical to include in this study (approximately 300 pages). Stratigraphic sequences mapped on large-scale (1:12,000 or 1:24:000) work maps described in Chapter 3 were grouped into formations to compile the small-scale map (approximately 1:80,000) **Plate 1a**, a composite of 24 7.5' quadrangles (**Figure 3**). **Plate 6** is an example of a map compilation from large-scale work maps (approx. 1:1,000) which also shows mapped sequences and section segments at TMS. Therefore, **Plate 1a**, a revised geologic map of the Timpahute Range 30' X 60' quadrangle, is a generalized geologic map illustrating the main structural elements that separate measured sections of contrasting Upper Devonian facies.

## Thrust Faults

Thrust faults provide the greatest evidence for crustal shortening of the greater Timpahute Range. Chapter 1 shows how the thrust faults in the study area fit into the Sevier fold-and-thrust belt. Three main imbricated thrust sheets containing contrasting Upper Devonian stratigraphy make up the Paleozoic rocks of the greater Timpahute Range (**Figure 32**). They are from lower to upper: 1) Meadow Valley Mountain, 2) Pahroc, and 3) Silver Canyon. A thrust sheet is the package of rock above a thrust fault (Marshak and Mitra, 1988). Three contrasting Upper Devonian facies help distinguish the thrust sheets. Upper Devonian rocks of the Meadow Valley thrust sheet are not exposed in the map area. However, where they are exposed in the Meadow Valley Mountains and Pahroc Range, to the southeast and east of the study area, respectively, they are mostly dolomitized. The exposed part of the Pahroc sheet at Tempiute Mountain is composed of thin-bedded limestone (facies 1), and the exposed part east of the Silver Canyon thrust fault is composed of cyclic carbonates and reefs (facies 3). Separating the two Pahroc sheet facies is the Silver Canyon thrust sheet composed of thick quartz sandstones (facies 2). These facies and the significance of their structural position are discussed more fully in Chapter 7. Bounding the Silver Canyon thrust sheet are two east-west striking faults, the North Penoyer Springs and Reed Spring faults (Strike-Slip Faults, Appendix E). They are likely thrust tear faults.

Fortunately, erosion has cut through the Silver Canyon and Pahroc sheets at Tempiute Mountain, thus revealing a small sliver of the unnamed thrust sheet below the Tempiute Mountain thrust sheet (**Figure 32**). Only Mississippian shales and fusulinid-bearing Pennsylvanian-Permian rocks are exposed in the fenster. This fenster revealing the thrust sheet below the Pahroc and Silver Canyon thrust sheets is illustrated on the geologic profile on **Plate 1a** and on the structural cross section **Plate 4a**. The Tempiute Mountain thrust fault, a splay off the Pahroc thrust fault, separates the Pahroc and the unnamed thrust sheet (thrust faults, Appendix E). On the west end of the Timpahute

Range, the Chocolate Drop thrust fault separates the Pahroc and Silver Canyon thrust sheets. The Chocolate Drop and Silver Canyon thrust faults are probably the same thrust fault (geologic profile, **Plate 1a** and 3, 3a, and 3b on **Plate 4a**).

Lying on the Meadow Valley thrust sheet on the eastern greater Timpahute Range and below the Silver Canyon thrust sheet in the middle and western greater Timpahute Range is the Pahroc thrust sheet. In the greater Timpahute Range, it is divided into west and east segments by the overlying Silver Canyon thrust sheet (**Figure 32**). Upper Devonian strata in the Silver Canyon thrust sheet are composed of more than 1000 feet of quartz sandstones (facies 2). Exposed in a fenster of the Silver Canyon thrust sheet at Tempiute Mountain is a western segment of the Pahroc thrust sheet (**Plate 1a**). It contains a unique Upper Devonian thin-bedded limestone facies (facies 1) that is correlative with the thick sandstone facies in the Silver Canyon thrust sheet. In contrast, correlative strata in the eastern exposures of the Pahroc thrust sheet contain stromatoporoid reefs and lack thick sandstones (facies 3). Unconformities cut out many Devonian sequences in the Meadow Valley thrust sheet below the Pahroc thrust sheet (**Figure 17**). The three contrasting facies from different greater Timpahute Range thrust sheets were introduced in Chapter 1 and are discussed in Chapters 4 and 7. **Plate 4b** illustrates the location of the three facies after thrust restoration.

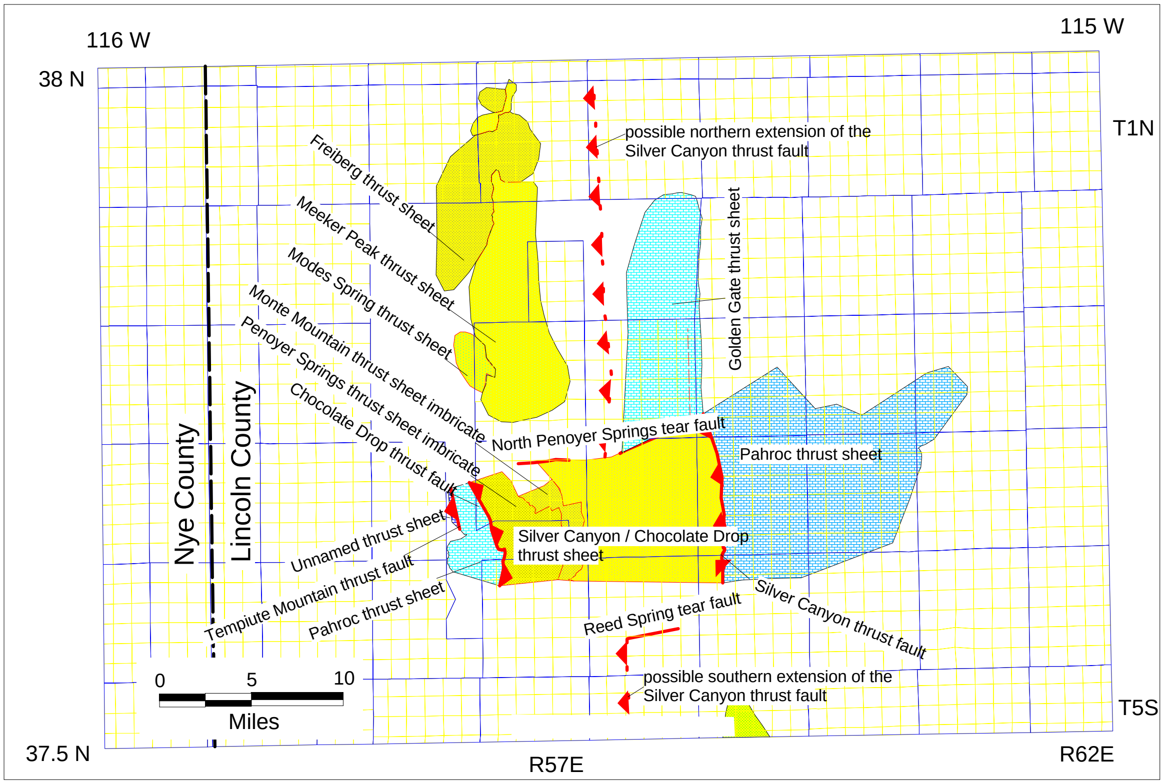


**Figure 32** Generalized tectonic map of the Timpahute Range quadrangle showing the major thrust sheets and some of their imbricate sheets that make up the greater Timpahute Range. The sandy (facies 2) Silver Canyon thrust sheet (yellow) and its imbricates (darker yellow) contrast sharply with the reefy (facies 3, east) Pahroc and thin-bedded limestone (facies 1, west) Pahroc thrust sheet (light blue bricks). Thin red lines separate imbricate thrust sheets within the Silver Canyon thrust sheet. Only a small sliver of an unnamed thrust sheet (dark blue bricks--see label) is exposed in a fenster of the Silver Canyon and Pahroc thrust sheets on the west end of the greater Timpahute Range.

The uppermost thrust sheet, the Silver Canyon thrust sheet, is well-exposed in the middle of the greater Timpahute Range and in the Worthington Range to the north. A deep (>30,000 feet) test on Mount Irish should cut two and perhaps three thrust sheets (**Plate 1a**).

Meadow Valley Mountain Thrust Sheet

The Meadow Valley Mountain thrust sheet is exposed in the North Pahroc Range, five miles northeast of the study area, and in the Meadow Valley Mountains, 25 miles southeast of the study area (**Figure 2**, Pahroc thrust fault, Appendix E, and **Plate 4**). Western dipping Paleozoic rocks of the Meadow Valley Mountain thrust sheet steepen westward in the North Pahroc Range (Cedar Strat proprietary geologic map, 1996). Unfortunately the trace of the thrust fault, or the normal fault of Taylor (1989), between the Seaman and North Pahroc ranges is buried by Tertiary volcanic rocks.

At Pahroc Summit, 14 miles east-northeast of Hiko, folded Paleozoic rocks in the Pahroc thrust sheet attest to an underlying thrust detachment (see Pahroc Spring anticline, Appendix E). However, the Pahroc thrust fault is concealed by Tertiary volcanic rocks in and next to the study area. The Pahroc thrust fault is the inferred northern extension of the Delamar thrust fault. Only in the southern Delamar Mountains, 35 miles south-southeast of the study area, has headward erosion by Colorado River tributaries exhumed the Delamar/Pahroc thrust fault.

A footwall syncline in the Meadow Valley Mountain thrust sheet in the southern Delamar Mountains suggests yet another thrust detachment below the Pahroc thrust fault. Therefore, the Pahroc thrust sheet is another imbricate in a stack of thrust sheets. Additional regional mapping, deep well bores, and seismic data will likely reveal deeper thrust detachments. However, the upper three thrust sheets are the main focus of this study.

Pahroc Thrust Sheet

Lying on the Meadow Valley thrust sheet and partly concealed by the overlying Silver Canyon thrust sheet, the Pahroc thrust sheet contains the TMS (facies 3) and the

Tempiute Mountain (facies 1) measured sections (**Plate 1a**). Exposures of the Pahroc thrust sheet are found east of the Silver Canyon thrust fault and west of the Chocolate Drop thrust fault (**Figure 32**). TMS, with its Upper Devonian stromatoporoid reef, lies about 1.5 miles east of the Silver Canyon thrust fault. The Tempiute Mountain measured section containing thin-bedded limestones lies 1.9 miles west of the Chocolate Drop thrust.

Folded Paleozoic rocks in the Pahroc thrust sheet suggest an underlying detachment. Its western exposure contains the Tempiute Mountain anticline. Folds of the eastern exposure include Silver Canyon syncline, Mail Summit anticline, Fossil Peak anticline, folds in the Hiko Range, and Pahroc Spring anticline (Appendix E). Fusulinid-bearing Permian-Pennsylvanian limestones on the eastern edge of the western exposure of the Pahroc thrust sheet near the Chocolate Drop thrust fault are vertical to overturned. These folded rocks provide evidence of an underlying detachment below the greater Timpahute Range. Folds in the Golden Gate and Seaman ranges north of the greater Timpahute Range also suggest a thrust fault detachment beneath the Pahroc thrust sheet.

The main stratigraphic differences between rocks of the Meadow Valley Mountain thrust sheet and the Pahroc thrust sheet include abrupt changes in the thickness of the Sequence Dgb2 breccia and the content of quartz sandstone in the Upper Devonian Guilmette Formation. The breccia is more than 100 feet thick in the hanging wall Pahroc thrust sheet (Hiko and Delamar ranges) and is less than 10 feet thick in the Meadow Valley Mountain thrust sheet (Meadow Valley Mountain (**Figure 17**) and North Pahroc Range). Quartz sandstone thickens from zero sandstone in the Meadow Valley Mountain thrust sheet to 10's of feet in the Pahroc (Delamar-Arrow Canyon) thrust sheet, to 100's of feet in the Pahranagat thrust sheet. The Pahranagat thrust sheet possibly correlates to the Silver Canyon thrust sheet (**Figure 32**).

In the northern Arrow Canyon Range (114.88 W Longitude; 36.76 N Latitude, 62 miles south-southeast of Hiko), the Dgb2 breccia is 3 feet thick. In the Delamar Range (114.98 W Longitude, 37.05 N Latitude, 40 miles south, southeast of Hiko) it is 260 feet thick. Thicknesses of the Ordovician Eureka Quartzite in both ranges are similar (164 feet in the north Arrow Canyon Range and 142 feet in the southern Delamar Range, Shell Oil Company proprietary measured sections). Webb (1958) reported 132 feet of Eureka Quartzite in the northern Arrow Canyon Range. If the two sections correlate and belong to the same thrust sheet, then the thickness of breccia decreases from 260 to 3 feet in approximately 22 miles. However the thickness of the Eureka Quartzite in the Meadow Valley Mountains, ten miles east of the Delamar Range, is approximately 20 feet (A Cedar Strat proprietary map). Therefore, the Meadow Valley Mountains lie in another thrust sheet, footwall to the Delamar-Arrow Canyon thrust sheet. If the breccia decreases in thickness linearly between the Delamar and Arrow Canyon ranges, then the same rate of decrease could be applied between the Delamar and Meadow Valley Mountain sections. Applying that rate of decrease (5.8 feet per mile), depositional or restored distance between the Delamar Range and the Meadow Valley Mountains should be approximately 44 miles. If the above assumptions in correlations and rate of change of thicknesses hold, the amount of crustal shortening on the Pahroc thrust fault is approximately 44 miles, based on Dgb2 stratigraphic considerations. Cumulative thrust slip on the Pahroc and underlying unnamed (8 on **Plate 4a**) thrust faults on **Plate 4a** is 20 miles. Other concealed thrust faults taking up addition displacement could lie between the Pahroc and Meadow Valley ranges. Therefore, crustal shortening between the ranges is at least 20 miles and could possibly be more.

The Ordovician Eureka Quartzite can also be used to estimate shortening on the Pahroc thrust fault (**Plate 1a** and Appendix E). It is approximately 120 feet thick in the east Arrow Canyon Range (Longwell et al., 1965) and 150 feet thick in the Delamar Range (Tschanz and Pampeyan, 1970), 22 miles away. Therefore, it thins an average of 1.36 feet per mile. The Eureka Quartzite is approximately 20 feet thick in the Meadow Valley Range sheet. If the thickness decreases linearly, then the Eureka Quartzite in the Delamar Range was deposited 96 miles from the Meadow Valley sheet, based on Eureka Quartzite stratigraphic considerations. However, crustal shortening was probably less than 96 miles on the Pahroc thrust fault. More accurate stratigraphic sections with gamma-ray logs and correlations based on sequences as presented herein should improve the estimates of crustal shortening.

Splay thrust faults in the Pahroc thrust sheet include the Fossil Peak thrust fault, Hiko Spring klippe, and the Golden Gate thrust fault. The Fossil Peak thrust sheet and the Hiko Spring klippe may both belong to the Fossil Peak thrust fault (Thrust Faults, Appendix E). The Golden Gate thrust fault superficially appears to terminate south of the Baseline Canyon fault in the Golden Gate Range (**Plate 1a** and Thrust Faults, Appendix E). However, folds north of the east-west trending Baseline Canyon fault and footwall splay thrust faults east of the Golden Gate thrust fault suggest that shortening on the Golden Gate thrust fault was taken up by other structures (see Golden Gate thrust fault, Golden Gate anticline, Golden Gate syncline, Garden Valley anticline and Baseline Canyon fault in Appendix E).

A group of east-west normal faults is restricted to the Pahroc thrust sheet east of the Silver Canyon thrust fault in the greater Timpahute Range (see Mail Summit faults, Appendix E). They are lacking in the overlying Silver Canyon thrust sheet. Another east-west striking fault cutting the Pahroc thrust sheet is the Wildcat Wash fault. It occurs 1.4 miles west of the Chocolate Drop thrust fault. South (1.3 miles) of Wildcat Wash fault, the Tempiute Mountain fault could have strike-slip displacement (Appendix E).

North of the greater Timpahute Range, the Pahroc thrust sheet, exposed in the Golden Gate Range, is also cut by east-west normal faults. However, similar faults are lacking in the Worthington Range interpreted to be part of the Silver Canyon thrust sheet. Another east-west trending fault in the Pahroc thrust sheet, the Crystal Springs Canyon fault, could have strike-slip displacement plus dip slip displacement (see Crystal Springs Canyon fault in Appendix E). Two east-west striking faults, the North Penoyer Springs and Reed Spring faults, are likely thrust tear faults. Other east-west striking faults in the Pahroc thrust sheet include: northeast Tikaboo Valley faults, faults north of Bactrian Mountain, and Logan Canyon fault.

Three significant north-south trending normal faults in the study area cut rocks of the Pahroc thrust sheet: Hiko Narrows, Coal Valley Reservoir, and Mail Summit faults. However, the Hiko Narrows fault could be a thrust fault revealing rocks in a fenster of a lower thrust sheet (see Hiko Narrows fault in Appendix E). The Coal Valley Reservoir fault, is likely a listric normal fault on the west side of Coal Valley with several hundred feet of displacement (see Coal Valley Reservoir fault in Appendix E). The west Mail Summit fault is exposed 2.9 miles east of the Silver Canyon thrust fault (**Plate 1a**). It also has several hundred feet of displacement. North-south trending normal faults with thousands of feet of displacement were not detected in the study area (see discussion of normal faults below and description of normal faults in the Timpahute Range 30' X 60' quadrangle in Appendix E).

## Silver Canyon Thrust Sheet

Exposures of the Silver Canyon thrust sheet in the middle of the greater Timpahute Range lie between the Chocolate Drop thrust fault on the west and the Silver Canyon thrust fault on the east (**Plate 1a**; **Figure 32**). North of the greater Timpahute Range, the Silver Canyon thrust sheet is exposed in the Worthington Range (**Figure 32**).

Folds within the Silver Canyon thrust sheet attest to underlying thrust detachments. Folds include Mount Irish anticline, Monte Mountain syncline, Penoyer Springs syncline, north Timpahute anticline, and the Worthington Mountain doubly plunging anticline (Appendix E).

Splay thrust faults within the Silver Canyon thrust sheet include Penoyer Springs and Monte Mountain thrust faults in the greater Timpahute Range and the Freiberg and Modes Spring thrust faults in the Worthington Range (Appendix E). The north Worthington fault may be a fenster into a deeper thrust sheet or it could be a normal fault (see Appendix E). Penoyer Springs and Monte Mountain thrust faults have footwall synclines. Footwall synclines are absent, however, in the Worthington Mountains. East-west striking strike-slip faults are generally restricted to the Silver Canyon thrust sheet. They include six faults: south Penoyer Springs, Tunnel Spring, Monte Spring, Chocolate Drop, south Timpahute Range and Logan Canyon faults (Strike-Slip Faults, Appendix E).

In the greater Timpahute Range, the Silver Canyon thrust sheet is bounded on the north and south by faults interpreted as thrust tear faults. Therefore, the greater Timpahute Range portion of the Silver Canyon thrust sheet moved eastward approximately two miles with respect to the northern or southern portions of the thrust sheet. Two miles is the measured distance between the north and south sides of the Logan Canyon fault (**Plate 1a**).

Thick (1000+ feet) Upper Devonian quartz sandstone (facies 2), abnormally thin (≈200- feet) Sequence Dgb2 breccia, and limey Ordovician Ely Springs Dolomite distinguish the strata of the Silver Canyon thrust sheet from the underlying Pahroc thrust sheet. An isolith map of the Devonian quartz sandstones was used to estimate the 30 miles of crustal shortening on the Silver Canyon thrust fault (Chapter 7). Also, in Chapter 7, isolith maps of the Dgb2 breccia were used to estimate about 100 miles of relative cumulative crustal shortening of the three thrust sheets of the greater Timpahute Range.

## Conclusions

Newly mapped thrust sheets in the Timpahute 30' X 60' quadrangle geologic map explain the abrupt change in Upper Devonian facies separated by thrust faults. Approximately 62 miles of structural shortening shuffled the thrust sheets and required thrust restoration to accurately interpret the Devonian paleogeography. Unique stratigraphic components such as the distribution of the Dgb2 breccia and Upper Devonian quartz sandstone provide tools to aid in thrust reconstruction.

**Figure 32** is a conceptual tectonic map of the study area summarizing the major thrust sheets of the greater Timpahute Range. Cenozoic cover conceals most of the thrust sheets and thrust fault traces in the Paleozoic rocks. Strike-slip faults on the north and south sides of the greater Timpahute Range are probably thrust tear faults that separate contrasting stratigraphic facies of the different thrust sheets. The Silver Canyon thrust sheet in the greater Timpahute Range moved eastward approximately two miles with respect to portions of the sheet north and south of the greater Timpahute Range. Tempiute Mountain is a fenster in the Silver Canyon thrust sheet revealing a western segment of the Pahroc thrust sheet. A second fenster on the west side of Tempiute Mountain in the Pahroc thrust sheet reveals a sliver of an unnamed thrust sheet. Folding in exposures of the Meadow Valley thrust sheet east of the Pahroc thrust fault suggest another, deeper detachment. Therefore, the greater Timpahute Range is interpreted to be composed of a stack of at least three thrust sheets: Meadow Valley Mountain, Pahroc, and Silver Canyon.

This stack of thrust sheets probably has ridden eastward on yet deeper detachments. Other than minor splay thrust faults, all the thrust faults in the study area glide on Carboniferous strata and especially on Mississippian shale (**Plate 4a**). The master detachment probably involves Lower Cambrian or older rocks on Carboniferous or younger rocks. Probably all of the exposed thrust faults in the study area are merely thrust fault splays of a large system (Sevier orogenic belt?).

## Folds

Twenty-one folds in the study area testify of the intensity of crustal shortening of this part of the Sevier fold-and-thrust belt. See Folds, Appendix E for a detailed description of each fold. The new map showing these folds contrasts sharply with previous mapping that shows only four folds in the study area (**Plate 1a** and **Plate 1b**).

Broken recumbent footwall synclines, an important signature of the region's structure style, provide strong evidence of deeper thrust faults. The study area represents only a small sample of the Sevier fold-and-thrust belt in Nevada. Many uncharted folds occur beyond the study area. All these folds attest to the amount of crustal shortening. However, newly mapped thrust faults discussed above provide a stronger witness to the amount of crustal shortening that occurred in this part of the Sevier fold-and-thrust belt. Without an understanding of the amount of crustal shortening accurate reconstruction of Devonian paleogeography is not possible.

## Strike-Slip Faults

Little work has been done to date on strike-slip faults within the Timpahute Range quadrangle. More than thirteen strike-slip faults are documented on the Timpahute Range quadrangle geologic map (Appendix E, **Plate 1a**). Most of them are newly mapped and all of them are newly named. All the strike-slip faults, except the Tempiute Mountain and Reed Spring faults, have sinistral strike-slip displacement. The most obvious ones with the most strike-slip displacement include Logan Canyon, Tunnel Springs and South Penoyer Springs faults. Dip-slip normal displacement on these faults is measured in hundreds of feet and strike-slip displacement is measured in thousands of feet or miles. Dip-slip normal displacement probably took place along pre-existing zones of weakness caused by the strike-slip displacement. As Tschanz and Pampeyan (1970) point out, strike-slip displacement may be related to tear faults.

An important diagnostic feature of these strike-slip faults is that, despite highly divergent domains of structural dip, the sense of displacement remains the same along their trace. The diagnostic features that are sporadically observed include slickensides, dikes, hydrothermal alteration zones, discontinuities in structural grain, and outcrop patterns. Descriptions of the newly named faults appear in Strike-Slip Faults, Appendix

E.

This study documents several strike-slip faults. Most of them are east-west trending or parallel with thrust fault movement. Strike-slip faults, confined to a single thrust sheet, could be tear faults created synchronously with thrust fault emplacement. Some exhibit dip-slip movement and could have been reactivated during Cenozoic extension. Faults most likely having dip-slip displacement are described in normal faults of Appendix E.

Strike-slip Faults as Thrust Tear Faults In 1964, Gwinn stated that abrupt changes in structure and stratigraphy or outcrop patterns along strike-slip faults in the Appalachians are probably caused by tear-faults. Strike-slip faults in the Timpahute Range quadrangle may be tear faults. As mentioned above Tschanz and Pampeyan (1970) suggested that the Arrowhead Mine fault, twenty miles south of the study area, could be a tear fault. Some sets of faults in the study area are confined to certain thrust sheets. This implies they formed synchronously with formation of the thrust sheet in the Late Mesozoic. Four strike-slip faults described in this section are restricted to the Silver Canyon thrust sheet. The Mail Summit faults presented in the section on normal faults are restricted to the Fossil Peak thrust sheet. The Reed Spring fault may be a right-lateral tear fault on the south edge of the Silver Canyon thrust sheet. The Penoyer Springs fault may be a left-lateral tear fault on the north side of the Silver Canyon thrust sheet.

## Normal Faults

Continuous outcrops in the greater Timpahute Range provide an opportunity to study the results of Cenozoic extension in this region of the Great Basin. These faults and fractures greatly enhance the reservoir qualities of the rocks of the region. However, only eight faults with significant displacement or features were documented, as described in detail in Appendix E.

Five of the eight significant normal faults in the study area strike north-south, parallel with the structural grain of the region. Two of the five have 10,000 feet or more stratigraphic displacement and may be thrust faults. Stratigraphic displacement on the other three is 2000 feet or less. No classical Basin and Range normal faults with tens of thousands of feet of displacement are found in the study area. Either the study area is a unique area that has escaped regional Cenozoic extension or the region has been misinterpreted to have been severely affected by Cenozoic extension.

Geologic mapping beyond the study area revealed few possible Basin and Range normal faults constrained by outcrop data. Many published classical Basin and Range normal faults are shown in valleys where they are unconstrained by outcrops. Some have used seismic data to justify their interpretation of a classical Basin and Range faults such as on the east side of Eagle Springs field in Railroad Valley (Effimoff, and Pinezich, 1986; Dolly, 1979; Vreeland and Berrong, 1979). No mention is made of the westward steeply dipping Paleozoic rocks in the pediment and at the foot of Grant Range on the east end of the seismic lines. If a normal valley-bounding fault occurs as suggested by Bortz and Murray (1979), then it is subparallel to bedding in Paleozoic rocks. Clearly, all Great Basin inselbergs containing Paleozoic rocks need to be mapped more carefully before sweeping interpretations of this complex region are made.

## Extensional vs. Compressional Models

Mayer (1986), using topographic constraints to model lithospheric stretching or crustal thinning of the Basin and Range province, concluded that the thinning resulted in “a topographic pattern characterized by normal-fault-bounded mountain blocks separated by alluvial valleys superimposed on a broad regional uplift." The most widely accepted model of Tertiary Basin and Range extension in the region of the study area emphasizes north-south trending faults of major displacement (thousands of feet) bounding the ranges (horsts) and valleys (grabens). Effimoff and Pinezich (1986) concluded, from their study of selected basins in the region, that the basins are bounded by listric normal faults with displacements of 10,000 to 15,000 feet.

Taylor (1989) attributed the tilted Paleozoic rocks in the North Pahroc Range, 10 miles northeast of the study area, to normal faults. Though he misidentified several key outcrops, Hurtubise (1989) found no evidence for thrust faults in the Seaman Range, from Fossil Peak to Black Cliff, 25 miles north. He also attributed tilting in Paleozoic rocks to normal faults caused by Cenozoic extension. However, Bartley et al. (1988) described the area from the Seaman Range to the Golden Gate Range, five miles north of the study area, as an area of minor normal faults caused by Cenozoic extension. North-south normal faults related to Cenozoic extension are rare in the study area. Most of the exposed normal faults cut across the north-south structural grain in the study area. The few normal faults that are subparallel with the north-south structural grain have stratigraphic displacement of no more than several hundred feet. An exception is the Hiko Narrows fault exposed in Sec 7 T3N R61E with about 5000 feet of stratigraphic displacement (See Fossil Peak thrust in Appendix E). Normal north-south trending faults with tens of thousands of feet of displacement are not recognized in the study area. In contrast, thrust faults with tens of miles of displacement are documented in the study area. Significant normal faults in the study area with their locations and approximate throws are listed in Appendix E.

Some normal fault models depict 20-40,000 feet of vertical stratigraphic separation and many miles of horizontal extension. Axen et al. (1993), for example, speculated that a major normal fault is situated just east of the study area, between the Seaman and North Pahroc ranges, and is concealed by Tertiary volcanics and sediments. They concluded that the ranges in the region of the Timpahute Range quadrangle were extended during the Tertiary. However, I find no evidence in my mapping that supports their conclusion. Furthermore, it is shown in Appendix E that steep gradients in an isostatic gravity contour map supporting their postulated normal fault are lacking. In contrast to their model, I postulate that a major thrust fault (Pahroc/Delamar thrust fault) is situated just east of the study area. As with the postulated normal fault, it is concealed by Tertiary volcanics. However, the Pahroc Spring anticline, exposed through a window of volcanic rocks and exposures of the Delamar thrust fault to the south, supports the crustal shortening model. The current study provided the opportunity to test, within the Timpahute Range quadrangle, both models and their inherent ramifications.

## Conclusions

New mapping clearly shows more compressional structural elements in the Paleozoic rocks of the Timpahute Range quadrangle than was previously known. The new mapping combined with well and gravity data (Appendix E) dispute the existence of published hidden normal faults believed to have been caused by Cenozoic extension. No classic, north-south trending Basin and Range normal faults were found cutting the greater Timpahute Range. Therefore, the region likely underwent more Late Mesozoic compressional deformation and much less Cenozoic extension than was previously thought. **Plate 4**, a structural cross section, constrained by the new mapping, shows significant displacement between thrust sheets. Therefore, paleogeographic reconstructions based on unrestored locations for measured sections are misleading. The stratigraphic significance of structural interpretations in Chapter 6 sets the stage for paleogeographic reconstructions based on restored sections (Chapter 7).

# CHAPTER 6

# STRATIGRAPHIC SIGNIFICANCE OF STRUCTURAL INTERPRETATIONS

The magnitude of the Sevier-age compressional event on the Paleozoic rocks of the study area estimated in this chapter, shows how the newly mapped folds and faults on **Plate 2a** contribute to a new tectonic model. The new model helps explain contrasting post-Guilmette Formation Sequence Dgb facies in juxtaposed thrust sheets. The new geologic map of the greater Timpahute Range, with its more detailed analysis of Great Basin thrust styles, also provides constraints for a more accurate tectonic model. It will be shown in Chapter 7 that knowledge of the assumed original distribution of Dgb2 breccia provides a unique opportunity to restore thrust sheets with a greater degree of confidence and further constrains the structural model. This new tectonic model is illustrated by a geometrically balanced structural cross section of the greater Timpahute Range (**Plate 4a**) and its restoration (**Plate 4b**). The tectonic model is supported by other data including biostratigraphic dislocation, structural implications of the "Oxyoke Formation," contrasting facies in the Ordovician Ely Springs Dolomite between structural sheets, and the distribution of Tertiary-Cretaceous synorogenic rocks

## Tectonic Model

A tectonic model of the greater Timpahute Range is supported by a balanced cross section (**Plate 4**). Restoration of the cross section shows that cumulative displacement of thrust faults within the greater Timpahute Range is approximately 63 miles. An explanation of the distribution of contrasting facies in different structural sheets is shown by the model.  It also provides new opportunities for oil and gas exploration and helps predict the location of the Dg2 breccia impact site.

Balanced Cross Section

An advantage of a balanced cross section is that it helps isolate possible geometric solutions and eliminate impossible ones.  Normally, balanced cross sections in eastern Nevada are impossible to construct because of the lack of constraint or control that ties the deformed region to an undeformed region (Chapter 3).  However, because of its unique nature, the distribution of the Dgb2 breccia may provide the constraint necessary to construct a balance cross section of the greater Timpahute Range (Chapter 7).  **Plate 4a**, a cross section along A-A’ of the greater Timpahute Range geologic map, was made using *Thrustbelt*, a software program described in Chapter 3.

Fundamental parameters needed to construct a balanced cross section included spacing and scales. Spacing affects the smoothness of the appearance of lines in the cross sections.  Centimeters were used as the unit of measurement to construct **Plate 4a** and **Plate 4b** because they were easier to use than English measurements.  Distances and elevations on the 30' X 60' Timpahute Range topographic quadrangle are in meters.  The metric system simplified relating distances and thicknesses on the cross section.  Horizontal and vertical scale factors were kept constant to avoid vertical exaggeration.

Once the fundamental parameters were established, geologic parameters were added.  First, a stratigraphic section was made by building up layer by layer, starting at the lowest layer of interest, the Upper Cambrian.  Rocks of the Upper Cambrian are the oldest exposed in the greater Timpahute Range (**Plate 1a**).  A topographic profile of the greater Timpahute Range transect A-A’, showing the surface geology and formation thicknesses that constrain the structural cross section, **Plate 4a**, lies below the geologic map on **Plate 1a**.  Formation thicknesses were taken from measured sections and wells (Well Data,

Appendix F) in the region. The base of each formation was entered from oldest to youngest along with its x-coordinate on the stratigraphic cross section.

An angle in degrees, compared with the base of each rock unit at which a hypothetical fault would cut through the unit, was specified. A higher angle ($25^{o}$) was chosen for more massive, resistant units (Laketown, Sevy, Simonson, and Ely formations). A lower angle ($20^{o}$) was assigned to more platy, less resistant units (Pogonip, Guilmette, and Joana formations. Because of its shaley nature, the lowest angle ($15^{o}$) was assigned to the Mississippian Antler clastics. The differences in thrust fault angle can be seen on **Plate 4b**.

Each fault is described as to the unit it is rooted in, its position in the cross section, the layer to which it climbs and the x-coordinate of the ramp of the next sub-fault, and the direction and amounts of movement along the fault plane. These fault parameters were changed and tested until a satisfactory solution was found and thrust fault traces and units matched the topography, geology, and faults on the geologic map (**Plate 1a**). Any of the 50 or so iterations are geometrically possible but the final solution, **Plate 4a**, most closely matches the new geologic map. The model could always be improved with additional mapping and more rigorous structural analysis.

## <u>**Plate 4a** and **Plate 4b**</u>

**Plate 4a** illustrates the deformed Paleozoic rocks along transect A-A’ (**Plate 1a**). Rocks above the erosional profile have been removed by erosion. The erosional profile is shown by the thick, solid line that begins on the left-hand side at 16.5 kilometers above the base of the section. Several topographic features along the erosional profile are labeled for reference. Sea level is the horizontal, straight line below the erosion profile at 15 kilometers above the base of the section. A legend for rock units is on the right-hand end of both **Plate 4a** and **Plate 4b**. The darkest gray unit, Mississippian Antler clastics, is the last prominent shale unit in the Paleozoic rocks and contains the main thrust detachments. It is also the main source rock in Nevada (Poole and Claypool, 1984). How much compression to cause the folds and faults in the greater Timpahute Range can be seen on the left-hand end of **Plate 4a**. The missing rock units above the Upper Cambrian were moved 104 kilometers or about 64 miles to the east.

Thrust faults are labeled consecutively from left to right on **Plate 4b**. The oldest faults are on the left and the youngest are on the right. In the deformed area, they are curved, solid, dark-gray lines that separate wedges of different formations. Left of the deformed area on **Plate 4a**, the faults root in the Upper Cambrian and are parallel to bedding. Right of the deformed area, the faults lie within the upper detachment in the Carboniferous. Undoubtedly, thrust faults east and west of the greater Timpahute Range will further complicate the cross section and will show more compression in this region of the Sevier fold-and-thrust belt.

## Amount of Displacement

The cumulative amount of thrust displacement shown on **Plate 4b** is 105 kilometers or about 64 miles. Thrust faults east and west of the greater Timpahute Range were not taken into account on **Plate 4a**. Another model using “snip reconstruction” and thrust displacement within and beyond the greater Timpahute Range estimated 98 miles (**Table 10**) of cumulative compression (Chamberlain and Chamberlain, 1990). Snip restoration is a technique of thrust fault restorations introduced by D. Roeder to Esso in 1967 (D. Roeder, 1998, personal communication). Each thrust slice is snipped or cut from a cross section and laid out in sequence like a puzzle to preserve area of the beds. Bed-length measurement from **Plate 4a** suggests that the Silver Canyon thrust fault have a displacement of approximately 22 miles. Snip reconstruction of the Chocolate Drop-Silver Canyon thrust fault suggested that the fault have about 28 miles of lateral displacement (Chamberlain and Chamberlain, 1990). **Table 10** lists the approximate displacement of faults estimated from snip reconstruction and from **Plate 4a**.

**Table 10** Bed length displacement scaled from a snip reconstruction model and the amount of slip for each thrust in **Plate 4a**.

| Thrust Fault | Approximate Displacement snip reconstruction | Approximate Displacement **Plate 4a** |
|---|---|---|
| Pahroc | 50 miles | 18 miles |
| Silver Canyon | 28 miles | 22 miles |
| Tempiute Mountain splays | 12 miles | 9 miles |
| Penoyer Springs | 3 miles | 3 miles |
| Fossil Peak | 3 miles | 9 miles |
| Monte Mountain | 2 miles | 2 miles |
| Unnamed thrust fault | | 1 miles |
| Cumulative displacement | 98 miles | 64 miles |

Much of the compressional displacement of the greater Timpahute Range was taken up by folding. Most of the thrust faults in the greater Timpahute Range along transect A-A’ (**Plate 1a**) are characterized by an anticline with a gentle west back limb and a steep east forelimb in the hanging wall sheet. They are also characterized by a broken recumbent syncline in the footwall. Typically, a footwall thrust fault places the recumbent limb on Mississippian Antler shales (Chainman facies, **Table 1**). Unless Pennsylvanian rocks are included, the upper sandy facies (Scotty Wash facies) of the Antler clastics are usually sheared off by thrust faults. The shales extend for an unknown distance under the thrust faults. Examples of this style of thrust faults include the Golden Gate (Stop 10,

Appendix D), Penoyer Springs (geologic profile, **Plate 1a**), Monte Mountain (Stop 14, Appendix D and Appendix E), and Silver Canyon thrust faults (a geologic profile, **Plate 1a**). Examples of older Paleozoic rocks thrust over Pennsylvanian rocks include the Chocolate Drop (geologic profile, **Plate 1a**) and Pahroc thrust faults (Stop 2, Appendix D, and Appendix E). In all these examples, Mississippian organic-rich, oil-prone source rocks are placed advantageously below potential reservoir rocks. The economic significance of this thrust style is discussed in Chapter 8.

Facies Restoration and Devonian Paleogeography

On the cross section, prominent geographic features are labeled along the present-day erosional surface for correlating the cross section with the geologic map (**Plate 1a**). Three of these features associated with measured sections in **Figure 30** include Tempiute Mountain (TMP or 53 on **Figure 9**), Monte Mountain thrust (TMM or 52 on **Figure 9**) and Mail Summit three miles east of Mount Irish (TMS or 51 on **Figure 9**). Without a structural reconstruction, the spacial distribution of facies represented by these sections is puzzling. However, restoration of the thrust model to its prethrust configuration (**Plate 4b)** allows reconstruction of a probable Devonian basin and depositional model (Chapter 7). The thrust restoration places the three stratigraphic sections with contrasting upper Guilmette facies in a spacial relationship that is more reasonable than their present post-thrust positions. It also causes the Tempiute impact basin to become more concentric.

The new tectonic model suggests that the source for the siliciclastics at Monte Mountain was an emergent region to the west. The emergent region is likely the Antler forebulge of Carpenter et al. (1994). Erosion of Ordovician Pogonip limestones from the forebulge is the likely source of the recycled Ordovician conodonts in Sequence Dgb2 impact breccia reported by Warme and Sandberg (1996). It is also the likely source of recycled early Paleozoic microfossils in Devonian rocks throughout the Sunnyside basin (T. Hutter, 1998, personal communication). Conodont paleontologists have yet to take advantage of Devonian sequences defined in this work. A restricted basin of deeper-water mixed siliciclastics and carbonates at Tempiute Mountain lies between the sandy emergent region on the west and the reef-bearing carbonate platform at Mail Summit to the east (**Figure 33**). The paleogeography of the Sunnyside basin was similar to the paleogeography of the Late Pennsylvanian Oquirrh-Wood River basin of southern Idaho where shallow-marine siliciclastics filled the basin from the west and the bioclastic limestone facies filled the basin from the east (Geslin, 1994, 1998).

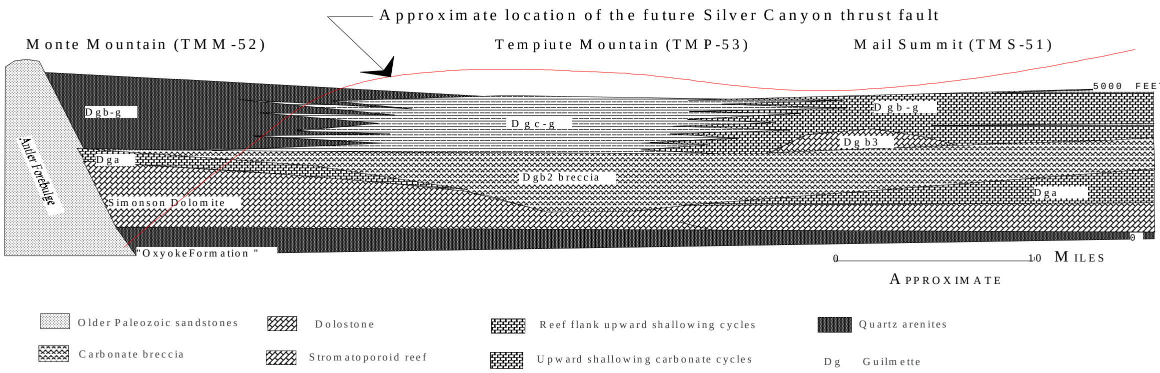


**Figure 33** Diagrammatic stratigraphic cross section showing strata restored about Guilmette Sequence Dgb2 (Alamo Breccia) time. TMM is an abbreviation for Timpahute Range, Monte Mountain measured section. TMP is an abbreviation for Timpahute Range, Tempiute Mountain measured section. TMS is an abbreviation for Timpahute Range, Mail Summit measured section. The number after the section abbreviation is the number of the section on **Figure 9**. The future Silver Canyon thrust fault shown as a red line indicates how western Monte Mountain facies is placed between Tempiute Mountain and Mail Summit facies. Subsequent movement and erosion created the present relationship as seen in the geologic profile (**Plate 1a**) and the balanced cross section (**Plate 4**).

Bed-length restoration of the structural cross section (**Plate 4b)** suggests that the Monte Mountain (TMM) hanging wall lies about two miles west of Monte Mountain footwall (**Figure 33** and **Table 10**). Displacement is the amount the thrust fault had to be shifted to fit the model. It can also be scaled off **Plate 4a**. Evidence that the rocks of the TMM hanging wall were closer to the siliciclastic source area than the rocks of the TMM footwall include thicker and coarser sandstones and lack of *Amphipora*-bearing interbeds in the TMM hanging wall in contrast to thinner and finer grained sandstones and *Amphipora*-bearing interbeds in the footwall. Section restoration shows that both sections at TMM originated not east of TMP, but west (see faults one and two on **Plate 4b** and **Figure 33** for the restored Tempiute basin). Bed-length restoration (**Plate 4b)** suggests that TMM originated at least twenty miles west of TMP. The distance is measured between fault cut offs on **Plate 4a** and is the amount the fault was shifted to fit the model.

TMP is more basinward than TMM or TMS, contains basinal carbonates (facies 1), and lacks abundant well-sorted sandstones (facies 2) or reefs (facies 3). About twenty miles east of TMP, the reef of TMS was constructed in up-dip, shallow basin margin carbonates. The reef was discussed in Chapter 4. A schematic cross section illustrates the principal depositional environments of the Devonian Guilmette and the relative positions of the three measured stratigraphic sections (**Figure 33**). The provenance and distribution of quartz sandstones shed off the Antler forebulge are discussed in Chapter 7.

**Figure 33** shows the Dgb2 impact breccia to be thicker at TMP than at TMM on the west and TMS on the east. Warme and Kuehner (1998) suggested that the thicker breccia at TMP is a crater fill. Thickness of the crater fill thins radially and provides another structural tool in this part of the Sevier thrust belt (Chapter 7).

Biostratigraphic Dislocations

Biostratigraphic dislocations across the Silver Canyon thrust fault support the notion of significant shortening. Fossil occurrences above the Sequence Dgb2 breccia in the greater Timpahute Range are summarized in **Table 11**. Megalodonts are common in Devonian carbonates in the hanging wall of the Silver Canyon thrust plate (TMM) and are rare in the footwall (TMS). They are absent in the Tempiute Mountain thrust sheet (TMP). Stromatoporoid reefs are conspicuous in the Devonian rocks of the footwall (TMS) and are absent in the Silver Canyon hanging wall (TMM) and at Tempiute Mountain (TMP). *Amphipora* is abundant at TMS and is common in the carbonate facies of TMM. They are absent at TMP. Corals are abundant at TMS but are rare at TMM and absent at TMP. Crinoids are rare at TMS and absent at TMM and TMP. Perhaps crinoids are lacking at TMM and TMP because those sections were in restricted marine conditions on the west side of the Sunnyside basin.

**Table 11** Fossil occurrences in Devonian Guilmette rocks above Sequence Dgb2 breccia in three different thrust sheets of the greater Timpahute Range.

| Fossil | TMM | TMP | TMS |
|---|---|---|---|
| Corals | R | N | A |
| Amphipora | C | N | A |
| Stromatoporoids | R | N | A |
| Stromatoporoid Reefs | N | N | C |
| Megalodonts | A | N | R |
| Crinoids | N | N | R |
| N= None or Absent R= Rare C= Common A= Abundant<br>TMM= Timpahute Monte Mountain TMP= Tempiute Mountain<br>TMS= Timpahute Mail Summit | | | |

Structural Implications of the "Oxyoke Formation"

An isopach map of structurally unrestored sections of the "Oxyoke Formation" in Chapter 7 gives an anomalous thickness of 430 feet at Monte Mountain (TMM), in the middle of the greater Timpahute Range. This section is in the hanging wall of the Silver Canyon and Chocolate Drop thrust faults. East of Monte Mountain, in the footwall of the Silver Canyon thrust fault (TMS), the "Oxyoke Formation" is 195 feet thick. West of Monte Mountain, in the footwall of the Chocolate Drop thrust fault (TMP), the "Oxyoke Formation" is 285 feet thick. If the structural reconstruction of the greater Timpahute Range presented in Chapter 5 is correct, and the Monte Mountain section was deposited west of Tempiute Mountain, then the "Oxyoke Formation" thickened progressively to the west (**Plates 1** and **4**). If the Monte Mountain section was deposited between the other two sections, then some sort of depression caused a thicker "Oxyoke Formation" section in the middle of the greater Timpahute Range. All three sections appear to have been deposited in shallow water making it difficult to resolve the depositional position using "Oxyoke Formation" facies distributions alone.

<u>Ely Springs Dolomite</u>

An independent argument that supports this new structural model is found by examining the Ordovician Ely Springs Dolomite in the different structural sheets. See **Figure 8** and **Table 1** to see the position of the Ely Springs Dolomite in the stratigraphic column. In the Silver Canyon sheet (TMM), the formation contains open-marine limestones in contrast to the sections exposed in the Silver Canyon footwall (TMS) and in the Chocolate Drop footwall (TMP) at Tempiute Mountain (**Plates 1** and **4**). In those sections, and in most sections of Ely Springs Dolomite in this part of Nevada, the formation is pervasively dolomitized (Cedar Strat proprietary measured sections, 1984-1989).

However, Reso (1960) noted that the Ely Springs Dolomite contains more limestone in the hanging wall of the Pahranagat thrust fault than in the footwall, 15 miles south-southwest of Mount Irish. I correlated his Pahranagat hanging wall thrust sheet to the Silver Canyon hanging wall thrust sheet. However, my interpretation shows that the Silver Canyon thrust sheet in the Timpahute salient traveled farther east than the Pahranagat thrust sheets. A structural salient is part of a thrust fault, bounded by thrust tears, that moved farther than the rest of the thrust fault. The Pahranagat hanging wall thrust sheet is exposed 18 miles south of Silver Canyon. Pervasive dolomitization of the Ely Springs is related to the

Ordovician-Silurian paleogeography. Ordovician rocks in the Silver Canyon sheet, containing more open-marine fossils including crinoids and corals, were deposited more seaward and, being less emergent, were less affected by dolomitizing processes than equivalent rocks to the east, higher on the shelf and containing fewer abundant open-marine fossils.

An argument that paleogeography controlled dolomitization of equivalent rocks comes from outcrops west of Eureka, Nevada (**Figure 2**). The Ely Springs Dolomite is equivalent to the Hanson Creek Formation in the Eureka area. Duhnam and Olson (1980) argued that dolomitization of the Hansen Creek was related to paleogeography of the region. Similarly, Ely Springs Dolomite in the Silver Canyon thrust sheet is composed of open-marine limestone (abundant open-marine fossils) in contrast to restricted-marine dolomites (less open-marine fossils) in the Pahroc and Meadow Valley Mountain thrust sheets. Therefore, it is likely that Ordovician rocks in the Silver Canyon thrust sheet were deposited seaward or west of Ordovician rocks at Tempiute Mountain.

### Tertiary/Cretaceous Synorogenic Rocks

The newly discovered Late Cretaceous or Early Tertiary rock unit (TKs) southwest of Monte Mountain that lies between Paleozoic rocks and Tertiary volcanic rocks (Chamberlain, et al., 1992b) was introduced in Chapter 2. It may provide insight into the age of formation of Late Mesozoic to Early Tertiary structures in the region. As presented in Chapter 2, the upper lacustrine limestone beds of the unit probably correlate to the Lower Eocene lacustrine Sheep Pass Formation in Nevada and the Flagstaff Limestone and Claron Formation in Utah. The underlying conglomerate beds may correlate to Late Cretaceous conglomerates of the Newark Canyon Formation in central Nevada or the North Horn Formation in central Utah.

The Sevier fold-and-thrust belt produced folds in Paleozoic rocks. Erosion cut down and exposed the folded Paleozoic rocks before deposition of the Monte Mountain

Tertiary/Cretaceous strata. Because of folding in the Monte Mountain footwall, the Tertiary/Cretaceous strata lie on younger Paleozoic rocks westward. Where they overlie resistant Mississippian Joana Limestone in the footwall sheet of the Monte Mountain thrust fault, they are 300 feet thick. However, the unit is about 500 feet thick where it lies over the nonresistant Mississippian shales and sandstones. In contrast, the Tertiary/Cretaceous strata are less than 100 feet thick where they lie over Mississippian carbonates of the Monte Mountain hanging wall thrust sheet. Tertiary/Cretaceous strata lying on breached structures of Paleozoic rocks are not unique to the greater Timpahute Range. Eocene lacustrine limestones lie on Mississippian shales in the breached Illipah anticline in the White Pine Range, 120 miles to the north. I have mapped similar beds in the Grant, Pancake, and Egan ranges. Sparse well and outcrop data in central Nevada suggest that the Tertiary/Cretaceous strata thin and pinch out over Mesozoic anticlines and are thicker in synclines. The distribution of the Tertiary/Cretaceous strata along the Sevier fold-and-thrust belt is similar to the distribution of the Tertiary/Cretaceous strata over folds in central Utah.

Interbedded with and below the limestone beds at Monte Mountain are conglomerate beds with limestone clasts containing *Receptaculites*, a marker fossil found near the top of the Ordovician Pogonip Formation. The conglomerate also contains clasts of Eureka Quartzite and other Pogonip units. Erosion has exposed the nearest outcrops of *Receptaculites*-bearing Ordovician rocks in the Penoyer Springs plate 1.3 miles to the west.

Interbedded with cross-bedded sandstone, the well rounded, exotic clasts are in stream deposits. Imbrication of the clasts and cross-bedding suggests a paleocurrent direction of 165° at Monte Spring (see Monte Spring fault, **Plate 1a**). Exotic clasts shed from thrust sheets are not unique to the Monte Mountain locality, but also occur to the south and north. Carpenter and Carpenter (1994a, b), for example, described exotic clasts in Albian synorogenic beds in the Muddy Mountains, 90 miles south-southeast of the greater Timpahute Range. They found Ordovician clasts but no Ordovician outcrops. I found clasts of Ordovician Eureka Quartzite and *Receptaculites*-bearing limestone in a Tertiary/Cretaceous conglomerate unit ninety miles north of the study area at Big Louis Spring in the Pancake Range (near Wood Canyon thrust fault, **Figure 2**). There, nearly flat-lying Ordovician-bearing conglomerates lie unconformably on steeply-dipping Mississippian strata. The Tertiary/Cretaceous rocks are overlain by a thrust sheet of Devonian Guilmette Formation (Cedar Strat proprietary map, 1997). Volcanic rocks conceal the thrust klippe in most of the area. The clasts must have come from the nearest outcrops of Eureka Quartzite in the Moody Peak thrust sheet six miles to the west (**Figure 2**). I believe that the Late Mesozoic to Early Tertiary compressional event allowed Tertiary/Cretaceous strata rocks to be deposited in interthrust and foreland basins. The Monte Mountain Tertiary/Cretaceous basin may be similar to the Axhandle piggyback basin of central Utah. That basin contains Cretaceous to Tertiary North Horn conglomerates overlain by Eocene Flagstaff lacustrine limestones (Talling et al., 1995). Unfortunately, the most widespread area of exposed Tertiary/Cretaceous strata near the study area is in the restricted area of the Nellis Bombing Range (Tschanz and Pampeyan, 1970). Map patterns on their map show that the Tertiary/Cretaceous strata are closely associated with thrust faults. A detailed study of these strata may shed more light on the timing and style of this part of the Sevier fold-and-thrust belt. It is recommended that the United States Department of Defense remove restrictions and allow access to study these rocks (Chapter 9).

## Conclusions

A cumulative bed-length reconstruction of all the thrust faults in the greater Timpahute Range suggests at least 64 and possibly 98 miles of horizontal displacement in this part of the Sevier fold-and-thrust belt. It was pointed out in Chapter 2 that workers in other parts of the thrust belt suggested similar amounts of displacement. Elison (1991) concluded that the western North American Cordillera from southeastern British Columbia to northern Nevada experienced 180 miles of east-west crustal shortening. The magnitude of crustal shortening strongly affected the position of thrust sheets containing Devonian rocks and had a strong impact on interpreting the Devonian paleogeography.

My structural interpretation of the greater Timpahute Range improves significantly the stratigraphic analysis of this area, and the stratigraphic interpretation adds rigor to the structural model. Together, the merging of the structural (Chapter 5) and stratigraphic (Chapter 4) data illustrates the complexities of this part of the Sevier fold-and-thrust belt. The combination of the structural and stratigraphic analysis aids the paleogeographic interpretation of the Devonian rocks in Chapter 7. The new structural model and recognition of Devonian sequences herein also have economic implications (Chapter 8).

# CHAPTER 7

# DEVONIAN PALEOGEOGRAPHY

In the previous chapters the groundwork was laid for reconstructing the Devonian paleogeography of the study area. Chapter 4 provided the basis for dividing the Devonian into mappable sequences and contains sequence descriptions. In Chapter 5 and Appendix E the sequences are used to document structural features shown on **Plate 1a**. A structural model based on new mapping and distribution of contrasting sequence facies appears in Chapter 6. In the present chapter results of the previous chapters are combined and synthesized into an interpretation of the Devonian paleogeography.

The 21 mappable sequences at TMS introduced in Chapter 1 were identified and refined by correlating them to other sections and wells in the region (Chapter 4, **Figure 9**). An east-west correlation chart through the greater Timpahute Range was presented in Chapter 4. Other examples of some of these correlations are provided in this chapter. Formation names from previous work, introduced in Chapter 2, were retained wherever possible. Methods used to construct surface gamma-ray logs and isopach maps used in this chapter were presented in Chapter 3.

After correlating and refining sequences between sections listed in **Table 2**, correlations between sections and wells listed in Appendix F provided additional control to construct isopach maps. An isopach map of each sequence was constructed, two of which are shown in this chapter. A comparison of the isopach maps from the oldest to the youngest sequence shows that the center of the Sunnyside basin, described in Chapter 1, migrated from central Nevada in Lower Devonian (Sevy Dolomite Sequences) to western Utah in Late Devonian (Pilot Formation Sequences). All of the sequences were combined into a composite isopach map for the total Devonian (**Plate 3**). The map shows the form of the Sunnyside basin with the basin center near Sunnyside, Nevada, 54 miles north of Hiko. The axis of the Sunnyside basin trends north-northeast and intersects the basin center.

## Sequence Correlations

Three contrasting facies of Upper Devonian rocks from different thrust sheets in the greater Timpahute Range were introduced in Chapter 1. Structural elements of the thrust sheets were introduced in Chapter 5, illustrated on **Plate 1a**, and described in detail in Appendix E. The Chocolate Drop thrust fault separates facies 1 (thin-bedded limestone of the western exposure of the Pahroc thrust sheet) from the overlying facies 2 (sandy Silver Canyon thrust sheet). Facies 2 is separated from facies 3 (reefy, cyclic carbonates of the eastern exposure of the Pahroc thrust sheet) by the Silver Canyon thrust fault (**Plate 1a**). These contrasting facies are illustrated in **Figure 30**. The uniqueness of the Silver Canyon thrust sheet sandy facies is also illustrated by north-south correlation charts (**Figure 34** and **Figure 35**. Tear faults separate the Silver Canyon thrust sheet in the Pahranagat and Golden Gate ranges from the Silver Canyon thrust sheet in the greater Timpahute Range (**Plate 1a** and **Figure 32**). **Figure 34**, a correlation chart from the Pahranagat Range (correlative with the Silver Canyon thrust sheet) through Monte Mountain (Silver Canyon thrust sheet) and to the Golden Gate Range (Pahroc thrust sheet) shows the Guilmette sequence thicknesses to be more similar than those in a correlation chart from the Pahranagat Range through TMS (Pahroc thrust sheet) and to the Golden Gate Range (**Figure 35**). This is because the Silver Canyon thrust sheet and the correlative Pahranagat Range section are more genetically related than sections in the Pahroc thrust sheet.

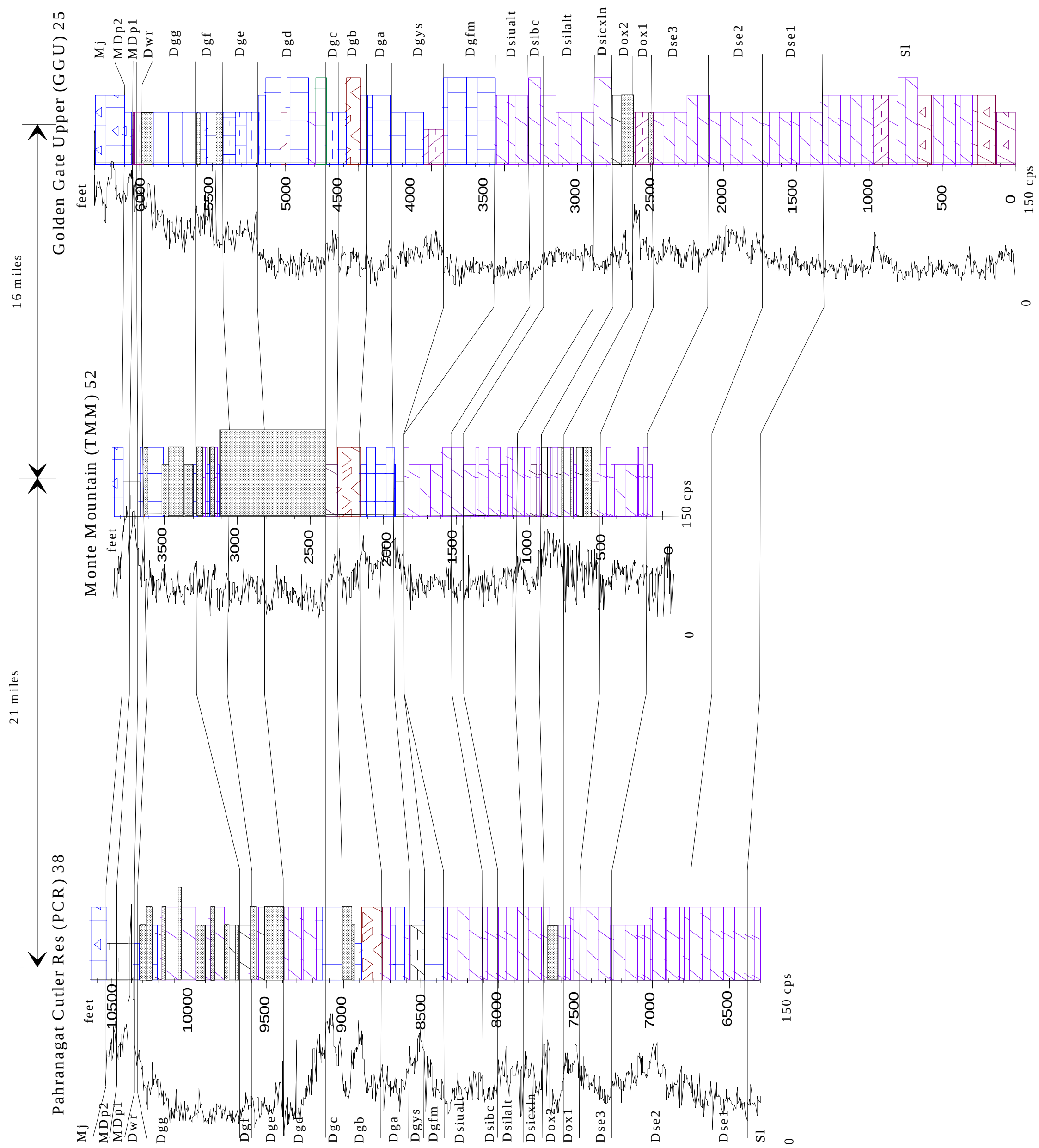


**Figure 34** North-south correlation of sections in the region showing the northward thickening of the pre-b2 breccia units toward the Sunnyside basin and the uniform thickness of the post-b2 breccia units within the Silver Canyon (Gass Peak?) thrust sheet (**Figure 2** for Gass Peak thrust in Clark County). See **Figure 9** for locations of sections.

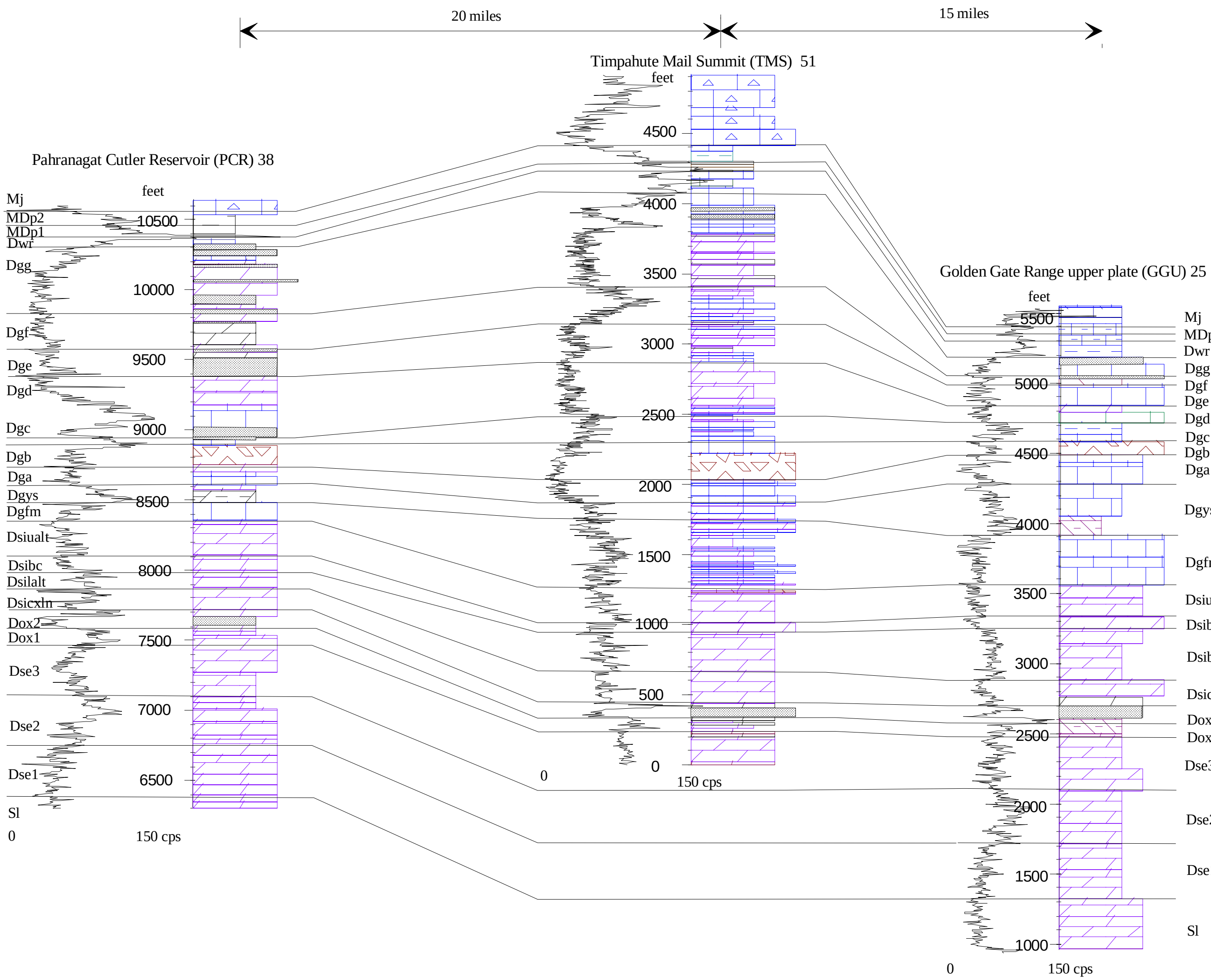


**Figure 35** North-south correlation of sections in the region showing the northward thickening of the pre-b2 breccia units toward the Sunnyside basin and the nonuniform thickness of the post-b2 breccia units between the Silver Canyon (Gass Peak?) and Pahroc (TMS) thrust sheets (**Figure 2**). See **Figure 9** for locations of sections

The trend of sandy facies thrust over reefy facies can be followed southward to the Gass Peak thrust fault that may be correlative with the Silver Canyon thrust fault (**Figure 2**). The Pahranagat Range is in the hanging wall of the Gass Peak thrust fault and contains a Guilmette sandy facies above Sequence Dgb. It contrasts with the footwall exposed in the southern Delamar Range, 25 miles south of the study area, that lacks the sandstone facies.

## Sunnyside Basin

**Plate 3** and **Figure 36** provide an example of an unrestored regional isopach map of the total Great Basin Devonian. Isopach maps of each of the 21 Devonian sequences were composited to make the total Great Basin Devonian isopach map (Chapter 4). The map implies an intrashelf basin centered near Sunnyside, 60 miles north Hiko. Therefore, the basin is named the Sunnyside basin (Chamberlain and Birge, 1997). The greater Timpahute Range lies on the southwest flank of the basin.

The Sunnyside basin is a northeast-southwest trending Devonian intrashelf basin about 400 miles long and 200 miles wide before structural restoration (**Figure 36**). Devonian strata thicken from approximately 500 feet near the basin edges to more than 6,600 feet in the basin (**Figure 8**). The steepest contour gradient is on the southeast flank of the basin between the Meadow Valley Mountains in south central Lincoln County, Nevada, and Blue Mountain in the Wah Wah Range, western Utah (**Plate 3** for locations). It lies within the area of known Sevier-age thrust faults. Contours on the western edge of the basin, western Eureka and Nye Counties, Nevada, also show steep gradients. The steep gradients are probably due to crustal shortening. Along the northeast structural strike within the basin, contour gradients are gentle, and probably more representative of original depositional trends. Restoration of the thrust sheets causes the steep gradients to flatten.

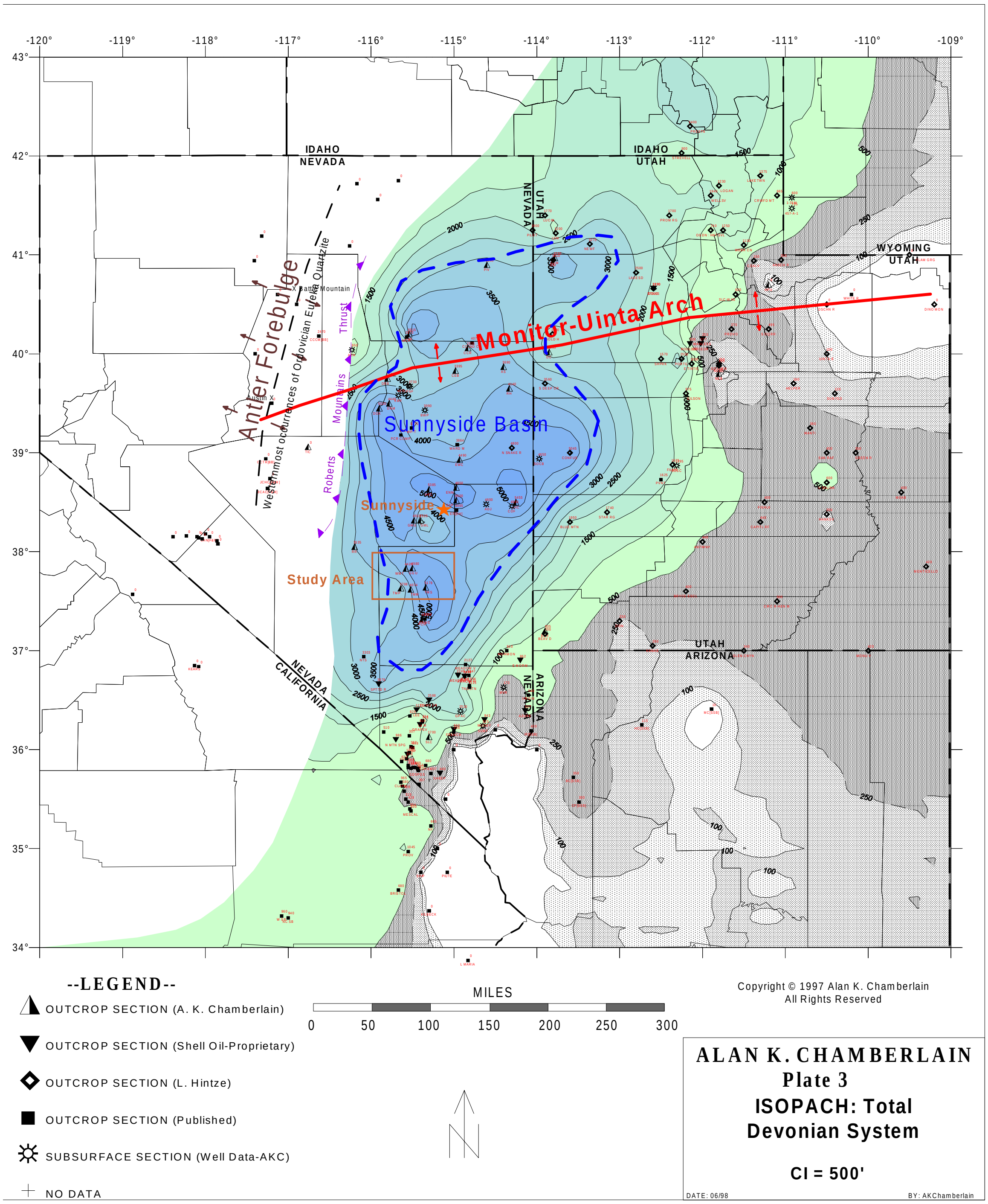


**Figure 36** Isopach map of all 21 Devonian sequences of the Sunnyside basin shows the configuration of the basin, some Paleozoic tectonic features including the Antler forebulge, Utah hingeline, and Monitor-Uinta arch, and the steep gradient on the southeast side of the basin caused by Mesozoic Sevier crustal shortening. The blue dashed line is the outline of the unrestored Sunnyside basin.

As mentioned in Chapter 6, at least 64 and possibly 98 miles of crustal shortening occurred in the greater Timpahute Range. Chapter 5 presented evidence of deeper thrust faults. They probably carried the Timpahute Range eastward some unknown distance. Elison (1991) estimated 180 miles of cumulative crustal contraction of the Cordilleran fold-and-thrust belt (see Chapter 6). If this cumulative displacement was restored then the northeast trending steep isopach gradient would flatten significantly. Furthermore, the size of the Sunnyside basin would approach the size of the Williston basin. As LeFever (1996) pointed out, the Williston basin is also approximately 300 by 600 miles in size. However, the Williston basin is a cratonic basin and the Sunnyside basin is an intrashelf basin. Strata of equivalent ages are much thicker in the Sunnyside basin than in the Williston basin, and the Sunnyside basin strata lack the evaporate-bearing strata of the Williston basin.

Guilmette rocks on the east side of the Sunnyside basin are characterized by reefs, bioherms, and other organic buildups. Thick quartz sandstones occur along the edges of the basin, shoreward of the organic buildups. Guilmette rocks on the west side (i.e., Pancake Range) of the basin are characterized by thick strata bearing *Amphipora*. Westward of the *Amphipora* wackestones are quartz sandstone beds. These mature quartz sandstones were probably derived from erosion of older Paleozoic rocks on the Antler forebulge. Evidence of a forebulge associated with the Antler Orogeny is found in fensters in the Roberts Mountain allochthon between Battle Mountain and Austin (Carpenter et al., 1994). Thousands of feet of lower Paleozoic rocks, including the Eureka Quartzite, were removed by erosion and shed eastward into the Sunnyside basin. Webb (1958) showed the upper sandstone member of the Eureka Quartzite thickening toward the study area. He also showed thickening of the highest two members of the Eureka Quartzite (up to 500') toward the Antler forebulge. An example of a fenster in the Roberts Mountains allochthon is in the Toquima Range (TIC), north-central Nye County, where a thin section of Devonian rocks lies on Ordovician Pogonip rocks (**Figure 36**, **Plate 3**). In other fensters, the Roberts Mountain allochthon lies directly on Cambrian and Lower Ordovician carbonates (Carpenter et al., 1994). Younger strata, including the Eureka Quartzite, have been removed. Most of the eroded strata were carbonate rocks. Consequently the insoluble residues from these older rocks in Sunnyside basin Devonian rocks testify to the erosional event. Devonian quartz sandstones that thicken westward are probably residues of the eroded Eureka Quartzite. Erosion of the lower Paleozoic rocks from the Antler forebulge was arrested by emplacement of the Roberts Mountain thrust sheet in Late Devonian and Lower Mississippian. Erosion of the allochthon resulted in a thick wedge of Mississippian Antler siliciclastics that attest to the emplacement of the Roberts Mountains allochthon that followed the development and eastward migration of the Antler forebulge.

An isopach of Guilmette Dgb2 breccia (Alamo Breccia) shows a sub-basin within the southwestern end of the Sunnyside basin that was probably created by the cosmolite impact at Tempiute Mountain (**Figure 37**). I named this impact basin the Tempiute basin (Chamberlain, 1999). Devonian strata in this part of the Sunnyside basin should be thinner and composed of shallowing-upward cycles with abundant *Amphipora* and supratidal, fine-grained stratal dolomite cycle caps. However, *Amphipora* and shallowing-upward cycles capped with supratidal dolomite are absent in the Tempiute basin. Instead, the unique thin-bedded limestone facies 1, commonly exhibiting soft-sediment deformation and containing rare thin quartzose turbidite sandstone beds, fill the Tempiute impact basin. No other section or well in the region exhibits these unique facies (facies 1).

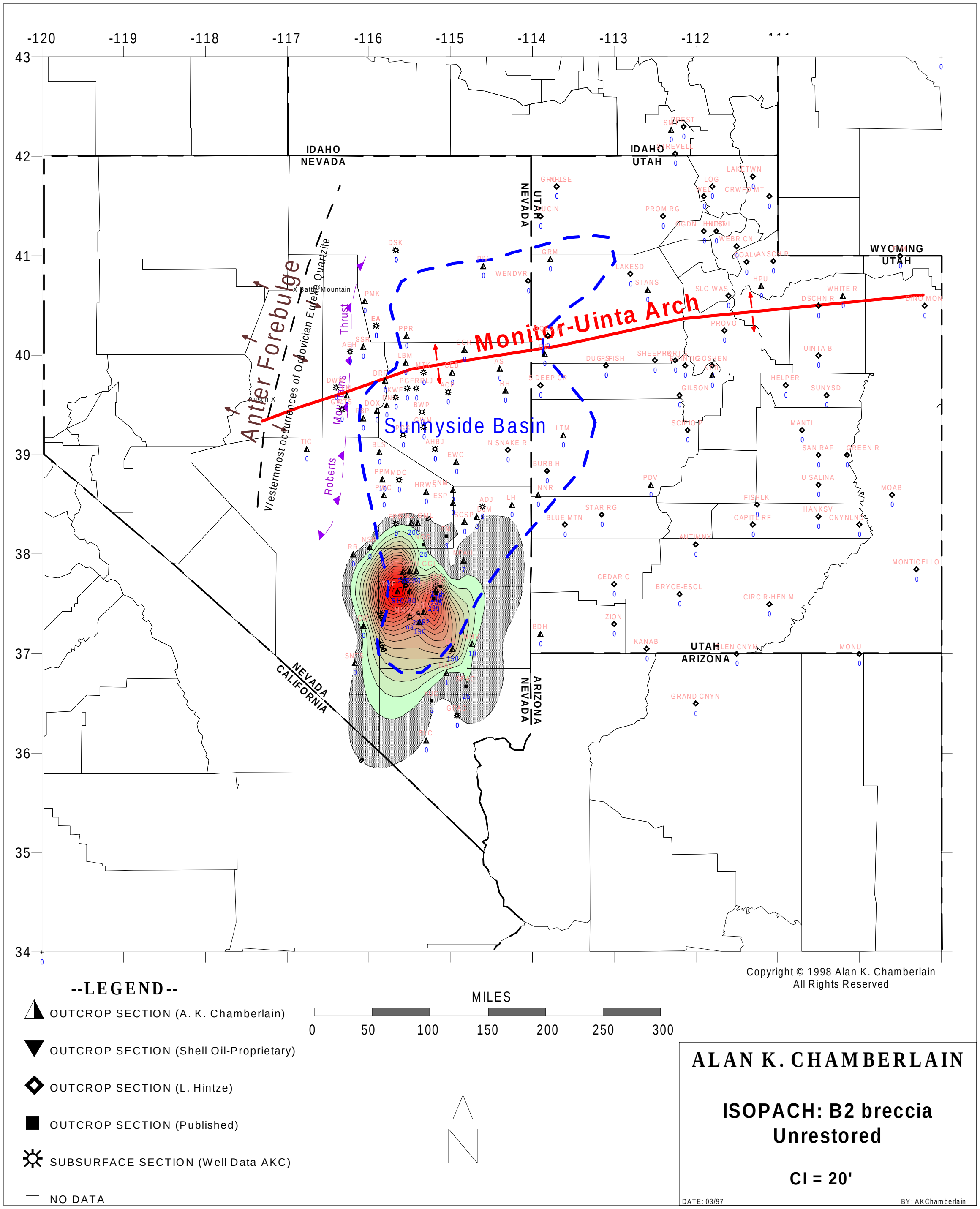


**Figure 37** An unrestored isopach map of Guilmette Dgb2 breccia shows the form of the unrestored Tempiute basin in the Sunnyside basin. It shows an oval pattern 160 miles long and 60 miles wide with two pods of thicker breccia separated by a ridge of thinner breccia. The blue dashed line is the outline of the unrestored Sunnyside basin.

The isopach of Sequence Dgb also shows that the thickest Sequence Dgb is in the Egan Range, near Sunnyside (**Figure 38**). **Figure 34** and **Figure 35** show this northward thickening in sequences below Sequence Dgb. Being continuous with the north-northeast trending axis of the Sunnyside basin, another thick area occurs in southwestern White Pine County. It occurs in an area of known Sevier thrust and strike-slip faults. If the sections containing thinner Sequence Dgb strata west of Sunnyside were restored to the west, then the Sunnyside basin axis and the southwest White Pine thick area would converge into a single basin (**Plate 3**). Because the axis of the Sunnyside basin appears to have moved eastward with time, the axis of the basin during Sequence Dgb2 time is farther to the west than the average basin axis in **Figure 36**. This would imply that the Antler forebulge migrated from central Nevada toward western Utah during the Devonian. Giles (1994) concluded that the Pilot basin reflected the flexural downwarping of the Antler back-bulge basin. She suggested that the flexural features remained fixed throughout the history of the Pilot basin and that the forebulge moved eastward across eastern Nevada into western Utah during the Early Mississippian. Giles (1996) suggested that the Lower Mississippian Joana Limestone shows a retrograde stratigraphic pattern interpreted to have been forced by lithospheric flexural subsidence during the Antler orogeny. The relationships all suggest that the Antler forebulge migrated eastward from central Nevada in Early Devonian to western Utah in Early Mississippian.

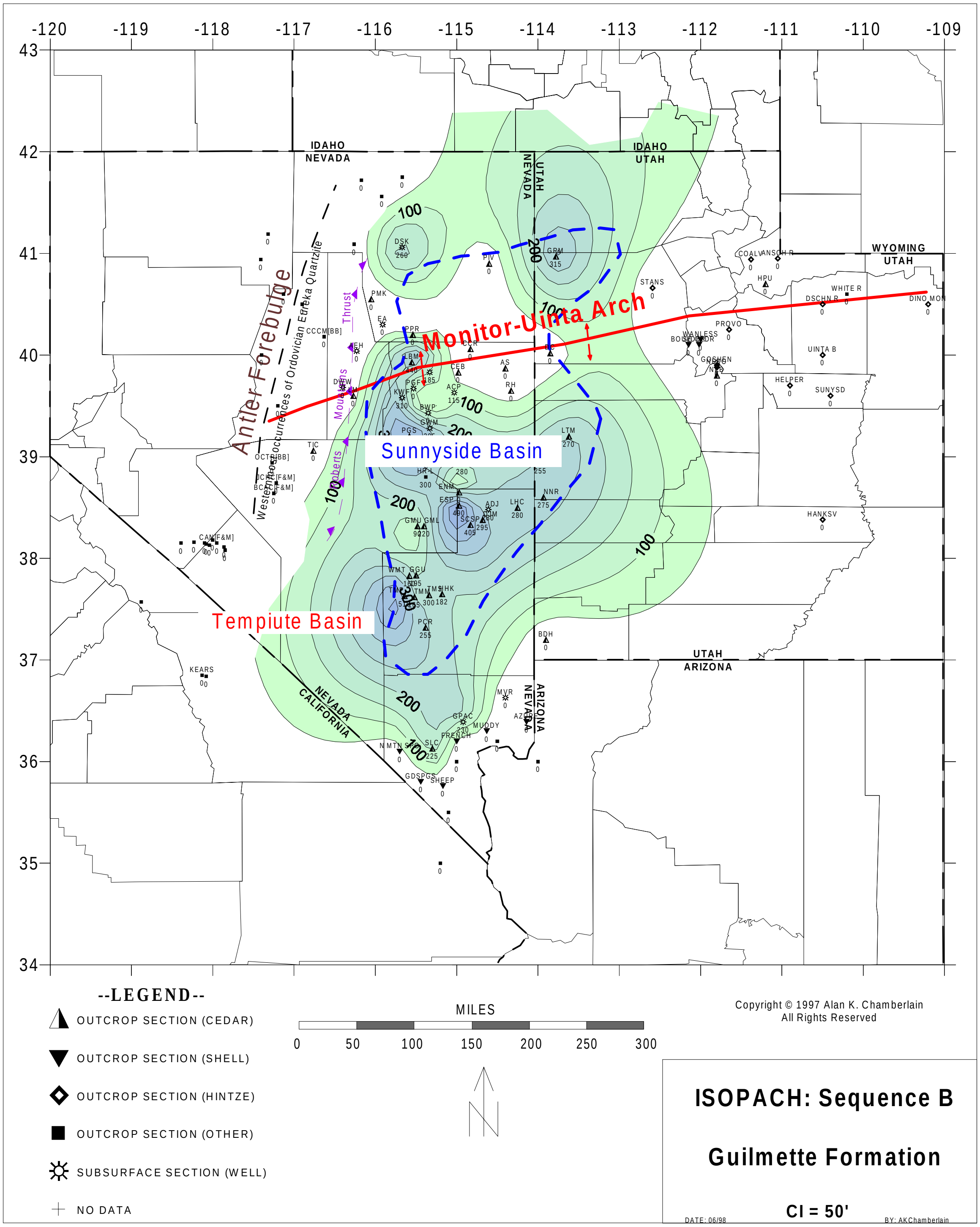


**Figure 38** Isopach map of unrestored Guilmette Sequence Dgb shows contours closing on the Dgb2 breccia basin (Tempiute basin) in the southern end of the Sunnyside basin. The blue dashed line is the outline of the unrestored Sunnyside basin.

Generally, Sequence Dgb thins northward to the Monitor-Uinta arch. The thinning of Sequence Dgb near the Monitor-Uinta arch suggests that the arch was a positive area during Sequence Dgb time. North of the arch, Sequence Dgb thickens again. The blue dashed line in the isopach maps, **Figure 36**, **Figure 37**, **Figure 38**, **Figure 39**, **Figure 40**, **Figure 41** and **Plate 3**, represents the unrestored outline of the Sunnyside basin.

## Tempiute Basin

The subbasin discussed above within the southern end of the Sunnyside basin was likely created by a Devonian cosmolite impact that disrupted Sequence Dgb strata and is named Tempiute basin herein. The impact likely created a concentric basin, similar to other terrestrial impact basins including: Chesapeake Bay (Johnson et al., 1998), Bosumtwi, Ghana (Reimold et al., 1998), Morokeng, South Africa (Koeberl et al., 1997a), Popigai, Russia (Koeberl et al., 1997b), and Chicxulub, Yucatan Peninsula, Mexico (Hildebrand et al., 1991) and many others. However, subsequent tectonic events have deformed some impact basins such as the Sudbury structure, Canada (Fueten and Redmond, 1997; Ames et al., 1998). Mesozoic thrusting deformed the Tempiute impact basin. Well-preserved impact basins, such as Chicxulub, exhibit distinct topographic rings and predictable morphology including a central uplift, terrace zone of slumped blocks, and inward-facing asymmetric scarps (Morgan and Warner, 1999). These morphologic features are yet to be found in the deformed Tempiute impact basin.

Within the Tempiute basin, a central crater is marked by an abrupt thickening of the impact breccia (**Plate 4b**). An unrestored isolith map of the Tempiute basin shows two thick areas, delimiting the central crater, within the basin (**Figure 37**). The ridge between the two lows is caused by thinner (126-200 feet) Dgb2 breccia in the Silver Canyon thrust sheet than in the thicker Pahroc (east) thrust sheet (392 feet) and in the Pahroc (west) thrust sheet (510 feet). The isolith contours should have produced a concentric pattern.

However, the unrestored distribution of the breccia forms a large oval pattern 160 miles long in the longest dimension (north-south) and 60 miles wide in its shortest dimension (east-west). Its size can be compared with other terrestrial impact craters. The Chesapeake Bay (Johnson et al., 1998) and Popigai (Koeberl et al., 1997b) craters are about 60 miles in diameter, Chicxulub (Hildebrand et al, 1991) is about 160 miles in diameter, and the Morokeng (Koeberl et al., 1997a) is approximately 210 miles in diameter. Lunar mare crater counts, the terrestrial impact flux, and astronomical observations of asteroids and comets provided data to predict 11 continental craters with 155-186 miles of diameter (Glikson, 1999). Only three craters of this rank are reported in literature (Glikson, 1999). Timpahute may be the fourth.

According to the emerging structural model presented in Chapter 6, the Tempiute Mountain section was deposited in an intrashelf basin west of the reef-bearing TMS section and east of the Monte Mountain sandstone facies. In other words, the Monte Mountain section (TMM), which is now between TMS and TMP, was probably originally deposited west of TMP (**Plate 4b**). Thrust restoration suggests that TMP facies 1 of the central crater were probably deposited approximately 30 miles to the west (**Plate 4b**). Post impact strata at TMS are deepwater, rhythmic, thin bedded limestones (facies 1) that are unique in the region. They intertongue with the shallowing-upward cycles of TMM (facies 2). Evidence of the intertonguing is found by comparing post impact sequences in the Monte Mountain hanging wall, to the Monte Mountain footwall and the northernmost exposures of the sequences in the Pahranagat Range (NPR, T5N R58E Sec 5, **Plate 1a**). Thick-bedded, sandy, burrowed limestone and dolomite lies immediately above the Dgb2 breccia at TMM hanging wall. The carbonates are more limey, less sandy and thinner bedded in the TMM footwall. Correlative beds at NPR are rhythmically, thin-bedded limestone and are similar to those at TMP. Therefore the rocks in the Silver Canyon thrust sheet deepen eastward toward the restored position of TMP. Cycles at NPR contain a greater proportion of deeper-water facies than those at Down Drop Mountain (DDM) which is nearer the edge of the Tempiute basin. For example, the abundance of

*Amphipora*, which suggest restricted marine conditions, increases from NPR to DDM. All these sections, TMM, NRP, and DDM lie within the Silver Canyon thrust sheet. Thicknesses and the number of tongues of deepwater, thin-bedded limestones in the sequences and especially cycles in Sequence C increase eastward, toward the Tempiute basin and decrease toward the edge of the basin. Similarly, basinal post impact strata of the Chesapeake Bay impact structure, Virginia, intertongues with offshore shoal deposits (Johnson et al., 1998). From assumptions within this study, it appears that the TMM section was likely deposited on the west edge of the Sunnyside intrashelf basin. Restoration of the sections places TMP near the axis of the Sunnyside basin with the sandy TMM on the west side and the reefy TMS on the east side. This restoration provides for a thicker Dgb2 breccia near the center of the circular impact crater and a consistent thinning radially. Similarly, the Exmore Breccia of the Chesapeake Bay impact structure thins rapidly from 984 feet in the annular trough to zero outside the outer rim (Johnson et al., 1998).

Providing an ideal chronostratigraphic bed, the unique nature of the single-event Dgb2 breccia can be used to unshuffle thrust sheets not only in the Timpahute region but beyond. The cosmolite impact crater was most likely circular. The impact ejecta blanket and associated disturbed seabed rocks were probably distributed radially. Channel-like occurrences of the breccia in the Golden Gate hanging wall thrust sheet and in the south Seaman Range could be associated with ejecta rays or breccia-filled grooves radiating from the impact crater. In the southern Golden Gate range thick (100's feet) of breccia occur between ridges of undisturbed Sequence Dgb. In the southern Seaman Range, thinner (10's feet) of breccia occur between intervals of undisturbed Sequence Dgb. See **Figure 37** and **Figure 39** for isolith maps of the breccia. In the third dimension, these bodies of breccia may be channels or valleys cut into undisturbed Sequence Dgb. They thicken and widen toward Tempiute Mountain.

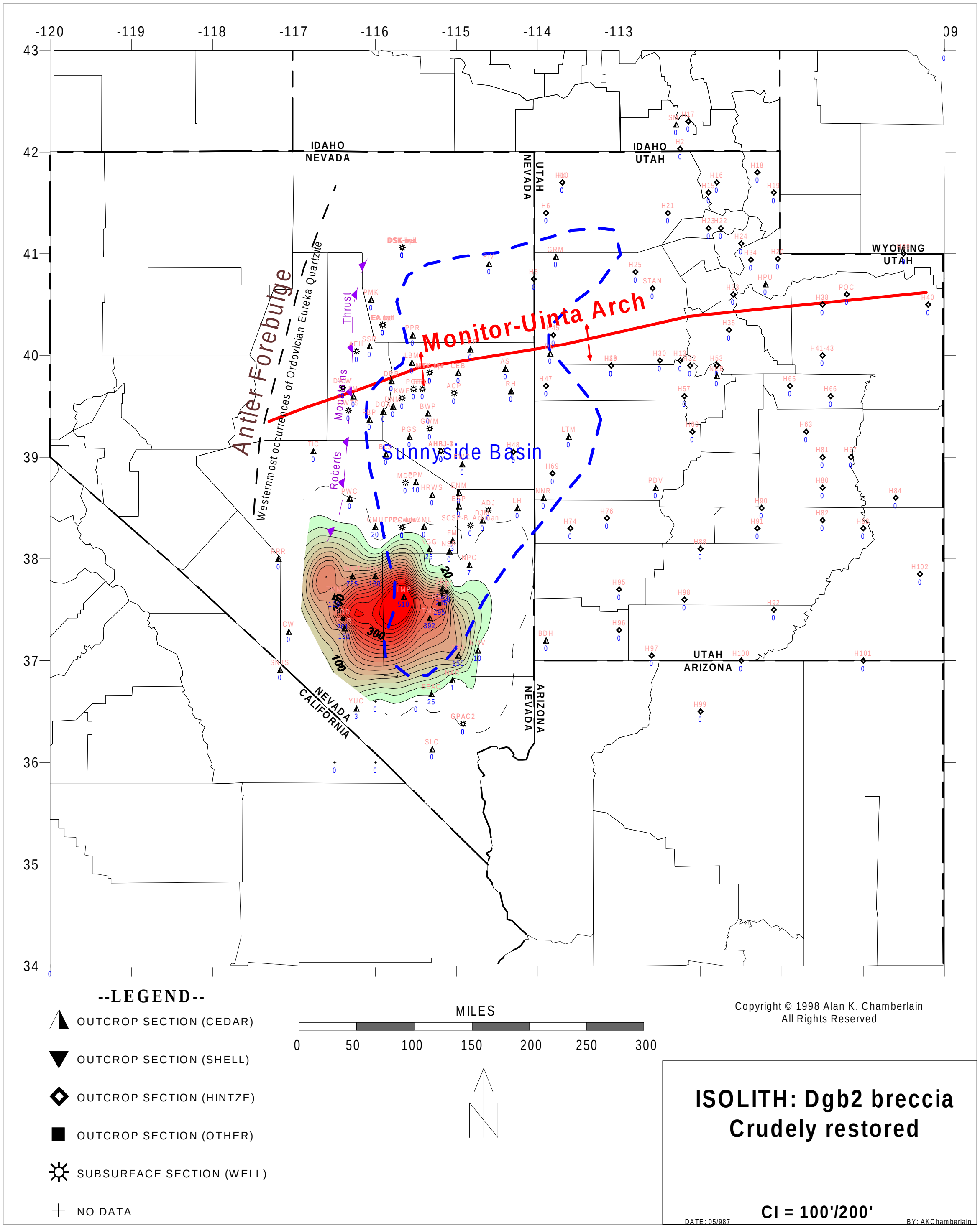


**Figure 39** Crudely restored isolith map of the Guilmette Sequence Dgb2 breccia shows a more concentric distribution of the breccia in the Tempiute sub-basin. The restoration eliminates the ridge of thinner breccia between pods of thicker breccia. The blue dashed line is the outline of the unrestored Sunnyside basin.

Once the Silver Canyon thrust sheet is restored west of Tempiute Mountain, a consistent thinning of the breccia occurs radially from the circular impact site. Beyond the major changes in thickness across the Silver Canyon and Chocolate Drop thrust faults, other major changes in thickness occur across the Pahroc, Forest Home, and Wood Canyon thrust faults (**Figure 2**). The breccia is more than 100 feet thick in the hanging wall of the Pahroc/Delamar thrust sheet in the southern Delamar, Hiko, and southern Seaman ranges (**Figure 5**). However, it is about 10 feet thick in the footwall sheet exposed in the northern Meadow Valley and northern Pahroc ranges (**Figure 17**). The breccia is absent in Sequence Dgb exposed in a fenster of the Forest Home thrust sheet 20 miles north of the study area (Stop 12, Appendix D). Nevertheless, it is about 8 feet thick in the Forest Home hanging wall thrust sheet (**Figure 2**). In the Pancake Range, 40 miles northwest of the study area, the breccia is about 6 feet thick in the Portuguese Mountain thrust sheet, footwall to the Wood Canyon thrust fault. It is absent in the Wood Canyon hanging wall thrust sheet (**Figure 2**).

Thrust fault restorations using the structural model presented in Chapter 6 provide constraints on the circular Tempiute sub-basin created within the Sunnyside basin by the cosmolite impact (Chamberlain, 1999). An isolith map of the present-day distribution of the breccia manifests an ellipsoidal areal distribution (**Figure 37**). The Tempiute sub-basin, in which Dgb2 breccia is found, extends from the southern Arrow Canyon Range on the south to Portuguese Mountain on the north, a distance of about 160 miles. In contrast, the east-west distribution covers only about 60 miles from west of Tempiute Mountain to east of the Pahroc Range. The compressed, ellipsoidal shape was likely due to, or accentuated by, the Sevier orogeny. A knowledge of the assumed distribution of breccia before thrusting provides a unique opportunity to restore thrust sheets with a greater degree of confidence and could help predict the center of the impact.

A crudely restored isolith map was made by moving sections west of the Gass Peak/Silver Canyon thrust one degree, or about 55 miles, to the west (**Figure 39**). Cumulative shortening of the Silver Canyon, Monte Mountain and Penoyer Springs thrust faults is approximately 50 miles (**Table 11**). Restoration of the Pahroc thrust sheet would move the Tempiute basin an additional 50 miles to the west. Cumulative shortening of the entire greater Timpahute Range, including the Pahroc thrust fault, is approximately 100 miles (Chapter 6). Because the traces of some thrust faults extend more than 200 miles along the north-south structural strike, then 100 miles of east-west crustal shortening is reasonable. Though maximum displacements are not linearly related to thrust lengths, worldwide three-dimensional seismic surveys show length exponents vary from 0.8 to 1.55 (Fermor, 1999).

The crudely restored isolith map (**Figure 39**) shows a more concentric basin than the unrestored isolith map (**Figure 37**). Although these isopach maps are constructed with limited preliminary control, refined maps with many more control points could be adjusted until the breccia basin is perfectly concentric. As pointed out in Chapter 3, without additional constraints for this unique region, accurate balanced cross sections and restorations cannot be constructed. Distribution of the Dgb2 breccia provides the additional constraints needed to make accurate balanced cross sections in the area. It could be a powerful tool to restore the sections and obtain accurate values for crustal shortening for each thrust sheet. Accurate balanced cross sections constrained by those values would greatly improve the structural model and provide a better template for structural analysis along strike.

## Devonian Sandstone

Quartz sandstone in the Devonian rocks of Nevada have largely been overlooked. Ryan and Langenheim (1973) attempted to describe and interpret sandstones in the Upper Devonian regionally. They cite many workers who mentioned local sandstone occurrences, but they were first to put the sandstones into a regional setting. In my analysis, the Upper Devonian sandstones and sandstone intervals of the Middle Devonian "Oxyoke Formation" are also put into a regional setting.

As mentioned in Chapter 2, provenance of Devonian sandstones is problematic. C. Sandberg (1998, personal communication) suggested that the source of the Devonian sandstones in the study area was the Stansbury uplift in north central Utah. According to Sandberg et al. (1988) the Stansbury uplift was initiated after the Pilot basin formed in the Famennian. However, most of the Guilmette sandstones were deposited below the Pilot Formation in the study area and are Frasnian. Sandberg and Ziegler (1973), at Bactrian Mountain within the study area, documented the base of the West Range Limestone in the Middle *crepida* conodont zone at the base of the Famennian. This implies that the sandy beds of the Guilmette lie well below Stansbury siliciclastics. This chapter shows that a probable Antler forebulge bordered the west side of the Sunnyside basin and was the likely source area for the mature sandstones there. Sandstones along the eastern edge of the Sunnyside basin were derived from highlands in northeastern and east-central Utah. The distribution of Devonian sandstones also provides another tool for restoring structural cross sections in the study area.

## "Oxyoke Formation"

Carbonate deposition predominated between deposition of the Ordovician Eureka Quartzite to the Devonian "Oxyoke Formation" in the Sunnyside basin. The "Oxyoke Formation" recorded the first pulse of the Antler forebulge as containing the first significant quartz sandstone above the Eureka Quartzite. Sandstone beds of the "Oxyoke Formation" consist of mature quartz grains. They generally overlie argillaceous dolomite beds. A detailed description of the "Oxyoke Formation" sequences and cycles are presented in Chapter 4 and in Appendix B.

An isopach of the "Oxyoke Formation" shows that the formation increases in thickness on the western side of the Sunnyside basin (**Figure 40**). It is thickest near the intersection of the Sunnyside basin and the western extension of the Monitor-Uinta arch. Hurtubise (1989) described the Timber Mountain strike-slip fault as a major fault cutting the northern end of the Seaman and Golden Gate ranges with sinistral movement. Isopach contours show a sinistral offset of thicker "Oxyoke Formation" in the axis of the Middle Devonian Sunnyside basin (**Figure 40**). Thrust restoration of the Timpahute area westward would place the north-south trending thick or basin axis south of the fault in line with the thick or basin axis north of the fault. It would also place the Timpahute area closer to sandstone source areas on the Antler forebulge. The structural model (**Plate 4a)** that supports this thrust restoration is presented in Chapter 6 (**Plate 4b)**.

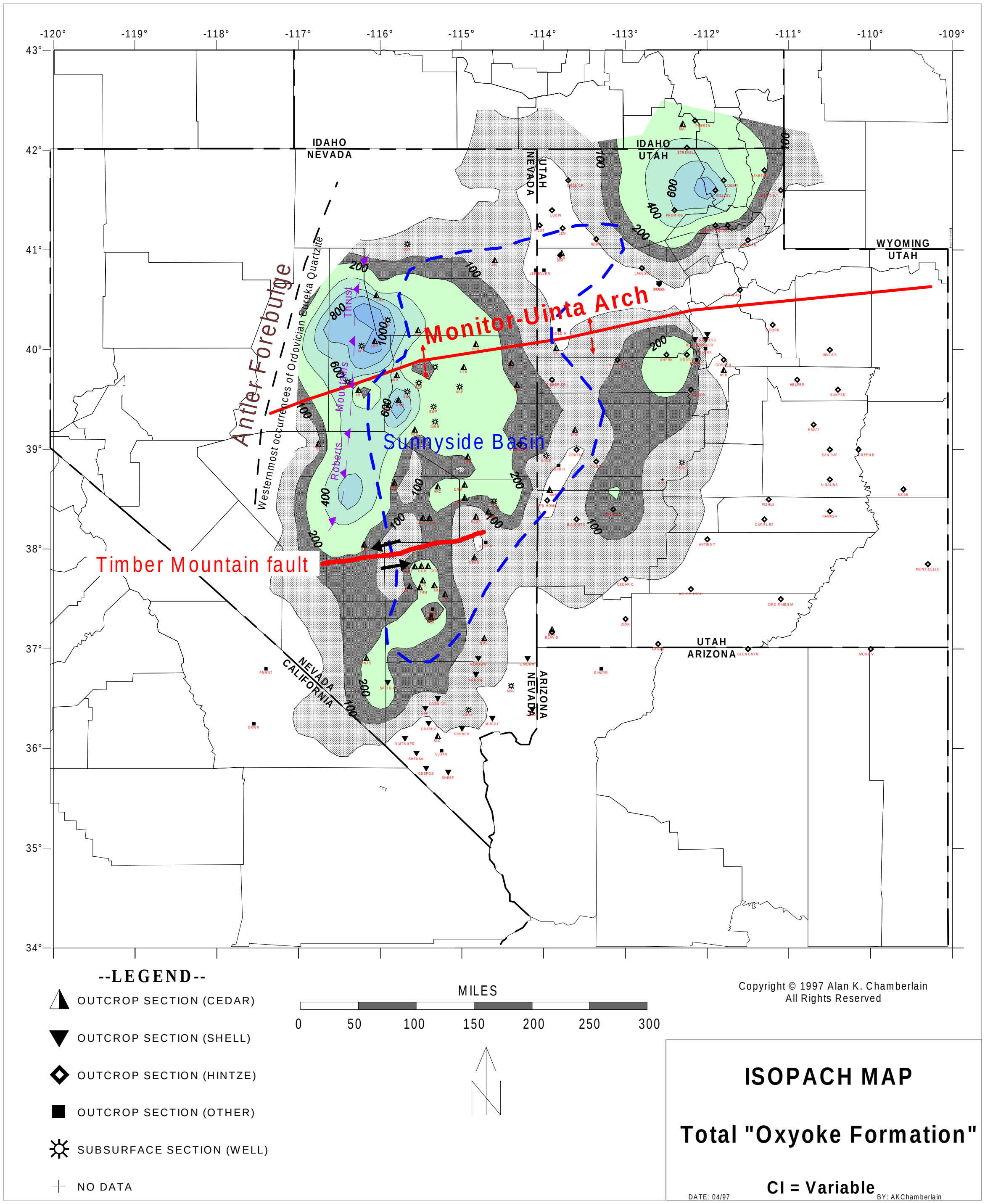


**Figure 40** An isopach map of "Oxyoke Formation" in the Sunnyside basin shows that the basin axis was farther west during Oxyoke time than during younger Devonian time (**Figure 38**). It also suggests that the western extent of the Monitor-Uinta arch was a source area for quartz sandstones and that the Timber Mountain strike-slip fault offsets the basin axis. The blue dashed line is the outline of the unrestored Sunnyside basin.

Guilmette Sandstones

Siliciclastic rocks above the "Oxyoke Formation" next occur in the Yellow Slope Sequence of the Guilmette. Carpenter et al. (1994) and Carpenter (1997) recognized the importance of these siliciclastic rocks and suggested that rocks equivalent to the Yellow Slope Sequence represented the initial filling of the backbulge basin east of the Antler forebulge. Occurrence of quartz sand grains in the Yellow Slope Sequence is persistent in much of the Sunnyside basin and a careful study of them may provide insight into the paleogeography of the Sunnyside basin. However, thick sandstone occurrences above Sequence Dgb were the main topic of Ryan and Langenheim (1973) and are the subject of this section. This discussion begins with the Guilmette quartz sandstones in the study area, then includes the regional setting of the study area sandstones within the Sunnyside basin.

Guilmette Sandstones in the Study Area A number of conspicuous features that differ across the Silver Canyon thrust fault suggest eastward displacement of tens of miles. First, an abrupt change in the volume and characteristics of Guilmette sandstones occur across the thrust fault (**Table 12** and **Figure 41**). Reef-bearing rocks (facies 3) occur in Guilmette Sequence Dgb east of the thrust, and thick (up to 860 feet) quartz sandstone units (facies 2) make up Sequences Dgb through Dgg in the hanging wall west of the thrust.

**Table 12** Net Sandstone thickness of the Guilmette Formation in the Timpahute area and beyond providing data used to generate **Figure 41**.

| LONG LAT | NET FEET | SECTION | SECTION NAME |
|---|---|---|---|
| -115.42 37.83 | 75 | GGL | GOLDEN GATE RANGE, LOWER PLATE |
| -115.50 37.83 | 100 | GGU | GOLDEN GATE RANGE, UPPER PLATE |
| -115.38 37.32 | 320 | PCR | PAHRANAGAT RANGE, CUTLER RESERVOIR |
| -115.37 37.34 | 330 | PCR | PAHRANAGAT RANGE, CARBONATE RIDGE |
| -115.36 37.40 | 830 | PHS | PAHRANAGAT RANGE, HANCOCK SUMMIT |
| -116.20 8.05 | 0 | RR | REVEILLE RANGE |
| -114.83 38.33 | 20 | SCSP | SCHELL CREEK, SIDEHILL PASS |
| -115.35 37.63 | 150 | TMS | TIMPAHUTE RANGE, MAIL SUMMIT |
| -115.65 37.63 | 40 | TMP | TIMPAHUTE RANGE, TEMPIUTE MOUNTAIN |
| -115.52 37.63 | 1070 | TMM | TIMPAHUTE, MONTE MOUNTAIN |
| -115.48 37.69 | 965 | TPS | TIMPAHUTE PENOYER SPRINGS |
| -115.58 37.83 | 190 | WMT | WORTHINGTON MOUNTAIN |

Net Guilmette quartz sandstone in the Silver Canyon thrust sheet (TMM) is 1,070 feet thick in contrast with 150 feet in the Pahroc (east) thrust sheet (TMS). Note the unusual thickness for the sandstone in the Silver Canyon thrust sheet in **Figure 41**. Sandstone bodies in the hanging wall are lenticular, occur throughout the Guilmette, exhibit bidirectional cross bedding, and are interbedded with *Amphipora*-bearing carbonates. They are interpreted as tidal deposits in channels and flats. Thin sandstone units of the Pahroc thrust sheet, by contrast, mostly occur in the uppermost Guilmette.

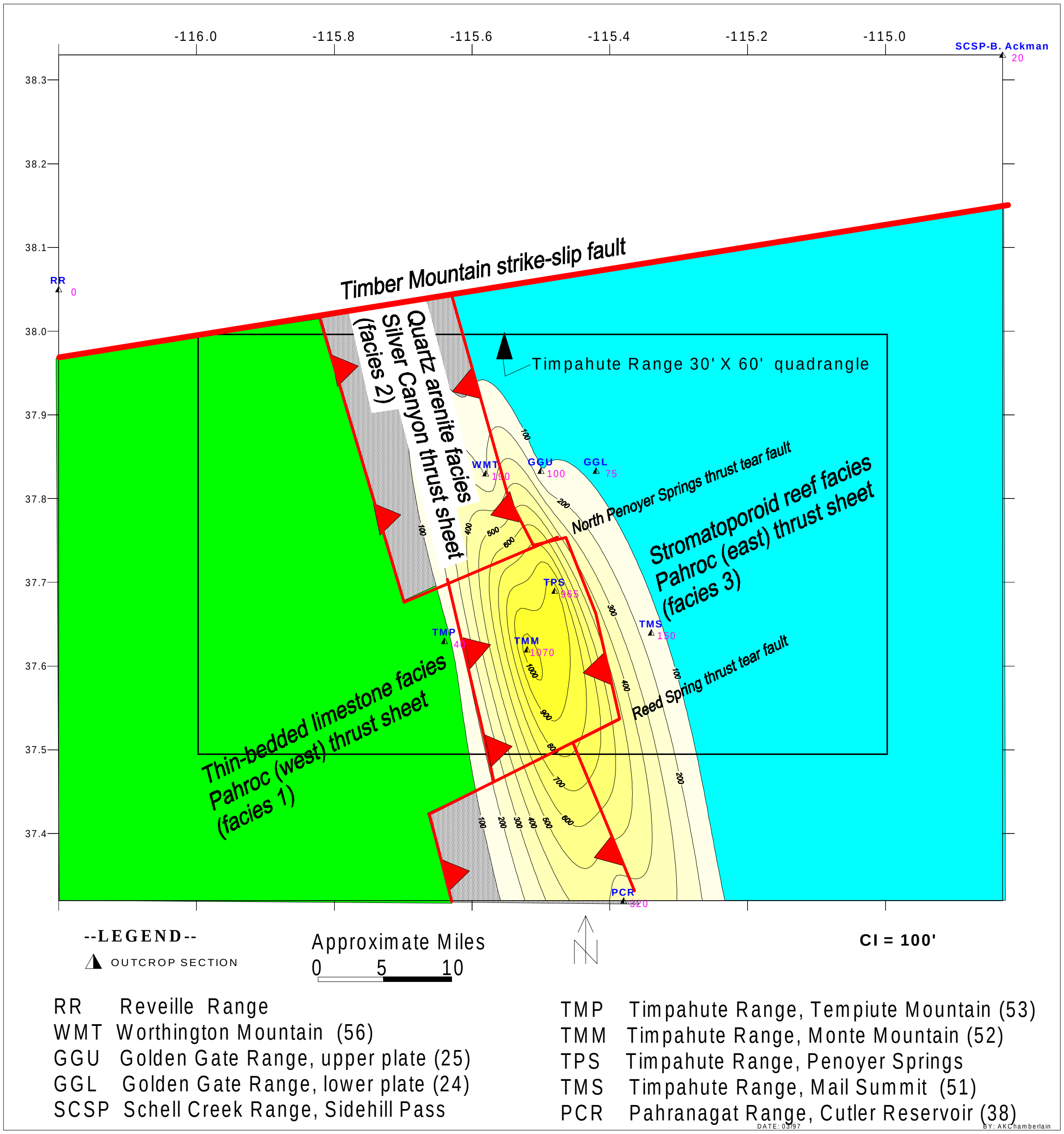


**Figure 41** Guilmette Formation net quartz sandstone isolith map in the Timpahute area shows the abrupt changes in sandstone thicknesses between structural plates. Compare with the generalized tectonic map showing the structural plates of the greater Timpahute Range (**Figure 32**). Sections with capital letters are from Appendix F and **Table 2**. The value adjacent to the triangles are net sandstone thicknesses in feet. Thrust faults and thrust sheets are schematic. See Timber Mountain strike-slip fault on **Figure 38**.

Composite sandstone thickness in the Guilmette Formation increases northward from the southern Pahranagat Range to the Timpahute Range and then rapidly decreases to zero sandstone north of the Timber Mountain fault. Thickness of the sandstones increases from 320 feet in the Pahranagat Range to more than a thousand feet at Monte Mountain. North of the greater Timpahute Range, quartz sandstone thickness decreases rapidly to no sandstone in the southern Egan Range, 60 miles north-northeast of Hiko (**Figure 8**, **Figure 9**, No. 20 and **Table 2**). If the original thickness trends were gradual, then the present abrupt trends could be due to thrust tear faults that bound the north and south sides of the Silver Canyon thrust sheet in the Timpahute salient. Structural salient is defined in Chapter 6. These thrust tear faults may be related to basement fractures caused by the cosmolite impact. Glikson (1999) suggested a potential correlation between mega-impacts and crustal magmatic and tectonic episodes. Cedar Strat measured 190 feet in the Worthington Range and 100 feet in the Golden Gate Range of net quartz sandstones (proprietary measured sections, 1986, 1987). I measured 40 feet of net quart sandstone in the Guilmette Formation in the western exposure of the Pahroc thrust sheet at Tempiute Mountain. In the Pahranagat Range, south of the study area, Estes (1992) reported 830 feet of net Guilmette sandstone near Hancock Summit and Downdrop Mountain. Similar thicknesses were reported for Downdrop Mountain (Shell Oil Company and Cedar Strat proprietary measured sections). Reso (1960) reported 330 feet west of Badger Spring, six miles south of Hancock Summit.

The change in net sandstone thickness between the central Pahranagat Range and Monte Mountain, a distance of 23 miles along structural strike, is 740 feet or an average of 32 feet per mile. Assuming the same gradient, net sandstone thickness would decrease to 150 feet, the thickness at Mail Summit, nine miles from Monte Mountain. If the gradient were similar between Monte Mountain and Mail Summit, Monte Mountain should be restored 29 miles west of Mail Summit. Approximate crustal shortening estimated by balancing bed lengths in a snip reconstructed structural cross section is 28 miles and the amount of slip on the Silver Canyon thrust fault on **Plate 4a** is 22 miles (**Table 10**).

Regional setting of Guilmette Sandstones An isolith map of net sandstone (**Figure 42**) of the Guilmette Formation in the Sunnyside basin sheds light on possible source areas for the sandstones. Generally quartz sandstones are thickest on the edges of the Sunnyside basin. Some thickest sandstones occur where the Monitor-Uinta arch intersects the edges of the Sunnyside basin. Thick uppermost Devonian sandstones are focused in the Stansbury uplift area in north central Utah. The sandstones become thinner southwestward, parallel with the Utah hingeline. Another area of thick uppermost Devonian sandstones occurs near the Utah/Nevada border at latitude 38.75°. Isolith contours suggest that another positive area could have occurred in an east-west belt in central Utah. Sand moving westward from eastern and central Utah would have been trapped at the edge of the Sunnyside basin near the Nevada border. The sandstones are mature. Ryan and Langenheim (1973) suggested that the sandstones must have moved from the environment of maturation to the site of deposition. The maturation of the sandstones could be a result of recycling sandstones from earlier mature sandstones such as the Eureka Quartzite.

Thick middle Upper Devonian sandstone occurrences in the Silver Canyon thrust sheet in the Timpahute region occur on the southwest edge of the Sunnyside basin. These sandstones are described in Chapter 4 and in Appendix B. Generally they are composed of mature, fine- to medium-grained, well-sorted, well-rounded, and frosted quartz grains. They occur in lenticular channels tens to hundreds of feet wide and tens of inches to tens of feet deep. They exhibit planar crossbedding and are rippled. Ryan and Langenheim (1973) reported a predominant current direction from the northeast for Guilmette sandstones exposed in the Arrow Canyon Range, 62 miles south-southeast of Hiko. Mudcracks are common at the top of the sandstone beds in the study area.

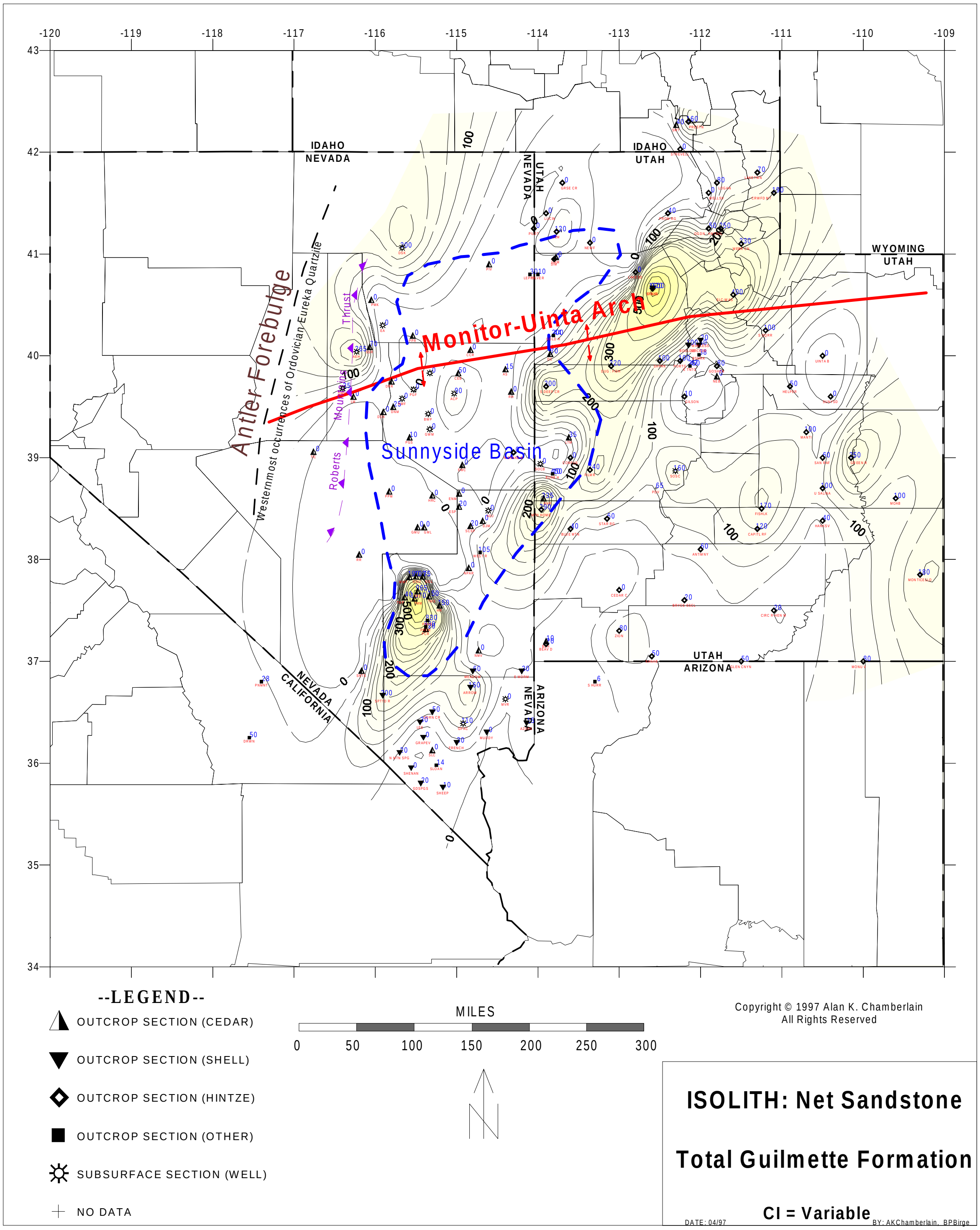


**Figure 42** An isolith map of the net quartz sandstone of the Guilmette Formation of the Sunnyside basin, Nevada and Utah shows that sandstones are concentrated along the edges of the Sunnyside basin (see Appendix F for data locations). The blue dashed line is the outline of the unrestored Sunnyside basin.

Thrust restoration of the greater Timpahute Range would place the thick quartz sandstones even closer to the Antler forebulge, a likely source of the mature sandstones. The steep gradient on the north side of the Timpahute sandstone accumulation is probably due to strike-slip displacement along the north Penoyer Spring tear fault and more especially along the Timber Mountain fault four miles north of the study area.

On the northwest edge of the Sunnyside basin, another sandstone thick occurs below the Mississippian Roberts Mountain allochthon near the Monitor-Uinta arch. The source area for these mature sandstones is likely from erosion of lower Paleozoic sandstones such as the Eureka Quartzite on the Antler forebulge.

## Conclusions

Isopach maps of correlated Devonian sequences reveal the form of the Sunnyside basin, an intrashelf basin with restored dimensions similar to the Williston basin. The Sunnyside basin may be a precursor to the Antler foreland basin. It was bordered on the west by the Antler forebulge. Recycled sandstones, and perhaps insoluble residues including conodonts, from lower Paleozoic rocks were eroded from the forebulge and were deposited in the Sunnyside basin. Thick accumulations of the "Oxyoke Formation," with the first significant accumulations of quartz sandstone above the Eureka Quartzite near the Antler foreland bulge, may record the first pulse of the Antler orogeny.

*Amphipora*-bearing facies is more common on the west side of the basin and coral and stromatoporoid-bearing facies is more common on the east side of the basin. Thick, mature, quartz sandstone beds accumulated on the edges of the basin. A cosmolite impact created the Tempiute basin, a sub-basin in the south end of the Sunnyside basin, during Sequence Dgb time. The oval-shaped sub-basin is more concentric when sections are restored closer to their prethrust locations (Chamberlain, 1999).

# CHAPTER 8

# APPLICATIONS

This study has academic applications dealing with stratigraphy and structure. It also has economic implications for oil and gas, mineral, and groundwater exploration.

## Economic Applications

The new structural model presented in this report suggests considerable displacement on thrust faults in the study area thus creating viable structural targets for oil and gas. Most of the thrust faults place porous middle and lower Paleozoic carbonates on Mississippian source rocks (Chamberlain et al., 1992a). Devonian carbonates, with karsted regional unconformities, reefs, sandstones, breccias, and fractures may be the best reservoir rocks in the region (Chamberlain 1986a, b). Skarns in Devonian and Mississippian rocks associated with intrusives at Tempiute are enriched with tungsten and other metals. Silver and molybdenum mineralization favors the fractures and hydrothermal alteration associated with the Silver Canyon thrust fault. An understanding of the regional Devonian paleogeography will not only help predict reservoir and host rock trends but help predict gold occurrences. Devonian rocks in the Great Basin contain significant amounts of syngenetic gold (Emsbo et al., 1999). This section briefly reviews some economic applications of this research.

Oil and Gas Exploration

In the Golden Gate Range, organically rich, thermally mature Mississippian source rocks containing 4-6% Total Organic Carbon (TOC)(Chamberlain, 1990a) occur within the oil-generation window (Ro > 0.65)(Scott and Chamberlain, 1986; Chamberlain, 1998b). Specifically, these rocks lie in the footwall of the Golden Gate thrust fault. Devonian reefs and karsted intervals below unconformities occur in the hanging wall of large fault folds (Stop 10, Appendix D). Open fractures, perpendicular to the underlying source rocks, could have served as conduits for fluids migrating into the porous beds above. Before erosion, thousands of feet of Mississippian shales and thin beds of anhydrites draped the structure and could have served as effective regional seals over the now breached Golden Gate structure. Therefore, the Golden Gate anticline serves as a model for traps along the central Nevada Oil and Gas Fairway, a north-south trending region in east central Nevada where organic-rich Mississippian source rocks are thermally mature (Scott and Chamberlain, 1986; Chamberlain, 1988d, Chamberlain, 1999). Pine Valley, containing the Blackburn Oil Field (210 miles north, northwest of Hiko), marks the northern end of the fairway. The Nevada Test Site marks the southern end of the fairway (Trexler et al., 1999). All of the existing oil production in Nevada lies within this trend (Chamberlain, 1988a). The well exposed and well preserved Golden Gate anticline provides an excellent opportunity to study sources, reservoirs, traps, and seals that could exist in similar, unbreached structures along the fairway. The structural model presented in Chapter 5 (**Plate 4)** could serve as a template to find structures like the Golden Gate feature along strike, where they are concealed by Tertiary volcanics and valley fill.

The axis of the 15-mile-long Worthington Mountain doubly-plunging anticline is convex eastward, analogous to the giant 14-mile-long Whitney Canyon-Carter Creek Gas Field (Bishop, 1982) and the giant five-mile-long Anschutz Ranch East Field (Lelek, 1982) in the Utah-Wyoming thrust belt. The Worthington Mountain anticline provides another model for folded structures in this part of the Sevier thrust belt. It also provides an example of a folded thrust fault. Such structures could have contained significant quantities of hydrocarbons if they are not breached. Similar, unbreached structures along the Central Nevada Oil and Gas Fairway (Chamberlain, 1988b, Chamberlain et al., 1999) could contain significant hydrocarbon reserves.

Sequence Boundaries in Exploration Recognition of sequence boundaries not only provides a practical basis for correlating strata, but also guides explorationists to intervals of potential economic significance. For example, a sequence boundary expressed as a karst surface at the top of the Simonson Dolomite separates dolomites below from varied lithologies of limestone, dolomite, sandstone, megabreccia, and siltstone above. The karsted, coarsely-crystalline dolomite below the unconformity has favorable reservoir properties. Reservoir properties include interconnecting coarsely-crystalline dolomite pores, interconnecting vugs and karst cavities, and fractures that interconnect karst cavities, vugs, and coarsely-crystalline dolomite pores (Stop 7, Appendix D). Thus, it is a major hydrocarbon exploration target and could correlate to the reservoir rocks at the Grant Canyon oil field 65 miles north-northwest of Hiko.

Hulen et al. (1994) described the Grant Canyon and closely associated Bacon Flat reservoirs as vuggy, brecciated, Paleozoic dolomites. They suggested an early period (Devonian?) of fracturing followed by dissolution that could be karsting related to the regional unconformity. A later event (Tertiary?) of major brecciation and fracturing followed by dissolution described by Hulen et al. (1994) could suggest a period of reactivation of the karsted interval that enhanced the reservoir porosity.

Devonian Reefs Reefs in the Devonian Guilmette Formation are similar to those in the hydrocarbon-producing reef trend in the Alberta Basin of Canada. The reefs in the Hiko Range, up to 3,000 feet long and more than 100 feet thick (Stops 5 and 16, Appendix

D), are composed of stromatoporoids and corals. Porosity in the reefs has been enhanced by episodes of karstification and diagenetic alteration.

Devonian Porosity and Permeability Much of the Devonian section in the Timpahute area is dolomitized. Dolomitization could have either improved or destroyed porosity and permeability. Porosity in the pervasively dolomitized carbonates below the Simonson Dolomite unconformity could be similar to that of the Mississippian Burlington-Keokuk Formation in Iowa, Illinois and Missouri. Within the Burlington-Keokuk, three pervasively dolomitized microfacies comprise up to 70% of the formation and contain > 80% of the formation's pore volume (Choquette et al., 1992).

Permeability is the hardest characteristic of potential oil reservoirs to evaluate without knowledge of how the fluids interacted with the rock at burial temperatures and pressures (Longman, 1982). Outcrops provide some information about permeability, but without more exploratory drilling and testing, fluid/rock interactions at burial temperatures and pressures and subsequent diagenetic alterations are poorly known. The paucity of Devonian penetrations hinders testing various hypotheses of diagenesis of the rocks and predicting porosity and permeability trends. Compensated neutron-density logs in mature oil provinces such as the Williston basin provide the ability to trace different carbonate units through their complex facies changes across that basin. They also help distinguish limestones, dolomites, anhydrites, and even partly-dolomitized limestones and determine porosity with remarkable accuracy (Longman, 1982). Lacking these logs, surface gamma-ray logs and descriptions of outcrops in the Great Basin provide the basic information to begin to understand the complex history of Devonian sedimentation (Chamberlain, 1983).

Descriptions of porous and permeable zones such as the karst interval below the Simonson Dolomite unconformity and dolomitized reefs in Sequence Dgb provide some empirical data that may help quantify porosity and permeability in the rocks. Furthermore, descriptions and measurements of fracture patterns such as those associated with the crest of large thrust fault structures may further help quantify permeability for migration paths and reservoirs. Locally, fractured reservoirs may have developed because of the cosmolite impact into Devonian seas during Sequence Dgb time. Reservoirs in other regions that could have developed as fossil meteorite or cosmolite impacts include Viewfield field in Saskatchewan and Red Wing Creek and Newporte fields in North Dakota. In each case, a highly disturbed and brecciated crater is surrounded by a structurally high rim of highly fractured rock (Longman, 1982). The impact responsible for the Guilmette Dgb2 breccia Sequence could have also produced a similar crater.

Although most exploration is focused on structural traps, stratigraphic traps could play an important role in successful oil and gas exploration in the Great Basin. Commonly, porous dolomites in the Guilmette grade laterally into tight limestones. Porous, coarsely-crystalline Simonson Dolomites grade into tight, finely-crystalline dolomite. Development of an exploration model is partly dependent on dolomitization mechanisms. Possible mechanisms of dolomitization and descriptions of Devonian dolomite occurrences in TMS are reviewed in Chapter 4.

<u>Sevy Dolomite Reservoir Potential</u> For petroleum exploration, the Sevy Dolomite may be the poorest Devonian reservoir target in Nevada, as it lacks any visual porosity. The density of the Sevy Dolomite is an obvious attribute noticed by most field geologists. However, the correlative Beacon Peak Member of the Nevada Formation is likely the primary reservoir unit at the Blackburn Field in Pine Valley (Scott and Chamberlain, 1988a, b). Fenestral vugs do occur in the Sevy Dolomite locally. These tiny (<0.2" diameter) vugs are neither persistent, abundant, nor interconnected. They would provide a poor reservoir unless somehow enhanced in the subsurface. In areas where interstitial anhydrite is present in the Sevy Dolomite, hydrocarbon accumulation could occur because: 1) anhydrite can be diagenetically removed differentially creating secondary intercrystalline porosity; and (2) where the anhydrite remains intact, the Sevy Dolomite

may act as a competent roof seal on the underlying Laketown Dolomite or on the footwall of any age where the Sevy Dolomite occurs in a hanging wall plate.

Roof Seal Potential  All the Yellow Slope Sequence Cycles have low permeability and lack visual porosity. The tight, laminated, dolomudstones may provide a hydrocarbon roof seal above the unconformity at the top of the Fox Mountain Sequence. A thin-section of a core from Grant Canyon No. 3 at 3,961.9 feet has a striking resemblance to a Cycle 3 thin-section (MI-301 in Appendix C). It is likely they are both of the Yellow Slope Sequence because of the similarity in the stratigraphic sequence and the rare occurrence of detrital quartz grains in a dolomicrite of the lower Guilmette Formation. Nearly five hundred thin sections taken at 2.5 foot intervals of the lower Guilmette at TMS revealed no detrital sand grains between the "Oxyoke Formation" and Sequence Dgd above Dgb2 breccia except in the Yellow Slope Sequence. Therefore, the main producing reservoir at Grant Canyon is likely just below the major unconformity at the top of the Simonson Dolomite. Large cavities were encountered while drilling. This suggests that part of the prolific production from Grant Canyon may be due to karsting. Karst cavities associated with the unconformity were probably reactivated and enlarged before being charged with oil. The impermeability of the overlying Yellow Slope Sequence could be responsible for the roof seal of some oil at the Grant Canyon oil field. If the Yellow Slope Sequence functions as a reservoir seal over karsted reservoirs at the tops of the Simonson Dolomite and Fox Mountain sequences at Grant Canyon, then this model may serve as an exploration target in other prospective areas. Hulen et al. (1994) suggested that karst is not important at Grant Canyon Field. In other localities including Lake, White Pine, Coal, and Long valleys, drill stem tests and wireline logs show that the karst interval below the Simonson Dolomite unconformity is very porous; they commonly produce water with minor oil shows (Cedar Strat well files).

Mineral Exploration

Correlative with Upper Devonian Guilmette rocks in the Timpahute Range, Upper Devonian Slaven Chert rocks in the Robert Mountains allochthon, north-central Nevada, host the world's largest resources of barite in sedimentary exhalative deposits (Emsbo et al., 1999). Auriferous sedimentary exhalative deposits are hosted in the underlying autochthon. They could be the source of gold in the world-class Carlin gold trend (Emsbo et al., 1999). Therefore, a better understanding of Great Basin Devonian depositional systems could have economic significance.

The structural model presented herein provides insight into the distribution of precious metals in the greater Timpahute Range. Geochemical analyses of several hundred jasperoid occurrences in the Timpahute Range show elevated gold values in the footwall of the Chocolate Drop thrust fault (Cedar Strat proprietary data). Gold production at the old Tempiute Mining District in the late 1800's complement these analyses (Tschanz and Pampeyan, 1970). Geochemical analysis of jasperoids in the Silver Canyon thrust sheet provide only trace amounts of precious metals and their associated pathfinding elements. Pathfinding elements include Cu, As, Pb, Sb, Mo, and Zn. For example, no pathfinding elements occur in unaltered carbonates, but trace concentrations of precious metals and precious metal pathfinder elements occur in jasperoids near the Penoyer Springs thrust fault footwall contact. Higher concentrations were found in footwall jasperoids near the Silver Canyon thrust fault. Silver production came from mines along the Silver Canyon thrust fault in Silver Canyon during the late 1800's (Tingley, 1991). Silver production matches the elevated values near the thrust fault. Thus, a knowledge of structural relationships can guide exploration companies to appropriate areas for further evaluation.

Groundwater Exploration

Devonian rocks in the study area provide the major aquifer for the region. Hiko Spring and Crystal Springs both occur in the Guilmette Formation where east-west structures intersect the north-south structural grain. Hiko Spring is in the axis of the east-west trending Hiko syncline where Dgb2 breccia is in thrust fault contact with the Pilot Formation (Appendix E). The porous Dgb2 breccia serves as the aquifer in the hanging wall plate and the Pilot Formation serves as an aquitard or floor seal. The artesian spring flows about 2700 gallons per minute (E. Hansen, 1998, personal communication).

Crystal Springs flows from fractured upper Guilmette rocks near the projected position of the Crystal Springs Canyon fault (Appendix E). It flows about 5400 gallons per minute. About four miles south of the study area, Ash Springs flows about 8000 gallons per minute (B. Tanner, 1998, personal communication). Both are artesian springs.

Results of this study provide additional information on the structure and stratigraphy of this regionally important Devonian aquifer. This information coupled with well data and geophysical data could help identify potential targets for water exploitation.

Academic Applications

Results of this work have structural academic applications. For example, the concentric Tempiute basin constrains the construction of retrodeformable balanced cross sections. Also, results of this work have stratigraphic academic applications. For example, exposed stratigraphic sequences can be tied to seismic stratigraphy by correlating between surface and subsurface gamma-ray logs and tying well data to the seismic lines. Furthermore, geologic maps based on sequences rather than formations and members depict complex structures more accurately and clearly.

Structural Applications

Construction of retrodeformable balanced cross sections should involve undoing the total displacement field. However, Mukel (1998) pointed out that most restorations only account for translation and rotation components and ignore the penetrative internal deformation of thrust sheets. He also pointed out that the most accurate restorations are obtained by retrodeforming the deformation profile incrementally using strain history of the thrust sheet as a guide. Incremental strain data are not always available. Estimates of spacial variability of strain in a thrust sheet causes the cross section to be less accurate. However, the restored concentric Tempiute basin constrains assumptions and estimates of the spatial variability of strain in the thrust sheets. Thrust restoration of the Dgb2 basin provides a unique opportunity to test various thrust models. If the assumptions about the strain variations that lead to the retrodeformable balanced cross section that most closely restores the concentric Tempiute basin are regarded as correct (**Plate 4a**), they could be used to construct other cross sections in this part of the Sevier fold-and-thrust belt.

Stratigraphic Applications

Devonian sequences in the study area have characteristic gamma-ray patterns that are regionally mappable in surface and subsurface sections. As a result, surface gamma-ray logs tie exposed sequences to well logs that can be tied to seismic data. Thus, sequence stratigraphy can be tied to seismic stratigraphy with surface gamma-ray logs.

Furthermore, this study shows the utility of mapping sequences instead of formations and members in structurally complex areas (**Plate 6**). Therefore, structural stratigraphy, the application of sequence stratigraphy to solve structural problems, greatly refined the structural detail of the study area.

# CHAPTER 9

# CONCLUSIONS AND RECOMMENDATIONS

Twelve conclusions summarize this research. Because of the scope and limitations of this study, 19 recommendations suggest directions for future work.

## Conclusions

1. A well-exposed 5,000-foot-thick composite stratigraphic section, comprised of 21 mappable sequences in the greater Timpahute Range, provides a new and more detailed reference section for Devonian depositional cycles and sequences across the eastern Great Basin. A knowledge of these sequences is indispensable for mapping this complex region. For example, recognition of overturned beds associated with thrust faults in the study area was eased by applying detailed knowledge of stratigraphic sequences and shallowing-upward patterns of the carbonate cycles.

2. The Simonson Dolomite unconformity, a karsted sequence boundary, divides the pervasively dolomitized Paleozoic rocks below from undolomitized rocks above in most of the Sunnyside basin.

3. Guilmette sequences can be distinguished regionally on surface gamma-ray logs. Surface gamma-ray logs provide a way to tie exposed sequences to wells. From the wells the sequences could be tied into seismic data. Thus, exposed sequence stratigraphy can be tied to seismic stratigraphy.

4. The most common occurrence of dolomite in Devonian rocks exposed on the southwestern part of the Mail Summit and northwestern part of the Mount Irish SE 7.5' quadrangles is the finely-crystalline stratal dolomite that caps most of the shallowing-upward cycles. They are most obvious in the Guilmette Formation where the dolomite cycle caps lie on limestone bases. In the Simonson Dolomite, they are the light bands between the alternating dark bands. Most of the Sevy Dolomite is composed of finely-crystalline stratal dolomite.

5. Isopach maps of Devonian sequences and isolith maps provide insight to Devonian paleogeography. A composite isopach map of all the Devonian sequences reveals the unrestored shape of the Sunnyside basin, an intrashelf basin, that is a precursor of the Mississippian Antler basin. A sandstone isolith map shows that quartz sandstones were deposited on the edges of the basin. It also suggests that the Antler forebulge was the probable source area for Devonian quartz sandstones on the west side of the basin. Additionally, the forebulge was probably the source of Cambrian, Ordovician and Silurian conodonts and other microfossils found in Devonian carbonates of the Sunnyside basin.

6. The Sunnyside basin lies between the Antler forebulge in central Nevada and the Utah hingeline in central Utah. Sequence isopach maps show that the axis of this Antler backbulge basin migrated eastward from around Eureka, Nevada, in Early Devonian Sevy Dolomite time to western Utah by Early Mississippian Pilot Formation time.

7. Thinning of Devonian sandstones and sequences shown by regional isolith and isopach maps, and unconformities cutting out lower Paleozoic rocks beneath the Devonian-Mississippian Roberts Mountains allochthon, imply an active tectonic high on the western side of the Devonian Sunnyside basin. These maps and unconformities suggest that the “Oxyoke Formation” resulted from a siliciclastic pulse marking the onset of the Antler Orogeny.

8. The methods used to produce the new geologic map for the greater Timpahute Range took advantage of mapping, contouring, and graphic software and satellite global positioning systems. Other methods and resources that proved useful include surface gamma-ray logging, recently available low-altitude color aerial photography, and 7.5-minute topographic base maps. The application of these methods and tools and others described in Chapter 3 provide a new, more effective way to acquire geologic data and annotate and animate images and document and express the geologic data and interpretations to others. Such technology coupled with GIS mapping led to a new level of mapping efficiency, viewing, and geologic interpretation.

9. The new geologic map of the Timpahute Range quadrangle reveals many newly identified compressional features in Paleozoic rocks associated with of the Sevier compressional event (Appendix E). Thrust restoration suggests at least 30 miles of east-west crustal shortening on the Silver Canyon thrust and at least 63 miles of cumulative crustal shortening along the length of the greater Timpahute Range. When restored, the Tempiute impact crater becomes more concentric.

10. The new geologic map of the Timpahute Range quadrangle reveals abundant compressional elements of the Mesozoic Sevier fold-and-thrust belt, but failed to reveal major north-south trending faults associated with Cenozoic extension. Models of Cenozoic extension should probably be revised.

11. The new structural cross section of the greater Timpahute Range provides a template that can be used to decipher structural complexities along strike where thrust fault relationships are hidden by Tertiary cover. For example, Cenozoic cover in Coal, Garden and Sand Springs valleys conceal all but the crests of the Golden Gate and Worthington ranges north of the greater Timpahute Range. However, by projecting thrust faults northward from the greater Timpahute Range and adjusting for strike-slip faults, the

Freiburg thrust fault probably correlates to the Penoyer Springs thrust fault. It is likely that a thrust fault, correlative with the Monte Mountain thrust fault, is concealed in the Freiburg thrust footwall. The outcrop of Guilmette Formation exposed below the north Worthington fault, described in Appendix E, may be a small window into the thrust fault correlative with the Monte Mountain thrust fault.

12. Application of data and interpretations presented herein may lead to new mineral and hydrocarbon discoveries and to a better understanding of the regional Devonian carbonate groundwater aquifer. Three major sea-level lowstand events that produced regionally and economically significant karst intervals occur in the reference section of Devonian rocks at TMS.

## Recommendations

1. Detailed analysis of the Sevy Dolomite could reveal the source of dolomitizing fluids and the potential for preserved evaporites in the subsurface. It may be worth further study to learn if the Sevy Dolomite becomes sufficiently anhydritic to serve as a competent reservoir roof seal for the Laketown Dolomite.

2. Additional research, including measured sections, isotope studies, and petrographic analysis, on the “Oxyoke Formation” and Guilmette quartz sandstones could test the hypothesis that some of these sandstones were derived from the Antler forebulge and provide additional insight into the evolution of the Antler orogeny. The sandstones may be important hydrocarbon reservoir rocks in some areas.

3. Detailed stratigraphic analysis of the Devonian sequences of the TMS has led to the identification of regional karsted intervals associated with major sequence boundaries. Additional work on these karsted intervals, occurring in many sections of the region, could provide attractive targets for hydrocarbon exploration. Additional work could include more measured sections, well log analyses, petrographic analyses, etc.

4. In Chapter 4, it was suggested that an isopach map of the depth of karsting could provide a rough estimate of the paleotopography at the end of Fox Mountain time. Such a map could serve as a potential reservoir trend map for hydrocarbon exploration.

5. An isopach map and facies maps of Fox Mountain Sequences would provide additional insight into the paleotopography and nature of the Guilmette transgression.

6. The unique structural grain in eastern Nevada provides an opportunity to compare and contrast cycles over large (10's miles) distances along strike. A series of closely spaced measured sections could provide insight into the processes and causes of carbonate cycles in the Sunnyside basin.

7. This study provides the criteria for recognizing Devonian sequences in the Sunnyside basin. Using these criteria, a systematic study of recycled pre-Devonian microfossils in the sequences could shed light on the unroofing of the Antler forebulge. Of particular interest is Sequence Dgb in and beyond the Tempiute impact basin.

8. A more rigorous approach using Guilmette Dgb2 breccia isolith maps to restore thrust faults could refine the tectonic model and may provide insight into constructing retrodeformable internal thrust belt cross sections in the region.

9. Documentation of the reef at TMS and the reefs in the Hiko Range and their position in the Sunnyside basin could lead to the discovery of additional reefs on outcrops and hidden reefs buried beneath valley fill and Sevier thrust sheets. Some reefs may be important hydrocarbon reservoirs.

10. Isopach maps of each sequence provide clues to the evolution of the Sunnyside basin centered north of the study area. Further research and mapping of this basin will result in better facies maps that can be used to predict hydrocarbon reservoir rocks, depositional trends, and tectonic imprint on the rocks.

11. A rigorous analysis of coalescing sequence boundaries from the middle to the eastern edge of the Sunnyside basin would provide insight into the evolution of the basin and the effects of relative sea-level changes on the Devonian strata. Such analyses should provide trends of unconformities. Hydrocarbon reservoir rocks or seals may have formed at the unconformities

12. This study has laid the groundwork for a comprehensive analysis of dolomite in Devonian rocks of the region. Regional isotope and trace element trends could lead to a better understanding of the dolomitizing events and should provide additional information about the tectonic and diagenetic history of the region. Fluid inclusions could provide clues on timing and fluid conditions of the dolomitizing events. Identification of dolomitization processes and timing could lead to better predictions of possible hydrocarbon reservoirs and subtle mineralization trends.

13. Rigorous structural modeling that includes gravity, magnetic, seismic and new surface mapping could add insight into the region's complex structural evolution and could result in economic benefits.

14. A corollary study that will complement this work is a detailed gravity profile of the greater Timpahute Range. A rigorous structural analysis coupled with a detailed gravity and magnetic survey of the exposed greater Timpahute Range may provide a refined structural template that could help interpret the structure in fewer exposed areas along strike.

15. A more detailed study of fracture patterns within the study area should reveal additional fault patterns related to the Dgb2 impact event, Cretaceous compression, and Cenozoic extension of this part of the Sevier fold-and-thrust belt.

16. The surface gamma-ray technique developed in this study can be applied to other regions of the world to tie exposed stratigraphic sequences to sequence and seismic stratigraphy. Future work on the Great Basin Devonian rocks would benefit from detailed surface gamma-ray logs. For example, the gamma-ray signature of a sequence from where conodonts or other microfossils were collected could be correlated to gamma-ray logs of wells and outcrops where sample quality is inadequate to provide fossil zones. The definition of sequences, formations and members should include their gamma-ray signature as I suggested in 1983.

17. The technique of integrating a Global Positioning System (Trimble Pathfinder) with a Geographic Information System (*MapInfo*) used to make the geologic map of the Timpahute Range quadrangle has worldwide applications for rapid precision mapping. Additional mapping and sample collection in the Great Basin would be greatly enhanced with GPS and GIS techniques.

18. Data and interpretations presented herein may be helpful in evaluating the natural resource potential of several wilderness study areas in and near the study area. For example, extensive mapping of Nellis Air Force bombing range and the Nevada test site

should yield information on Mississippian source rocks, Devonian sequences including the Guilmette Formation Sequence Dgb2 (Alamo Breccia), Mesozoic thrust faults and associated synorogenic strata, and possible hydrocarbon and mineral prospects, when the areas are declassified and made accessible to researchers. Independent evaluation of the region may result in interpretations that contrast with those of federal geologists. For example, Barker (1999) concluded that the Nevada Test Site lacks oil and gas potential. In contrast, Trexler et al. (1999) provided evidence for oil and gas potential. Neither considered the additional potential by projecting thrust faults from the Timpahute quadrangle south, along strike to the Nevada Test Site. With further evaluation, significant hydrocarbons may be found in the Nevada Test Site region (Chamberlain, 1991).

19. All the text and figures of this dissertation fit on one compact disk. Availability of this dissertation in digital form and a comment form for suggestions and comments can be found at www.cedarstrat.com. Because it is in digital form, it is easily updated as suggestions, comments, and new data and technology become available.

## REFERENCES


Ackman, B.W., 1991, Stratigraphy of the Guilmette Formation, Worthington Mountains and Schell Creek Range, southeastern Nevada: unpublished M.S. thesis, Colorado School of Mines, Golden, 207 p.

Albright, G.R., 1991, Late Devonian and Early Mississippian paleogeography of the Death Valley region, California: *in* Cooper J.D., and Stevens, D.H., eds., Paleozoic paleogeography of the western United States-II: Pacific Section Society of Economic Paleontologists and Mineralogists, v. 67, p. 253-269.

Altschuld, N., and Kerr, S.D.Jr., 1982, Mission Canyon and Duperow reservoirs of the Billings Nose, Billings County, North Dakota: *in* Christopher, J.E., and Kaldi, J., eds., Fourth International Williston Basin symposium: Special Publication Number 6, Saskatchewan Geological Society, p. 103-112.

Ames, D.E., Watkinson, D.H., and Parrish, R.R., 1998, Dating of a regional hydrothermal system induced by the 1850 Ma Sudbury impact event: Geology, v. 26, p. 447-450.

Arabasz, W.J., and Julander, D.R., 1986, Geometry of seismically active faults and crustal deformation within the Basin and Range-Colorado Plateau transition in Utah, *in* Mayer, L., ed., Extensional tectonics of the southwestern United States: a perspective on processes and kinematics: Geological Society of America Special Paper 208, p. 75-96.

Armstrong, J.A., 1980, Correlation of Devonian rocks in southwestern Nevada--southeastern California with reference to central Nevada: unpublished Master’s thesis, California State University, Fresno, 112 p.

Armstrong, P.A., 1991, Displacement and deformation associated with a lateral thrust propagation: an example form the Golden Gate Range, southern Nevada: unpublished M.S. thesis, University of Utah, Salt Lake City, 162 p.

Armstrong, P.A., and Bartley, J.M., 1993, Displacement and deformation associated with a lateral thrust termination, southern Golden Gate Range, southern Nevada, U.S.A.: Journal of Structural Geology, v. 15, p. 721-735.

Armstrong, R.L., 1968, Sevier orogenic belt in Nevada and Utah: Geological Society of America Bulletin, v. 79, p. 429-458.

Arthur, M.A., and Garrison, R.E., 1986, Cyclicity in the Milankovitch band through geologic time: an introduction: Paleooceanography, v. 1, p. 369-372.

Asquith, D.O., 1970, Depositional topography and major marine environments, Late Cretaceous, Wyoming: American Association of Petroleum Geologists Bulletin, v. 54, p. 1184-1224.

Axen, G.J., Taylor, W.J., and Bartley, J.M., 1993, Space-time patterns and tectonic controls of Tertiary extension and magmatism in the Great Basin of the western United States: Geological Society of America Bulletin, v. 105 p. 56-76.

Axen, G.J., Wernicke, B.P., Skelly, M.F., and Taylor, W.J., 1990, Mesozoic and Cenozoic tectonics of the Sevier thrust belt in the Virgin River Valley area, southern Nevada, *in* Wernicke, B.P., ed., Basin and Range extension tectonics near the latitude of Las Vegas, Nevada: Geological Society of America Memoir 176, p. 123-153.

Baer, J.L., 1962, Geology of the Star Range, Beaver County, Utah: Brigham Young University Studies v. 9, pt. 2, p.29-52.

Baer, J.L., R.L Davis, and George, S.E., 1982, Structure and stratigraphy of the Pavant Range, central Utah: *in* Nielson, D.L., ed., Overthrust belt of Utah, 1982 Symposium and Field Conference: Utah Geological Association Publication 10, p.31-48.

Baker, W.H., 1959, Geologic setting and origin of the Grouse Creek pluton, Box Elder County, Utah: unpublished Ph.D. thesis, University of Utah, 150 p.

Barker, C.E., 1999, Middle Devonian-Mississippian stratigraphy on and near the Nevada Test Site: implications for hydrocarbon potential: discussion: American Association of Petroleum Geologists, v. 83, p. 519-522.

Barosh, J.P., 1960, Beaver Lake Mountains, Beaver County, Utah: Utah Geological and Mineral Survey Bulletin 68, 89 p.

Bartley, J.M., Axen, G.J., Taylor, W.J., and Fryxell, J.E., 1988, Cenozoic tectonics of a transect through eastern Nevada near 38º N. latitude, *in* Weide, D.L., and Faber, M.I., eds., This extended land, geological journeys in the souther Basin and Range: Geological Society of America Cordilleran Section Field Trip Guide, p. 1-20.

Bates, R.L., and Jackson, J.A., 1987, Glossary of geology: American Geological Institute, third edition, 788 p.

Baum, G.R., and Vail, P.R., 1988, Sequence stratigraphic concepts applied to Paleogene outcrops, Gulf and Atlantic basins, *in* Wilgus, C.K., ed., Sea-level changes: an integrated approach: Society of Economic Paleontologists and Mineralogists Special Publication 42, p. 309-328.

Beales, F.W., and Hardy, J.L., 1980, Criteria for the recognition of diverse dolomite types with an emphasis on studies on host rocks for Mississippi Valley-type ore deposits: *in* Zenger, D.H., Dunham, J.B., and Ethington, R.L., eds. Concepts and models of dolomitization: Society of Economic Paleontologists and Mineralogists Special Publication 22, p. 197-213.

Beck, A.S., 1981, Stratigraphic analysis, Lippincott member, Lost Burro Formation, California-Nevada: unpublished Master's thesis, California State University, Fresno, 149 p.

Bereskin, S.R., 1982, Middle and Upper Devonian stratigraphy of portions of southern Nevada and southeastern California: *in* Powers, R.B., ed., Geologic studies of the Cordilleran thrust belt: Rocky Mountain Association of Geologists, p.751-764.

Berry, W.B.N., 1977, Great Basin Devonian western assemblage rocks, *in* Murphy, M.A., Berry, W.B.N., and Sandberg, C.A., eds., Western North America: Devonian: University of California, Riverside, Campus Museum Contribution 4, p. 204-219.

Best, M.G., Scott, R.B., Rowley, P.D., Swadley, W.C., Anderson, R.E., Gromme, C.S., Harding, A.E., Deino, A.L., Christiansen, E.H., Tingey, G., and Sullivan, K.R., 1993, Oligocene-Miocene caldera complexes, ash-flow sheets, and tectonism in the central and southeastern Great Basin, *in* Lahren, M.M., Trexler, J.H.Jr., and Spinosa, C., eds., Crustal evolution of the Great Basin and the Sierra Nevada: Cordilleran/Rocky Mountain sections of the Geologic Society America Field Trip Guide, p. 285-312.

Beus, S.S., 1965, Devonian faunule from the Jefferson Formation, central Blue Springs Hills, Utah-Idaho: Journal of Paleontology, v. 39, p. 21-30.

Beus, S.S., 1980, Late Devonian (Frasnian) paleogeography and paleoenvironments in northern Arizona, *in* Fouch, T.D., and Magathan, E.R., Rocky Mountain Paleography Symposium 1 Paleozoic Paleogeography of the west-central U.S.: Rocky Mountain section of the Society of Economic Paleontologists and Mineralogists, p. 55-69.

Bick, K.F., 1959, Stratigraphy of Deep Creek Mountains, Utah: American Association of Petroleum Geologists Bulletin, v.43, p.1064-1069.

Biller, E.J., 1976, Stratigraphy and petroleum possibilities of lower Upper Devonian (Frasnian and lower Famennian) Strata, southwestern Utah, U.S. Geological Survey open-file report 75-343, 105 p.

Bishop, R.A., 1982, Whitney Canyon-Carter Creek gas field southwest Wyoming: *in* Powers, R.B.I., ed. Geologic Studies of the Cordilleran thrust belt: Rocky Mountain Association of Geologists, p. 591-599.

Bissell, H.J., Rigby, J.K., Proctor, P.D., and Moyle, R.W., 1959, Geology of the southern Oquirrh Mountains and Five-Mile Pass--northern Boulter Mountain area, Tooele and Utah Counties, Utah: Utah Geological Society Guidebook, no. 14, 262 p.

Blair, T.C., and McPherson, J.G., 1999, Grain-size and texture classification of coarse sedimentary particles: Journal of Sedimentary Research, v. 69, p. 6-19.

Blue, D.M., 1960, Geology and ore deposits of the Lucin Mining District, Box Elder county, Utah, and Elko County, Nevada: unpublished M.S. thesis, University of Utah, 162 p.

Bohannon, R.G., 1983, Mesozoic and Cenozoic tectonic development of the Muddy, North Muddy, and northern Black Mountains, Clark County, Nevada, *in* Miller, D.M., Todd, V.R., and Howard, K.A., eds., Tectonic and stratigraphic studies in the eastern Great Basin: Geological Society of America Memoir 157, p. 125-148.

Bond, G.C., and Kominz, M.A., 1984, Construction of tectonic subsidence curves for the early Paleozoic miogeocline, southern Canadian Rocky Mountains; Implications for subsidence mechanisms, age of breakup, and crustal thinning: Geological Society of America Bulletin, v. 95, p. 155-173.

Bortz, L.C., 1998, Blackburn oil field, Pine Valley, Nevada--a case history update: Nevada Petroleum Society Newsletter, v. 13, issue 2, p. 1-2.

Bortz, L.C., and Murray, D.K., Eagle Springs oil field, Nye County, Nevada, *in* Newman, G.W., and Goode, H.D., eds., Basin and Range Symposium: Rocky Mountain Association of Geologists and Utah Geological Association, p. 441-453.

Boucot, A.J., and Potter, A.W., 1977, Middle Devonian orogeny and biogeographical relations in areas along the North American rim, *in* Murphy, M.A., Berry, W.B.N., and Sandberg, C.A., eds., Western North America: Devonian: University of California, Riverside, Campus Museum Contribution 4, p. 210-219.

Boyer, S.E. and Elliot, D., 1982, Thrust systems: American Association of Petroleum Geologists Bulletin, v. 66, p. 1196-1230.

Brown, H.J., 1991, Stratigraphy and Paleogeographic setting of Paleozoic rocks in the San Bernardino Mountains, California *in* Cooper, J.D. and Stevens, C.H., Paleozoic paleogeography of the western United States-II: Pacific Section Society Economic Paleontologists and Mineralogists, v. 1, p. 193-208.

Buelter, D.P., and Guillemette, R.N., 1988, Geochemistry of epigenetic dolomite associated with lead-zinc mineralization of the Viburnum trend, southeast Missouri: a reconnaissance study, *in* Shukla, V., and Baker, P.A., eds., Sedimentology and geochemistry of dolostones: Society of Economic Paleontologists and Mineralogists Special Publication 43, p. 85-93.

Burchfiel, B.C., 1961, Structure and stratigraphy of the Specter Range quadrangle, Nye County, Nevada: unpublished Ph.D. thesis, Yale University, 197 p.

Burchfiel, B.C., 1964, Precambrian and Paleozoic stratigraphy of Specter Range Quadrangle, Nye County, Nevada: American Association of Petroleum Geologists Bulletin, v. 48, p. 40-56.

Burke, R.B., and Stefanosvsky, G.L., 1984, Porosity types, geometry and interpore minerals of the lower Duperow Formation, Billings nose area, Williston Basin, North Dakota: *in*: Christopher, J.E., and Kaldi, J., eds., Fourth International Williston Basin symposium: Special Publication Number 6, Saskatchewan Geological Society, p. 92-100.

Calkins, F.C., and Butler, B.S., 1943, Geology and ore deposits of the Cottonwood American Fork District, Utah: U.S. Geological Survey Professional Paper 201, 150 p.

Cameron, G., and Chamberlain, A.K., 1987, Reevaluation of late Mesozoic thrusting in east-central Nevada: American Association of Petroleum Geologists Bulletin v. 71, p. 536.

Cameron, G., and Chamberlain, A.K., 1988, Delineation of late Mesozoic thrust belt in east-central Nevada: Geological Society of America, Cordilleran Section, 84th annual meeting. Abstracts-with-Programs, Geological Society of America, v. 20, p. 148.

Camilleri, P.A., 1999, Reevaluation of metamorphic “klippen” in the Diamond Mountains, Nevada and the implications for Mesozoic (?) Shortening and Cenozoic extension: Rocky Mountain Association of Geologists, The Mountain Geologist, *in press*.

Carlisle, D., Murphy, M.A., Nelson, C.A., and Winterer, E.L., 1957, Devonian stratigraphy of Sulphur Springs and Pinyon ranges, Nevada: American Association of Petroleum Geologists Bulletin, v. 41, p. 2175-2191.

Carpenter, D.G., and Carpenter, J.A., 1994a, Fold-thrust structure, synorogenic rocks, and structural analysis of the north Muddy and Muddy Mountains, Clark County, Nevada: southern Nevada, southwest Utah, and northwest Arizona: *in* Dobbs, S.W., and Taylor, W.J., eds., Structural and stratigraphic investigations and petroleum potential of Nevada, with special emphasis south of the Railroad Valley producing trend: Nevada Petroleum Society Conference Volume II, p. 65-94.

Carpenter, D.G., Carpenter, J.A., Dobbs, S.W., and Stuart, C.K., 1993, Regional structural synthesis of the Eureka fold-and-thrust belt, east-central Nevada: *in* Gillespie, C.W., ed., Structural and stratigraphic relationships of Devonian reservoir rocks, east central Nevada: 1993 Field trip Guidebook, Nevada Petroleum Society, Reno, Nevada, p. 59-72.

Carpenter, J.A., 1997, Antler tectonic system and global analogs in the Mediterranean and Asia: American Association of Petroleum Geologists Annual Convention, Abstracts with programs, p. A17-A18.

Carpenter, J.A., and Carpenter, D.G., 1994b, Analysis of basin-range and fold-thrust structure, and reinterpretation of the Mormon Peak detachment and similar features as gravity slide systems: southern Nevada, southwest Utah, and northwest Arizona: *in* Dobbs, S.W., and Taylor, W.J., eds., Structural and stratigraphic investigations and petroleum potential of Nevada, with special emphasis south of the Railroad Valley producing trend: Nevada Petroleum Society Conference Volume II, p. 15-52.

Carpenter, J.A., Carpenter, D.G., and Dobbs, S.W., 1993a, Structural analysis of the Pine valley area, Nevada: *in* Gillespie, C.W., ed., Structural and stratigraphic relationships of Devonian reservoir rocks, east central Nevada: 1993 Field trip Guidebook, Nevada Petroleum Society, Reno, Nevada, p. 9-49.

Carpenter, J.A., Carpenter, D.G., and Dobbs, S.W., 1993b, Fault reactivation and deactivation in the Basin-Range, western United States: *in* Gillespie, C.W., ed., Structural and stratigraphic relationships of Devonian reservoir rocks, east central Nevada: 1993 Field trip Guidebook, Nevada Petroleum Society, Reno, Nevada, p. 73-87.

Carpenter, J.A., Carpenter, D.G., and Dobbs, S.W., 1994, Antler Orogeny: Paleostructural analysis and constraints on plate tectonic models with a global analogue in southeast Asia: *in* Dobbs, S.W., and Taylor, W.J., eds., Structural and stratigraphic investigations and petroleum potential of Nevada, with special emphasis south of the Railroad Valley producing trend: Nevada Petroleum Society Conference Volume II, p. 187-240.

Carr, M.D., 1980, Upper Jurassic to Lower Cretaceous (?) Synorogenic sedimentary rocks in the southern Spring Mountains, Nevada: Geology, v. 8, p. 385-389.

Castonguay, S., and Price, R.A., 1995, Tectonic heredity and tectonic wedging along an oblique hanging wall ramp: the southern termination of the Misty thrust sheet, southern Canadian Rocky Mountains: Geological Society of America Bulletin, v. 107, p. 1304-1316.

Chafetz, H.S., and Zhang, J., 1998, Authigenic euhedral megaquartz in a Quaternary dolomite: Journal of Sedimentary Research, v. 68, p. 994-100.

Chamberlain, A.K., 1981, Biostratigraphy of the Great Blue Formation: Brigham Young University Geology Studies. v. 28, p. 8-17.

Chamberlain, A.K., 1983, Surface gamma-ray logs: a correlation tool for frontier areas: American Association of Petroleum Geologists Bulletin, v. 68, p. 1040-1043.

Chamberlain, A.K., 1986a, A new Paleozoic play in East Great Basin: American Association of Petroleum Geologists Bulletin, v. 70, p. 1034.

Chamberlain, A.K., 1986b, New Paleozoic play in East Great Basin: Oil and Gas Journal. v. 84, no. 38, p. 52-54.

Chamberlain, A.K., 1987, Depositional environments and hydrocarbon occurrence of Mississippian Antler basin, Nevada and Utah: American Association of Petroleum Geologists Bulletin v. 71, p. 1002-1003.

Chamberlain, A.K., 1988a, Petroleum exploration in Nevada, then and now: Geological Society of America, Cordilleran Section, 84th annual meeting; Abstracts with Programs, 20, p. 149.

Chamberlain, A.K., 1988b, A Mississippian thermal maturation map of the eastern Great Basin illustrates regions of thermal and tectonic events: Geological Society of America, Rocky Mountain Section, 43rd annual meeting; Abstracts with Programs, v. 22, p. 5-6.

Chamberlain, A.K., 1988c, Three lobes of higher organic content may be related to three Mississippian Antler basin delta systems, Utah and Nevada: Geological Society of America, Rocky Mountain Section, 43rd annual meeting; Abstracts with Programs, v. 22, p. 5.

Chamberlain, A.K., 1988d, Depositional environments and hydrocarbon occurrence of the Mississippian Antler basin, Nevada and Utah: Geological Society of America, Cordilleran Section, 84th annual meeting; Abstracts with Programs, v 20, p. 149.

Chamberlain, A.K., 1990a, Three lobes of higher organic content may be related to three Mississippian Antler basin delta systems, Utah and Nevada: American Association of Petroleum Geologists Bulletin, v. 74, p. 1319.

Chamberlain, A.K., 1990b, Stigmaria; indicator for erosional surfaces of low sea level stands in the Mississippian Antler basin, Utah and Nevada: American Association of Petroleum Geologists Bulletin, v. 74, p. 1319.

Chamberlain, A.K., 1990c, A Mississippian thermal maturation map of the eastern Great Basin illustrates regions of thermal and tectonic events: American Association of Petroleum Geologists Bulletin, v. 74, p. 1318.

Chamberlain, A.K., 1991, Yucca Mountain, high-level nuclear waste repository over a billion barrel oil field?: American Association of Petroleum Geologists Bulletin, v 75, p.3, p. 551.

Chamberlain, A.K., 1998, Rapid precision mapping: American Association of Petroleum Geologists National Convention, Salt Lake City Abstracts with Programs, p. 82.

Chamberlain, A.K., 1999, Thrusted Devonian Tempiute meteorite crater, Nevada: American Association of Petroleum Geologists National Convention, San Antonio, Texas, Abstracts with Programs, p. A23.

Chamberlain, A.K., and Birge, B.P., 1997, Devonian Sunnyside Basin, Nevada: American Association of Petroleum Geologists Abstract Volume, p. A19.

Chamberlain, A.K., and Chamberlain, R.L., 1990, Monte Mountain Thrust, additional confirmation of the central Nevada thrust: American Association of Petroleum Geologists Bulletin v. 74, p. 626.

Chamberlain, A.K., Chamberlain, R.L., and Roeder, D., 1992a, Oil and gas exploration of the central Nevada thrust belt: American Association of Petroleum Geologists, 1992 annual convention; Abstracts with Programs, p.18-19.

Chamberlain, A.K., Chamberlain, R.L., and Roeder, D., 1992b, Tertiary/Cretaceous syntectonic sediments of the central Nevada thrust belt: American Association of Petroleum Geologists, 1992 annual convention; Abstracts with Programs, p. 19.

Chamberlain, A.K., and Gillespie, C.W., 1993, Evidence of late Mesozoic thrusting, Timpahute Range, south-central Nevada, *in* C.W. Gillespie, ed., Structural and stratigraphic relationships of Devonian reservoir rocks, east-central Nevada: 1993 Field trip Guidebook, Nevada Petroleum Society, Reno, Nevada, p. 139-155.

Chamberlain, A.K., Graham, A.T., and Connelly, M.S., 1999, Channel sandstones, Mississippian Antler basin, Nevada: American Association of Petroleum Geologists National Convention, San Antonio, Texas, Abstracts with Programs, p. A22-23.

Chamberlain, A.K., Hook, S.C., and Frost, K.R., 1996, Digital field trip to the Central Nevada thrust belt: American Association of Petroleum Geologists 1996 annual convention; Abstracts with Programs, p. 25.

Chamberlain, A.K., and Warme, J.E., 1996, Devonian sequences and sequence boundaries, Timpahute Range, Nevada: *in* Longman, M.W., and Sonnenfeld, M.D., eds., Paleozoic Systems of the Rocky Mountain Region: Rocky Mountain Association of Geologists and SEPM (Society for Sedimentary Geology), p. 63-84.

Chamberlin, T.C., 1897, The method of multiple working hypotheses: Journal of Geology, v. V, p. 837-848.

Chan, M.A., 1999, Triassic loessite of north-central Utah: stratigraphy, petrophysical character, and paleoclimate implications: Journal of Sedimentary Research, v. 69, p. 477-485.

Choquette, P.W., Cox, A., and Meyers, W.J., 1992, Characteristics, distribution and origin of porosity in shelf dolostones: Burlington-Keokuk Formation (Mississippian), U.S. mid-continent: Journal of Sedimentary Research, v. 62, p. 167-189.

Coats, R.R., 1987, Geology of Elko County, Nevada: Nevada Bureau of Mines and Geology Bulletin 101, 112 p.

Cohenour, R.E., 1959, Sheeprock Mountains, Precambrian and Paleozoic stratigraphy, igneous rocks, structure, geomorphology, and economic geology: Utah Geological and Mineral Survey Bulletin 63, 201 p.

Compton, J.S., 1988, Sediment composition and precipitation of dolomite and pyrite in the Neogene Monterey and Sisquoc Formations, Santa Maria basin area, California, *in* Shukla, V., and Baker, P.A., eds., Sedimentology and geochemistry of dolostones: Society of Economic Paleontologists and Mineralogists Special Publication 43, p. 53-64.

Constenius, K.N., 1996, Late Paleogene extensional collapse of the Cordilleran foreland fold-and-thrust belt: Geological Society of America Bulletin, v. 108, p. 20-39.

Cook, H.E., and Taylor, M.E., 1985, Paleozoic carbonate continental margin: facies transitions, depositional processes and exploration models--the Basin and Range Province: American Association of Petroleum Geologists Field Seminar, 177 p.

Cornwall, H.R., and Kleinhampl, F.J., 1960, Preliminary geologic map of the Bare Mountain Quadrangle, Nye county, Nevada: U.S. Geological Survey Map MF-239.

Costain, J.K, 1960, Geology of the Gilson Mountains and vicinity, Juab County, Utah: unpublished Ph.D. dissertation, University of Utah, 139 p.

Cowell, P.F., 1986, Structure and stratigraphy of part of the northern Fish Creek Range, Eureka County, Nevada: unpublished MS thesis, Oregon State University, Corvallis, 96 p.

Crosby, G.W., 1959, Geology of the South Pavant Range, Millard and Sevier Counties, Utah: Brigham Young University Research Studies, Geology Series v.6, n.3, p.59.

Currie, B.S., 1997, Sequence stratigraphy of nonmarine Jurassic-Cretaceous rocks, central Cordilleran foreland-basin system: Geological Society of America Bulletin, v. 109, p. 1206-1222.

Dahlstrom, C.D.A., 1969, Balanced cross sections: Canadian Journal of Earth Sciences, v. 6, p. 743-757.

Dahlstrom, C.D.A., 1977, Structural geology I the eastern margin of the Canadian Rocky Mountains: *in* Heisey, E.L., Lawson, D.E., Norwood, E.R., Wach, P.H., and Hale, L.A., eds., Rocky Mountain thrust belt geology and resources: Wyoming Geological Association 29th annual field conference in conjunction with Montana geological Society and Utah Geological Society, p. 407-439.

Decals, P.G., 1994, Late Cretaceous-Paleocene synorogenic sedimentation and kinematic history of the Sevier thrust belt, northeast Utah and southwest Wyoming: Geological Society of America Bulletin, v. 106, p. 32-56.

Decals, P.G., and Mitra, G., 1995, History of the Sevier orogenic wedge in terms of critical taper models, northeast Utah and southwest Wyoming: Geological Society of America Bulletin, v. 107, p. 454-462.

Decker, R.W., 1953, Geology of southern Centennial Range, Elko County, Nevada: Unpublished Ph.D. dissertation, Colorado School of Mines, 150 p.

Dilles, J.H., and Gans, P.B., 1995, The chronology of Cenozoic volcanism and deformation in the Yerington area, western Basin and Range and Walker Lane: Geological Society of America, v. 107, p. 474-486.

Dix, G.R., 1993, Patterns of burial and tectonically controlled dolomitization in an Upper Devonian fringing-reef complex: Leduc Formation, Peace River Arch area, Alberta, Canada: Journal of Sedimentary Research, v. 63, p. 628-640.

Dolly, E.D., 1979, Geologic techniques utilized in Trap Spring field discovery, Railroad Valley, Nye County, Nevada, *in* Newman, G.W., and Goode, H.D., eds., Basin and Range Symposium: Rocky Mountain Association of Geologists and Utah Geological Association, p. 455-467.

Donovan, J.T., 1951, Devonian rocks of the Confusion Basin and vicinity, *in* Guidebook to the geology of Utah, Intermountain Association of Petroleum Geologists guidebook second annual field conference, Geology of the Canyon, House and Confusion Ranges, Millard County, Utah, (Guidebook to the Geology of Utah, no. 6), p.47-53.

Dott, R.H., 1955, Pennsylvanian stratigraphy of Elko and northern Diamond Ranges, northeastern Nevada: American Association of Petroleum Geologists, v. 39, p. 2211-2305.

Drummond, C.N., and Wilkinson, B.H., 1993, Carbonate cycle stacking patterns and hierarchies of orbitally forced eustatic sea level change: Journal of Sedimentary Research, v. 63, p. 369-377.

DuBray, E.A., and Hurtubise, D.O., 1994, Geologic map of the Seaman Range, Lincoln and Nye Counties, Nevada: U.S. Geological Survey, Miscellaneous Investigation map I-2282.

Duey, H.D., 1979, Trap Spring oil field, Nye County, Nevada: *in* Newman, G.W., and Goode, H.D., eds., Basin and Range Symposium and Great Basin field Conference: Rocky Mountain Association of Geologists and Utah Geological Association, p. 469-476.

Dunham, J.B., and Olson, E.R., 1978, Diagenetic dolomite formation related to Paleozoic paleogeography of the Cordilleran miogeocline in Nevada: Geology, v. 33, p. 556-559.

Dunham, J.B., and Olson, E.R., 1980, Shallow subsurface dolomitization of subtidally deposited carbonate sediments in the Hanson Creek formation (Ordovician-Silurian) of central Nevada: *in* Concepts and models of dolomitization, Zenger, D.H., Dunham, J.B., and Ethington, R.L., eds., Society of Economic Paleontologists and Mineralogists Special Publication 22, p. 139-161.

Dunham, R.J., 1962, Classification of carbonate rocks according to depositional texture: *in* Ham, W.E. ed., Classification of carbonate rocks: American Association of Petroleum Geologists, Memoir 1, p. 108-121.

Dunn, M.J., 1979, Depositional history and peleoecology of an Upper Devonian (Frasnian) bioherm Mount Irish, Nevada: unpublished M.S. thesis, State University of New York at Binghamton, 133p.

Eardley, A.J., 1944, Geology of the north-central Wasatch Mountains: Geological Society America Bulletin, v.55, p.819-94.

Edwards, B.R., and Russell, J.K., 1999, Northern Cordilleran volcanic province: a northern Basin and Range?: Geology, v. 27, p. 243-246.

Effimoff, I., and Pinezich, A.R., 1986, Tertiary structural development of selected basins: Basin and Range Province, northeastern Nevada, *in* Mayer, L., ed., Extensional tectonics of the southwestern United States: a perspective on processes and kinematics: Geological Society of America Special Paper 208, p. 31-42.

Einsele, G., 1982, Limestone-marl cycles (periodites): diagnosis, significance, causes- a review, *in* Einsele, G., and Seilacher, A., Cyclic and event stratification: Springer-Verlag, New York, p. 8-53.

Ekren, E.B., Rogers, C.L., and Dixon, G.L., 1973, Geologic and Bouguer Gravity Map of the Reveille Quadrangle, Nye County, Nevada, U.S. Geological Survey Map I-806.

Elison, M.W., 1991, Intracontinental contraction in western North America: continuity and episodicity: Geological Society of America Bulletin, v. 103, p. 1226-1238.

Elrick, M., 1986, Depositional and diagenetic history of the Devonian Guilmette Formation southern Goshute Range, Elko, County, Nevada: unpublished MS thesis, Oregon State University, Corvallis, 109 p.

Elrick, M., 1995, Cyclostratigraphy of Middle Devonian carbonates of the eastern Great Basin: Journal of Sedimentary Research, v. B65, p. 61-79.

Elrick, M., 1996, Sequence stratigraphy and platform evolution of Lower-Middle Devonian carbonates, eastern Great Basin: Geological Society of America Bulletin, v. 108, p. 392-416.

Emsbo, P., Hutchinson, R.W., Hofstra, A.H., Volk, J.A., Bettles, K.H., Baschuk, G.J., and Johnson, C.A., 1999, Syngenetic Au on the Carlin trend: implications for Carlin-type deposits: Geology, v. 27, p. 59-62.

Erken, E.B., Bucknam, R.R.C., Carr, W.J., Dixon, G.L., and Quinlivan, W.D., 1976, East-trending structural lineaments in central Nevada: U.S. Geological Survey, Professional Paper 986, p. 16.

Erskine, M.C., 1999, The Oquirrh basin revisited: reply: American Association of Petroleum Geologists, v. 83, p. 367-369.

Estes, J.E., 1992, Stratigraphy of the Devonian Guilmette Formation, Pahranagat Range, Lincoln County, Nevada: unpublished M.S. thesis, Colorado School of Mines, Golden, 94 p.

Farmer, G.L., and Ball, T.T., 1997, Sources of Middle Proterozoic to Early Cambrian siliciclastic sedimentary rocks in the Great Basin: a Nd isotope study: Geological Society of America Bulletin, v. 109, p. 1193-1205.

Farr, M.R., 1992, Geochemical variation of dolomite cement within the Cambrian Bonneterre Formation, Missouri: evidence for fluid mixing: Journal of Sedimentary Research, v. 62, p. 636-651.

Felix, C.E., 1956, Geology of the eastern part of the Raft River Range, Box Elder County, Utah, *in* Guidebook to the geology of Utah, n.11: Utah Geological Society, p. 76-97.

Ferguson, H.G., 1952, Paleozoic of Western Nevada: Washington Academy of Science Journal, v.42, n.3, p.72-74.

Ferguson, H.G., and Muller, S.W., 1949, Structural geology of the Hawthorne and Tonopah Quadrangles, Nevada: U.S. Geological Survey Professional Paper 216, p.55.

Fermor, P., 1999, Aspects of the three-dimensional structure of the Alberta Foothills and Front Ranges: Geological Society of America Bulletin, v. 111, p. 317-346.

Finney, S.C., Berry W.B.N., Cooper, J.D., Ripperdan, R.L., Sweet, W.C., Jacobson, S.R., Soufiane, A., Achab, A., and Noble, P.J., 1999, Late Ordovician mass extinction: a new perspective from stratigraphic sections in central Nevada: Geology, v. 27, p 215-218.

Fischer, H.J., 1988, Dolomite diagenesis in the Metaline Formation, northeastern Washington State, *in* Shukla, V., and Baker, P.A., eds., Sedimentology and geochemistry of dolostones: Society of Economic Paleontologists and Mineralogists Special Publication 43, p. 209-219.

Flugel, E., 1982, Microfacies analysis of limestones: translated by Christenson, K., Springer-Verlag, Berlin-Heidleberg-New York, 633 p.

Folk, R.L., 1962, Spectral classification of limestone types: *in* Ham, W.E., ed., Classification of carbonate rocks: American Association of Petroleum Geologists, Memoir 1, p. 62-84.

Foster, N.H., 1979, Geomorphic exploration used in the discovery of Trap Spring oil field, Nye County, Nevada, *in* Newman, G.W., and Goode, H.D., eds., Basin and Range Symposium: Rocky Mountain Association of Geologists and Utah Geological Association, p. 477-486.

Foster, N.H., Howard, E.L., Meissner, F.F., and Veal, H.K., 1979, The Bruffey oil and gas seeps, Pine Valley, Eureka County, Nevada: *in* Newman, G.W., and Goode, H.D., eds., Basin and Range Symposium and Great Basin field Conference: Rocky Mountain Association of Geologists and Utah Geological Association, p. 531-540.

Fouch, T.D., Hanley, J.H., and Forester, R.M., 1979, Preliminary correlation of Cretaceous and Paleogene lacustrine and related nonmarine sedimentary and volcanic rocks in parts of the eastern Great Basin of Nevada and Utah, *in* Newman, G.W., and Goode, H.D., eds., Basin and Range Symposium and Great Basin field Conference: Rocky Mountain Association of Geologists and Utah Geological Association, p. 395-312.

Fouch, T.D., Lund, K., Schmitt, J.G., Good, S.C., and Hanley, J.H., 1991, Late Cretaceous(?) basins in the region of the Egan and Grant ranges, and White river and Railroad valleys, Nevada: their relation to Sevier and Laramide contractional basins in the southern Rocky Mountains and Colorado Plateau, *in* Flanigan, D.M.H., Hansen, M., and Flanigan, T.E., eds., Geology of White River Valley and western Egan Range, Nevada: Nevada Petroleum Society 1991 Field trip Guidebook, p. 15-23.

Frank, J.R., Cluff, S., Bauman, J.M., 1982, Painter Reservoir, East Painter Reservoir and Clear Creek fields, Uinta County, Wyoming: *in* Powers, R.B., ed., Geologic Studies of the Cordilleran thrust belt: Rocky Mountain Association of Geologists, p. 601-611.

Friedman, G.M., 1990, Dolomite is an evaporite mineral: evidence from the rock record and from sea-marginal ponds of the Red Sea: *in* Concepts and models of dolomitization, Zenger, D.H., Dunham, J.B., and Ethington R.L., eds., Society of Economic Paleontologists and Mineralogists Special Publication 22, p. 69-80.

Friedman, G.M., 1995, A reappraisal of dolomite abundance and occurrence in the Phanerozoic--discussion: Journal of Sedimentary Research, v. A65 p. 244-245.

Friedman, G.M., and Sanders, J.E., 1967, Origin and occurrence of dolostones *in* Chilingar, G.V., Bissell, H.J., and Faribridge, R.W., eds., Carbonate Rocks: Elsevier Publishing Company, New York, 267-348.

Fueten, F., and Redman, D.J., 1997, Documentation of a 1450 Ma contractional orogeny preserved between the 1850 Ma Sudbury impact and the 1 Ga Grenville orogenic fron, Ontario: Geological Society of America Bulletin, v. 109, p. 268-279.

Furlong, K.P., and Londe, M.D., 1986, Thermal-mechanical consequences of Basin and Range extension, *in* Mayer, L., ed., Extensional tectonics of the southwestern United States: a perspective on processes and kinematics: Geological Society of America Special Paper 208, p. 23-30.

Geslin, J.K., 1994, Carbonate pseudomatrix in mixed siliciclastic-carbonate turbidite from the Oquirrh-Wood River basin, southern Idaho: Journal of Sedimentary Research, v. A64, p. 55-58.

Geslin, J.K. 1998, Distal ancestral Rocky Mountains tectonism: evolution of the Pennsylvanian-Permian Oquirrh-Wood River basin, southern Idaho, Geological Society of America Bulletin, v. 110, p. 644-663.

Geslin, J.K., Link, P.K., Mahoney, J.B., and Burton, B.R., 1999, The Oquirrh basin revisited: Discussion: American Association of Petroleum Geologists Bulletin, v. 83, p. 362-366.

Giles, K.A., 1994, Stratigraphic and tectonic framework of the Upper Devonian to lowermost Mississippian Pilot Formation Basin in east-central Nevada and Western Utah: *in* Dobbs, S.W., and Taylor, W.J., eds., Structural and stratigraphic investigations and petroleum potential of Nevada, with special emphasis south of the Railroad Valley producing trend: Nevada Petroleum Society Conference Volume II, p. 165-185.

Giles, K.A., 1996, Tectonically forced retrogradation of the Lower Mississippian Joana Limestone, Nevada and Utah: *in* Longman, M.W., and Sonnenfeld, M.D., eds., Paleozoic Systems of the Rocky Mountain Region: Rocky Mountain Association of Geologists and SEPM (Society for Sedimentary Geology), p. 154-164.

Ginsburg, R.N., 1991, Controversies about stromatolites: vices and virtues: Controversies in Modern Geology, Academic Press, p. 25-36.

Glikson, A.Y., 1999, Oceanic-impacts and crustal evolution: Geology, v. 27, p. 387-390.

Goddard, E.N., Trask, P.D., DeFord, R.K., Rove, O.N., Singewald J.T.Jr., and Overbeck, R.M., 1984, Rock-Color Chart: National Research Council and The Geological Society of America.

Goldhammer, R.K., Lehmann, P.J., and Dunn, P.A., 1993, the origin of high-frequency platform carbonate cycles and third-order sequences (Lower Ordovician El Paso Gp, West Texas): Constraints from outcrop data and stratigraphic modeling: Journal of Sedimentary Research, v. 63, p. 318-359.

Goldstrand, P.M., 1992, Evolution of Late Cretaceous and Early Tertiary basins of southwest Utah based on clastic petrology: Journal of Sedimentary Research, v. 62, p. 495-507.

Goldstrand, P.M., 1994, Tectonic development of Upper Cretaceous to Eocene strata of southwestern Utah: Geological Society of America Bulletin, v. 106 p. 145-154.

Goodwin, P.W., and Anderson, E.J., 1985, Punctuated aggradational cycles: a general hypothesis of episodic stratigraphic accumulation: The Journal of Geology, v. 93, p. 515-533.

Granger, A.E., 1953, Stratigraphy of the Wasatch Range near Salt Lake City, Utah: U.S. Geological Survey Circular 296, 14 p.

Gretener, P.E., 1972, Thoughts on overthrust faulting in a layered sequence: Bulletin of Canadian Petroleum Geology, v. 20, p. 583-607.

Gupta, S., and Allen, P.A., 1999, Fossil shore platforms and drowned gravel beaches: evidence of high-frequency sea-level fluctuations in the distal Alpine foreland basin: Journal of Sedimentary Research, v. 69, p. 394-413.

Guth, P.L., Schmidt, D.L., Deibert, J., and Yount, J.C., 1988, Tertiary extensional basins of northwestern Clark County, Nevada, *in* Weide, D.L., and Faber, M.I., eds., This extended land, geological journeys in the souther Basin and Range: Geological Society of America Cordilleran Section Field Trip Guide, p. 239-254.

Gwinn, V.E., 1964, Thin-skinned tectonics in the plateau of northwestern Valley and Ridge provinces of the central Appalachians: Geological Society of America Bulletin, v. 75, p. 863-900.

Hague, A., and Emmons. S.F., 1877, Descriptive geology: U.S. Geological Exploration, 40$^{th}$ Parallel Rport, v. 2.

Hamblin, W.K., 1985, The Earth’s dynamic systems a textbook in physical geology, fifth edition: MacMillian Publishing Company, New York, 576 p.

Hanson, A.M., 1949, Geology of the southern Malad Range and vicinity in northern Utah: unpublished Ph.D. thesis, University of Wisconsin, 150 p.

Harland, W.B., Cox, A.V., Llewellyn, P.G., Pickton, C.A.G., Smith, A.G., and Walters, R., 1982, a geologic time scale: Cambridge university Press, 131 p.

Harris, L.D., and Milcici, R.C., 1977, Characteristics of thin-skinned style of deformation in the southern Appalachians, and potential hydrocarbon taps: U.S. Geological Survey Professional Paper 1018, 40 p.

Harris, S.H., Land, C.B.Jr., and McKeever, J.H., 1966, Relation of Mission Canyon stratigraphy to oil production in north-central North Dakota: American Association of Petroleum Geologists Bulletin, v. 50, p. 2269-2276.

Harry, D.L., Oldow, J.S., and Sawyer, D.S., 1995, The growth of orogenic belts and the role of crustal heterogeneities in decollement tectonics: Geological Society of America Bulletin, v. 107, p. 1411-1426.

Hazzard, J.C., 1954, Revision of Devonian and Carboniferous section, Nopah Range, Inyo County, California: American Association of Petroleum Geologists Bulletin, v.38, p.878-885.

Hazzard, J.C., 1954, Rocks and structure of the northern Providence Mountains, San Bernardino County, California: California Division Mines Bulletin 170, Chapter IV, Contribution 4, p 27-36.

Henry, C.D., and Boden, D.R., 1998, Eocene magmatism: the heat source for Carlin-type gold deposits of northern Nevada: Geology, v. 26, p. 1067-1070.

Hess, R.H., and Johnson, G., 1997, County digital geologic maps of Nevada, scale 1:250,000: Nevada Bureau of Mines and Geology Open File 97-1, 1 CD disk.

Hewett, D.F., 1956, Geology and mineral resources of the Ivanpah Quadrangle, California and Nevada: U.S. Geological Survey Professional Paper 275, p.172.

Hildebrand, A.R., Penfield, G.T., Kring, D.A., Pilkington, M., Camargo, A.Z, Jacobsen, S.B., and Boynton, W.V., 1991, Chicxulub Crater: a possible Cretaceous/Tertiary boundary impact crater on the Yucatan Peninsula, Mexico: Geology, v. 19, p. 867-871.

Hintze, L.F., 1988, Geologic History of Utah: Brigham Young University Geology Studies Special Publication 7, 202 p.

Hoffman, M.E., and Balcells-Baldwin, R.N., 1982, Gas Giant of the Wyoming thrust belt: Whitney Canyon-Carter Creek field: *in* Powers, R.B., ed., Geologic Studies of the Cordilleran thrust belt: Rocky Mountain Association of Geologists, p. 613-618.

Holail, H., Lohmann, K.C., and Sanderson, I., 1988, Dolomitization and delolomitization of Upper Cretaceous carbonates: Bahariya Oasis, Egypt, *in* Shukla, V., and Baker, P.A., eds., Sedimentology and geochemistry of dolostones: Society of Economic Paleontologists and Mineralogists Special Publication 43, p. 191-207.

Hoggan, R.D., 1975, Paleoecology of the Guilmette Formation in eastern Nevada and western Utah: Brigham Young University Geological Studies, v.22, pt.1, p.141-198.

Hook, S.C., Chamberlain, A.K., and Frost, R.K., 1998, Digital field trip to the central Nevada thrust belt: Society for Sedimentary Geology (SEPM) Continuing Education Digital Field Trip No.1.

Horita, J., Weinberg, A., Das, N., and Holland, H.D., 1996, Brine inclusions in halite and the origin of the Middle Devonian Prairie Evaporites of western Canada: Journal of Sedimentary Research, v. 66, 956-964.

Horton, B.K., and Schmitt, J.G., 1998, Development and exhumation of a Neogene sedimentary basin during extension, east-central Nevada: Geological Society of America Bulletin, v. 110, p. 163-172.

Hose, R.K., and Blake, M.C.Jr., 1976, Geology and mineral resources of White Pine County, Nevada: Nevada Bureau of Mines and Geology Bulletin 85, 105 p.

Hose, R.K., Repenning, C.A., and Ziony, J.I., 1960, Generalized geologic map of a part of the Confusion Range, Utah: U.S. Geological Survey Open File Report, 150 p.

Hulen, J.B., Goff, F., Ross, J.R., Bortz, L.C., and Bereskin, S.R., 1994, Geology and geothermal origin of Grant Canyon and Bacon Flat oil fields, Railroad Valley, Nevada: American Association of Petroleum Geologists Bulletin, v. 78, p. 596-623.

Humphrey, F.L., 1960, Geology of the White Pine Mining District, White Pine County, Nevada: Nevada Bureau of Mines Bulletin 57, 119 p.

Humphrey, J.D., and Quinn, T.M., 1989, Coastal mixing zone dolomite, forward modeling, and massive dolomitization of platform margin carbonates: Journal of Sedimentary Petrology, v. 59, p. 438-454.

Humphrey, J.D., and Quinn, T.M., 1990, Coastal mixing zone dolomite, forward modeling, and massive dolomitization of platform margin carbonates-Reply: Journal of Sedimentary Petrology, v. 60, p. 1013-1016.

Hurtubise, D.O., 1989, Stratigraphy and structure of the Seaman Range, Nevada, with an emphasis on the Devonian System: unpublished Ph.D. dissertation, Colorado School of Mines, Golden, 443 p.

Hurtubise, D.O., 1994, Silver King lineament, the missing link of a 50 km east-trending structure in the southern Great Basin: *in* Dobbs, S.W., and Taylor, W.J., eds., Structural and stratigraphic investigations and petroleum potential of Nevada, with special emphasis south of the Railroad Valley producing trend: Nevada Petroleum Society Conference Volume II, p. 127-139.

Hurtubise, D.O., and DuBray, E.A., 1988, Stratigraphy and structure of the Seaman Range and Fox Mountain, Lincoln and Nye Counties, Nevada: U.S. Geological Survey Bulletin 1988-B, 31 p.

James, N.P., 1984a, Carbonate slopes, *in* Walker, R.G., ed., Facies Models: Geological Association of Canada Geoscience Canada, Reprint Series 1, p. 245-257.

James, N.P., 1984b, Reefs, *in* Walker, R.G., ed., Facies Models: Geological Association of Canada Geoscience Canada, Reprint Series 1, p. 224-257.

James, N.P., 1984c, Shallowing-upward sequences in carbonates, *in* Walker, R.G., ed., Facies Models: Geological Association of Canada Geoscience Canada, Reprint Series 1, p. 213-228.

Johnson, G.H., Kruse, S.E., Vaughn, A.W., Lucy, J.K., Hobbs, C.H.III, and Powers, D.S., 1998, Postimpact deformation associated with the late Eocene Chesapeake Bay impact structure in southeastern Virginia: Geology, v. 26, p. 507-510.

Johnson, J.G., 1962, Lower Devonian-Middle Devonian boundary in central Nevada: American Association of Petroleum Geologists Bulletin, v.46, p.542-545.

Johnson, J.G., 1977, Status of Devonian studies in western and arctic North America, *in* Murphy, M.A., Berry, W.B.N., and Sandberg, C.A., eds., Western North America: Devonian: University of California, Riverside, Campus Museum Contribution 4, p. 1-15.

Johnson, J.G., Klapper, G., and Sandberg, C.A., 1985, Devonian eustatic fluctuations in Euramerica: Geological Society of America Bulletin, v. 96, p. 567-587.

Johnson, J.G., and Murphy, M.A., 1984, Time-rock model for Siluro-Devonian continental shelf, western United States: Geological Society of America Bulletin, v. 95, p. 1349-1359.

Johnson, J.G., and Pendergast, A., 1981, Timing and mode of emplacement of the Roberts Mountain allochthon, Antler orogeny: Geological Society of America Bulletin, v. 92, p. 648-658.

Johnson, J.G., and Sandberg, C.A., 1989, Devonian eustatic events in the western United States and their biostratigraphic responses, *in* McMillan, N.J., Embry, A.F., and Glass, D.J., Devonian of the World: Canadian Society of Petroleum Geologists, Calgary, Memoir 14, v. 1, Regional Syntheses, p. 171-178.

Johnson, J.G., Sandberg, C.A., and Poole, F.G., 1989, Early and Middle Devonian paleogeography of western United States, *in* McMillan, N.J., Embry, A.F., and Glass, D.J., Devonian of the World: Canadian Society of Petroleum Geologists, Calgary, Memoir 14, v. 1, Regional Syntheses, p. 161-182.

Johnson, J.G., Sandberg, C.A., and Poole, F.G., 1991, Devonian lithofacies of the western United States, *in* Cooper J.D, and Stevens, C.H., eds., Paleozoic Paleogeography of the western United States II: Pacific Section Society of Economic Paleontologists and Mineralogists, p. 83-105.

Johnson, M.S., and Hibbard, D.E., 1957, Geology of the Atomic Energy Commission, Nevada Proving Grounds Area, Nevada: U.S. Geological Survey Bulletin, 1021-k, p. 333-384.

Jones, C.H., Sonder, L.J., and Unruh, J.R., 1999, Lithospheric gravitational potential energy and past orogenesis: implications for conditions of initial Basin and Range and Laramide deformation: Reply: Geology, v. 27, p. 475-476.

Jones, B, and Hunter, I.G., 1994, Messinian (Late Miocene) karst on Grand Cayman, British West Indies: an example of an erosional sequence boundary: Journal of Sedimentary Research, v. B64, n. 4, p. 531-541.

Jordan, D.W., 1991, Outcrop gamma-ray logging: truck-mounted and hand held scintillometer methods are useful for exploration, development, and training purposes: 66th Annual Technical Conference and Exhibition of the Society of Petroleum Engineers, p. 841-852.

Kay, M., 1952, Late Paleozoic orogeny in central Nevada: Geological Society of Amercia Bulletin, v. 63, p. 1269-1270.

Kellogg, H.E., 1959, Stratigraphy and structure of the southern Egan Range; unpublished Ph.D. thesis, Columbia University, 150 p.

Kellogg, H.E., 1960, Geology of the Southern Egan Range, Nevada; *in* Boettcher, J.W. and Sloan, W.W. Jr., Guidebook to the Geology of east-central Nevada: Intermountain Association of Petroleum Geology and Eastern Nevada Geological Society, 11th Annual Field Conference, Salt Lake City, Utah, p.189-197.

Kellogg, H.E., 1963, Paleozoic Stratigraphy of the Southern Egan Range, Nevada; Geological Society of America Bulletin. v. 74, p.685-708.

Kendall, G.W., Johnson, J.G., Brown, J.O., and Klapper, G., 1983, Stratigraphy and facies across Lower Devonian-Middle Devonian boundary, central Nevada: American Association of Petroleum Geologists Bulletin, v.67, p. 2199-2207.

Kennedy, M.J., 1996, Stratigraphy, sedimentology, and isotopic geochemistry of Australian Neoproterozoic postglacial cap dolostones: deglaciation, $\delta^{13}C$ excursions, and carbonate precipitation: Journal of Sedimentary Research, v. 66 p. 1050-1064.

Ketner, K.B., 1970, Limestone trubidite of Kinderhook age and its tectonic significance, Elko County, Nevada: U.S. Geological Survey Professional Paper 700-D, p. D18-D22.

Ketner, K.B., 1977, Deposition and deformation of lower Paleozoic western facies rocks, northern Nevada, *in* Stewart, J.H., Stevens, C.H., and Fritsche, A.E., eds., Paleozoic paleogeography of the western United States: Society of Economic Paleontologists and Mineralogists, Pacific Section, Pacific Coast Paleogeography Symposium 1, p. 251-258.

King, C., 1870, U.S. Geological Exploration 40$^{th}$ Parallel Report, v 3, p. 451-473.

King, P.B., 1969, Tectonics of North America-a discussion to accompany the tectonic map of North America: U.S. Geological Survey Prof. Paper 628, 95p.

Kirk, E., 1918, The stratigraphy of the Inyo Range: *in* Knopf, A., A geologic reconnaissance of the Inyo Range and the eastern slope of the southern Sierra Nevada, California: U.S. Geological Survey Professional Paper 110, p.19-48.

Kirk, E., 1933, The Eureka quartzite of the Great Basin region, American Journal of Science, 5th ser., v. 26, p. 27-43.

Kleinhampl, F.J., and Ziony, J.I., 1984, Mineral resources of northern Nye County, Nevada, Nevada Bureau of Mines and Geology Bulletin 99B, 243 p.

Kleinhampl, F.J., and Ziony, J.I., 1985, Geology of northern Nye County, Nevada, Nevada Bureau of Mines and Geology Bulletin 99A, 172 p.

Kuehner, Hans-Cristian, 1997, A genetic model of the Devonian Alamo Breccia, southeastern Nevada: unpublished Ph. D. dissertation, Colorado School of Mines, Golden, 321 p.

Koeberl, C., Armstrong, R.A., and Reimold, W.U., 1997a, Morokweng, South Africa: a large impact structure of Jurassic-Cretaceous boundary age: Geology, v. 25, p. 731-734.

Koeberl, C., Masaitis, V.L., Shafranosky, G.I., Gilmour, I., Langenhorst, F., and Schrauder, M., 1997b, Diamonds from the Popigai impact structure, Russia: Geology, v. 25, p. 967-970.

LaMaskin, T.A., and Elrick, M., 1997, Sequence stratigraphy of the Middle to Upper Devonian Guilmette Formation, southern Egan and Schell Creek Ranges, Nevada: Geological Society of America Special Paper 321, p. 89-112.

Langenheim, R.L. Jr., 1956, Mississippian stratigraphy in eastern Nevada: Geological Society America Bulletin, v.67, p.1714.

Langenheim, R.L. Jr., 1960a, Early and Middle Mississippian Stratigraphy of the Ely Area: in Intermountain Association Petroleum Geologists, Guidebook 11th Annual Field Conference, Geology of east-central Nevada, 1960, p.72-80.

Langenheim, R.L. Jr., 1960b, Preliminary report on the geology of the Ely No.3 Quadrangle, White Pine County, Nevada, in Guidebook to the geology of east-central Nevada: Intermountain Association of Petroleum Geologists, p.148-156.

Langenheim, R.L. Jr., 1960c, The Pilot Shale, West Range Limestone, and the Devonian-Mississippian boundary in eastern Nevada: Illinois Academy of Science, v.53, n.3-4, p.122-131.

Langenheim, R.L. Jr., Carss, B.W., Kennerly, J.B., McCutcheon, V.A., and Waines, R.H., 1960, Paleozoic section in the Arrow Canyon Range, Clark County, Nevada (abs): Geological Society America Bulletin, v.71, p.2064.

Langenheim, R.L. Jr., Carss, BW, Kennerly, J.B., McCutcheon, V.A., and Waines, R.H., 1962, Paleozoic section in Arrow Canyon Range, Clark County, Nevada: American Association of Petroleum Geologists Bulletin, v.46, p.592-609.

Langenheim, R.L. Jr., and Larson, E.R., 1973, Correlation of Great Basin stratigraphic units: Nevada Bureau of Mines and Geology, Bulletin 72, 36 p.

Langenheim, R.L. Jr., and Tischler, H., 1960, Mississippian and Devonian paleontology and stratigraphy, Quartz Spring area, Inyo County, California: California University Publications, Geologic Science, v.38, n.2, p.89-150.

Lawton, T.F., and Trexler, J.H.Jr., 1991, Piggyback basin in the Sevier orogenic belt, Utah: implications for development of the thrust wedge: Geology, v. 19, p. 827-830.

LeFever, R.D., 1996, Sedimentology and stratigraphy of the Deadwood-Winnipeg interval (Cambro-Ordovician, Williston Basin: *in* Longman, M.W., and Sonnenfeld, M.D., eds., Paleozoic Systems of the Rocky Mountain Region: Rocky Mountain Association of Geologists and SEPM (Society for Sedimentary Geology), p. 11-28.

Lehmann, C., Osleger, D.A., and Montañez, I.P., 1998, Controls on cyclostratigraphy of Lower Cretaceous carbonates and evaporites, Cupido and Coahuila platforms, northeastern Mexico: Journal of Sedimentary Research, v. 68, p. 1109-1130.

Lelek, J.J., 1982, Anschutz Ranch East field, northeast Utah and southwest Wyoming: *in* Powers, R.B., ed., Geologic studies of the Cordilleran thrust belt: Rocky Mountain Association of Geologists, p. 619-631.

Lewis, C.J., Wernicke, B.P., Selverstone, J., and Bartley, J.M., 1999, Deep burial of the footwall of the northern Snake Range decollement, Nevada: Geological Society of America Bulletin, v. 111, p. 39-51.

Link, P.K., 1983, Glacial and tectonically influence sedimentation in the upper Proterozoic Pocatello Formation, southeastern Idaho, *in* Miller, D.M., Todd, V.R., and Howard, K.S. eds., Tectonic and stratigraphic studies in the eastern Great Basin: Geological Society of America Memoir 157, p. 165-181.

Liu, M., and Shen, Y., 1998, Sierra Nevada uplift: a ductile link to mantle upwelling under the Basin and Range province: Geology, v. 26, p. 299-302.

Longman, M.W., 1982, Carbonate diagenesis as a control on stratigraphic traps (with examples from the Williston Basin): American Association of Petroleum Geologists Education course note series #21, 159 p.

Longwell, C.R., 1928, Geology of the Muddy Mountains, Nevada: U.S. Geological Survey Bulletin, 798, 152 p.

Longwell, C.R., 1952, Basin and Range geology west of the St. George Basin, Utah: Guidebook to the Geology of Utah, Intermountain Association of Petroleum Geologists, n. 7, p.27-42.

Longwell, C.R., Pampeyan, E.H., Bowyer, B., and Roberts, R.J., 1965, Geology and mineral deposits of Clark County, Nevada: Nevada Bureau of Mines Bulletin 62, 218 p.

Loucks, G.G., 1977, Geologic history of the Devonian northern Alberta to southwest Arizona, *in* Heisey, E.L., Lawson, D.E., Norwood, E.R., Wach, P.H., and Hale, L.A., eds., Rocky Mountain thrust belt geology and resources: Wyoming Geological Association 29th annual field conference in conjunction with Montana geological Society and Utah Geological Society, p. 119-134.

Lu, F.H., and Meyers, W.J., 1998, Massive dolomitization of a late Miocene carbonate platform: a case of mixed evaporative brines with meteoric water, Nijar, Spain: Sedimentology, v. 45, p. 263-277.

Lumsden, W.W.I. Jr., 1964, Geology of the southern White Pine Range and northern Horse Range, Nye and White Pine Counties, Nevada: unpublished Ph.D. dissertation, University of California, Los Angeles, 249 p.

MacCready, T., Snoke, A.W., Wright, J.E., and Howard, K.A., 1997, Mid-crustal flow during Tertiary extension in the Ruby Mountain core complex, Nevada: Geological Society of America Bulletin, v. 109, p. 1576-1594.

Machel, H.G., Cavell, P.a., and Patey, K.S., 1996, Isotopic evidence for carbonate cementation and recrystallization and for tectonic expulsion of fluids into the Western Canadian Sedimentary Basin: Geological Society of America Bulletin, v. 108, p. 1108-1119.

Machel, H.G., and Mountjoy, E.W., 1987, General constraints on extensive pervasive dolomitization--and their application to the Devonian carbonates of western Canada: Bulletin Canadian Petroleum Geology, v. 35, p. 143-158.

Machel, H.G., and Mountjoy, E.W., 1990, Coastal mixing zone dolomite, forward modeling and massive dolomitization of platform margin carbonates-Discussion: Journal of Sedimentary Petrology, v. 60, p. 1008-1012.

Marshak, S., and Mitra, G., 1988, Basic methods of structural geology: Prentice Hall, New Jersey, 446 p.

Martin, M.W., 1987, The structural geology of the Worthington Mountains, Lincoln County, Nevada: unpublished M.S. thesis, University of North Carolina, 112 p.

Matthews, V., 1988, Reinterpretation of the relations between the Keystone, Red Spring, Contact, and Cottonwood faults; eastern Spring Mountains, Clark County, Nevada: The Mountain Geologist, v. 25, p. 181-191.

Matti, J.C.D., 1979, Depositional history of middle Paleozoic carbonate rocks deposited at an ancient continental margin, central Nevada: unpublished Ph.D. dissertation, Stanford University, 486 p.

Matti, J.C., and McKee, E.H., 1977, Silurian and Lower Devonian paleogeography of the outer continental shelf of the Cordilleran miogeocline, central Nevada, *in* Stewart, J.H., Stevens, C.H., and Fritsche, A.E., eds., Paleozoic paleogeography of the western United States: Society of Economic Paleontologists and Mineralogists, Pacific Section, Pacific Coast paleogeography symposium I, p 181-215.

Mayer, L., 1986, Topographic constraints on models of lithospheric stretching of the Basin and Range province, western United States, *in* Mayer, L., ed., Extensional tectonics of the southwestern United States: a perspective on processes and kinematics: Geological Society of America Special Paper 208, p. 1-14.

Mayo, E.B., 1931, Fossils from the eastern flank of the Sierra Nevada, California: Science, v. 74, p. 514-515.

McAllister, J.F., 1952, Rocks and structure of the Quartz Spring area, northern Panamint Range, California: California Department of Natural Resources, Division of Mines, Special Report 25, 38 p.

McAllister, J.F., 1974, Silurian, Devonian, and Mississippian formations of the Funeral Mountains in the Ryan quadrangle, Death Valley region, California: U.S. Geological Survey Bulletin 386, 35 p.

McKee, E.H., 1968, Geology of the Magruder Mountain area, Nevada-California: U.S. Geological Survey Bulletin 1251-H, 40 p.

McKee, E.H., 1976, Geology of the northern part of the Toquima Range, Lander, Eureka, and Nye Counties, Nevada: U.S. Geological Survey Professional Paper 931, 49 p.

McLean, D.J., and Mountjoy, E.W., 1994, Allocyclic control on Late Devonian buildup development, southern Canadian Rocky Mountains: Journal of Sedimentary Research, v. B64, p. 326-340.

McNair, A.H., 1951, Paleozoic stratigraphy of part of northwestern Arizona: American Association of Petroleum Geologists Bulletin, v.35, p.503-541.

McNair, A.H., 1952, Summary of the Pre-Coconino stratigraphy of southwestern Utah, northwestern Arizona and southeastern Nevada, in Guidebook to the geology of Utah, n. 7: Utah Geological and Mineral Survey, p.45-51.

Merriam, C.W., 1940, Devonian stratigraphy and paleontology of the Roberts Mountains region, Nevada: Geological Society of America Special Paper 25, 114 p.

Merriam, C.W., and Anderson, C.A., 1942, Reconnaissance survey of the Roberts Mountains, Nevada: Geological Society of America Bulletin, v. 53, p. 1675-1728
.

Meyers, W.J., Lu, F.H., and Zachariah, J.K., 1997, Dolomitization by mixed evaporative brines and freshwater, Upper Miocene carbonates, Nijar, Spain: Journal of Sedimentary Research, v. 67, p. 898-912.

Miller, E.L., Gans, P.B., Wright, J.E., and Sutter, J.F., 1988, Metamorphic history of the east-central Basin and Range Province: tectonic setting and relationship to magmatism, *in* Ernst, W.G., ed., Metamorphism and crustal evolution of the western United States, (Rubey Volume VII): Englewood Cliffs, New Jersey, Prentice-Hall, p. 649-682.

Miller, G.M., 1959, The Pre-Tertiary structure and stratigraphy of the southern portion of the Wah Wah Mountains, southwestern Utah: unpublished Ph.D. thesis, University of Washington, Seattle, 150 p.

Miller, M.G., and Friedman, R.M., Early Tertiary magmatism and probable Mesozoic fabrics in the Black Mountains, Death Valley, California: Geology, v. 27, p. 19-22.

Misch, P., 1960, Regional structural reconnaissance in central-northeast Nevada and some adjacent areas observations and interpretations: Intermountain Association of Petroleum Geologists and Eastern Nevada Geological Society Guidebook Geology of East Central Nevada, p. 17-42.

Mitchum, R.M., Vail, P.R., and Thompson, S. III, 1977, Seismic stratigraphy and global changes of seal level, Part 2: The depositional sequence as a basic unit for stratigraphic analysis *in* Payton, C.E., ed., Seismic Stratigraphy--Applications to Hydrocarbon Exploration: American Association of Petroleum Geologists Memoir 26, p. 53-62.

Morgan, J., and Warner, M., 1999, Chicxulub: the third dimension of a multi-ring impact basin: Geology, v. 27, p. 407-410.

Morris, H.T., and Lovering, T.S., 1961, Stratigraphy of the East Tintic Mountains, Utah: U.S.Geological Survey Professional Paper 361, 145 p.

Mossop, G., and Shetsen, I., 1994, Geological Atlas of the Western Canadian Sedimentary Basin: Canadian Society of Petroleum Geologists and Alberta Research Council, 510 p.

Mountjoy, E.W., Qing, H., and McNutt, R.H., 1992, Strontium isotopic composition of Devonian dolomites, Western Canada Sedimentary Basin: significance of sources of dolomitizing fluids: Applied Geochemistry, v. 7, p. 59-75.

Mountjoy, E., Whittaker, S., Williams-Jones, A., Qing, H., Drivet, E., and Marquez, X., 1997, Variable fluid and heat flow regimes in three Devonian dolomite conduit systems, Western Canada Sedimentary Basin: isotopic and fluid inclusion evidence/constraints: *in* Basin-wide diagenetic patterns: integrated petrologic, geochemical, and hydrologic considerations: SEPM (Society of Sedimentary Geology) Special Publication No. 57, p. 119-137.

Mukul, M., 1998, A spatial statistics approach to the quantification of finite strain variation in penetratively deformed thrust sheets: an example from the Sheeprock thrust sheet, Sevier fold-and-thrust belt, Utah: Journal of Structural Geology, v. 20, p. 371-384.

Mukul, M., and Mitra, G., 1998, Finite strain and strain variation analysis in the Sheeprock thrust sheet: an internal thrust sheet in the Provo salient of the Sevier fold-and-thrust belt, central Utah: Journal of Structural Geology, v. 20, p. 385-405.

Nelson, R., 1959, Stratigraphy and structure of the northernmost part of the northern Snake Range and the Kern Mountains in eastern Nevada and the southern Deep Creek Range in western Utah: unpublished Ph.D. thesis, University of Washington, Seattle, 165 p.

Nelson, S.L., 1994, Lower and Middle Devonian carbonate platform and outer-shelf basin deposits from the southern end of Railroad Valley, Nevada: *in* Dobbs, S.W., and Taylor, W.J., eds., Structural and stratigraphic investigations and petroleum potential of Nevada, with special emphasis south of the Railroad Valley producing trend: Nevada Petroleum Society Conference Volume II, p. 157-164.

Nelson, S.T., and Tingey, D.G., 1997, Time-transgressive and extension-related basaltic volcanism in southwest Utah and vicinity, Geological Society of America Bulletin, v. 109, p. 1249-1265.

Newman, G.W., 1979, Late Cretaceous(?)-Eocene faulting in the east central Basin and Range, *in* Newman, G.W., and Goode, H.D., eds., Basin and Range Symposium: Rocky Mountain Association of Geologists and Utah Geological Association, p.245-257.

Niebuhr, W.W., 1979, Biostratigraphy and paleoecology of the Guilmette Formation (Devonian) of eastern Nevada: unpublished Ph.D. dissertation, University of California, Berkeley, 246 p.

Nichols, K.M., and Silberling, N.J., 1980, Eogenetic dolomitization in the pre-Tertiary of the Great Basin: *in* Zenger, D.H., Dunham, J.B., and Ethington, R.L., Concepts and models of dolomitization, eds. Society of Economic Paleontologists and Mineralogists Special Publication 22, p. 237-246.

Nolan, T.B., 1935, The Gold Hill mining district, Utah: U.S. Geological Survey Professional Paper 177, 172 p.

Nolan, T.B., 1943, The Basin and Range Province in Utah, Nevada, and California: U.S. Geological Survey Professional Paper 197-D, 196 p.
Nolan, T.B., 1962, The Eureka mining district, Nevada: U.S. Geological Survey Professional Paper 406.

Nolan, T.B., Merriam, C.W., and Williams, J.S., 1956, The stratigraphic section in the vicinity of Eureka, Nevada: U.S. Geological Survey Professional Paper 276, 77 p.

Nolan, T.B., Merriam, C.W., and Brew, D.A., 1971, Geologic map of the Eureka quadrangle, Eureka and White Pine Counties, Nevada: U.S. Geological Survey Map I-612.

Nolan, T.B., Merriam, C.W., and Blake, M.C. Jr., 1974, Geologic map of the Pinto Summit quadrangle, Eureka and White Pine Counties, Nevada: U.S. Geological Survey Map I-793.

North, F.K., 1988, The state of the system and economic survey of the whole Devonian: *in* McMillan, N.J., Embry, A.F., and Glass, D.J., Devonian of the World: Canadian Society of Petroleum Geologists, Calgary, Memoir 14, v. 1, Regional Syntheses, p. 1-14.

Okaya, D.A., and Thomspson, G.A., 1986, Involvement of deep crust in extension of Basin and Range province, *in* Mayer, L., ed., Extensional tectonics of the southwestern United States: a perspective on processes and kinematics: Geological Society of America Special Paper 208, p. 15-22.

Olson, R.H., 1956, Geology of Promontory Range, *in* Geology of parts of northwestern Utah: Utah Geological Society, p.41-75.

Osmond, J.C., 1953, Mottled carbonate rocks in the Middle Devonian of Eastern Nevada: Geological Society America Bulletin, v.64, p.1460.

Osmond, J.C., 1954, Dolomites in Silurian and Devonian of east-central Nevada: American Association of Petroleum Geologists Bulletin, v. 38, p.1911-1156.

Osmond, J.C., 1962, Stratigraphy of Devonian Sevy Dolomite in Utah and Nevada: American Association of Petroleum Geologists Bulletin, v. 46, p. 2033-2056.

Paddock, R.E., 1956, Geology of the Newfoundland Mountains, Box Elder County, Utah: unpublished MS thesis, University of Utah, Salt Lake City, 101 p.

Page, W.R., 1993, Stratigraphy and structure of the Paleozoic rocks in the southern Delamar Mountains, Lincoln County, Nevada: unpublished M.S. thesis, Colorado School of Mines, Golden, 95 p.

Page, W.R., and Ekren, E.B., 1995, Preliminary geologic map of the Bristol Well Quadrangle, Lincoln County, Nevada: U.S. Geological Survey Open-File Report 95-580, 27 p.

Page, W.R., Swadely, W.C., and Scott, R.B., 1990, Preliminary geologic map of Delamar three SW quadrangle, Lincoln County, Nevada: U.S. Geological Survey Open-File Report 90-336, 17 p.

Paulsen, T., and Marshak, S., 1998, Charleston transverse zone, Wasatch Mountains, Utah: structure of the Provo salient's north margin, Sevier fold-thrust belt: Geological Society of America Bulletin, v. 110, p. 512-522.

Perkins, R.F., 1955, Structure and stratigraphy of the lower American Fork Canyon--Mahogany Mountain area, Utah County, Utah: Brigham Young University Research Studies, Geology Series, v.2, n.1, 38 p.

Perry, W.J.Jr., and Sando, W.J., 1982, Sequence of deformation of Cordilleran thrust belt in Lima, Montana region, *in* Powers, R.B., ed., Geologic studies of the Cordilleran thrust belt: Rocky Mountain Association of Geologists, v. 1, p. 137-144.

Peterson, J.A., and MacCary, L.M., 1987, Regional stratigraphy and general petroleum geology of the U.S. portion of the Williston basin and adjacent areas: *in* Longman, M.W., ed., Williston Basin: Anatomy of a cratonic oil province: Rocky Mountain Association of Geologists, p. 9-43.

Petersen, M.S., 1956, Devonian strata of central Utah: Brigham Young University Research Studies, Geology Series, v.3, n.3, 37 p.

Picha, F.J., 1996, Exploring for hydrocarbons under thrust belts-a challenging new frontier in the Carpathians and elsewhere: American Association of Petroleum Geologists, v. 80, p. 1547-1564.

Ponce, D.A., 1997, Gravity data of Nevada: U.S. Geological Survey Digital Data Series DDS-42.

Poole, F.G., 1974, Flysch deposits of Antler foreland basin, western United States, in Dickinson, W.R., ed., Tectonics and sedimentation: Society of Economic paleontologists and Mineralogists Special Publication 22, p. 58-83.

Poole, F.G., and Claypool, G.E., 1984, Petroleum source-rock potential and crude-oil correlation in the Great Basin, *in* Woodward, J., Meissner, F.F., and Clayton, J.L., eds., Hydrocarbon source rocks of the greater Rocky Mountain region: Rocky Mountain Association of Geologists, p. 179-228.

Poole, F.G., Sandberg, C.A., and Boucot, A.J., 1977, Silurian and Devonian paleogeography of the western United States, *in* Stewart, J.H., Stevens, C.H., and Fritsche, A.E., eds., Paleozoic paleogeography of the western United States: Society of Economic Paleontologists and Mineralogists, Pacific Section, Pacific Coast Paleogeography Symposium 1, p. 39-65.

Poole, F.G., Stewart, J.H., Palmer, A.R., Sandberg, C.A., Madrid, R.J., Ross, R.J. Jr., Hintze, L.F., Miller, M.M., and Wrucke, C.T., 1992, Latest Precambrian to latest Devonian time: Development of a continental margin, *in* Burchfiel, B.C., Lipman, P.W., and Zoback, M.L., eds., The Cordilleran Orogen: Conterminous U.S.: Boulder, Colorado, Geological Society of America, The Geology of North America, v. G-3, p. 9-56.

Quennell, A.M., 1987, Rift Valleys: *in* Seyfert, C.K., ed., the encyclopedia of structural geology and plate tectonics: Van Nostrand Reinhold Company, New York, p. 671-688.

Rankey, E.C., and Walker, K.R., 1994, Gradual establishment of Iapetan “passive” margin sedimentation: stratigraphic consequences of Cambrian episodic tectonism and eustasy, southern Appalachians: Journal of Sedimentary Research, v. B64 p. 298-310.

Read, D.L., and Zogg, W.D., 1988, Description and origin of the Devonian dolomite reservoir, Grant Canyon field, Nye County, Nevada, *in* Goolsby, S.M., and Longman, M.W., eds., Occurrence and petrophysical properties of carbonate reservoirs in the Rocky Mountain region: Rocky Mountain Association of Geologists, Denver, p. 229-240.

Read, J.F., and Goldhammer, R.K., 1988, Use of Fischer plots to define third-order sea-level curves in Ordovician peritidal cyclic carbonates, Appalachians: Geology, v. 16, p. 895-899.

Rehig, W.A., 1986, Processes of regional Tertiary extension in the western Cordillera: insights from the metamorphic core complexes, *in* Mayer, L., ed., Extensional tectonics of the southwestern United States: a perspective on processes and kinematics: Geological Society of America Special Paper 208, p. 97-122.

Reid, R.K., and Dorobek, S.L., 1993, Sequence stratigraphy and evolution of a Paleozoic foreland carbonate ramp in the Mississippian Mission Canyon Formation and stratigraphic equivalent, Montana and Idaho: *in* Loucks, R.G and Sarg, J.F., eds., Carbonate sequence stratigraphy: recent developments and applications: American Association of Petroleum Geologists Memoir 57, p. 327-352.

Reimold, W.U., Brandt, D., and Koeberl, C., 1998 Detailed structural analysis of the rim of a large, complex impact crater: Bosumtwi Crater, Ghana: Geology, v. 26, p.543-546.

Reso, A., 1960, The geology of the Pahranagat Range, Lincoln County, Nevada: unpublished Ph.D. dissertation, Rice University, Houston, Texas, 656 p.

Reso, A., 1963, Composite columnar section of exposed Paleozoic and Cenozoic rocks in the Pahranagat Range, Lincoln County, Nevada: Geological Society of America Bulletin, v. 74, p. 901-918.

Reso, A., and Corneis, C.G., 1959, Devonian system in the Pahranagat Range, southeastern Nevada: Geological Society of America Bulletin, v. 70, p. 1249-1252.

Rey, P.F., and Costa, S., 1999, Lithospheric gravitational potential energy and past orogenesis: implications for conditions of initial Basin and Range and Laramide deformation: Comment: Geology, v. 27, p. 475-476.

Riciputi, L.R., Machel, H.G., and Cole, D.R., 1994, An ion microprobe study of diagenetic carbonates in the Devonian Nisku formation of Alberta, Canada: Journal of Sedimentary Research, v. A64, p. 115-127.

Rigby, J.K., 1958, Geology of the Stansbury Mountains, eastern Tootle County, Utah, *in* Guidebook to the geology of Utah, n.13: Utah Geological Society, 134 p.

Rigby, J.K., 1959, Stratigraphy of the southern Oquirrh Mountains, Lower Paleozoic succession, *in* Guidebook to the geology of Utah, n.14: Utah Geological Society, p.9-36.

Rigby, J.K., 1960, Geology of the Buck Mountain-Bald Mountain area, southern Ruby Mountains, White Pine County, Nevada: *in* Intermountain Assoc. Petroleum Geologists, Guidebook 11th Ann. Field Conference, Geology of east-central Nevada, 1960, p.173-180.

Rinehart, C.D., Ross, D.C., and Huber, N.K., 1959, Paleozoic and Mesozoic fossils in a thick stratigraphic section in the eastern Sierra Nevada, California: Geological Society America Bulletin, v.70, p.941-946.

Roberts, R.J., 1949, Structure and stratigraphy of Antler Peak Quadrangle, north-central Nevada: Geological Society America Bulletin, v.60, p.1917.

Roberts, R.J., 1972, Evolution of Cordilleran fold belt: Geological Society of America Bulletin, v. 83, p. 1989-2004.

Roberts, R.J., Hotz, P.E., Gilluly, J., and Ferguson, H.G., 1958, Paleozoic rocks of north-central Nevada: American Association of Petroleum Geologists Bulletin, v.42, p.2813-2857.

Roberts, R.J., Montgomery, K.M., and Lehner, R.E., 1967, Geology and Mineral Resources of Eureka County, Nevada: Nevada Bureau of Mines and Geology Bulletin 64, 152 p.

Roeder, D., 1989, Thrust belt of central Nevada, Mesozoic compressional events, and the implications of petroleum prospecting, *in* Garside, L.J., and Shaddrick, D.R., eds., Compressional and extensional structural styles in the northern Basin and Range seminar proceedings: Reno, Nevada Petroleum Society and Geological Society of Nevada, p. 21-34.

Roeder, D., Gilbert, O.C., and Witherspoon, W.D., 1978, Evolution and macroscopic structure of the Valley and Ridge thrust belt, Tennessee and Virginia: Studies in Geology 2, University of Tennessee Department of Geology Sciences, 25 p.

Rodgers, J., 1949, Evolution of thought on structure of middle and southern Appalachians: American Association of Petroleum Geologists Bulletin, v. 33, p. 1643-1654.

Ross, D.C., 1961, Geology and mineral deposits of Mineral County, Nevada: Nevada Bureau of Mines Bulletin 58, 98 p.

Ross, D.C., 1962, Preliminary geologic map of the Independence Quadrangle, Inyo County California: U.S. Geological Survey Mineral Field Studies Map MF254.

Ross, G.M., 1991, Precambrian basement in the Canadian Cordillera: an introduction: Canadian Journal of Earth Sciences, v. 28, p. 1133-1139.

Rush, R.W., 1951, Stratigraphy of the Burbank Hills, Western Millard County, Utah: Utah Geological and Mineral Survey Bulletin 38, 23 p.

Rush, R.W., 1956, Silurian rocks of western Millard County, Utah: Utah Geological and Mineral Survey Bulletin 53, 66 p.

Ryan, J.F., and Langenheim, R.L. Jr., 1973, Upper Devonian sandstone in Arrow Canyon Quadrangle, Clark County, Nevada: American Association of Petroleum Geologists Bulletin, v.57, p.1734-1742.

Sadler, P.M., Osleger, D.A., and Montañez, I.P., 1993, On the labeling, length, and objective basis of Fischer plots: Journal of Sedimentary Research, v. 63, p. 360-368.

Sami, T.T., and James, N.P., 1994, Peritidal carbonate platform growth and cyclicity in an early Proterozoic foreland Basin, Upper Pethei Group, northwest Canada: Journal of Sedimentary Research, v. B64, p. 111-131.

Sandberg, C.A., Morrow, J.R., and Warme, J.E., 1997, Late Devonian Alamo impact event, global Kellwasser events, and major eustatic events, eastern Great Basin, Nevada and Utah, *in* Link, P.K. and Kowallis, B.J., eds., Proterozoic to recent stratigraphy, tectonics, and volcanology, Utah, Nevada, southern Idaho and central Mexico: Brigham Young University Geology Studies, v. 42, part 1, p. 129-160.

Sandberg, C.A., and Poole, F.G., 1977, Conodont biostratigraphy and depositional complexes of the Upper Devonian cratonic-platform and continental-shelf rocks in the western United States, *in* Murphy, M.A., Berry, W.B.N., and Sandberg, C.A., eds., Western North America: Devonian: University of California, Riverside, Campus Museum Contribution 4, p. 144-182.

Sandberg, C.A., Poole, F.G., and Johnson, J.G., 1988, Upper Devonian of western United States, *in* McMillan, N.J., Embry, A.F., and Glass, D.J., Devonian of the World: Canadian Society of Petroleum Geologists, Calgary, Memoir 14, v. 1, Regional Syntheses, p. 183-220.

Sandberg, C.A., and Ziegler, W., 1973, Refinement of standard Upper Devonian conodont zonation based on sections in Nevada and West Germany: Geologica et Paleaontologica, v. 7, p. 97-122.

Sandberg, C.A., and Ziegler, W., 1996, Devonian conodont biochronology in geologic time calibration: Senckenbergiana lethae, v. 76, p. 259-265.

Sandberg, C.A., Ziegler, W., Dreesen, R., and Butler, J.L., 1988, Late Frasnian mass extinction: Conodont event stratigraphy, global changes, and possible causes, Courier Forschungs-Institute Senckenberg, v. 102, p. 263-307.

Satterley, A.K., 1996, Cyclic carbonate sedimentation in the Upper Triassic Dachstein Limestone, Austria: the role of patterns of sediment supply and tectonics in a platform-reef-Basin system: Journal of Sedimentary Research, v. 66, p. 307-323.

Schaeffer, M.E., 1960, Stratigraphy of the Silver Island Mountains, *in* Guidebook to the geology of Utah, n.15: Utah Geological Society, p.15-111.

Scott, C.H., Chamberlain, A.K., 1986, Mississippian source rock maturation and richness, eastern Nevada: American Association of Petroleum Geologists Bulletin, v. 70; p. 1055.

Scott, C.H., and Chamberlain, A.K., 1988a, Blackburn Field, Nevada; a case history: Geological Society of America, Abstracts with Programs; v. 20, p. 229.

Scott, C., and Chamberlain, A.K., 1988b, Blackburn Field Nevada: a case history: *in* Goolsby, S.M., and Longman, M.W. eds., Occurrence and petrophysical properties of carbonate reservoirs in the Rocky Mountain region: 1988 Rocky Mountain Association of Geologists, Denver, Colorado, p. 241-250.

Sengör, A.M.C., 1987, Aulacogen: *in* Seyfert, C.K., ed., the encyclopedia of structural geology and plate tectonics: Van Nostrand Reinhold Company, New York, p. 18-25.

Sharp, R.P., 1942, Stratigraphy and structure of the southern Ruby Mountains, Nevada: Geological Society America, v.53, p.647-690.

Shukla, V., 1988, Sedimentology and geochemistry of a regional dolostone: correlation of trace elements with dolomite fabrics, *in* Shukla, V., and Baker, P.A., eds., Sedimentology and geochemistry of dolostones: Society of Economic Paleontologists and Mineralogists Special Publication 43, p. 145-157.

Simpson, R.W., Jachens, R.C., and Blakley, R.J., 1986, A new isostatic residual gravity map of the conterminous United States with a discussion on the significance of isostatic residual anomalies: Journal of Geophysical Research, v. 91, p. 8348-8372.

Skinner, B.J., and Porter, S.C., 1989, The dynamic Earth an introduction to physical geology: John Wiley & Sons, New York, 541 p.

Skipp, B., and Hiat, M.H., Jr., 1977, Allochthons along the northeast margin of the Snake River Plain, Idaho: *in* Heisey, E.L., Lawson, D.E., Norwood, E.R., Wach, P.H., and Hale, L.A. eds., Rocky Mountain Thrust Belt Geology and Resources: Wyoming Geological Association-Montana Geological Society-Utah Geological Society Joint Field Conference, p. 499-515.

Sloss, L.L., 1963, Sequences in the cratonic interior of North America: Geological Society of America Bulletin, v. 74, p. 93-113.

Smith, M.T., Dickinsen, W.R., and Gehrels, G.E., 1993, Contractional nature of the Devonian-Mississippian Antler tectonism along the North American continental margin: Geology, v. 21, p. 21-24.

Smith, J. Jr., and Ketner, K.B., 1968, Devonian and Mississippian rocks and the date of the Roberts Mountains thrust in the Carlin-Pinon range area, Nevada: U.S. Geological Survey Bulletin 1251-I, 18 p.

Smith, J. Jr., and Ketner, K.B., 1975, Stratigraphy of Paleozoic rocks in the Carlin-Pinon range area, Nevada: U.S. Geological Survey Professional Paper 867-A, 87 p.

Snyder, D. B., 1983, Interpretation of the Bouguer gravity map of Nevada: Caliente sheet: Nevada Bureau of Mines and Geology, Report 37, 8 p.

Spencer, A.C., 1917, The geology and ore deposits of Ely, Nevada: United states Geological Survey Professional Paper 96, 189 p.

Spurr, J.E., 1903, Descriptive geology of Nevada south of the fortieth parallel and adjacent portions of California: U.S. Geological Survey Bulletin 208, 229 p.

Staatz, M.H., and Osterwald, F.W., 1959, Geology of the Thomas Range fluorspar district, Juab County, Utah: U.S. Geological Survey Bulletin 1069, 97 p.

Stamatakos, J.A., Ferrill, D.A., and Spivey, K.H., 1998, Paleomagnetic constraints on the tectonic evolution of Bare Mountain, Nevada: Geological Society of Geology Bulletin, v. 110, p. 1530-1546.

Stanley, K.O., and Collison, J.W., 1979, Depositional history of Paleocene-Lower Eocene Flagstaff Limestone and coeval rocks, central Utah: American Association of Petroleum Geologists Bulletin, v. 63, p. 311-323.

Stevens, C.H., 1986, Evolution of the Ordovician through Middle Pennsylvanian carbonate shelf in east-central California: Geological Society of America Bulletin, v. 97, p. 11-25.

Stewart, J.H., 1980, Geologic Map of Nevada: Nevada Bureau of Mines and Geology Special Publication 4, 136 p.

Stewart, J.H., and Carlson, J.E., 1978, 1:500,000 scale geologic map of Nevada, U.S. Geological Survey and Nevada Bureau of Mines and Geology.

Stewart, J.H., and Poole F.G., 1974, Lower Paleozoic and uppermost Precambrian Cordilleran miogeocline, Great Basin, western United States, *in* Dickenson, W.R., ed., Tectonics and sedimentation: Society of Economic Paleontologists and Mineralogists, Special Publication, n. 22, p. 28-57.

Stewart, S.A., 1996, Influence of detachment layer thickness on style of thin-skinned shortening: Journal of Structural Geology, v. 18, p. 1271-1274.

Stokes, W.L., 1979, Stratigraphy of the Great Basin region, *in* Newman, G.W., and Goode, H.D., eds., Basin and Range Symposium: Rocky Mountain Association of Geologists and Utah Geological Association, p. 195-220.

Suek, D.H., and Knaup, W.W.I, 1979, Paleozoic carbonate buildups in the Basin and Range Province *in* Newman, G.W., and Goode, H.D., eds., Basin and Range Symposium: Rocky Mountain Association of Geologists and Utah Geological Association, p.245-257.

Suppe, J., 1985, Principles of structural geology: Prentice-Hall, New Jersey, 537 p.

Swadley, W.C., Page, W.D., Scott, R.B. and Pampeyan, E.H., 1994, Geologic map of the Delamar three SE Quadrangle, Lincoln County, Nevada: U.S. Geological Survey Map GQ-1754.

Swart, P.K., 1988, The elucidation of dolomitization events using nuclear-track mapping, *in* Shukla, V., and Baker, P.A., eds., Sedimentology and geochemistry of dolostones: Society of Economic Paleontologists and Mineralogists Special Publication No. 43, p. 11-23.

Talling, P.J., Lawton, T.F., Burbank, D.W., and Hobbs, R.S., 1995, Evolution of latest Cretaceous-Eocene nonmarine deposystems in the Axhandle piggyback Basin of central Utah: Geological Society of America Bulletin v. 107, p. 297-315.

Taylor, W.J., 1989, Geometry of faulting, timing of extension and their relationship to volcanism, near 38$^{o}$ N latitude, eastern Nevada: Unpublished dissertation, University of Utah, Salt Lake City, 204 p.

Taylor, W.J., Bartley, J.M., Fryxell, J.E., Schmitt, J., and Vandervoort, D.S., 1993, Mesozoic central Nevada thrust belt, *in* Lahren, M.M., Trexler., J.H., and Spinosa, C., eds., Crustal evolution of the Great Basin and the Sierra Nevada: Geological Society of America Cordilleran/Rocky Mountain Section Field Trip Guidebook, p. 57-96.

Taylor, W.J., Dobbs, S.W., Nelson, S.L., and Armstrong, P.A., 1994, Generation of four-way closure through multiple tectonic events: structures of the Timpahute Range, southern Nevada: *in* Dobbs, S.W., and Taylor, W.J., eds., Structural and stratigraphic investigations and petroleum potential of Nevada, with special emphasis south of the Railroad Valley producing trend: Nevada Petroleum Society Conference Volume II, p. 141-156.

Tingley, J.V., 1991, Mineral resources of the Timpahute Range 30' x 60' quadrangle: Nevada Bureau of Mines and Geology Report 46, 40 p.

Trexler, J.H.Jr., Cole, J.C., and Cashman, P.H., 1999, Middle Devonian-Mississippian stratigraphy on and near the Nevada Test Site: implications for hydrocarbon potential: reply: American Association of Petroleum Geologists, v. 83, p. 523-524.

Tschanz, C.M., and Pampeyan, E.H., 1970, Geology and Mineral Deposits of Lincoln County, Nevada: Nevada Bureau of Mines and Geology Bulletin 73, 188 p.

Vail, P.R., Mitchum, R.M., and Thompson, S. III, 1977a, Seismic stratigraphy and global changes of seal level, Part 3: Relative changes of sea level from coastal onlap, *in* Payton, C.E., ed., Seismic Stratigraphy--Applications to Hydrocarbon Exploration: American Association of Petroleum Geologists Memoir 26, p. 83-97.

Vail, P.R., Mitchum, R.M., Todd, R.G.Jr., Widmier, J.M., Thomson S. III, Sangree, J.B., Bubb, J.N., and Hatlelid, W.G., 1977b, Seismic stratigraphy and global changes of sea level, *in* Payton, C.E. ed., Seismic stratigraphy--Applications to hydrocarbon exploration: American Association of Petroleum Geologists Memoir 26, p. 49-212.

Vandervoort, D.S., 1987, Sedimentology, provenance, and tectonic implications of the Cretaceous Newark Canyon Formation, east-central Nevada: unpublished M.S. thesis, Montana State University, Bozeman, Montana, 145 p.

Vreeland, J.H. and Berrong, B.H., 1979, Seismic exploration in Railroad Valley, Nevada, *in* Newman, G.W., and Goode, H.D., eds., Basin and Range Symposium: Rocky Mountain Association of Geologists and Utah Geological Association, p. 557-569.

Waines, R.H., 1961, Devonian sequence in the north portion of the Arrow Canyon Range, Clark County, Nevada (abs.), Geological Society America Special Paper 68, p. 62.

Waines, R.H., 1965, Devonian Stromotoporoids of Nevada: unpublished Ph.D. dissertation, University of California, Berkeley, 505 p.

Waite, R.H., 1953, Age of the "Devonian" of the Kearsarge area, California (abs.): Geological Society America Bulletin, v.64, p.1521.

Walker, J.D., Burchfiel, B.C., and Davis, G.A., 1995, New age controls on initiation and timing of foreland thrusting in the Clark Mountains, southern California: Geological Society of America Bulletin, v. 107, p. 742-750.

Walker, J.P., 1982, Hogback Ridge field, Rich County, Utah: thrust-belt anomaly or harbinger of further discoveries? *in* Powers, R.B., ed. Geologic Studies of the Cordilleran thrust belt: Rocky Mountain Association of Geologists, p.581-590.

Wang, K., Orth, D.J., Atreep, M.Jr., Chatterton, B.D.E., and Geldsetzer, H.H.J., 1991, Geochemical evidence for a catastrophic biotic event at the Frasnian/Famennian boundary in south China: Geology, v. 19, p. 776-779.

Warme, J.E., Chamberlain, A.K., and Ackman, B.W., 1991, The Alamo Event; Devonian cataclysmic breccia in southeastern Nevada: Geological Society of America, Cordilleran Section, 87th annual meeting, Abstracts with Programs; v. 23, p. 108.

Warme, J.E., and Kuehner, Hans-Christian, 1998, Anatomy of an anomaly: the Devonian catastrophic Alamo impact breccia of southern Nevada: International Geology Review, v. 40, p. 189-216.

Warme, J.E., and Sandberg, C.A., 1995, The catastrophic Alamo breccia of southern Nevada: record of Late Devonian extraterrestrial impact: Courier Forchungsinstitut Senckenberg, v. 188, W. Ziegler Commentuative Volume.

Warme, J.E., and Sandberg, C.A., 1996, Alamo megabreccia: record of a Late Devonian impact in southern Nevada: GSA Today, v. 6, n. 1, p.1-7.

Warme, J.E., Yarmanto, Chamberlain, A.K., and Ackman, B.W., 1993, The Alamo event: cataclysmic Devonian breccia, southeastern Nevada: *in*: Gillespie, C.W., ed., Structural and stratigraphic relationships of Devonian reservoir rocks, east central Nevada: 1993 Field trip Guidebook, Nevada Petroleum Society, Inc., Reno, NV, p. 157-170.

Warner, M.A., 1982, Source and time of generation of hydrocarbons in the Fossil Basin, western Wyoming thrust belt: *in* Powers, R.B., ed., Geologic studies of the Cordilleran thrust belt: Rocky Mountain Association of Geologists, p. 805-815.

Webb, G.E., 1998, Earliest known Carboniferous shallow-water reef, Gudman Formation (Tn1b) Queensland, Australia: implications for Late Devonian reef collapse and recovery: Geology, v. 26, p. 951-953.

Weimer, R.J., 1992, Developments in sequence stratigraphy: foreland and cratonic basins: American Association of Petroleum Geologists Bulletin, v. 76, p. 965-982.

Weinzapfel, A.C., and Neese, D.G, 1986, Gooseneck field, north Williston Basin: *in*: Noll, J.H. and Doyle, K.M., eds., Rocky Mountain oil and gas fields: 1986 symposium, Wyoming Geological Association, Casper, WY, p.61-82.

Wernicke, B.P., 1981, Low-angle normal faults in the Basin and Range Province: Nappe tectonics in an extending orogen: Nature, v. 291, p. 645-648.

Wernicke, B., Snow, J.K., and Walker, J.D., 1988, Correlation of Early Mesozoic thrusts in the southern Great Basin and their possible indication of 250-300 km of Neogene crustal extension, *in* Weide, D.L., and Faber, M.I. eds., This extended land, geological journeys in the souther Basin and Range: Geological Society of America Cordilleran Section Field Trip Guide, p. 255-268.

Westgate, L.G., and Knopf, A., 1932, Geology and ore deposits of the Pioche District, Nevada: U.S. Geological Survey Professional Paper 171, 79 p.

Wheeler, H.E., 1963, Post-Sauk and pre-Absaroka Paleozoic stratigraphic patterns in North America: American Association of Petroleum Geologists Bulletin, v. 47, p. 1497-1526.

Wilkinson, B.H., Diedrich, N.W., and Drummond, C.N., 1996, Facies successions in peritidal carbonate sequences: Journal of Sedimentary Research, v. 66, p. 1065-1078.

Wilkinson, B.H., Diedrich, N.W., Drummond, C.N., and Rothman, E.D., 1998, Michigan hockey, meteoric precipitation, and rhythmicity of accumulation on peritidal carbonate platforms: Geological Society of America Bulletin, v. 110, p. 1075-1093.

Wilkinson, B.H., Drummond, C.N., Diedrich, N.W., and Rothman, E.D., 1999, Poisson processes of carbonate accumulation on Paleozoic and Holocene platforms: Journal of Sedimentary Research, v. 69. P. 338-350.

Willden, R., and Kistler, R.W., 1979, Precambrian and Paleozoic stratigraphy in central Ruby Mountains Elko County, Nevada, *in* Newman, G.W., and Goode, H.D., eds., Basin and Range Symposium: Rocky Mountain Association of Geologists and Utah Geological Association, p. 221-243.

Williams, J.S., 1948, Geology of the Paleozoic rocks, Logan Quadrangle, Utah: Geological Society America Bulletin, v.59, p.1121-1164.

Williams, J.S., 1955, Resume of Paleozoic stratigraphy, Ordovician to Pennsylvanian, of the Green River Basin area, Wyoming, *in* Guidebook Tenth Annual Field Conference: Wyoming Geological Association, p.43-47.

Wilson, J. L., 1975, Carbonate facies in geologic history: Berlin-Heidelberg-New York, Springer-Verlag, 471 p.

Wilson, J.L., and Pilatzke, R.H., 1987, Carbonate-evaporite cycles in lower Duperow formation of the Williston Basin, *in* Longman, M.W., ed., Williston Basin: Anatomy of a cratonic oil province, Rocky Mountain Association of Geologists, p. 119-146.

Winfrey, W.M.Jr., 1960, Stratigraphy, correlation, and oil potential of the Sheep Pass Formation, east-central Nevada: *in* Boettcher, J.W. and Sloan, W.W. Jr., Guidebook to the Geology of east-central Nevada: Intermountain Association of Petroleum Geology and Eastern Nevada Geological Society, 11th Annual Field Conference, Salt Lake City, Utah, p.126-133.

Winterer, E.L., and Murphy, M.A., 1958, Silurian reef complex and associated facies, central Nevada: Geological Society America Bulletin, v.69, p.1711.

Wire, J.C.D., 1961, Geology of the Currant Creek District, Nye and White Pine Counties, Nevada: unpublished MA thesis, University of California, Los Angeles, 154 p.

Woodhead, J.D., Herst, J.M., and Simonson, B.M., 1998, Isotopic dating of an Archean bolide impact horizon, Hamersley basin, Western Australia: Geology, v. 26, p. 47-50.

Xun, Z., and Fairchild, I.J., 1987, Mixing zone dolomitization of Devonian carbonates, Guangxi, south China, *in* Marshall, J.D., ed., Diagenesis of sedimentary sequences: Geological Society Special Publication n. 36, p. 157-170.

Yang, W., 1989, Facies analysis of the middle member of Devonian Lost Burro Formation, Death Valley, California: Journal of Natural Science, California State University, Fresno, v. 4, p. 31-35.

Yang, W., Harmsen, F., and Kominz, M.A., 1995, Quantitative analysis of a cyclic peritidal carbonate sequence, the Middle and Upper Devonian Lost Burro Formation, Death Valley, California--a possible record of Milankovitch climatic cycles: Journal of Sedimentary Research, v. B65, p. 306-322.

Yang, W., Kominz, M.A., and Major, R.P., 1998, Distinguishing the roles of autogenic versus allogenic processes in cyclic sedimentation, Cisco Group (Virgilian and Wolfcampian), north-central Texas: Geological Society of America Bulletin, v. 110, p. 1333-1353.

Yarmanto, 1992, Sedimentology and stratigraphic setting of a Devonian carbonate breccia, northern Pahranagat Range, Nevada: unpublished M.S. thesis, Colorado School of Mines, Golden, 218 p.

Yoshida, S., Willis, A., and Miall, A.D., 1996, Tectonic control of nested sequence architecture in the Castlegate Sandstone (Upper Cretaceous), Book Cliffs, Utah: Journal of Sedimentary Research, v. 66, p. 737-748.

Young, J.C.D., 1955, Geology of the southern Lakeside Mountains, Utah: Utah Geological and Mineral Survey Bulletin 56, 110 p

Zhang, M., O'Reilly, S.Y., and Chen, D., 1999, Location of Pacific and Indian mid-ocean ridge-type mantle in two time slices: Evidence from Pb., Sr, and Nd isotopes for Cenozoic Australian basalts: Geology, v. 27, p. 39-42.

Zenger, D.H., and Pearson, F.E., 1969, Stratigraphy and petrology of the Lost Burro Formation, Panamint Range, California: California Department of Natural Resources, Division of Mines, Special Report 100, p. 45-65.

Ziegler, W., and Sandberg, C.A., 1990, The Late Devonian standard conodont zonation: Courier Forschungsinstitut Senckenberg, v. 121, p. 1-115.